Wind Turbine
Structural Dynamics

A workshop held at
Lewis Research Center
Cleveland, Ohio
November 15-17, 1977

Wind Turbine
Structural Dynamics

A workshop held at
Lewis Research Center
Cleveland, Ohio
November 15-17, 1977

1978

FOREWORD

A workshop on wind turbine structural dynamics was held at the NASA Lewis Research Center in Cleveland, Ohio, on November 15-17, 1977. The workshop was sponsored by the Department of Energy. It was attended by DOE and NASA personnel, their contractors and university grantees, and other invited speakers. Information was exchanged on the following topics:

- Methods for calculating dynamic loads
- Aeroelastic stability
- Wind loads, both steady and transient
- Critical design conditions
- Drive train dynamics
- Systems dynamics
- Behavior of operating wind turbines

The workshop had two purposes: First, to review and document current United States work on the dynamic behavior of large wind turbines, primarily of the horizontal-axis type; second, to identify and discuss other wind turbine configurations that may have lower cost and weight. Current work was reviewed during two days of technical presentations. Questions from the audience were answered after each presentation. Future large wind turbines were discussed at three panels: Analysis Methods, Structural Configurations, and Power Train Configurations. Questions and comments from the audience followed each panel. The discussion leader and the session chairman then summarized the main points made by both the panel and the audience. These proceedings present the papers, the panel summaries, and all questions and answers.

The success of this workshop was the result of the cooperative efforts of many people, among whom were Prof. Holt Ashley of Stanford University, the panel discussion leader, and the session chairmen.

Workshop Committee:

David A. Spera, Chairman
Joseph M. Savino, Co-Chairman
Dean R. Miller, Proceedings Editor
Karen J. Wester, Administrative Assistant

CONTENTS

COMPARISON OF COMPUTER CODES FOR CALCULATING DYNAMIC

LOADS IN WIND TURBINES

David A. Spera

National Aeronautics and Space Administration
Lewis Research Center
Cleveland, Ohio 44135

INTRODUCTION

The development of computer codes for calculating dynamic loads in horizontal-axis wind turbines has been part of the Federal Wind Energy Program for almost four years.

During this period of time the Energy Research and Development Administration (ERDA) has sponsored the development of at least seven codes by NASA and its contractors. As might be expected in an area of new technology, these codes differ considerably in approach and technique. Because of the generally complicated nature of any structural dynamics analysis, a detailed comparison of seven computer codes is extremely difficult. Therefore, the objectives of this study have been limited to the following: (1) To present a brief overview of each code and identify sources for further detailed information, and (2) to compare the performance of each code against two sets of test data measured on the 100 kW Mod-0 wind turbine, an experimental machine in operation at NASA's Plum Brook Station near Sandusky, Ohio. Comparison on the basis of cyclic loads, peak loads, and harmonic contents was selected. The results of this study are given in detail in Reference 1.

DESCRIPTION OF CODES

The seven computer codes compared in this study are listed in Table 1. All codes are aeroelastic (i.e., air loads and blade deformations are coupled) and include loads which are gravitational, inertial, and aerodynamic in origin. Three of the codes (MOSTAB-WT, -WTE, and -HFW) analyze only rotor loads, while the remaining four codes (REXOR-WT, GETSS, F-762, and MOSTAS) are complete system codes which include rotor-tower interaction.

MOD-0 DATA CASES

For purposes of establishing reference test data, two sets of blade load data have been defined, which were measured on the Mod-0 wind turbine (Ref. 1). These data sets have been designated as Mod-0 Data Cases I and IV. The data sets contain time histories and harmonic analyses of bending moment loads measured in the Mod-0 blades by means of strain-gage load cells. Moment loads in the flatwise and edgewise directions at Station 40 (shank area, 5% span) and Station 370 (midblade area, 49% span) were measured. Additional data are also available for these two cases, including shaft bending and torque loads, nacelle accelerations, and tower deflections. However, for purposes of

comparing computer codes, blade moment loads were judged to be critical, so other measured data were not used in this study.

Operating Conditions

Data Case I, with single yaw drive and stairs in the tower, presents a high level of rotor-tower interaction. These data were measured on December 18, 1975. On the other hand, Data Case IV with the yaw drive locked (relatively rigid nacelle-to-tower connection) were measured on September 11, 1976, after the tower stairs were removed and therefore exhibit little rotor-tower interaction. Thus, these two cases represent relatively high and low levels of blade loading sustained by the Mod-0 wind turbine operating at nominal wind speeds between 25 and 28 mph.

Typical Time-History Curves

A typical cycle of flatwise bending load during one rotor revolution is shown in Figure 1. A positive flatwise moment bends the blade toward the tower causing tensile stresses on the low-pressure (downwind) surface. In Figure 1, flatwise moment M_y is plotted versus the blade azimuth ψ_b, which is zero and 360^0 when the blade points downward. As shown in the figure, the flatwise time history for a rotor located downwind of the tower is dominated by the impulse applied to the blade each time it passes through the tower's wake or "shadow." For purposes of stress and fatigue analysis it is convenient to define cyclic load δM and steady load $\overline{M}$, as shown in Figure 1.

Figure 2 illustrates a typical time history of edgewise load, M_z, measured during one revolution. A positive edgewise load on the blade tends to stop the rotor, causing tensile stresses on the blade's leading edge. An edgewise moment time history is usually composed of three components, as shown in Figure 2: (1) A relatively steady bending moment which produces shaft torque and power, (2) a sinusoidal moment caused by the blade's own weight plus a small wind shear effect (90^0 out of phase) and (3) high frequency dynamic loads attributable to motions of the nacelle and tower.

RESULTS AND DISCUSSION

Cyclic Moment Load Comparisons

Figures 3(a) and (b) illustrate how cyclic moments calculated using the seven codes compare not only with the specific data cases defined but also with the trend of data measured over a period of time on the Mod-0 wind turbine. This trend is represented by a nominal variation of load with wind speed plus a band of variation which is estimated to be ± 1σ in width, thereby containing loads for about 70% of the machine's revolutions. This band is approximately equal to ± 20% of the nominal loads with the exception of Case IV edgewise loads. Variations are caused by changes in wind direction and velocity, control changes, and unsteady factors not yet identified.

The empirical constants used in the MOSTAB-WTE code were selected to place its results at the top of the variation band, as shown in Figures 3(a) and (b).

Data Cases I and IV do not necessarily represent the nominal loads. Other general observations concerning the results shown in Figures 3 are as follows:

1. Loads calculated by all codes fall within the data variation band, with the exception of edgewise loads for Case I which were calculated using the MOSTAB-WT and MOSTAB-HFW codes. MOSTAB codes are able to predict only the gravity component of cyclic edgewise load because shaft motion is absent in these codes.

2. REXOR-WT results generally coincide with nominal loads.

3. Results for the remaining codes tend to be mixed, falling both above and below nominal load values.

Table 2 presents data for a more complete comparison of measured and calculated cyclic loads.

Peak Moment Load Comparisons

A second comparison of calculated and measured moment loads will be made on the basis of their peak values, defined as the maximum absolute value occurring during one revolution. Measured and calculated peak moment loads are listed in Table 3. Inspection of the normalized results shows a wide range of values, from 0.57 to 1.30. With the exception of the empirical code MOSTAB-WTE, all the codes exhibit load ratios both larger and smaller than unity, without any significant trends being apparent.

Summary of Load Ratios

All the load ratios listed in Tables 2 and 3 for cyclic and peak loads, respectively, were averaged and appear in Table 4. These average ratios signify the general level of loading calculated using the various codes in comparison with a blend of high and low nominal loads. MOSTAB-WTE, with its empirical constants selected to place calculated loads well above nominal, was found to have an average load ratio of 1.15, slightly lower than expected. Of the remaining codes, all produced average load ratios within 97% ± 3% of nominal. Load ratios obtained with the REXOR-WT code showed significantly less deviation than ratios for all the other codes.

Load Predictions

The MOSTAB-WTE and REXOR-WT were used to predict the effect on blade loads of a new dual yaw drive system for the Mod-0 wind turbine (Ref. 2). The results are shown in Figures 4(a) and (b). The MOSTAB-WTE code provided an estimate of nominal + 1σ cyclic flatwise moment (Fig. 4(a)) in good agreement with data obtained later. Prediction of edgewise loading using MOSTAB-WTE (Fig. 4(b)) appears to be somewhat conservative, at least in comparison with load bank data. Additional synchronized operation data are required before the level of conservation can be judged.

SUMMARY OF RESULTS

1. Six of the seven codes studied (MOSTAB-WT and -HFW, MOSTAS, REXOR-WT, GETSS, and F-762) calculated loads which on the average were within 4% of nominal loads measured on the Mod-0 wind turbine.

2. Loads calculated using an empirical code (MOSTAB-WTE) were 18% above nominal levels, in accordance with the objective of this code to provide load margin.

3. Among the four system codes evaluated (MOSTAS, REXOR-WT, GETSS, and F-762), the REXOR-WT code appeared to be the most consistent in producing calculated loads close to nominal loads.

4. All codes except MOSTAB-WT and -HFW satisfactorily calculated the general pattern of both flatwise and edgewise loads for the two cases studied. These two codes contain the assumption of rigid rotor support which eliminates some edgewise load harmonics.

5. The empirical code MOSTAB-WTE was verified on the basis of comparisons with the results of the system codes and test data obtained from the Mod-0 wind turbine with dual yaw drive.

CONCLUSIONS

1. WTG load prediction codes are in an advanced state of development.

2. Present system codes tend to predict nominal loads, so load margins must be explicitly introduced into input or output data.

3. System codes have been validated for "stiff" WTG systems, but are not yet validated for "flexible" systems.

REFERENCES

1. Spera, D. A.: Comparison of Computer Codes for Calculating Dynamic Loads in Wind Turbines. NASA TM (to be published).

2. Spera, D. A.; Janetzke, D. C.; and Richards, T. R.: Dynamic Blade Loading in the ERDA-NASA 100 kW and 200 kW Wind Turbines. NASA TM-73711, 1977.

DISCUSSION

Q. How broadly applicable are the empirical corrections in MOSTAB-WTE?

A. The empirical equations apply to two-bladed hingeless rotors. However, the two empirical constants have been evaluated only for stiff or semi-stiff towers, to date.

Q. What accuracy is associated with the experimental bending moment data?

A. About 5% accuracy for cyclic bending moments. However, zero errors can be significant (see Ref. 1, Table 7).

Q. Has the yaw brake dramatically improved rotor/tower coupling effects in the Mod-0 WTG?

A. Yes. Blade loads are definitely lower when the yaw brake is on.

Q. What causes the significant variation in blade loads for the same nominal wind speed?

A. Variations in wind direction, control changes, yaw maneuvers, and other factors we don't understand.

Q. What is the frequency distribution of load variations?

A. Both normal and log normal distributions have been observed. More data are definitely needed.

Q. Have these codes been used to calculate stress levels?

A. No. The output of these codes is loads. Auxiliary stress codes are used subsequent to these codes.

Q. Please comment on costs per case and input/output format for the various codes.

A. I don't have specific information for all the codes but the contact persons listed in Table 1 do. For MOSTAB-WT and -WTE, typical input would consist of about 50 cards, running time would be two minutes (IBM 1110 computer) and typical output would be tabular listings of three moments and three shear forces at up to a dozen blade stations at each of 24 azimuthal blade positions. Parametric studies are conveniently and economically performed by non-specialists. My general comments about the remaining codes are that personnel must be well trained, running times of 30 to 60 minutes (or more) are to be expected, and your organization must be ready to provide dedicated support.

Q. During preliminary design, predicting load frequencies may be more important than predicting amplitudes. Do you plan to compare these programs on the basis of predicted frequencies?

A. Yes. The harmonic contents of the predicted loads are compared in Reference 1.

Q. Your experience has shown that softness in the Mod-0 yaw drive induced undesirable cyclic loads. How then can flexibility in future systems reduce costs?

A. Flexibility can lead to lighter, less costly structures only if resonances can be avoided. Unfortunately, softness in the Mod-0 yaw drive placed it at a resonance, leading to the undesired cyclic loads.

5

TABLE 1. - COMPUTER CODES PRESENTLY USED FOR AERO-ELASTIC ANALYSIS OF DYNAMIC
LOADS AND DEFORMATIONS IN HORIZONTAL-AXIS WIND TURBINES

Code	Type (domain)	Source for Information
MOSTAB-WT	Single blade; 1 DOF [a] (time)	Barry Holchin Mechanics Research Incorporated 9841 Airport Boulevard Los Angeles, CA 90045
MOSTAB-WTE	Same, plus empirical constants	David A. Spera NASA-Lewis 49-6 21000 Brookpark Road Cleveland, Ohio 44135
MOSTAB-HFW	Rotor; 4 DOF plus gimballing (time)	John A. Hoffman Paragon Pacific Incorporated 1601 E. El Segundo Boulevard El Segundo, CA 90245
REXOR-WT	System; multi-DOF (time)	Robert E. Donham Dept 75-21, Bldg. 360, Plant B-6 Lockheed-California Company Burbank, CA 91520
GETSS	System; multi-DOF (freq.)	Clyde Stahle General Electric Space Division Box 8661 Philadelphia, PA 19101
F-762	System; multi-DOF, (time)	Richard Bielawa United Technologies Research Center East Hartford, CT 06108
MOSTAS	System; multi-DOF, (time/freq.)	John A. Hoffman Paragon Pacific Incorporated 1601 E. El Segundo Boulevard El Segundo, CA 90245

[a]Degrees of freedom

TABLE 2. - COMPARISON OF RELATIVE CYCLIC MOMENT LOADS,

NORMALIZED WITH RESPECT TO NOMINAL CYCLIC LOADS

Source	Relative cyclic moment loads			
	Flatwise[a]		Edgewise[b]	
	Sta 40	Sta 370	Sta 40	Sta 370

(a) Data Case I

		Sta 40	Sta 370	Sta 40	Sta 370
Test data	Nominal	1.00	1.00	1.00	1.00
	Actual	1.02	0.97	0.87	0.95
MOSTAB rotor codes	-WT	1.00	1.00	0.60	0.50
	-WTE	1.20	1.20	1.20	1.20
	-HFW	1.00	0.99	0.66	0.58
REXOR-WT		0.96	1.00	0.94	0.87
GETSS		1.19	1.16	0.80	1.05
F-762		1.08	1.03	0.78	0.77
MOSTAS		0.92	0.97	0.82	0.78

(b) Data Case IV

		Sta 40	Sta 370	Sta 40	Sta 370
Test data	Nominal	1.00	1.00	1.00	1.00
	Actual	0.83	0.96	1.05	0.93
MOSTAB rotor codes	-WT	1.20	1.20	0.94	0.93
	-WTE	1.20	1.20	1.04	1.07
	-HFW	1.17	1.17	1.00	1.04
REXOR-WT		0.97	0.92	0.98	0.96
GETSS		0.92	0.86	0.98	1.01
F-762		0.87	0.91	1.05	1.11
MOSTAS		1.22	1.23	0.97	1.01

[a] $\delta M_y / \delta M_{y,nom}$

[b] $\delta M_z / \delta M_{z,nom}$

7

TABLE 3. - RELATIVE PEAK MOMENT LOADS, NORMALIZED WITH RESPECT TO NOMINAL PEAK LOADS

Source	Relative peak moment loads			
	Flatwise[a]		Edgewise[b]	
	Sta 40	Sta 370	Sta 40	Sta 370

(a) Data Case I

Test data	Nominal	1.00	1.00	1.00	1.00
	Actual	1.01	0.98	0.89	0.96
MOSTAB rotor codes	-WT	1.01	1.12	0.66	0.57
	-WTE	1.12	1.25	1.13	1.17
	-HFW	1.02	1.13	0.78	0.73
REXOR-WT		0.96	1.05	0.89	0.85
GETSS		0.98	0.96	0.72	1.11
F-762		1.11	1.19	0.84	0.95
MOSTAS		0.88	0.98	0.86	0.94

(b) Data Case IV

Test data	Nominal	1.00	1.00	1.00	1.00
	Actual	0.76	0.97	1.03	0.94
MOSTAB rotor codes	-WT	1.23	1.30	0.94	0.96
	-WTE	1.23	1.30	0.94	0.96
	-HFW	1.22	1.30	1.06	1.13
REXOR-WT		1.02	0.99	0.96	0.93
GETSS		0.76	0.67	0.77	1.17
F-762		0.92	0.92	1.01	1.27
MOSTAS		1.03	1.05	0.99	1.07

[a] $\left|M_y\right|_{max} / \left|M_{y,nom}\right|_{max}$

[b] $\left|M_z\right|_{max} / \left|M_{z,nom}\right|_{max}$

TABLE 4. - SUMMARY OF LOAD RATIOS OBTAINED USING VARIOUS COMPUTER CODES AND MOD-0

WIND TURBINE TEST DATA

Code Type and Name		Goal of Calc. Load	Blade Load Ratio [a]	
			Average	RMS Dev. [b]
Rotor Codes	MOSTAB-WTE	Nom. + 1σ	1.15	± 0.10
	MOSTAB-HFW	Nom.	1.00	± 0.20
	MOSTAB-WT	"	0.95	± 0.24
System Codes	F-762	"	0.99	± 0.14
	MOSTAS	"	0.98	± 0.12
	REXOR-WT	"	0.95	± 0.05
	GETSS	"	0.94	± 0.16

[a] Calculated to nominal measured; based on 16 ratios combining 2 data cases, 2 blade stations, flatwise and edgewise directions, and cyclic and peak bending moments.

[b] Root-mean-square deviation; includes approximately 11 of 16 ratios.

$$\overline{M}_y = \frac{1}{2}(M_{y,max} + M_{y,min})$$

$$\delta M_y = \pm\frac{1}{2}(M_{y,max} - M_{y,min})$$

M_y

160x10³

MAX LOAD, $M_{y,max}$

RESPONSE TO TOWER SHADOW

CYCLIC LOAD, δM_y

STEADY LOAD, $\overline{M}_y$

120

80

FLATWISE SHANK MOMENT, M_y, lb-ft

40

0

MIN LOAD, $M_{y,min}$

-40

0   90   180   270   360

BLADE AZIMUTH, ψ_b, deg
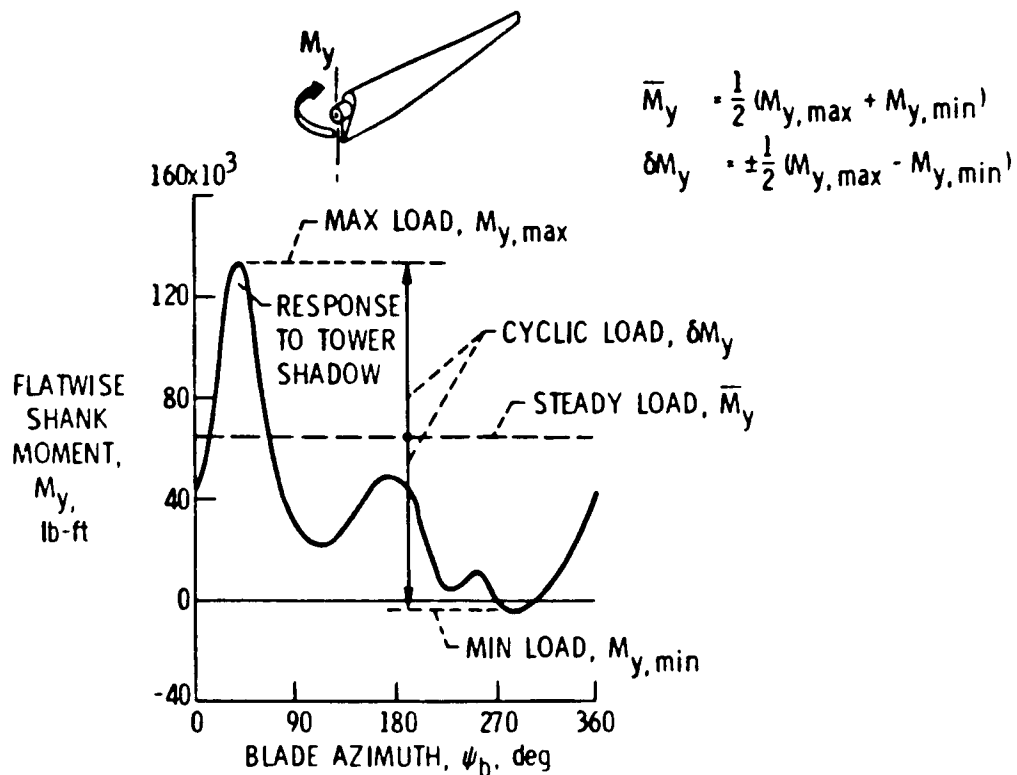
Figure 1. - Typical cycle of blade flatwise moment measured on ERDA-NASA 100-kilowatt Mod-0 wind turbine.

M_z

80x10³

RESPONSE TO NACELLE MOTION

GRAVITY, WIND SHEAR LOADS

STEADY LOAD PRODUCING POWER

40

EDGEWISE SHANK MOMENT, M_z lb-ft

0

-40

-80

0   90   180   270   360

BLADE AZIMUTH, ψ_b, deg
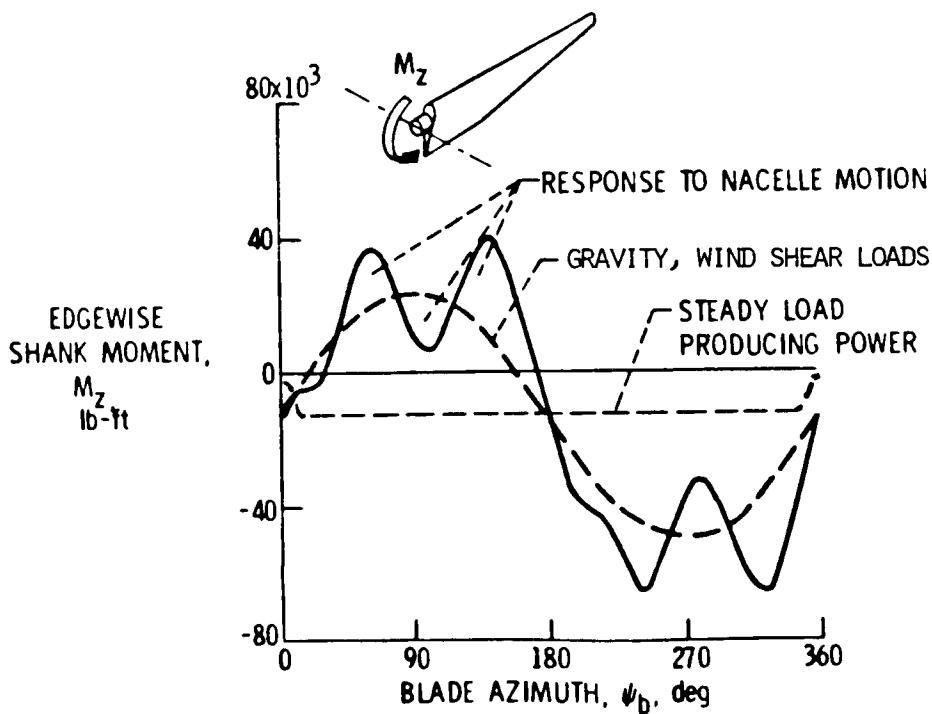
Figure 2. - Typical cycle of blade edgewise moment measured on Mod-0 wind turbine.

10
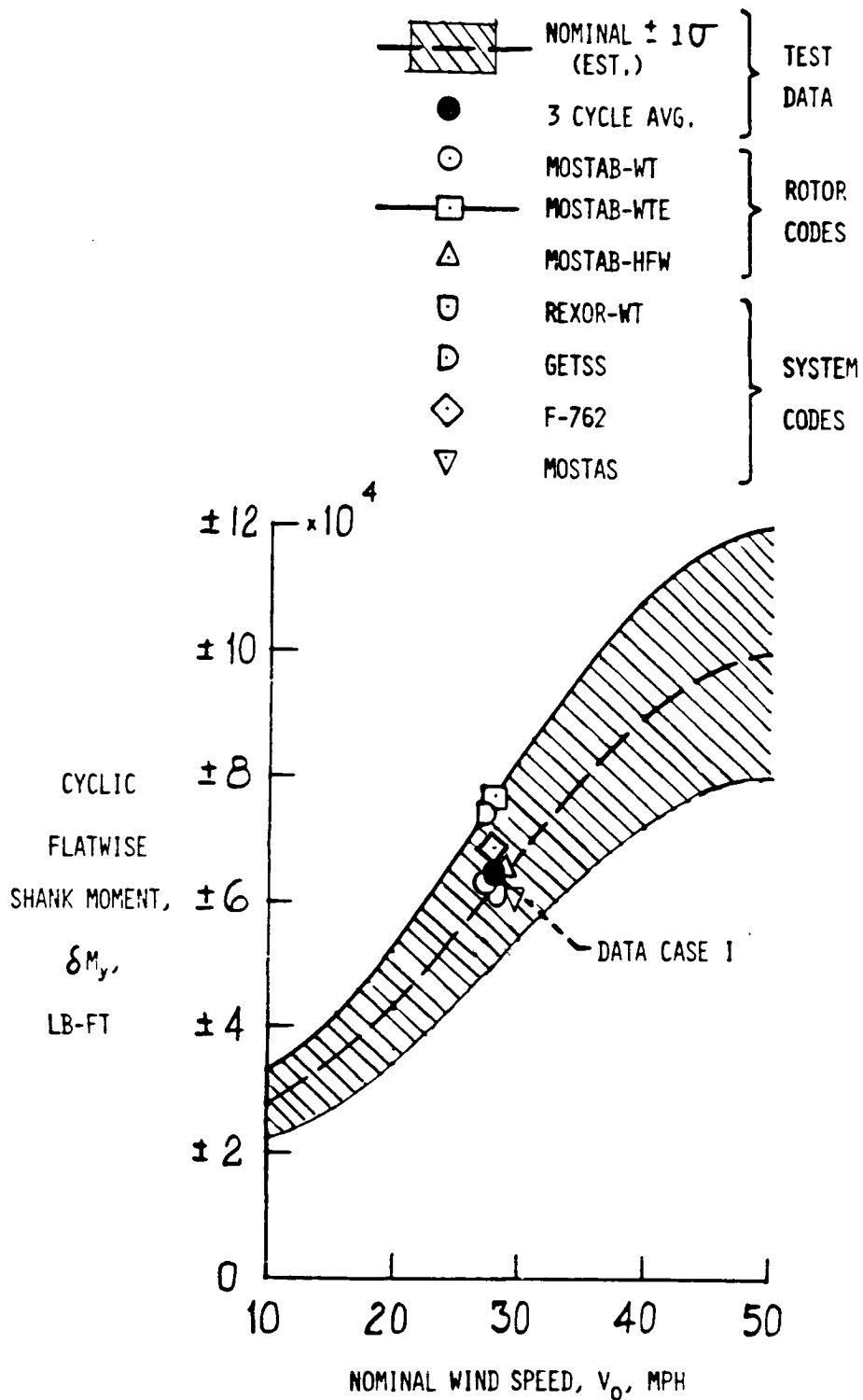
Figure 3. - Comparison of measured and calculated blade moment loads for Mod-0 wind turbine at various wind speeds with stairs and single yaw drive. Station 40; 5-percent span.
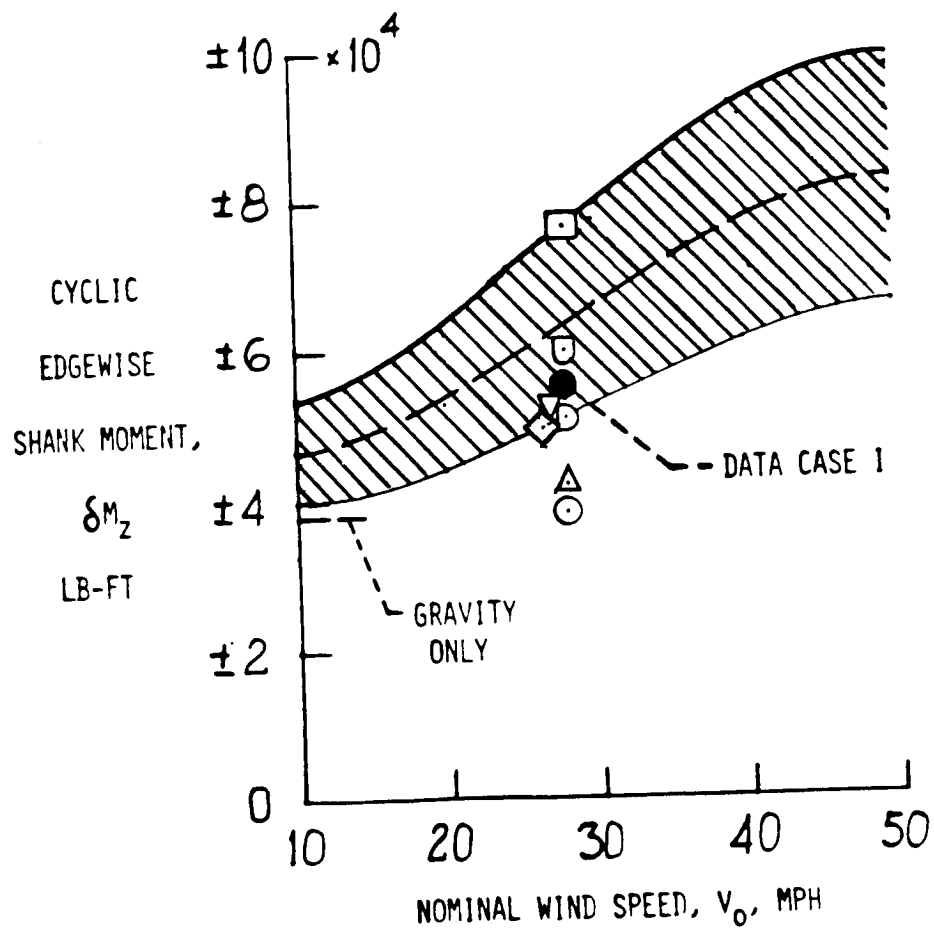
(b) Edgewise moment load.

Figure 3. - Concluded.

(a) Flatwise moment load.

(b) Edgewise moment load.

Figure 4. - Comparison of measured and calculated cyclic blade moment loads for Mod-0 wind turbine at various wind speeds with stairs removed and dual yaw drive installed. Station 40; 5-percent span.

13

MOD-1 WTG DYNAMIC ANALYSIS

Clyde V. Stahle, Jr.

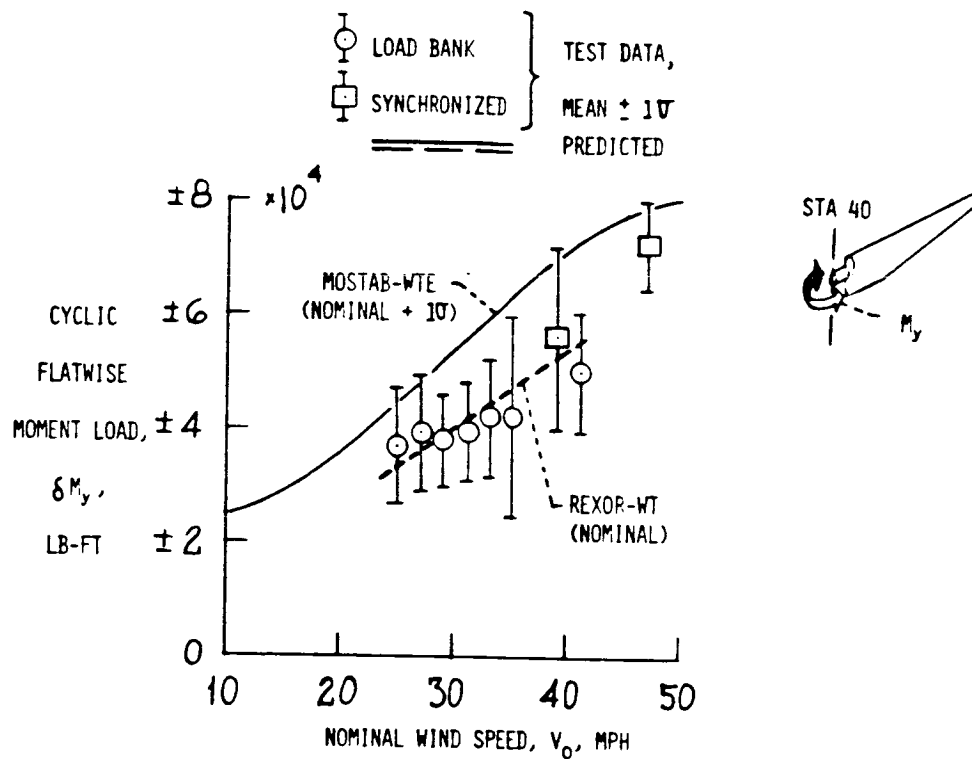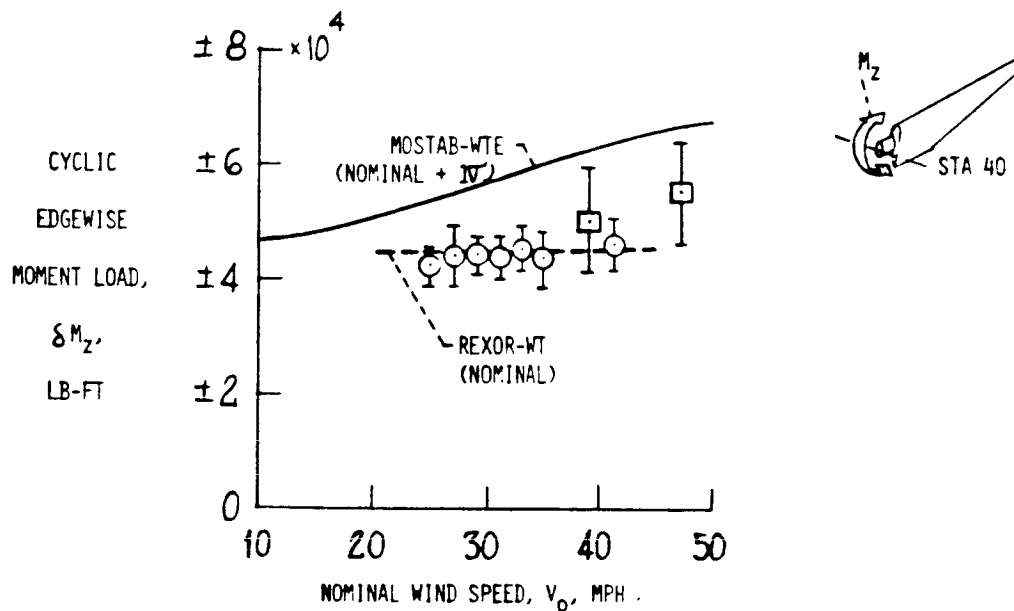General Electric Company
Valley Forge, Pennsylvania

ABSTRACT

This paper discusses the dynamic analysis of the MOD-1 2000 KW horizontal-axis wind turbine. After briefly describing the MOD-1 design, the dynamic analysis used to evaluate the dynamic loads and structual interactions is discussed. The resonant frequency placement, the treatment of unsteady wind loading and the dynamic load sensitivity to frequency shifts are reviewed for the design.

MOD-1 DESCRIPTION

As shown in Figure 1, the MOD-1 WTG incorporates a two-bladed, downwind rotor driving an AC generator through a speed increaser atop a steel, truss-type tower. The major characteristics of the MOD-1 WTG are summarized in Figure 2; its major elements are briefly described as follows:

a. Rotor: Two variable-pitch, steel blades are attached to the hub barrel via three-row roller bearings which permit about 105 deg. pitch excursion from full feather to max. power. Blade pitch is controlled by hydraulic actuators which provide a maximum pitch rate of 14 deg/sec.

The hub tailshaft provides the connection to the low-speed shaft and to the dual-tapered-roller main bearing, which supports the rotor and one end of the low-speed shaft.

b. Drive Train: Comprising the drive train are the low-speed shaft and couplings, the gearbox, and the high-speed shaft/slip-clutch which drives the generator. (Refer to Figure 3.) The slip-clutch precludes excessive torques from developing in the entire drive train due to extreme wind gusts and/or faulty synchronization.

c. Power Generation/Control: A General Electric synchronous AC generator is driven at 1800 RPM through the high-speed shaft. A shaft-mounted, brushless exciter controlled by a solid-state regulator and power stabilizer inputs provides voltage control.

15

d. Nacelle Structure: The core of the nacelle structure is the welded steel bedplate. All nacelle equipments and the rotor are supported by the bedplate, which provides the load path from the rotor to the yaw structure. Other equipments supported by the bedplate are the pitch control and yaw drive hydraulic packages, walkways, oil coolers, heaters, hydraulic plumbing, electronics boxes, cabling and the fairing. Redundant instrumentation booms, with wind speed, temperature and direction sensors are mounted on the upwind end of the fairing.

e. Yaw Drive: Unlimited yaw rotation is provided by the yaw drive system, comprising the upper and lower yaw structures, the two-motor hydraulic drive, the hydraulic yaw brake, and the large cross-roller yaw bearing. The yaw drive is capable of yawing the rotor/nacelle at 0.25 deg/sec. To provide adequate yaw drive stiffness, the yaw brake is fully activiated when not in a yaw maneuver and partially activated during the maneuver to avoid backlash in the yaw drive gear train.

f. Tower: The truss tower, as shown in Figure 4, is made up of seven vertical bays, including the base and top (pintle) sections. Tubular steel columns are used at the four corners to carry the main loads. Back-to-back channels serve as cross-members where loads permit. However, in most bays, tube-section cross-members are still required because of high loads and to reduce "tower shadow." Access to the yaw drive and nacelle area is provided via a cable-guided, gondola-type elevator.

g. WTG Weight: The final system weight (rotor, nacelle and tower) is expected to be about 650,000 lbs. This weight breaks down as shown in Figure 5.

GETSS COMPUTER CODE

The GETSS (GE Turbine System Synthesis) code was used to evaluate the dynamic loads of the complex MOD-1 WTG. Key objectives considered in the development of the code were: (1) to evaluate resonant frequency placements so that dynamic loads would be minimized, (2) to accurately determine the loads throughout the system so that adequate but not excessive design margins are provided, and (3) to determine the sensitivity to stiffness variations so that critical parameters can be careflly controlled. By minimizing dynamic interactions, dynamic loading can be alleviated assuring a long life design.

The analytical approach used in GETSS is to modal synthesize the system at various rotor positions and to analyze the system in a piecewise linear manner. The WTG system is analyzed as six major substructures, Figure 6, using NASTRAN

finite element models except for the blades which use a turbine blade code. These models serve the dual purpose of stress and dynamic analysis. The system is then synthesized from the substructure modes using a stiffness coupling synthesis code that includes the dynamic transformation. The stiffness matrices coupling the substructures together represent the bearing stiffnesses. The system is then analyzed at 45 degree rotor increments and the modal coordinates switched from model to model as the rotor turns. Using this approach the modal characteristics can readily be traced to the substructures and the modes contributing to the loads identified. The loads at various blade stations, the hub, the main rotor bearing, the yaw bearing and the tower base are determined for subsequent structural analysis. Accelerations and deflections at selected critical locations are also evaluated.

The code uses quasi-steady aerodynamics to evaluate the loads due to wind shear, tower shadow and gusts. The flow field includes a wind shear following the power law, Figure 7, and a three dimensional tower shadow that follows the tower geometry. The three dimensional tower shadow representation permits the sequential entering and exiting of the various blade stations into the retarded flow region.

GETSS CODE VERIFICATION

Prior to analyzing the MOD-1, the GETSS computer code was verified by analyzing the MOD-0 WTG for two operating conditions and comparing the analysis results with actual measurements, Reference 1. The comparisons included flatwise and chordwise bending moments at two blade stations, main shaft bending moments and torque, and tower accelerations and deflections. The comparison included waveform, harmonic content, peak and cyclic amplitudes. NASTRAN models of the tower and bedplate, similar to those used for MOD-1, were developed including the stairway and elevator rails, Figures 8 and 9. Excellent agreement of the predicted modes and resonant frequencies with modal test results verified the adequacy of the modeling of most of the structure. A typical comparison of the flatwise bending moment at the blade root is shown in Figure 10. More than 90 percent of the loads, accelerations and deflections were within 20 percent of the range of measured values. In general, the tower deflections and accelerations tended to be conservative. The waveform and harmonic content were reproduced and, in one condition, captured a 10P tower response caused by a tower stairway coupled mode. The tower shadow for each condition was based on NASA-LeRC wind tunnel duplicating the wind and rotor orientation relative to the tower. The good correlation of the analytical predictions with MOD-0 measurements permitted the use of minimum design margins for MOD-1.

17

MOD-1 RESONANT FREQUENCY PLACEMENT

The analysis of the MOD-1 used the same procedures described above. The NASTRAN tower and bedplate models are shown in Figures 11 and 12. The resulting resonant frequencies are shown in Figure 13. The lowest resonance results primarily from the effective stiffness of the electrical generation system. Blade flatwise bending is placed at approximately 2.6P and is below the tower lateral bending modes at approximately 3.0P. The first edgewise bending mode of the blade occurs at approximately 4.5P while tower torsion is above 8P. Blade torsion is at approximately 14.7P.

The sensitivity of the dynamic loads to variations in selected system parameters was investigated, Figure 14. Large variations in the soil stiffness, yaw bearing stiffness and shaft bearing stiffness were not found to significantly affect the loads. The position of the bedplate C.G. did not have a significant influence on the dynamic loads but, because of the weight, does have a significant effect on the tower loading. Variations on the order of 50 percent in the main rotor bearing and the blade retention bearing stiffness were, however, found to significantly influence the dyanmic loads. Critical to the dynamic loading are the yaw drive stiffness and twoer to blade frequency placements which can result in large load amplifications.

DESIGN LOAD DEFINITION

Design loads are determined considering the peak and cyclic loading that occurs for all operational environments throughout the life of the machine, Figure 15. Of major significance is the variation in the loads at a "constant" wind speed. Using a wind turbulance model and the WTG dynamic model, the dispersed loads are evaluated considering gust effects. Peak and cyclic load distributions are determined for nominal operating conditions by calculating the loads due to turbulence using a discrete gust analysis. MOD-0 load measurements were used to evaluate the adequacy of the load dispersions and correlate closely for flap bending moments on the blades. Significant load reductions are achieved by limiting the maximum operating wind velocity to a nominal 35 mph and an instantaneous value of 50 mph. Both positive and negative gusts are considered.

Additional design conditions include hurricane force winds and overspeed conditions due to desynchronism of the generator. Torsional loading of the system is dependent on pitch control system characteristics and is discussed in Reference 2.

CONCLUSIONS

Dynamic analysis of large horizontal-axis WTG systems involves complex structural interactions which can significantly affect dynamic loading and the resulting

18

design requirements. For the MOD-1 WTG design a comprehensive analytical treatment of the loads throughout the operating regime was used to assure adequate but realistic design margins and to enable interactions and sensitivities to be examined. Because of the early state of development of WTG technology, MOD-0 load measurements were essential to the evaluation of the analytical code and provide needed guidance to the determination of MOD-1 design loads and conditions.

REFERENCES

1. Spera, D. A., "Comparison of Computer Code for Calculating Dynamic Loads in Wind Turbines", Proceeding of the 1977 Wind Turbine Structural Dynamics Workshop, November 15-17, 1977, Cleveland, Ohio.

2. Barton, R., "MOD-1 WTG Analysis", Proceedings of the 1977 Wind Turbine Structural Dynamics Workshop, November 15-17, 1977, Cleveland, Ohio.

DISCUSSION

Q. Did you connect the analyses for the four rotor positions?

A. The analysis is performed using piecewise linear models for four rotor positions using a total of eight models during each revolution. Continuity of deflection and velocity is maintained at the model switching points.

Q. Did you compare results with more than four rotor positions?

A. Because of the good comparison with experimental results using the four rotor position models, a finer analysis using additional rotor positions was not performed.

Q. Why did you calculate frequencies at different blade azimuths and what significance does it have?

A. The analysis was performed using a piecewise linear modal analysis combining the solutions for a series of blade positions, i.e., the modes at eight rotor positions per revolution were combined to obtain the loads during a revolution. Because the system dynamic characteristics change with rotor azimuth, a system modal analysis is required for each range of rotor azimuth angles. By using this type of analysis, the dynamic loads are readily traced to the modal characteristics of the system and corrective action to reduce dynamic load magnification can be determined.

Q. How are the maximum loads determined?

A. The maximum loads are determined by evaluating the steady state loads at prescribed wind conditions during a complete revolution of the rotor. A continuous load time history for all rotor positions is determined. This

is then used with solutions for other wind conditions to determine the dispersed cyclic loads and the peak loads.

Q. Please elaborate on your turbulence model and its effect on loads.

A. The turbulence model was used to determine an equivalent gust velocity to use in calculating loads. The bandwidth considered spherical eddies having a size equivalent to one third the rotor radius or larger with pitch change to maintain constant torque. Analysis of partial rotor immersion with gusts of one third the rotor radius showed a negligible change in loading. The final loads analysis considered complete rotor immersion by a gust obtained by integrating the turbulence spectrum.

Q. What factors were used to set the cut out velocity of the MOD-1 at 35 mph (30 foot reference height)?

A. The cut out velocity was established from analysis of the peak and cyclic load variations with wind velocity and its effect on cost. Fatigue was a governing consideration. As the cut-out wind velocity increases the loads increase dramatically. The cut-out velocity of 35 mph was selected on the basis of cost and energy capture trade-offs which indicated a high cost for designing to higher wind velocities with little gain in yearly energy capture.

Q. Since you assessed frequencies and loads parametrically, did you take the opportunity to look at the effect of teetering or articulating the rotor?

A. Early in the design cycle, a preliminary evaluation of the effects of teetering the rotor was performed using the F762 code. The results did not indicate major reductions in blade loads in the most critical regions of the rotor, i.e., at the 50 percent span. The reduction in the loads on the bedplate and towers were not evaluated in depth in that the F762 code is primarily for rotor analysis and dis not determine loads throughout the system.

Q. How much time does a typical load analysis of the MOD-1 WTG require?

A. As the design evolves, changes are mde to the dynamic characteristics of all portions of the system. This includes the blades, bedplate, drive train, yaw drive and tower. Dynamic models of all these components are continually revised during the design process. Having established the dynamic characteristics of the various structural components, a set of ten design loads at critical interfaces throughout the system can be determined in approximately two weeks.
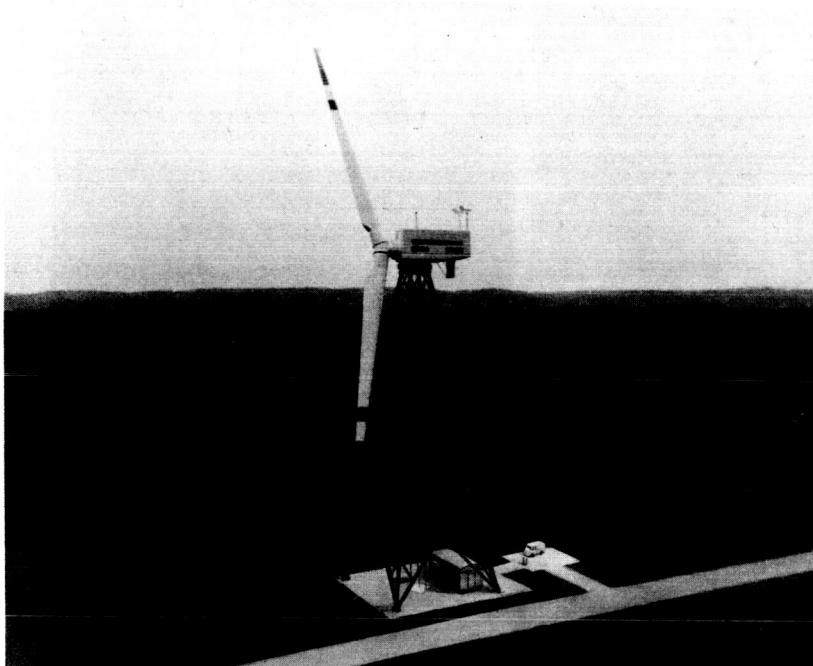
Figure 1. - MOD-1 wind turbine generator.

RATED POWER (SYSTEM)	2000 kW(e)
RATED WIND SPEED	25 MPH ⎞
CUT-IN WIND SPEED	11 MPH ⎬ AT 30 FT. ABOVE GROUND
CUT-OUT WIND SPEED	35 MPH ⎠
SURVIVAL WIND SPEED	150 MPH (AT ROTOR $\mathcal{C}_L$)
CONE ANGLE	12°
INCLINATION OF AXIS	0°
ROTOR SPEED	35 RPM
BLADE DIA.	$\sim$ 200 FT
BLADE TWIST	11°
AIRFOIL	NACA 230XX
BLADE-GROUND CLEARANCE	$\sim$ 40 FT.
LIFE	30 YEARS WITH MAINTENANCE
ENVIRONMENT	-31°F TO $+120^\circ$F

Figure 2. - Major characteristics of MOD-1 wind turbine generator.

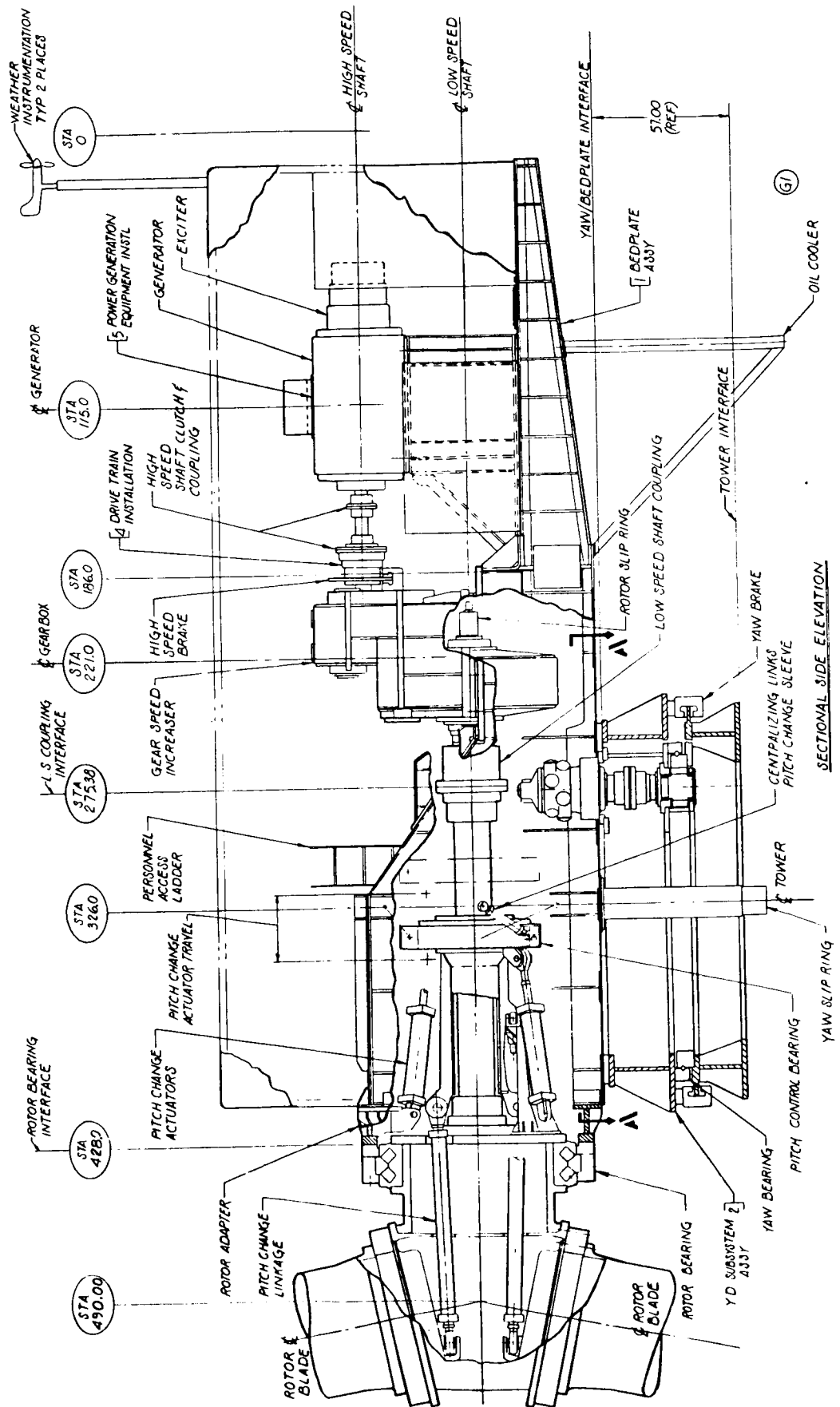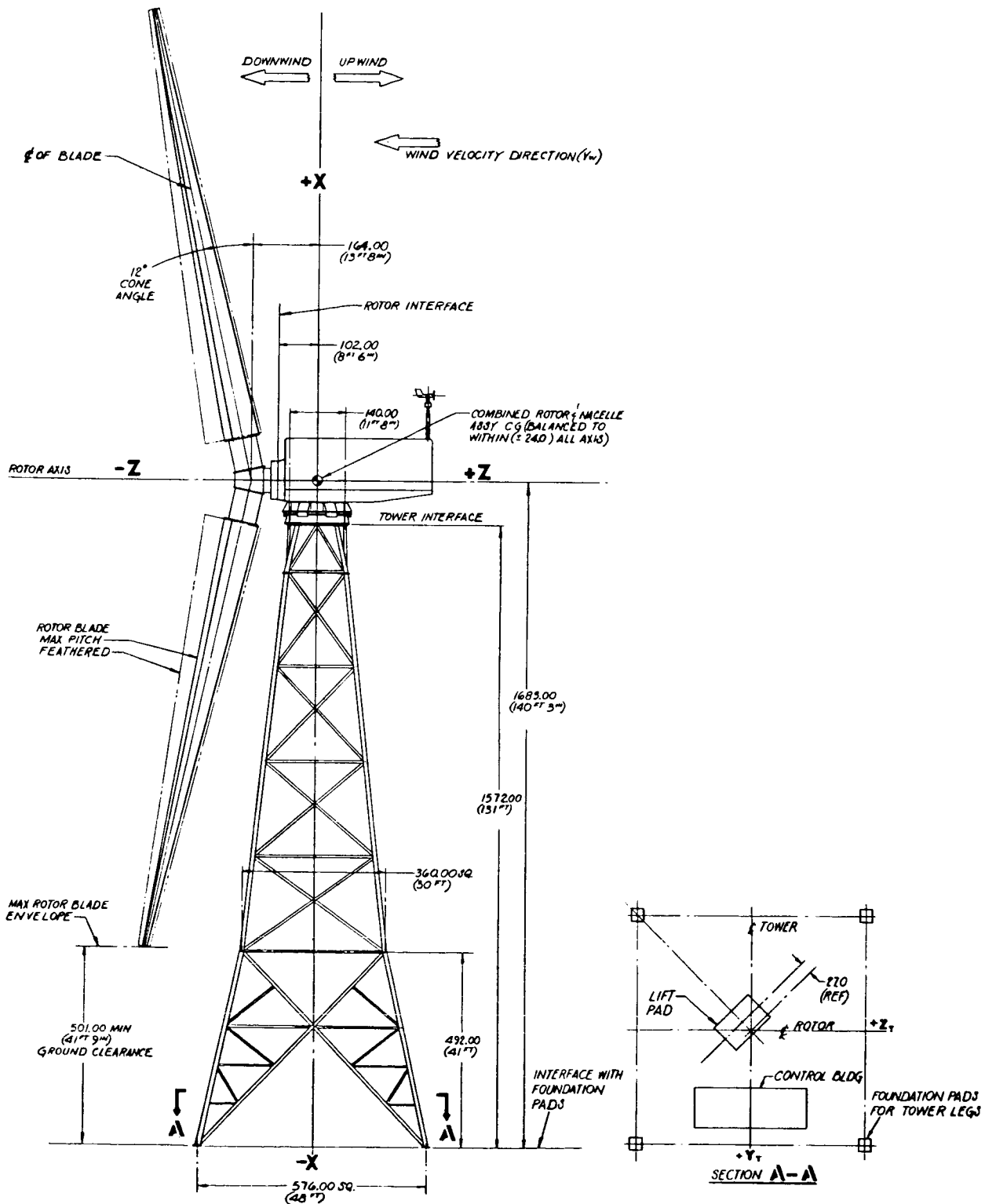Figure 3. - Nacelle installations.

22

Figure 4. – Schematic drawing of MOD-1 wind turbine generator.

23

ROTOR ASS'Y.		103,000 LBS.
HUB	15,000 LBS.	
BLADES	36,000 LBS.	
BEARINGS/STRUCTURE	29,000 LBS.	
PITCH CONTROL MECH.	11,000 LBS.	
PITCH CONTROL HYDR.	12,000 LBS.	
NACELLE ASS'Y.		171,000 LBS.
BEDPLATE	68,000 LBS.	
FAIRING	5,000 LBS.	
GENERATOR/EXCITER	14,000 LBS.	
POWER GEN. EQUIP.	1,000 LBS.	
SHAFTS/COUPLINGS/CLUTCH	18,000 LBS.	
GEARBOX	58,000 LBS.	
LUBE/HYD. SYSTEMS	4,000 LBS.	
DATA ACQUISITION	1,000 LBS.	
CABLES/LIGHTS/ETC.	2,000 LBS.	
YAW ASS'Y		56,000 LBS.
BEARING SUPPORTS	47,000 LBS.	
YAW BRAKE	1,000 LBS.	
YAW DRIVE	8,000 LBS.	
TOWER ASS'Y		320,000 LBS.
STRUCTURE	313,000 LBS.	
ELEVATOR/MISC.	1,000 LBS.	
CABLING/CONDUIT	6,000 LBS.	
TOTAL (EXCL. GROUND EQUIP.)		650,000 LBS.

Figure 5. - Weight breakdown for MOD-1 wind turbine generator.
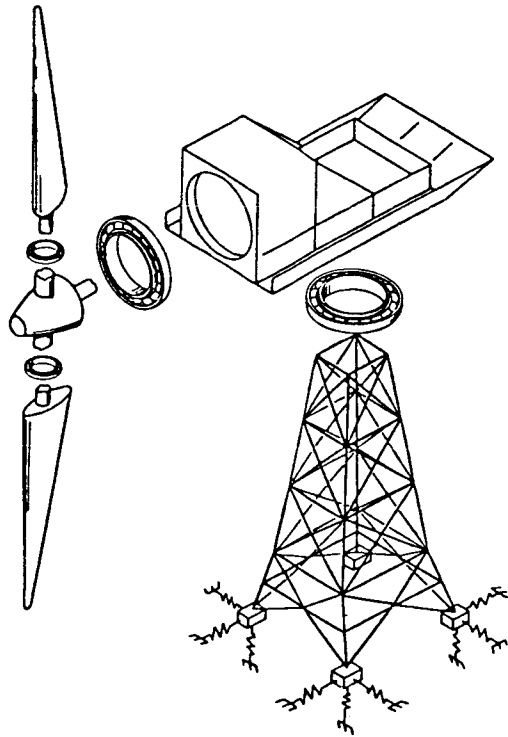
Figure 6. - Wind turbine generator
synthesized from substructures.

WIND SHEAR

$$V_0 = V_R \left(\frac{H}{H_R} \right)^{.167}$$

V_R = REFERENCE VELOCITY

H_R = REFERENCE HEIGHT

TOWER SHADOW

ω_t = TOWER WIDTH
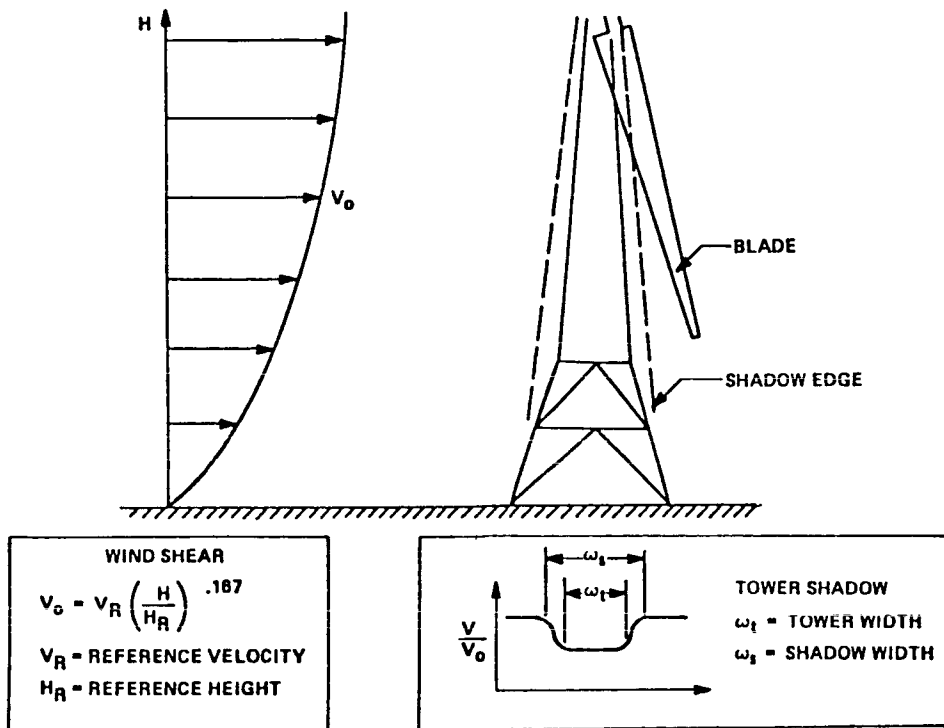
ω_s = SHADOW WIDTH

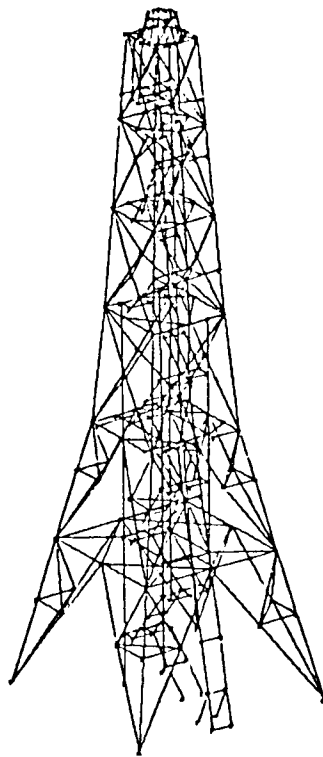Figure 7. - Wind shear and tower shadow representation.

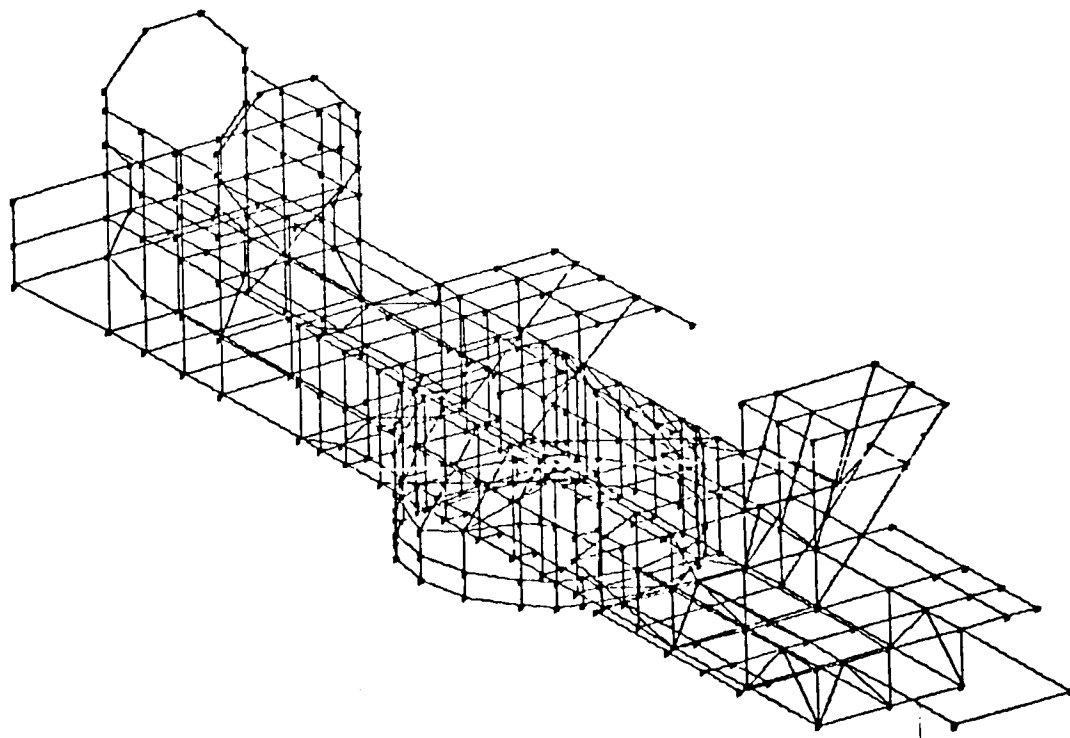25

Figure 8. - NASTRAN model of MOD-0 tower.

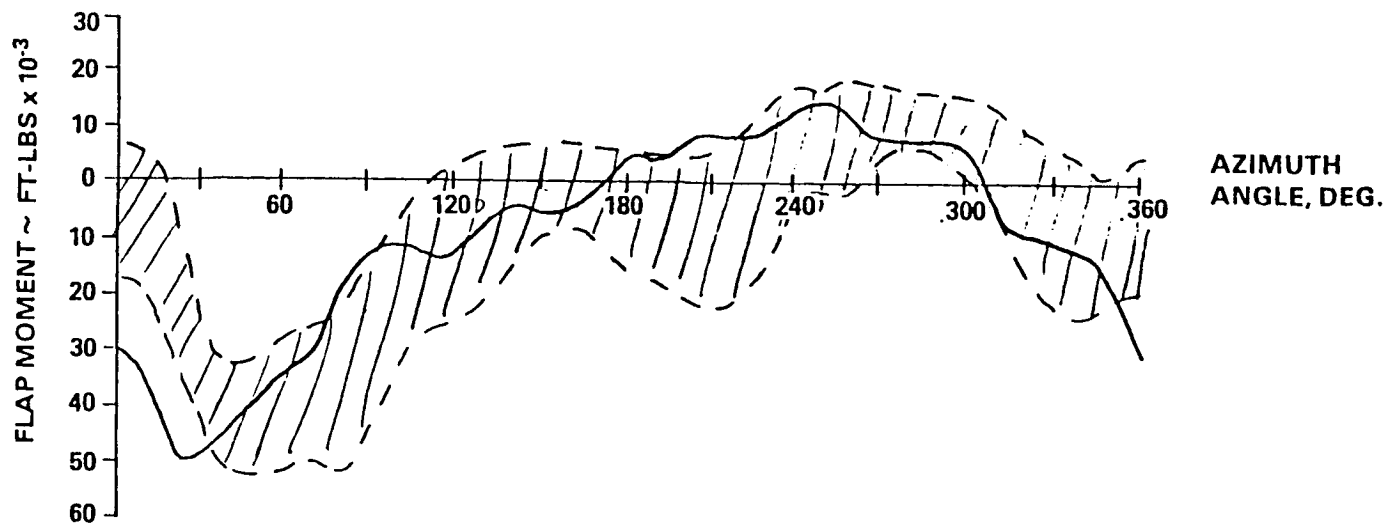Figure 9. - NASTRAN model of MOD-0 bedplate.

Figure 10. - Case 4 blade load comparison, flap moment at station 40.
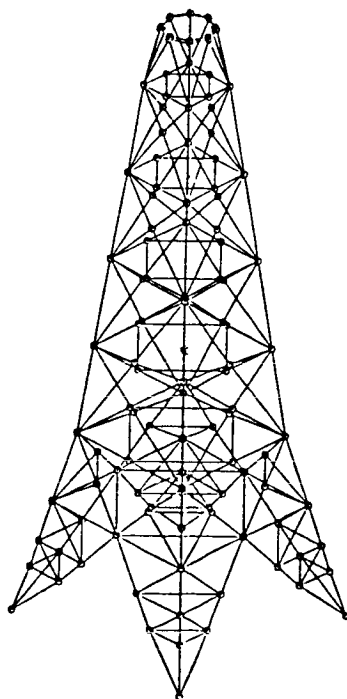
Figure 11. - Finite element
model of MOD-0 tower.
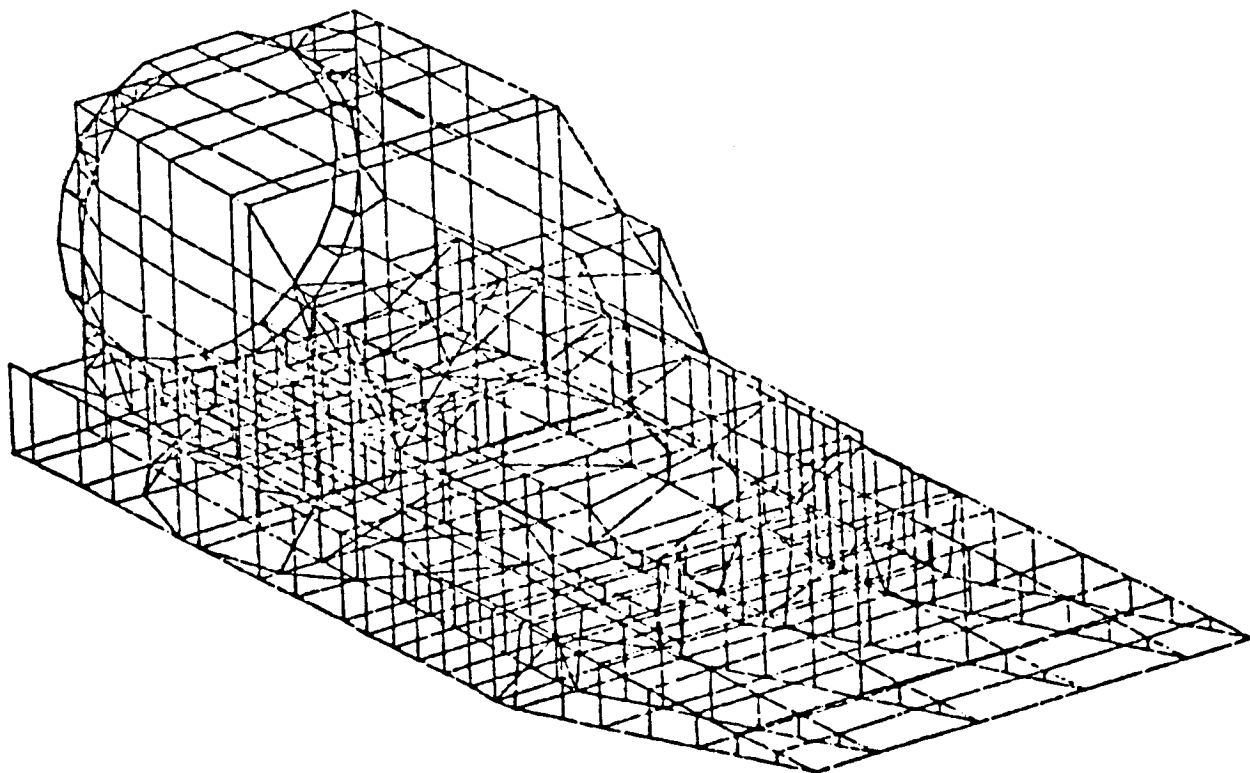
Figure 12. - Finite element model of MOD-O bedplate.

MODE NO.	DESCRIPTION	FREQ (Hz)	FREQ (1/REV)
1	ROTOR ROTATION	0.39	0.67
2	1ST ROTOR FLATWISE-CYCLIC	1.42	2.44
3	1ST ROTOR FLATWISE-COLLECTIVE	1.52	2.60
4	TOWER BENDING-Y AXIS	1.81	3.10
5	TOWER BENDING-Z AXIS	1.91	3.28
6	1ST ROTOR EDGEWISE-CYCLIC	2.43	4.16
7	2ND ROTOR FLATWISE-CYCLIC	3.28	5.63
8	2ND ROTOR FLATWISE-COLLECTIVE	3.64	6.25
9	SHAFT TORSION	4.00	6.86
10	TOWER TORSION	4.18	7.16
11	3RD ROTOR FLATWISE-CYCLIC	6.41	10.99
12	3RD ROTOR FLATWISE-COLLECTIVE	6.62	11.35
13	BLADE TORSION-ANTISYMMETRIC	6.76	11.60
14	BLADE TORSION-SYMMETRIC	6.78	11.63
15	2ND ROTOR EDGEWISE COLLECTIVE	7.54	12.92
16	TOWER 2ND BENDING ~ Z AXIS	8.37	14.35
17	TOWER 2ND BENDING ~ Y AXIS	8.70	14.91
18	2ND ROTOR EDGEWISE - CYCLIC	9.10	15.59

Figure 13. - Summary of resonant frequency (blade vertical position).

- SOIL STIFFNESS - NOT SIGNIFICANT

- YAW DRIVE TORSIONAL STIFFNESS - $\boxed{\text{CRITICAL}}$

- TOWER/BLADE TUNING - $\boxed{\text{CRITICAL}}$

- BLADE RETENTION BEARING STIFFNESS - SIGNIFICANT

- MAIN ROTOR BEARING - SIGNIFICANT

- YAW BEARING STIFFNESS - NOT SIGNIFICANT

- SHAFT BEARINGS - NOT SIGNIFICANT

- BEDPLATE C. G. - STATICALLY SIGNIFICANT

MOD-1 CRITICAL TUNING

PARAMETERS IDENTIFIED
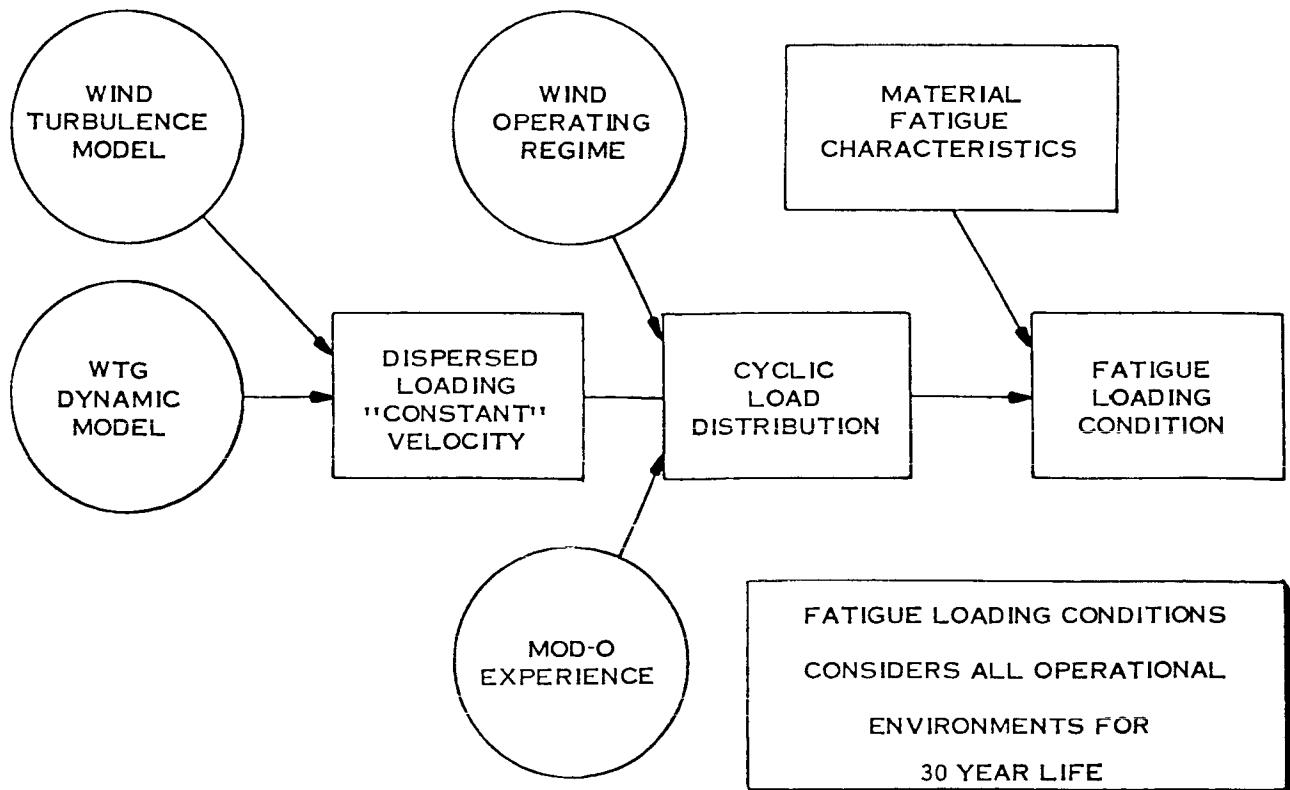
Figure 14. - Summary of parametric variations.

Figure 15. - Determination of design loads.

SIMPLIFIED MODELING FOR WIND TURBINE

MODAL ANALYSIS USING NASTRAN

Timothy L. Sullivan

National Aeronautics and Space Administration
Lewis Research Center
Cleveland, Ohio 44135

ABSTRACT

A simplified finite element model of the Mod-0 wind turbine tower is
described. Use of this model greatly reduces the computer time required
for modal analysis. The model provides good accuracy in predicting tower
frequencies and mode shapes as long as the tower bending mode shape resembles
the first bending mode shape of a cantilever beam. Several applications where
the simplified model was used for modal analysis are described.

INTRODUCTION

To reduce computing time and cost and, more importantly for us, to reduce turn-
around time from overnight to daytime runs, a detailed finite element model of
the Mod-0 wind turbine tower was reduced to six beam elements (stick model).
This paper explains the method used to calculate the properties of the beam
elements in the stick model, examines the accuracy of the stick model in
predicting natural frequencies and mode shapes, compares computer times, and
describes several applications where the stick model was used.

TOWER MODELS

Detailed Model

A detailed NASTRAN model of the Mod-0 tower was constructed for structural
and modal analysis. A side view of this model is shown in figure 1(a). This
view shows rails for an elevator that have since been removed from the tower.
This model, which includes the conical transition section at the top of the
tower, consisted of 143 nodes and 309 elements. Of these elements, 197 were
bar elements (CBAR), 88 were rod elements (CROD), and 24 were plate elements
(CQUAD2 and CTRIA2).

Simplified Model

The simplified or stick model of the tower consisted of just six NASTRAN bar
elements. This model is shown in figure 1(b). In order to calculate the bar
element properties, the detailed model was divided into six sections or bays.
A gravity vector was applied to determine the weight of each bay. This weight
determined the area used in each bar element of the stick model. The bending

31

and torsional stiffnesses of each bar were selected so that a bending load or torque produced the same deflection or rotation, respectively, in the bar as it did in the bay that the bar represented.

The remainder of the wind turbine (bedplate, drive train and blades) was also modeled with bar elements. The complete model with the stick tower is shown in figure 2. Details of the bedplate and blade models are given in ref. 1. The drive train model details are given in ref. 2.

RESULTS AND DISCUSSION

Comparison of Natural Frequencies and Mode Shapes

Table I compares the measured natural frequencies for the tower alone with those predicted by both the detailed and stick models. The agreement is very good for the first bending modes. For the second bending mode, the stick model predicts a much higher frequency.

Figure 3 compares mode shapes predicted by the detailed and stick models. For the first bending mode (figure 3(a)) the agreement is good. However, for the second bending mode (figure 3(b)) the agreement is poor. Because of the poor agreement for the second bending frequency and mode shape, it is concluded that the stick model will not provide accurate results when the tower mode shape resembles a cantilever beam second bending mode shape like that shown in figure 3(b).

In table II results are presented for the complete wind turbine model with rigid blades. The natural frequencies predicted using the stick tower model are in reasonably good agreement with those predicted using the detailed tower model. The fourth mode is one of combined tower and bedplate bending. Figure 4 shows the mode shapes for the three bending modes given in table II. For the first two modes (figure 4(a) and 4(b)) the agreement is good. There is some difference for the combined tower/pod bending mode (figure 4(c)). All three mode shapes were normalized with respect to the deflection at the hub.

From the results of table II and figure 4 it is concluded that the stick model will provide accurate results in modal analysis for tower torsional modes and tower bending modes when the tower mode shape resembles a cantilever beam first bending mode shape.

Comparison of Computer Times

Some representative computing times are given in table III for modal analysis of the complete wind turbine using both the detailed and stick tower models. The NASTRAN code gives an estimate of symmetric real decomposition time. When the stick tower model is used, this time is very small. Of greater concern are CPU and total time. For this representative case, the model with the detailed tower requires 17 times as much CPU time and about 8 times as much total computer time.

APPLICATIONS

The wind turbine model with a stick tower was first used to determine the effect of the yaw drive stiffness on system natural frequencies. The yaw drive was modeled as a bar element at the top of the tower. The analysis showed that a pod yaw mode frequency, that was initially close to two per revolution, could be significantly increased by using a double yaw drive. The Mod-0 wind turbine was subsequently modified to include a double yaw drive.

Other applications of this simplified model include studies to determine the effect of blade weight on system natural frequencies, and the effect of the tower/bedplate attachment location on frequencies and mode shapes. In addition, the natural frequencies, mode shapes, and generalized masses obtained from the simplified model with rigid blades were used as input to Lockheed's REXOR program for determining blade loads.

CONCLUSIONS

From the results obtained using a simplified model of the Mod-0 tower, it is concluded that a tower of this type can be modeled as a simple cantilever beam for modal analysis. However, this model should be limited to tower torsional modes and tower bending modes where the mode shape resembles a cantilever beam first bending mode shape.

REFERENCES

1. Chamis, C. C.; and Sullivan, T. L. : Free Vibrations of the ERDA-NASA 100 kW Wind Turbine. NASA TM X-71879, 1976.

2. Sullivan, T. L.; Miller, D. R.; and Spera, D. A.: Drive Train Normal Modes Analysis for the ERDA/NASA 100-Kilowatt Wind Turbine Generator. NASA TM-73718, 1977.

DISCUSSION

Q. Why not use a Guyan reduction to simplify your NASTRAN model?

A. A Guyan reduction is a satisfactory means of reducing degrees of freedom for modal analysis. However, the stick model has even fewer degrees of freedom than you would obtain by a Guyan reduction. In addition, while the stick model discussed in the paper was based on a detailed finite element model of the tower, a stick model can also be constructed from an engineering drawing of a tower.

Q. Did you consider shear deformations in your model? Perhaps this would account for the discrepancy in the higher tower bending modes.

A. No, the model did not consider shear deformations. We are presently investigating the effect of shear deformation.

Q. What is the preparation time required to perform a stick model analysis?

A. The time required to prepare a stick model of a tower from a detailed tower model should be less than 8 manhours.

Q. Are you looking at towers with guy wires, pinned joints or damping?

A. No, but the modeling method described is amenable to structures with guy wires, pinned joints and damping.

TABLE I. - MOD-0 TOWER NATURAL FREQUENCIES, Hz

Mode	Measured	Predicted	
		Detailed Model	Stick Model
1st bending-1	4.7	4.8	4.9
1st bending-2	5.1	5.2	5.0
2nd bending-2	9.4	9.2	20.1

TABLE II. - COMPLETE MOD-0 PREDICTED NATURAL FREQUENCIES, Hz

Mode	Detailed Model	Stick Model
Tower torsion	1.3	1.3
Tower 1st bending[a]	2.0	2.1
Tower 1st bending[b]	2.2	2.4
Tower/pod bending	3.8	3.9

[a]Motion at top of tower parallel to drive shaft

[b]Motion at top of tower normal to drive shaft

TABLE III. - COMPUTER TIME COMPARISONS

Computer Time	Detailed Model	Stick Model
Symmetric real decomposition time estimate, sec.	67	1
CPU time - 4 modes[a], min.	12.0	0.7
Total computer time - 4 modes[a], min.	24.4	3.2

[a]For the detailed model, 5 eigenvalues were extracted. One was a local mode.

Figure 2. - Complete model with stick tower.
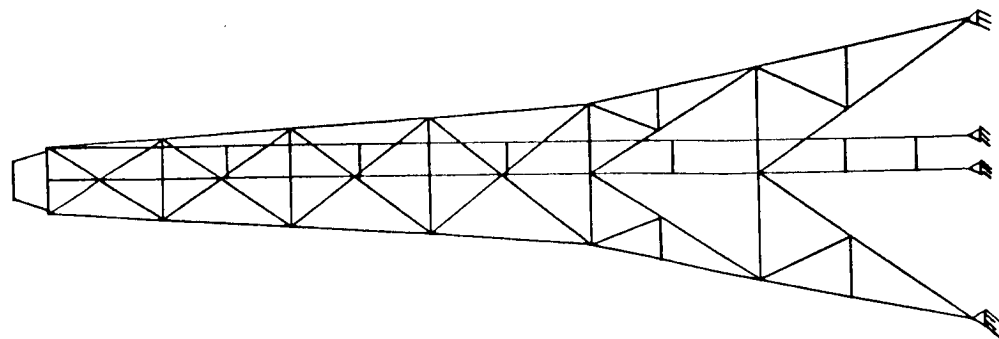
(a) Detailed model (143 nodes; 309 elements).
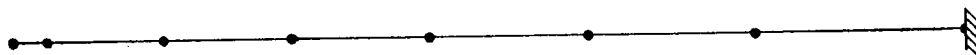
(b) Stick model (8 nodes; 7 elements).

Figure 1. - Mod-0 tower models.

36
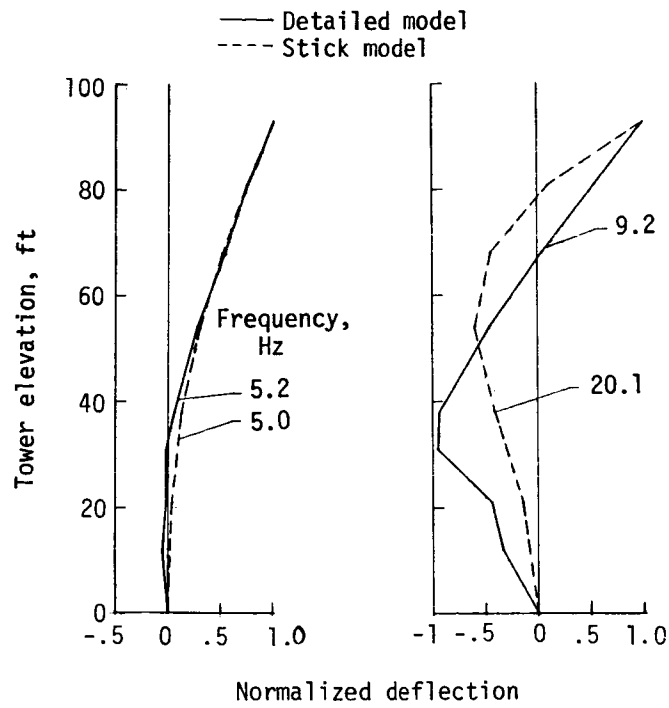
Figure 3. - Comparison of detailed and stick
tower model mode shapes for tower only.
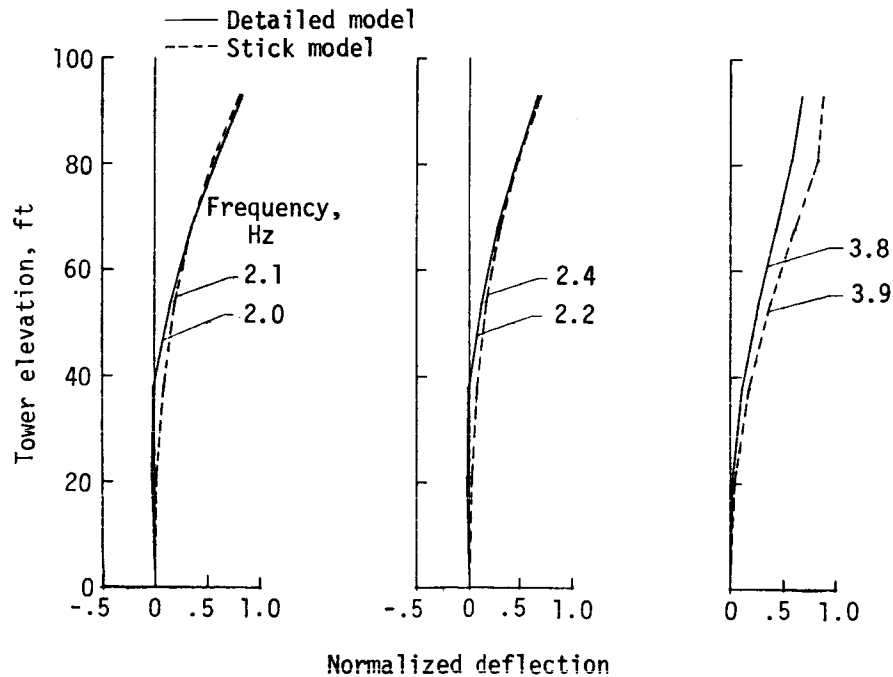
Figure 4. - Comparison of detailed and stick tower model
mode shapes for complete system.

37

USE OF ASYMPTOTIC METHODS IN VIBRATION ANALYSIS[*]

Holt Ashley

Department of Aeronautics & Astronautics
Stanford University
Stanford, Ca. 94305

ABSTRACT

Two subjects are discussed, which are believed relevant to the structural analysis of vertical-axis wind turbines. The first involves the derivation of dynamic differential equations, suitable for studying the vibrations of rotating, curved, slender structures. The Hamiltonian procedure is advocated for this purpose. Various reductions of the full system are displayed, which govern the vibrating <u>Troposkien</u> when various order-of-magnitude restrictions are placed on important parameters.

The final section discusses the possible advantages of the WKB asymptotic method for solving these classes of problems. A special case of this method is used illustratively to calculate eigenvalues and eigenfunctions for a "flat" turbine blade with small flexural stiffness.

PRINCIPAL SYMBOLS

k	Argument of elliptic integrals & functions
ℓ	Length of blade
$\overline{m}$	(Constant) mass per unit length of blade
s	Coordinate measuring distance along blade
t	Time
t_1, t_2	Limits in Hamiltonian integral
$\left.\begin{array}{l} x = x_o + \xi \\ y = y_o + \eta \\ z = \zeta \end{array}\right\}$	Instantaneous coordinates of point on vibrating blade
$x_o(s)$, $y_o(s)$	Coordinates of blade in rotational equilibrium
x_m	Coordinate of blade end
y_m	Maximum value of y_o
EI_s	Flexural rigidity for bending in x-y-plane

EI_z	Flexural rigidity for bending normal to x-y-plane
H_o	(Constant) x-component of equilibrium tensile force
K, K_o	Curvatures defined by Eqs. (4)
L	Kinetic minus potential energy
$T = T_o + \tau$	Instantaneous tensile force in blade
$T_o(s)$	Equilibrium value of T
$U(s)$	Vector of unknowns in WKB method
$\delta(\cdots)$	Variation of a quantity
λ	Eigenvalue in WKB method
μ	Parameter defined by Eq. (9)
ω	Circular frequency of simple harmonic motion
Ω	Angular velocity about support axis of blade

Superscripts, Etc.

$(\dot{\ })$	Partial derivative with respect to time.
$(\ )'$	Total derivative with respect to s

<div align="center">INTRODUCTION</div>

The title of this paper is somewhat misleading, since it actually addresses two subjects relevant to the structural analysis of vertical-axis wind turbines. The first involves the derivation of differential equations needed for the vibration and aeroelastic analysis of a rotating, curved, slender structure like a beam in the Troposkien shape. It is emphasized that a systematic procedure, such as that furnished by Hamilton's principle, can be useful both for ensuring that the results are correct and for developing a hierarchy of simplifications when various approximations are made.

The second subject concerns the possible advantages of what Steele (Ref. 1) chooses to call the WKB (Wentzel-Kramers-Brillouin) method for solving certain of these problems. An elementary illustrative example is offered.

Admittedly, detailed structural design studies of Darrieus-type wind turbines are best carried out by means of finite-element approximations. This approach is unavoidable when the designer is faced with such complications as interactions with the support structure, reinforcing struts, or variable properties along the blades. Calculations of operating stresses, vibration modes, etc. by finite elements appear in several published papers. Examples are Weingarten and Nickell (Ref. 2); Weingarten and Lobitz (Ref. 3); and Biffle (Ref. 4). Many other related citations are given in the survey paper by Blackwell et al. (Ref. 5).

Parametric studies and the goal of fundamental understanding are not so well served, on the other hand, by the purely numerical investigations of point designs. It is believed that Troposkien vibrations offer some interesting problems in applied mechanics, and the discovery of analytical or semi-analytical solutions to appropriate differential equations can certainly not be ruled out. The aim of this paper is to encourage that search.

Figure 1 depicts a Darrieus machine, with a typical blade both in its unperturbed equilibrium shape of $y_0(x_0)$ and slightly deformed. The instantaneous time-dependent position of mass element $\overline{m}$ ds is specified by coordinates x,y,z, measured in a frame rotating with the constant angular velocity Ω. Various simplifications are here adopted from the outset. Thus, attention is focused on a single, uniform blade by assuming its ends to be fully restrained at the points ($\pm x_m$, o, o). Gravitational force is neglected (cf. comparative studies cited by Weingarten and Lobitz Ref. 3).

The current experimental Darrieus configurations deviate somewhat from the true Troposkien shape (Blackwell and Reis, Ref. 6), and it is known that these deviations can produce substantial equilibrium bending stresses (Ref. 3). Here $y_0(x_0)$ is chosen, however, to be the perfect "skiprope." This is a restriction that is easy to remove, as are the prescribed limitations to essentially infinite torsional and elongational rigidity of the blade. In fact, during free vibration, torsion is often nearly uncoupled from the other degrees of freedom when the blade elastic axis and line of C.G.'s coincide — a design feature that would seem desirable in practice.

VIBRATION EQUATIONS FOR SEVERAL IDEALIZED TROPOSKIENS[*]

It is well known (e.g., Ref. 6) that the zero bending moment shape is governed by

$$\frac{d^2 y_0}{dx_0^2} + \frac{\Omega^2 m}{H_0} \left[1 + \left(\frac{dy_0}{dx_0} \right)^2 \right]^{\frac{1}{2}} y_0 = 0 \tag{1}$$

With support conditions as in Fig. 1, the solution of (1) is conveniently expressed as

$$\frac{y_0}{y_m} = sn \left[K(k) \left(1 + \frac{x_0}{x_m} \right); k \right] \tag{2}$$

Here sn is Jacobi's elliptic function, whereas K is the complete elliptic integral of the second kind with argument

$$k = \left[1 + \frac{4H_0}{\overline{m}\Omega^2 y_m^2} \right]^{-\frac{1}{2}} \tag{3}$$

Equation (3) introduces a dimensionless group $\overline{m}\,\Omega^2 y_m^2 / H_0$ which, with various slight modifications, is perhaps the key parameter for vibration and stability studies.

---

[*] Principal symbols are defined in Fig. 1 and the list at the beginning.

As suggested by Mallett in his work on the catenary (Ref. 7), distance s along the blade seems to be an efficient choice for the spatial independent variable. In terms of s, the instantaneous curvatures of the undeformed and deformed shapes can be written, respectively,

$$K_o = \left[\left(\frac{d^2 x_o}{ds^2} \right)^2 + \left(\frac{d^2 y_o}{ds^2} \right)^2 \right]^{\frac{1}{2}} \tag{4a}$$

$$K = \left[\left(\frac{\partial^2 x}{\partial s^2} \right)^2 + \left(\frac{\partial^2 y}{\partial s^2} \right)^2 \right]^{\frac{1}{2}} \tag{4b}$$

For the inextensible blade with flexural stiffnesses EI_s and EI_z, an appropriate Hamiltonian is

$$H = \int_{t_1}^{t_2} \left[L + (\text{Length constraint}) \right] dt = \frac{1}{2} \int_{t_1}^{t_2} \int_o^{\ell} \left\{ \bar{m} \left[\dot{x}^2 + \dot{y}^2 + \dot{z}^2 \right. \right.$$
$$+ 2\Omega y\dot{z} - 2\Omega z\dot{y} + \Omega^2 y^2 + \Omega^2 z^2 \Big] - EI_s \left[K - K_o \right]^2 - EI_z \left(\frac{\partial^2 z}{\partial s^2} \right)^2 \tag{5}$$
$$+ T(s,t) \left[1 - \left(\frac{\partial x}{\partial s} \right)^2 - \left(\frac{\partial y}{\partial s} \right)^2 - \left(\frac{\partial z}{\partial s} \right)^2 \right] \right\} ds\, dt$$

It is easily seen that the Lagrange multiplier on the constant-length constraint is simply the tension $T(s,t)$.

The principle $\delta H = 0$ is enforced by taking variations of (5) on x, y, z and T. Suitable integrations by parts with respect to s or t then lead to the general nonlinear dynamical system:

$$\frac{\partial^2}{\partial s^2} \left[EI_s \left(1 - \frac{K_o}{K} \right) \frac{\partial^2 x}{\partial s^2} \right] - \frac{\partial}{\partial s} \left[T \frac{\partial x}{\partial s} \right] + \bar{m}\, \ddot{x} = 0 \tag{6a}$$

$$\frac{\partial^2}{\partial s^2} \left[EI_s \left(1 - \frac{K_o}{K} \right) \frac{\partial^2 y}{\partial s^2} \right] - \frac{\partial}{\partial s} \left[T \frac{\partial y}{\partial s} \right] + \bar{m} \left[\ddot{y} - \Omega^2 y - 2\Omega \dot{z} \right] = 0 \tag{6b}$$

$$\frac{\partial^2}{\partial s^2} \left[EI_z \frac{\partial^2 z}{\partial s^2} \right] - \frac{\partial}{\partial s} \left[T \frac{\partial z}{\partial s} \right] + \bar{m} \left[\ddot{z} + 2\Omega \dot{y} - \Omega^2 z \right] = 0 \tag{6c}$$

$$\left(\frac{\partial x}{\partial s} \right)^2 + \left(\frac{\partial y}{\partial s} \right)^2 + \left(\frac{\partial z}{\partial s} \right)^2 - 1 = 0 \tag{6d}$$

42

Small perturbations ξ, η, ζ and τ are introduced on the dependent variables, products of small quantities are neglected, and the equilibrium relations corresponding to (1) are subtracted out. There results the most general system, governing the free dynamics of a uniform, inextensible Troposkien:

$$EI_s \frac{\partial^2}{\partial s^2}\left[\frac{x_o''}{K_o^2}\left(x_o'' \frac{\partial^2 \xi}{\partial s^2} + y_o'' \frac{\partial^2 \eta}{\partial s^2}\right)\right] - \frac{\partial}{\partial s}\left[T_o(s) \frac{\partial \xi}{\partial s} + x_o' \tau\right] + \bar{m} \ddot{\xi} = 0 \tag{7a}$$

$$EI_s \frac{\partial^2}{\partial s^2}\left[\frac{y_o''}{K_o^2}\left(x_o'' \frac{\partial^2 \xi}{\partial s^2} + y_o'' \frac{\partial^2 \eta}{\partial s^2}\right)\right] - \frac{\partial}{\partial s}\left[T_o(s) \frac{\partial \eta}{\partial s} + y_o' \tau\right] + \bar{m}\left[\ddot{\eta} - 2\Omega\dot{\zeta} - \Omega^2\eta\right] = 0 \tag{7b}$$

$$EI_z \frac{\partial^4 \zeta}{\partial s^4} - \frac{\partial}{\partial s}\left[T_o(s) \frac{\partial \zeta}{\partial s}\right] + \bar{m}\left[\ddot{\zeta} + 2\Omega\dot{\eta} - \Omega^2\zeta\right] = 0 \tag{7c}$$

$$x_o' \frac{\partial \xi}{\partial s} + y_o' \frac{\partial \eta}{\partial s} = 0 \tag{7d}$$

In principle, the assumption of simple harmonic time dependence at frequency ω converts Eqs. (7) into an ordinary system, whose eigenvalues and eigenfunctions describe the free vibration. It is also not difficult to add forcing terms, such as aerodynamic loads.

Equations (7), as written, offer little attraction to the analyst. Accordingly, several simpler versions will be discussed, along with the approximations that lead to them. For reasons of space, little attention is paid to boundary conditions, but their formulation is not a difficult matter.

1. The Rotating Rope or Chain

When $EI_s = EI_z = 0$, a catenary-like structure is left. Its linearized differential equations are

$$\bar{m} \ddot{\xi} - \frac{\partial}{\partial s}\left[T_o \frac{\partial \xi}{\partial s} + x_o' \tau\right] = 0 \tag{8a}$$

$$\bar{m}\left[\ddot{\eta} - 2\Omega\dot{\zeta} - \Omega^2\eta\right] - \frac{\partial}{\partial s}\left[T_o \frac{\partial \eta}{\partial s} + y_o' \tau\right] = 0 \tag{8b}$$

$$\bar{m}\left[\ddot{\zeta} + 2\Omega\dot{\eta} - \Omega^2\zeta\right] - \frac{\partial}{\partial s}\left[T_o \frac{\partial \zeta}{\partial s}\right] = 0 , \tag{8c}$$

with (7d) unchanged. Equations (8) are not relevant to wind turbines. The reason for displaying them is to make the point that, even in this case, the four variables remain coupled. In addition to the familiar centrifugal term

$- \Omega^2 \eta$, Coriolis effects couple the in- and out-of-plane degrees of freedom. These latter gain in importance relative to the centrifugal as the vibration frequency increases.

When (8) are made dimensionless, a two-parameter system is found, involving

$$\mu \equiv \frac{\overline{m} \, \omega^2 \, x_m^2}{H_o} \tag{9}$$

and the frequency ratio Ω/ω . It appears that $\mu \, \Omega^2/\omega^2$ is of $O(1)$ for all interesting designs. Ω/ω is less than unity, but it remains $O(1)$ for the lower vibration modes.

2. Small In-Plane and Large Out-of-Plane Bending Stiffnesses

It is obvious that Darrieus turbine blades with typical airfoil shapes will have

$$\frac{EI_z}{EI_s} \gg 1 \tag{10}$$

Indeed, Ref. 3 quotes a value over 40 for this ratio on the SANDIA 17-meter design. An interesting reduction of system (7) is found when both inequality (10) is satisfied and when

$$\frac{EI_s}{H_o x_m^2} \ll 1 \tag{11}$$

(this ratio is estimated to be 0.015 for the 17-meter). It can then be reasoned that $\zeta \ll \eta$, so that the Coriolis term in (7b) is negligible, and that the flexural terms may be dropped from (7a,b). The resulting equations are

$$\overline{m} \, \ddot{\xi} - \frac{\partial}{\partial s} \left[T_o \, \frac{\partial \xi}{\partial s} + x_o' \, \tau \right] = 0 \tag{12a}$$

$$\overline{m} \left[\ddot{\eta} - \Omega^2 \eta \right] - \frac{\partial}{\partial s} \left[T_o \, \frac{\partial \eta}{\partial s} + y_o' \, \tau \right] = 0 \tag{12b}$$

$$\frac{\partial \xi}{\partial s} + \frac{dy_o}{dx_o} \, \frac{\partial \eta}{\partial s} = 0 \tag{12c}$$

Three coupled dependent variables are involved in (12). Nevertheless, they constitute a considerable simplification and might form the basis for useful parametric studies. At considerable labor, one can eliminate $\zeta(s,t)$ among (12 a,b,c). The result does not seem of great value, however, and efforts to achieve a single equation in one unknown where unsuccessful.

3. The "Flat" Blade with Small Bending Stiffness

If in addition to the other assumptions behind system (12) the approximation is made that

$$\frac{dy_o}{dx_o} \ll 1 \quad , \tag{13}$$

then dropping the τ term in (12b) is justified. A further replacement of $T_o(s)$ by H_o/x_o', where H_o is its large, constant x-component leads to

$$\frac{\partial^2 \eta}{\partial x_o^2} - \frac{\overline{m}}{H_o} \frac{ds}{dx_o} \left[\ddot{\eta} - \Omega^2 \eta \right] = 0 \tag{14}$$

This is essentially the in-plane-deformation equation employed by Ham (Ref. 8), in his investigations on free vibration and flutter of the rotating blade. In view of the apparent limitations on its validity, further study would seem justified into the parameter ranges within which it can be used in practice.

DISCUSSION OF ASYMPTOTIC METHODS AND AN APPLICATION

The excellent review by Steele (Ref. 1) removes the need for any recapitulation here of how these methods are applied to ordinary differential equations arising in solid mechanics. The particular form useful in vibration problems with spatially-varying coefficients is known by such names as "phase integral," WKB and WKBJ. In the form most broadly applicable here, it starts with a homogeneous problem formulation in terms of a "state vector" $U(s)$:

$$\frac{dU(s)}{ds} = A(s;\lambda) U(s) \tag{15} \quad .$$

Here $A(s,\lambda)$ is a prescribed coefficient matrix, containing an eigenvalue λ which, in some sense, is a large quantity. A is expanded according to

$$A(s;\lambda) = \lambda A_o(s) + A_1(s) + \frac{1}{\lambda} A_2(s) + \cdots \tag{16}$$

The series in (16) may be convergent or asymptotic. In either event, clever changes of variable are employed to construct a corresponding succession of approximate solutions.

45

After the assumption of simple harmonic motion, it is worth noting that all the systems presented in the preceding section can be recast in state vector form. The same is true of equations for flutter stability or forced sinusoidal response. The principal recommendation of this paper is that the WKB theory should be put to work in order to determine what contribution it may make to the subject at hand.

All that can be offered at present is a simple example to illustrate the possibilities. For harmonic oscillations at frequency ω, with mode shape $\bar{\eta}(x_o)$, it is an easy matter to recast the "flat - _Troposkien_" eq. (14) as follows:

$$\frac{d^2\bar{\eta}}{dx_o^2} + \frac{\Lambda^2\bar{m}}{H_o}\left[1 + \frac{m\Omega^2 y_m^2}{H_o}\left(1 - \frac{y_o^2(x_o)}{y_m^2}\right)\right]\bar{\eta} = 0 \quad , \tag{17}$$

where

$$\Lambda \equiv \sqrt{\Omega^2 + \omega^2} \tag{18}$$

In view of (2), the quantity in brackets of (17) may be rewritten

$$[\cdots] = 1 + \frac{\bar{m}\,\Omega^2 y_m^2}{H_o} \, cn^2\left(K(k)\left(1 + \frac{x_o}{x_m}\right); \; k\right) \tag{19}$$

Now (17), with the associated boundary conditions $\bar{\eta}(\pm x_m) = 0$, is a special case of the problem solved by Steele (Ref. 1, Sect. 2), using the Green–Liouville transformation. In more general terms, Steele transforms the differential equation

$$\frac{d}{dx}\left[p(x)\frac{dy}{dx}\right] + \left[\lambda^2 q(x) - r(x)\right]y = 0 \tag{20}$$

by introducing

$$\zeta = \zeta(x) , \quad y = \psi(x)\,n(\zeta) \tag{21a,b}$$

With the following optimal choice of these functions:

$$(\zeta')^2 = p/q \tag{21c}$$

and $\psi = \left[pq\right]^{-\frac{1}{4}}$, $\qquad\qquad$ (21d)

(20) is reduced to

$$\frac{d^2\eta}{ds^2} + \left[\lambda^2 - \frac{\nu}{q}\right]\eta = 0 \quad , \tag{22}$$

46

where

$$\nu(x) = r - \frac{(p\psi')^l}{\psi} \tag{23}$$

When λ is large, the limiting form of the solution can be re-transformed to

$$y(x) = \psi(x) \exp\left[\pm i\lambda \zeta(x)\right], \tag{24}$$

where

$$\zeta(x) = \int_{x_b}^{x} \left[\frac{q}{p}\right]^{1/2} dx \tag{25}$$

has the name "phase integral." x_b is a point associated with one of the boundary conditions. Eigenvalues are readily estimated by combining (24), (25) and the second B.C.

In the present example, one associates Steele's x variable with x_o/x_m and y with $\bar{\eta}$. Here also

$$p(x) = 1 \tag{26a}$$

$$q(x) = 1 + \frac{\bar{m}\Omega^2 y_m^2}{H_o} \operatorname{cn}^2\left(K(k)\left(1 + \frac{x_o}{x_m}\right); k\right) \tag{26b}$$

$$r(x) = 0 \tag{26c}$$

$$\lambda^2 = \frac{\bar{m}\Lambda^2 x_m^2}{H_o} \tag{26d}$$

After specialization of the general solution, it is found that a first approximation to the free-vibration eigenvalues is

$$\tilde{\lambda}_n \cong \frac{n\pi}{\zeta_L}, \quad (n = 1, 2, \cdots), \tag{27a}$$

where [cf. (26b)]

$$\zeta_L = \int_{-1}^{1} \sqrt{1 + \frac{\bar{m}\Omega^2 y_m^2}{H_o} \operatorname{cn}^2} \, d\left(\frac{x_o}{x_m}\right) \tag{27b}$$

The mode shape corresponding to $\tilde{\lambda}_n$ is

$$\bar{\eta}_n \cong \psi \sin\left[\tilde{\lambda}_n \zeta\left(\frac{x_o}{x_m}\right)\right], \tag{28a}$$

where

$$\zeta\left(\frac{x_o}{x_m}\right) = \int_{-1}^{x_o/x_m} \sqrt{1 + \frac{\overline{m}\Omega^2 y_m^2}{H_o} \, cn^2} \; d\left(\frac{x_o}{x_m}\right)$$ (28b)

It is even possible, by one additional integration, to obtain a second approximation to the eigenvalues $\widetilde{\lambda}_n$ in accordance with a scheme developed in Sect. 3.3, Ref. 1. Details are not given here, since corrections are generally less than 5%.

In view of (18), (26d) and other knowledge of the properties of typical Darrieus turbines, one can conclude that λ is quite a large parameter, except possibly for the fundamental solution of (17). Accordingly, the WKB method was applied for values of the parameter k [eq. (3)] ranging from 0.2 to 0.8. ($k = 0.57$ characterizes a turbine with diameter equal to its height.) Table I furnishes some numerical results[*] for the first five eigenvalues and the corresponding dimensionless natural frequencies.

Figure 2 plots some representative vibration mode shapes for $k = 0.2$. This parameter was chosen because the condition (13), implied in (17), is most likely to be satisfied accurately in this rather "flat" case. The mode corresponding to $n = 1$ is not shown, because it involves a low-frequency, symmetrical stretching motion. Although not ruled out by (17), it obviously violates the condition (6d) of inextensibility and is regarded as a physical impossibility. For the same reason, $n = 1$ eigenvalues are enclosed by parentheses in Table I.

Time has not permitted extensive comparisons between the foregoing results and those of previous finite-element analyses. One possibility is furnished, however, by the data in Fig. 5 of Ref. 3. These relate to a blade like those of the SANDIA 17-meter turbine, but with the stiffening struts removed; the rotation rate is 75 RPM. From the modal symmetries, it is clear that their numbers are equivalent to $(\omega_2/\Omega) = 1.55$ and $(\omega_3/\Omega) = 2.95$ at $k = 0.57$. From the data in Table I, the corresponding numbers by the WKB approximation are 1.75 and 2.97, respectively.

The present computations were carried out on the digital computer only for convenience. Nothing more is involved than subroutines giving elliptic functions and the numerical evaluation of well-behaved integrals. It is believed unlikely that any much more efficient scheme exists for dealing with equations like (17). Further Troposkien dynamics investigations by means of the WKB method will hopefully be stimulated by this very elementary first attempt.

48

REFERENCES

1. Steele, C.R., "Application of the WKB Method in Solid Mechanics," Chapter VI, Vol. 3, pp. 243-295, Mechanics Today, Pergamon Press, London, 1976.

2. Weingarten, L.I., and Nickell, R.E., "Nonlinear Stress Analysis of Vertical-Axis Wind Turbine Blades," Journal of Engineering for Industry, ASME Transactions, Ser. B, Vol. 97, No. 4, Nov. 1975, pp. 1234-1237.

3. Weingarten, L.I., and Lobitz, D.W., "Blade Structural Analysis," Proceedings of the Vertical-Axis Wind Turbine Technology Workshop, Sandia Laboratories, Albuquerque, N.M., SAND 76-5568, May 1976, pp. II-137-150.

4. Biffle, J.H., "System Structural Response," Proceedings of the Vertical-Axis Wind Turbine Technology Workshop, Sandia Laboratories, Albuquerque, N.M., SAND 76-5568, May 1976, pp. II-168-179.

5. Blackwell, B.F., Sullivan, W.N., Beuter, R.C., and Bañas, J.F., "Engineering Development Status of the Darrieus Wind Turbine," Journal of Energy, Vol. 1, No. 1, Jan.-Feb. 1977, pp. 50-64.

6. Blackwell, B.F., and Reis, G.E., "Blade Shape for a Troposkien Type of Vertical-Axis Wind Turbine," Sandia Labs. Energy Rept. SLA-74-0154, April 1974.

7. Mallett, R.C., "On the Vibration of Suspended Cables," in preparation.

8. Ham, N.D., "Aeroelastic Analysis of the Troposkien-Type Wind Turbine," Proceedings of the Vertical-Axis Wind Turbine Technology Workshop, Sandia Laboratories, Albuquerque, N.M., SAND 76-5568, May 1976, pp. II-185-204.

DISCUSSION

Question:

Since torsion is structurally coupled with out-of-plane bending in a curved beam, isn't it true that whenever such bending occurs, torsion must occur?

Comment 1: Since coriolis forces dominate the coupling between in-plane and out-of-plane bending, blade chordwise elastic axis and center of gravity locations need not coincide, and blade design effort and manufacturing cost are greatly reduced.

Comment 2: In certain experimental cases of Darrieus blade flutter, in-plane and out-of-plane bending displacement perturbations are the same order of magnitude.

Answer: Agree with Comment 2. Feel we must gain more experience with various sizes of rotor and other structural details before Comment 1 can be accepted as a design principle for all Darrieus machines. Helicopter rotors also have important Coriolis couplings, yet practice with them is to massbalance so that the C.G. and quarter-chord axes coincide.

With regard to the question, author believes that the theory of his paper requires, as a strict condition, that the torsional rigidity GJ just be extremely large. He has found other possible circumstances, however, in which coupling with torsion may be negligible. This occurs when the C.G. is at the quarter chord and when a dimensionless parameter (involving GJ divided by the mass moment of inertia in torsion) is large compare to unity.

TABLE I. - SECOND-APPROXIMATE EIGENVALUES λ_n AND DIMENSIONLESS NATURAL

FREQUENCIES ω_n/Ω FOR TROPOSKIEN BLADES OF SEVEN

DIFFERENT ASPECT RATIOS

n	k	0.2	0.3	0.4	0.5	0.6	0.7	0.8
	y_m/x_m	0.2625	0.4100	0.5807	0.7908	1.071	1.486	2.226
1	$\tilde{\lambda}_1$	(1.511)	(1.525)	(1.489)	(1.440)	(1.376)	(1.057)	(1.181)
	ω_1/Ω	(0.7395)	(0.719)	(0.689)	(0.648)	(0.593)	(0.517)	(0.406)
2	$\tilde{\lambda}_2$	3.061	2.957	2.805	2.599	2.325	1.964	1.479
	ω_2/Ω	2.242	2.168	2.058	1.904	1.691	1.388	0.909
3	$\tilde{\lambda}_3$	4.593	4.444	4.235	3.966	3.638	3.251	2.801
	ω_3/Ω	3.545	3.446	3.306	3.126	2.907	2.649	2.356
4	$\tilde{\lambda}_4$	6.124	5.924	5.642	5.271	4.797	4.187	3.360
	ω_4/Ω	4.808	4.677	4.492	4.247	3.928	3.507	2.903
5	$\tilde{\lambda}_5$	7.655	7.405	7.053	6.593	6.016	5.304	4.433
	ω_5/Ω	6.057	5.895	5.665	5.364	4.983	4.510	3.926

$x_o = -x_m$

— — — Equilibrium
——— Perturbed

Ω

s

Equilibrium shape
$x_o(s), y_o(s)$

y_m

$z(\perp \text{ page})$

y, y_o

$y(s,t)$

$\overline{m}$ ds (coordinates x,y,z)

$x = x_o(s) + \xi(s,t)$
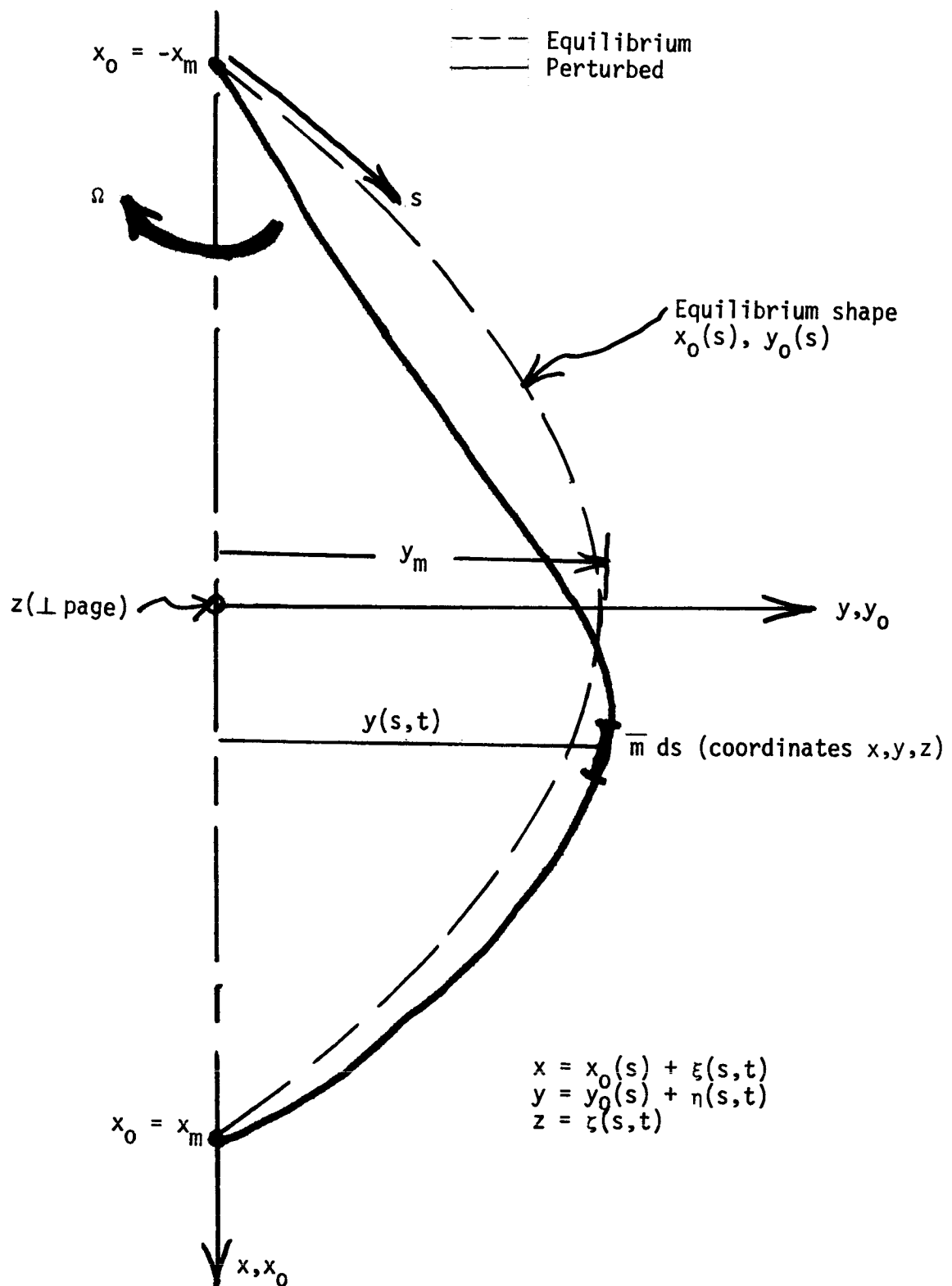$y = y_o(s) + \eta(s,t)$
$z = \zeta(s,t)$

$x_o = x_m$

x, x_o

Figure 1. - Equilibrium and perturbed positions of a Troposkien shape
which is vibrating while rotating about x_o-axis with constant
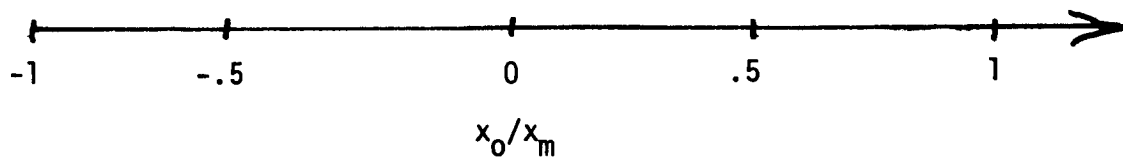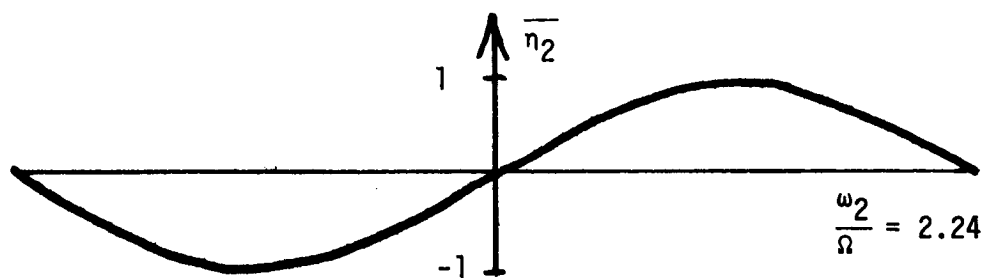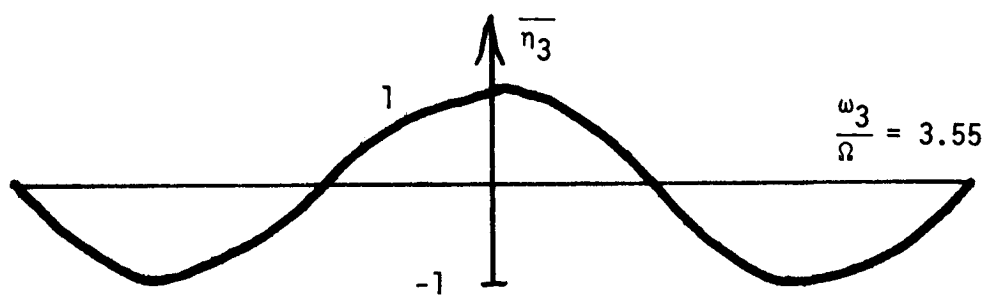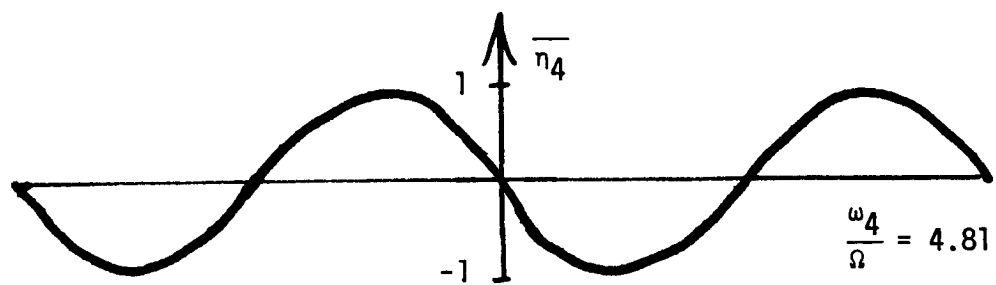angular velocity Ω.

51

Figure 2. - First three physically possible natural modes of vibration for the Troposkien with $(\bar{m}x_m^2\Omega^2/H_o)' = 1.555$, corresponding to $k = 0.2$.

AEROELASTIC ANALYSIS OF WIND ENERGY CONVERSION SYSTEMS

John Dugundji

Department of Aeronautics and Astronautics
Massachusetts Institute of Technology
Cambridge, Massachusetts   02139

ABSTRACT

An aeroelastic investigation of horizontal axis wind turbines is described. The study is divided into two simpler areas, namely, the aeroelastic stability of a single blade on a rigid tower, and the mechanical vibrations of the rotor system on a flexible tower. Some resulting instabilities and forced vibration behavior are described.

INTRODUCTION

The aeroelastic analysis of horizontal axis wind turbines may be divided into two convenient areas, namely, (a) the investigation of the aeroelastic stability and response of a single blade on a rigid tower, and (b) the investigation of the mechanical stability and vibrations of the rotor system on a flexible tower. With a reasonable understanding of the behavior in these two areas, the more complex problem involving a completely coupled blade-tower aeroelastic system can be better understood.

The present report deals with some work performed for ERDA in the two areas cited above. The aim has been to investigate the basic mechanisms and to reduce these analyses to forms in which they can be readily used for trade-off analyses.

AEROELASTIC STABILITY OF SINGLE BLADE

Using the equivalent hinge concept, the nonlinear equations of motion were written for large deflections of a rigid blade, with elastic hinges at the root, rotating about a rigid tower. The blade was assumed to have a flapping (β), lagging (ϕ), and feathering (θ) degree of freedom, and the effects of preconing of the blade relative to the feathering hinge (δ), and of the feathering hinge relative to the plane of rotation (β_H), were included. Quasi-steady aerodynamic forces were assumed. The equations were first solved to obtain the static, steady state displacement in flap (β_0) and lag (ϕ_0). Then the equations of motion were linearized by assuming small perturbations about the steady state flap and lag displacements found above. The resulting linear equations take the form

$$[A]\{\ddot{x}\} + [D]\{\dot{x}\} + [K]\{x\} = 0 \qquad (1)$$

where {x} represents the perturbation displacements in β, ϕ, θ and [A], [D], [K] represent the 3x3 mass, damping, and stiffness matrices respectively. These equations were investigated for stability by recasting them as standard first order equations, and extracting the eigenvalues $p_n = a_n + i\,b_n$ using standard procedures. The resulting a_n's indicate the damping characteristics, and the b_n's the frequencies of the resulting oscillations.

A wide range of parametric variations are being investigated. Figure 1 shows some typical results from this analysis showing effects of preconing on the stability margins. The results are presented in the form of modal critical damping ratio $\zeta \approx -a_n/b_n$ since it is believed this more clearly indicates the strength of the instability (or stability) than simple stability boundaries. It is seen here that positive droop angles (δ) can particularly decrease the stability margin.

The analyses described above have been based on equivalent hinges in order to provide a rapid and reasonably accurate tool for predicting stability characteristics. However, a more elaborate program is being developed which allows for distributed flexibility of all three hinges, and this program will be used to validate the results using equivalent hinges.

The linear aeroelastic stability analyses have been supplemented by some nonlinear, large deflection analyses again using equivalent hinges, to determine the nonlinear limit cycle behavior of these instabilities. The harmonic balance method was applied and the resulting nonlinear equations were solved by the Newton-Raphson technique. Both the self-excited aeroelastic instabilities and the dynamic response to gravity and wind shear loads were investigated. Figure 2 shows the nonlinear limit cycle behavior of a predominantly flapping-torsion type instability as rotation speed Ω is increased. The nonlinearity tends to be of a softening type, i.e., steady limit cycles can occur somewhat below the linear critical rotation speed if a large enough disturbance is given to the system.

MECHANICAL VIBRATIONS OF ROTOR-TOWER SYSTEM

The mechanical instabilities and vibrations that may result from the interaction of the flexible rotating blades with the base motions of the supporting tower were also investigated. The simplest of these interactions involves the coupling of the tower side motions (q_L) with the blade lagging motions (ϕ), which can give rise to a strong mechanical instability (the "gound resonance" effect of helicopters), as well as significant forced vibration effects due to blade unbalance and gravity forces. Using the equivalent hinge concept, the equations of motion for small vibrations of such a rotor-tower system are

$$M_L \ddot{q}_L + c_L \dot{q}_L + k_1 q_1 + \overset{i}{\underset{i}{\Sigma}} S_i \frac{d^2}{dt^2}(\phi_i \cos\psi_i) = \Omega^2 \overset{i}{\underset{i}{\Sigma}} S_i \sin\psi_i$$

$$S_i \cos\psi_i \, \ddot{q}_L + I_i \ddot{\phi}_i + c_\phi \dot{\phi}_i + k_\phi \phi_i = g[S_i \sin\psi_i + S_i \phi_i \cos\psi_i]$$

$$i = 1,2,\ldots N \tag{2}$$

54

where $\psi_i = \Omega t + 2\pi(i-1)/N$ represents the angular position of the ith blade, g is the acceleration of gravity, M_L is the equivalent tower mass of the tower and rotor, and S_i and I_i represent the static moment and moment of inertia of the ith blade about the lag hinge.

The mechanical stability of this rotor-tower system can be found by neglecting gravity and blade unbalance forces ($g = 0$, $S_i = $ const), and introducing the multiblade coordinate transformation

$$\phi_i = a(t)\,\sin\psi_i + b(t)\,\cos\psi_i \tag{3}$$

This eliminates all the periodic coefficients in Eqs. (2) for $N \geqslant 3$, and the stability of the resulting equations in q_L, a, b, can be investigated in the standard manner. Figure 3 shows the results for a typical 3-bladed rotor with varying amounts of critical damping ratio ζ_i in the tower and in the blades. In general adding damping stabilizes the system, but under certain circumstances, the addition of unequal amounts of damping can destabilize the system from the no damping case. For a 2-bladed rotor, effects are similar, but with additional small instability regions.

Effects of small, static unbalance can be found by assuming that $S_1 = S + \Delta S$, $S_2 = S_3 = \ldots = S$. The right hand side of Eqs. (2) then reduces to the forcing function $\Omega^2 S \sin \Omega t$. By neglecting the small ΔS variations in the periodic coefficients, and introducing again the multiblade coordinate transformation, Eq.(3), the basic equations reduce to the forced harmonic response of a conventional spring mass system involving the coordinates q_L, a, b. The resulting tower and rotor responses become

$$q_L(t) = q_{LS}\,\sin\Omega t + q_{LC}\,\cos\Omega t$$

$$\phi_1(t) = \frac{b_c + a_s}{2} + \left(\frac{b_s + a_c}{2}\right)\sin 2\Omega t + \left(\frac{b_c - a_s}{2}\right)\cos 2\Omega t \tag{4}$$

where a_s, a_c, b_s, b_c are the sine and cosine responses of the coordinates, a, b. Figure 4 shows the amplitude of the blade lagging response ϕ_1 for a typical case. It is seen that strong 2/rev resonance responses occur in the blade when the rotation speed Ω equals 1/2 the lagging natural frequency ω_ϕ or when Ω equals the tower natural frequency ω_L. Adding damping to the blade or to the tower reduces the respective amplitude accordingly.

The effects of gravity loading can similarly be investigated by examining Eqs.(2). Generally, gravity acts directly on each blade without much tower interaction. Strong 1/rev resonances may occur when Ω equals the lagging frequency ω_ϕ and weak .5/rev parametric resonances may possibly occur when Ω equals twice ω_ϕ.

More comprehensive rotor-tower interactions were investigated by including the tower yawing motions (θ_x) and the blade flapping motions (β) in the previous analyses. The mechanical instability regions occurred at slightly lower rotation speeds Ω than before, but the general mechanisms were not changed significantly. These additional degrees of freedom

55

also affected somewhat the static unbalance loads. Of more significance was the direct effect of wind shear and tower shadow on the blade flapping loads when these additional motions were introduced. The investigation of these mechanical vibrations are continuing.

REFERENCES

1. Miller, R.H., et al., "Wind Energy Conversion," Final Report, ERDA/NSF-00826/75-3, M.I.T. Aeroelastic and Structures Research Laboratory Report ASRL TR 184-3, October 1976.

2. Quarterly Progress Report, "Wind Energy Conversion," October-December 1976, COO-4131/76/1, M.I.T. Aeroelastic and Structures Research Laboratory Report ASRL TR 184-4, January 1977.

3. Quarterly Progress Report, "Wind Energy Conversion," January-March 1977, COO-4131/77/1, M.I.T. Aeroelastic and Structures Research Laboratory Report ASRL TR 184-5, April 1977.

4. Quarterly Progress Report, "Wind Energy Conversion," April-June 1977, COO-4131/77/2, M.I.T. Aeroelastic and Structures Research Laboratory Report ASRL TR 184-6, July 1977.

5. Chopra, I., "Nonlinear Dynamic Response of Wind Turbine Rotor," Ph.D. Thesis, Department of Aeronautics and Astronautics, M.I.T., Cambridge, Mass., February 1977.

DISCUSSION

Q. Comment: It is the flywheel resonance and mechanical instability problems that have primarily dictated natural frequencies of the tower well above the operating range of the rotor.

A. Yes. These factors play important roles, together with the forced vibrations due to rotor static unbalance, gravity loads, and air loads. Generally, I believe, to avoid significant "ground resonance" type mechanical instability, the blade lagging frequency (in-plane vibrations) would need to be above the rotation speed of the rotor. Low natural frequencies of the tower usually give rise to large forced vibration as the rotor speed passes through the tower natural frequency (and also through one half the tower natural frequency for two bladed rotors).
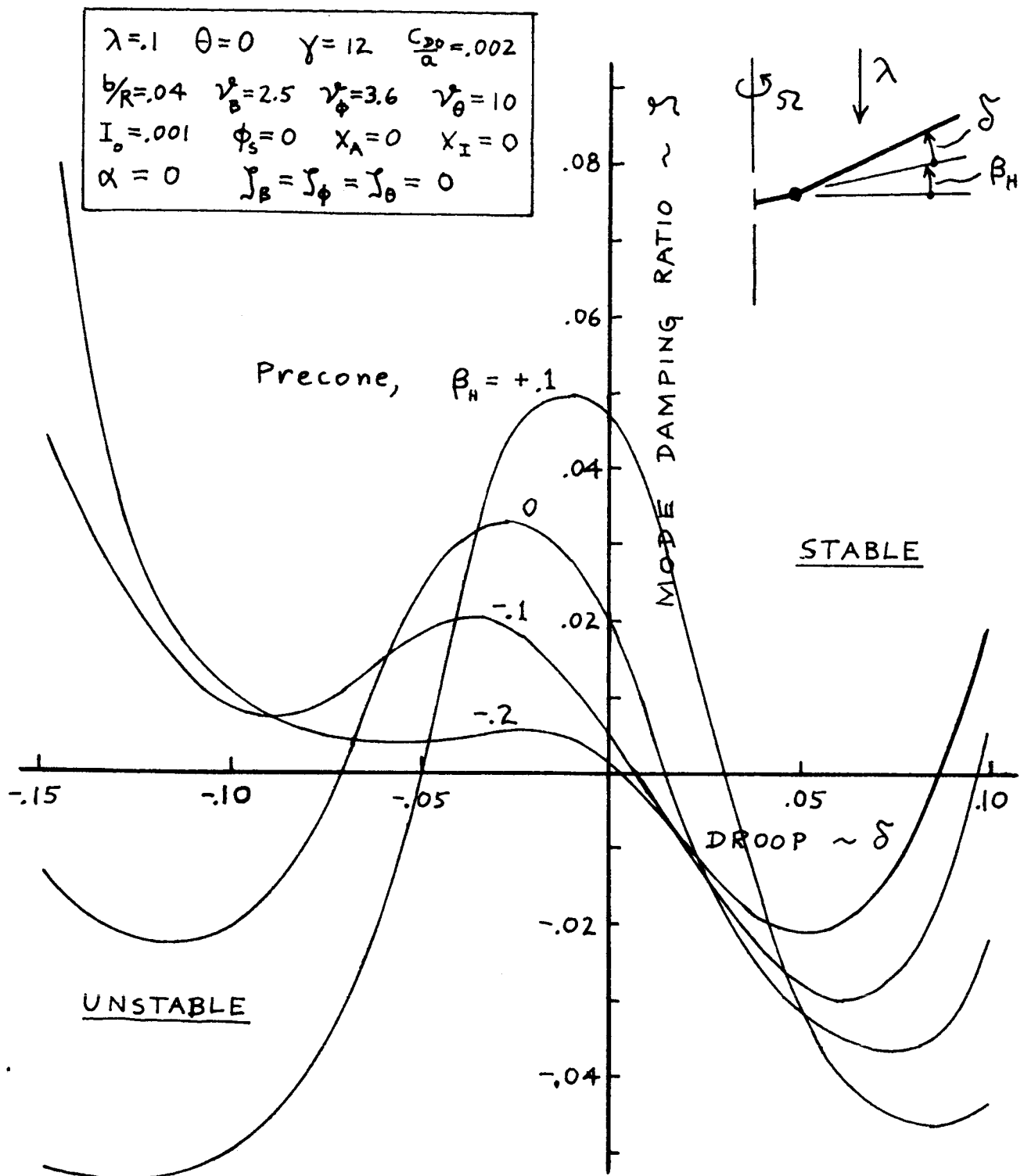
Figure 1 - Effect of precone and droop on aeroelastic stability of lag mode.
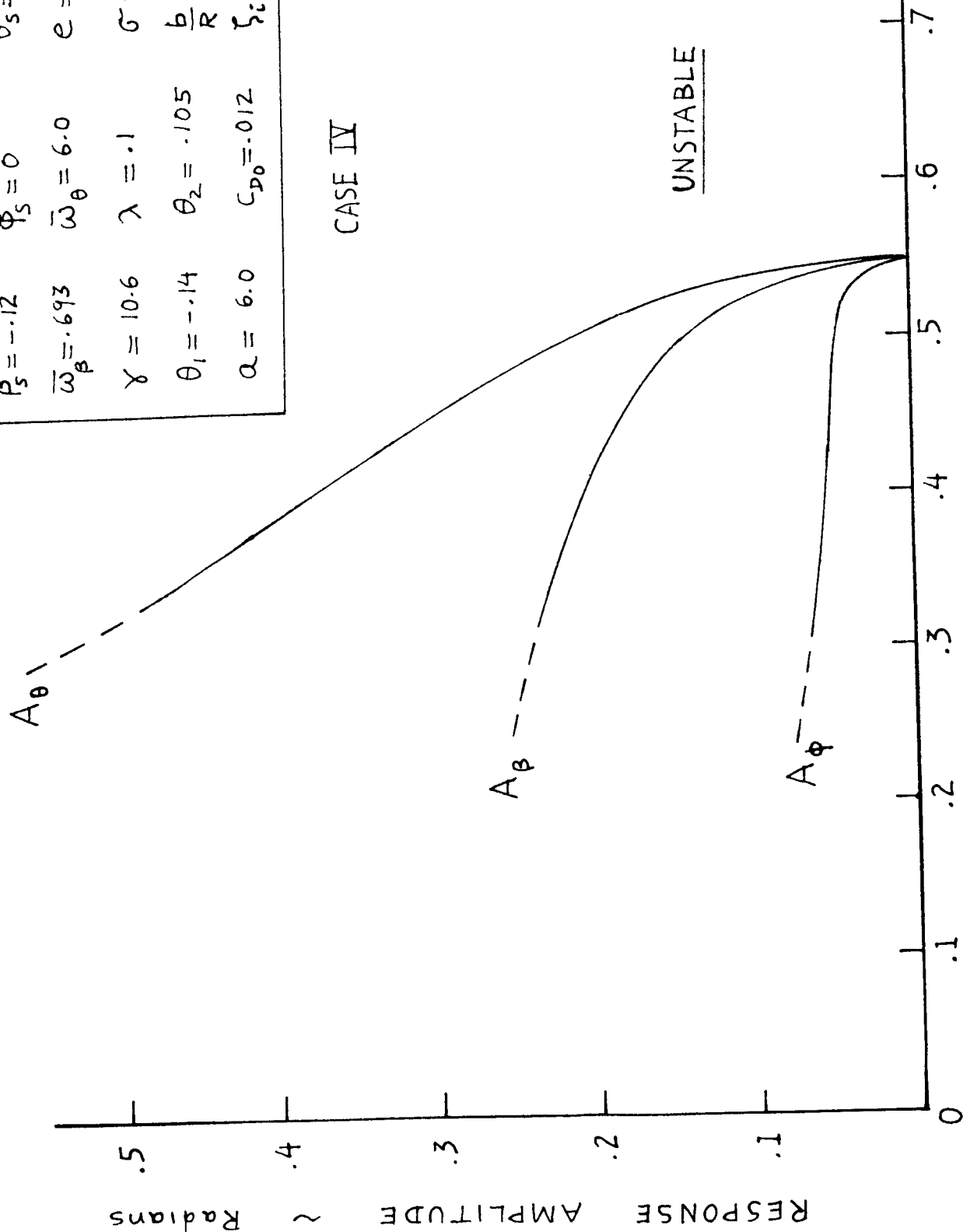
Figure 2. – Flutter solution (nonlinear limit cycles).

58

Figure 3. - Mechanical instability regions for a three-bladed rotor.

INSTABILITY REGION

NO DAMPIN

$\zeta_L = .1$, $\zeta_\phi = .01$

$.3 = \zeta_L = \zeta_\phi$

$\zeta_L = .01$, $\zeta_\phi = .1$

$\dfrac{S^2}{M_L I} = .128$

TOWER TO LAG FREQUENCY RATIO $\sim$ ω_L/ω_ϕ

ROTATION SPEED RATIO $\sim$ Ω/ω_ϕ

Figure 4. - Forced response of rotor to static unbalance.

The graph shows Blade Lagging Amplitude $A = \sqrt{\left(\frac{b_s + a_c}{2}\right)^2 + \left(\frac{b_c - a_s}{2}\right)^2}$ versus Rotation Speed Ratio $\sim \Omega/\omega_\phi$.

Curve labels:
$\begin{cases} \zeta_L = .1 \\ \zeta_\phi = .01 \end{cases}$

$\begin{cases} \zeta_L = .01 \\ \zeta_\phi = .1 \end{cases}$

$\frac{\Delta S}{M_L R} = .1$

$\frac{\omega_L}{\omega_\phi} = .924$

$\frac{N}{2}\frac{S}{M_L R} = .104$

$\frac{S R}{I} = 1.84$

AEROELASTIC STABILITY OF WIND TURBINE BLADES

Krishna Rao V. Kaza
The University of Toledo
Toledo, Ohio 43606

ABSTRACT

The second-degree nonlinear aeroelastic equations for a flexible, twisted, non-uniform wind turbine blade are developed using Hamilton's principle. The derivation of these equations has its basis in the geometric nonlinear theory of elasticity. These equations with periodic coefficients are suitable for determining the aeroelastic stability and response of large wind turbine blades. Methods for solving these equations are discussed.

INTRODUCTION

The recent renewed efforts in wind power machines is due to their prospective use as an alternate energy source. As a result of these efforts several wind turbine projects have been initiated by NASA Lewis Research Center as a part of ERDA's overall wind energy program. To make the wind energy cost effective, progressively larger wind turbines ranging from 100 kW with a rotor diameter of 125 feet to 2000 kW with a rotor diameter of 200 to 300 feet are being considered, and these wind turbines are now in conceptual design. However, as the blade flexibility increases, susceptibility to aeroelastic instability increases. Also, the efficient construction and operation of wind turbines require that the vibratory loads and stresses on the rotor as well as on the combined rotor-tower system be reduced to the lowest possible levels. Thus, the aeroelastic and structural dynamic considerations have a direct bearing on the manufacture, life, and operation of these large wind turbine systems. Although the structural dynamic and aeroelastic technology used to develop rotary wing aircraft appears to be adequate for the development of wind power machines, this technology has to be transformed from aircraft applications to wind power applications, and additional studies have to be conducted to determine the effects of the parameters peculiar to wind power machines on the aeroelastic and structural dynamic behaviour.

The aeroelastic considerations that are common to both the wind turbine blade and the helicopter blade are flap-lag-torsion, flap-torsion, flap-lag instabilities and torsional divergence. The wind velocity gradients due to earth's boundary layer and the gravity loads in the case of wind turbine rotor and the forward velocity in the case of helicopter rotor lead to timewise periodic coefficients in the equations of motion. Several previous studies have considered the helicopter blade and developed the nonlinear aeroelastic equations of motion. More recently reference 1 derived a set of nonlinear aeroelastic equations and compared them to some of the recent equations available in the literature. These comparisons indicated several descrepancies with the results of reference 1, particularly in the nonlinear terms. The reasons for these descrepancies were explained in reference 1. For wind turbine blades reference 2 presented a set of nonlinear aeroelastic equations. An examination of these equations reveals that the reference 2 fails to recover

several nonlinear elastic and aerodynamic terms which are of the same order as those retained. The reasons for this failure are the use of an incorrect torsional curvature and the linearization of the resultant transformation matrix between the undeformed and deformed blade coordinates while developing nonlinear equations of motion. In view of this, it is felt that a comprehensive development of the nonlinear aeroelastic equations of motion of wind turbine elastic blade is required. The purpose of this paper is to derive such a set of equations.

The derivation of the nonlinear elastic and dynamic forces follows essentially along the lines of reference 1. In this reference the pretwist of the blades was combined with the elastic twist, following the common practice in the helicopter blade literature. In the present paper, however, the pretwist together with the control inputs will be introduced before the elastic deformations, and a brief summary of the development will be presented. A formal NASA report which is under preparation will provide the details of the development. Methods for solving these equations will be discussed.

MATHEMATICAL MODEL AND COORDINATE SYSTEMS

The mathematical model chosen to represent the wind turbine blade consists of a straight, slender, variable twisted, nonuniform elastic blade. The elastic axis, the mass axis, and the tension axis are taken to be noncoincident; the elastic axis and the feathering axis are assumed coincident with the quarter-chord of the blade. The generalized aerodynamic forces are calculated from strip theory based on a quasi-steady approximation.

Several orthogonal coordinate systems will be employed in the derivation of equations of motion; those which are common to both the dynamic and aerodynamic aspects of the derivation are shown in figures 1 to 3. The axis system $X_I Y_I Z_I$ is fixed in an inertial frame with the origin at the centerline of the hub. The axis system XYZ is obtained by rotating about Z_I axis by the angle $\Psi = \Omega t$ and then about the negative Y_Ω axis by an angle β_{pc}, the angle of built-in coning. All the deformations of the blade are referenced to the XYZ system. The η and ζ axes with the origin at the elastic axis of the cross section are principal axes and are inclined to the Y and Z axes by an amount equal to the geometric pitch angle. The geometric pitch angle is given by $\theta = \theta_{pt} + \theta_c$ where θ_{pt} is the built-in twist angle (pretwist) and θ_c is the collective pitch angle.

The generalized coordinates defining the configuration of the deformed blade are shown in figure 3. The deformations u, v, w, and ϕ both displace and rotate the $x\eta\zeta$ coordinate system to $x_3 y_3 z_3$ where x_3 axis is tangent to the deformed elastic axis.

DEVELOPMENT OF EQUATIONS OF MOTION

The equations of motion are derived using Hamilton's principle

$$\int_{t_0}^{t_1} (\delta T - \delta V + \delta W)dt = 0 \tag{1}$$

where

$$\delta W = \delta W_D + \delta W_A \tag{2}$$

In equation (1), T is the kinetic energy, V is the strain energy, and δW is the virtual work done by all the nonconservative damping and aerodynamic forces. These are given by

$$V = \frac{1}{2} \int_0^R \iint_A (\sigma_{xx} \gamma_{xx} + \sigma_{x\eta}\gamma_{x\eta} + \sigma_{x\zeta} \gamma_{x\zeta})d\eta\, d\zeta\, dx \tag{3}$$

$$T = \frac{1}{2} \int_0^R \iint_A \rho \frac{d\overline{r_1}}{dt} \cdot \frac{d\overline{r_1}}{dt} d\eta\, d\zeta\, dx \tag{4}$$

$$\delta W_D = - \int_0^R E^* \iint_A \dot{\gamma}_{xx}\, \delta\gamma_{xx}\, d\eta\, d\zeta\, dx$$

$$- \int_0^R G^* \iint_A (\dot{\gamma}_{x\eta}\, \delta\gamma_{x\eta} + \dot{\gamma}_{x\zeta}\, \delta\gamma_{x\zeta})d\eta\, d\zeta\, dx \tag{5}$$

$$\delta W_A = \int_0^R (A_u \delta u + A_v \delta v + A_w \delta w + M_\phi \delta\phi)dx \tag{6}$$

For the strain energy, the stresses are proportional to strains $\sigma_{xx} = E\gamma_{xx}$; $\sigma_{x\eta} = G\gamma_{x\eta}$, and $\sigma_{x\zeta} = G\gamma_{x\zeta}$. In the kinetic energy, $d\overline{r_1}/dt$ is the velocity vector of an arbitrary point in the blade. The coefficients E^* and G^* account for internal damping of the material in tension and shear. The loads A_u, A_v, A_w, and M_ϕ are of aerodynamic origin. To develop the explicit expressions for strains and the aerodynamic loads, the expressions for curvatures ω_{x_3}, ω_{y_3}, and ω_{z_3} and the transformation matrix, $[T]$, between coordinate axes systems $x\eta\zeta$ and $x_3 y_3 z_3$ are needed. Imposing the geometric pitch rotation before the elastic deformation and following the procedures of reference 1, the second-degree expressions for curvatures and transformation matrix are given by

$$\omega_{x_3} = \phi' + \theta'_{pt}\left(1 - \frac{v'^2}{2} - \frac{w'^2}{2}\right) - (v'\cos\theta + w'\sin\theta)(-v'\sin\theta + w'\cos\theta)\Bigg)'$$

$$\omega_{y_3} = -w''(\cos\theta - \phi\sin\theta) + v''(\sin\theta + \phi\cos\theta) \Bigg\} \quad (7)$$

$$\omega_{z_3} = v''(\cos\theta - \phi\sin\theta) + w''(\sin\theta + \phi\cos\theta)$$

$$[T] = \begin{bmatrix} 1 - \dfrac{v'^2}{2} - \dfrac{w'^2}{2} & v'\cos\theta + w'\sin\theta & -v'\sin\theta + w'\cos\theta \\[2mm] \begin{matrix} -v'(\cos\theta - \phi\sin\theta) \\ -w'(\sin\theta + \phi\cos\theta) \end{matrix} & 1 - \dfrac{(v'\cos\theta + w'\sin\theta)^2}{2} - \dfrac{\phi^2}{2} & \begin{matrix} \phi - (v'\cos\theta + w'\sin\theta) \\ \cdot\ \overline{\overline{(-v'\sin\theta + w'\cos\theta)}} \end{matrix} \\[4mm] \begin{matrix} v'(\sin\theta + \phi\cos\theta) \\ -w'(\cos\theta - \phi)\sin\theta \end{matrix} & -\phi & \begin{matrix} 1 - \dfrac{(-v'\sin\theta + w'\cos\theta)^2}{2} \\[2mm] -\dfrac{\phi^2}{2} \end{matrix} \end{bmatrix}$$

$$(8)$$

Using equations (7) and (8) and following the procedure of reference 1, the following strain displacement relations can be derived.

$$\gamma_{xx} = u' + \zeta[-w''(\cos\theta - \phi\sin\theta) + v''(\sin\theta + \phi\cos\theta)]$$

$$-\eta[v''(\cos\theta - \phi\sin\theta) + w''(\sin\theta + \phi\cos\theta)]$$

$$+ (\eta^2 + \zeta^2)\left(\frac{\phi'^2}{2} + \phi'\,\theta'_{pt}\right)$$

$$\gamma_{x\eta} = -\zeta[\phi' + \underline{(v'v'' - w'w'')\cos\theta\sin\theta - v'w''\cos^2\theta}$$

$$+ w'v''\sin^2\theta + \theta'_{pt}\left(\frac{v'^2}{2}\cos2\theta + v'w'\sin2\theta - \frac{w'^2}{2}\cos2\theta\right)]$$

$$\gamma_{x\zeta} = \eta[\phi' + \underline{(v'v'' - w'w'')\cos\theta\sin\theta - v'w''\cos^2\theta + w'v''\sin^2\theta}$$

$$+ \theta'_{pt}\left(\frac{v'^2}{2}\cos2\theta + v'w'\sin2\theta - \frac{w'^2}{2}\cos2\theta\right)] \quad (9)$$

The position vector of a general point in the cross section of the deformed blade is given by

$$\overline{r_1} = \begin{Bmatrix} x_1 \\ y_1 \\ z_1 \end{Bmatrix} = \begin{Bmatrix} x + u - U_F \\ v \\ w \end{Bmatrix} + [T]^T \begin{Bmatrix} 0 \\ \eta \\ \zeta \end{Bmatrix} \quad (10)$$

64

where the axial foreshortening of the elastic axis due to bending is given by

$$U_F = \frac{1}{2} \int_0^x (v'^2 + w'^2)dx \tag{11}$$

The angular velocity of the triad $x\eta\zeta$ is obtained by projecting Ω and it is given by

$$\bar{\omega} = (\Omega\beta_{pc} \bar{e}_x + \Omega\theta_{pt} \bar{e}_\eta + \Omega\bar{e}_\zeta) \tag{12}$$

The remaining details of the derivation of the equations of motion follow from reference 1. An essential feature of the derivation is the introduction of a mathematical ordering scheme which is compatible with the assumption of a slender beam. This scheme was discussed in reference 1. Adapting the same scheme, the higher terms in the generalized elastic and inertia forces are dropped. The aerodynamic forces derived in reference 1 are modified so as to make them suitable for wind turbine blades. In this modification both the velocity gradients due to the earth's boundary layer and wind gusts are considered. The aerodynamic forces are retained in a general second-degree form because the ordering scheme which is imposed would depend on the order assigned to the inflow ratio, pretwist, collective pitch and other aerodynamic parameters. The final equations of motion of the blade are as follows:

$$S_u - Q_{D_u} - I_u = A_u + F_{Gu}$$

$$S_v - Q_{D_v} - I_v = A_v + F_{Gv} \tag{13}$$

$$S_w - Q_{D_w} - I_w = A_w$$

$$S_\phi - Q_{D_\phi} - I_\phi = A_\phi$$

In the above equations the generalized elastic forces S_u, S_v, S_w, and S_ϕ, the inertia forces I_u, I_v, I_w, and I_ϕ, the aerodynamic forces A_u, A_v, A_w, and A_ϕ are nonlinear coupled partial differential operators in u, v, w, and ϕ, and the generalized damping forces are linear uncoupled partial differential operators in u, v, w, and ϕ. The parameters F_{Gu} and F_{Gv} account for gravitational effects. Because of space limitations, the details of the development of the equations of motions and the explicit expressions for all the generalized forces are not presented herein. However, these details will be given in a formal NASA report which is under preparation.

METHODS OF SOLUTION

There are three methods to solve the equations of motion derived above. These are: (1) Galerkin's method[3] and Floquet-Liapunov theory[4]; (2) Integrating Matrix method[5] and Floquet-Liapunov theory; and (3) Approximate method[6] in conjunction with multiblade coordinates. Any one of these methods can be used to solve the above equations of motion. However, the choice depends on the system parameters.

The first two methods are independent of the number of blades whereas the third method is dependent upon the number of blades on the rotor since the multiblade coordinate transformations are functions of the number of blades. These multi-blade coordinate transformations have been developed and applied to rotors with polar symmetry, i.e., rotors with three or more blades. More recently, a similar transformation has been developed for rotors with only two blades in reference 7.

The first two methods involve a numerical integration of the equations of motion whereas the third method does not. But the validity of the third method depends on the parameters of the system in addition to the number of blades. Several studies have been conducted in the literature to determine the validity of the third method for rotors with three or more blades. Based on the results of these studies and the experience of the writer, it appears that the third method can be applied to wind turbine rotors with three or more blades in the preliminary analyses. However, for rotors with two blades the applicability of the transformation given in reference 7, and the validity of the third method which uses this transformation need further research.

CONCLUSIONS

A set of nonlinear second-degree coupled axial-flap-lag-torsional equations of motion for a single, flexible, twisted, nonuniform wind turbine blade were presented. Methods for solving these equations were discussed.

REFERENCES

1. Kaza, K. R. V.; and Kvaternik, R. G.: Nonlinear Aeroelastic Equations for Combined Flapwise Bending, Chordwise Bending, Torsion, and Extension of Twisted Nonuniform Blades in Forward Flight. NASA TM 74059, August 1977.

2. Friedman, P.: Aeroelastic Modeling of Large Wind Turbines. Journal of the American Helicopter Society, Vol. 21, No. 4, October 1976, pp. 17-27.

3. Bisplinghoff, R. L.; and Ashley, H.: Principles of Aeroelasticity. John Wiley and Sons, Inc., New York, 1962.

4. Hammond, C. E.: An Application of Floquet Theory to Prediction of Mechanical Instability. Journal of the American Helicopter Society, Vol. 19, No. 4, October 1974.

5. White, W. F., Jr.; and Malatino, R. E.: A Numerical Method for Determining the Natural Vibration Characteristics of Rotating Nonuniform Cantilever Blades. NASA TM X-72751, October 1975.

6. Kaza, K. R. V.; and Hammond, C. E.: An Investigation of Flap-Lag Stability of Wind Turbine Rotors in the Presence of Velocity Gradients and Helicopter Rotors in Forward Flight. Proceedings of AIAA/ASME/SAE 17th Structures, Structural Dynamics and Materials Conference, Pennsylvania, May 5-7, 1976, pp. 421-431.

7. Hoffman, J. A.: A Multiblade Coordinate Transformation Procedure for Rotors with Two Blades. Paragon Pacific Inc. Report No. PPI-1014-5, September 1976.

DISCUSSION

Q. Can you identify any reasons why earlier publications have not included your underlined terms especially if you contend that some are of the order of magnitude as the usually accepted terms?

A. Most of the earlier publications were unable to include these under-lined terms because of a partial linearization of the resultant rotational transformation matrix between the coordinates of the deformed and the undeformed blade or the use of an incorrect expression for the torsional curvature.

Q. Hodges and Friedmann had a long controversy on omitted terms. They finally agreed. How is your system different?

A. Examining the latest references of both Hodges and Friedmann, it is clear that they are not in complete agreement. Hodges partially linearized the transformation matrix between the coordinates of the deformed and the undeformed blade in his dissertation and hence obtained an incorrect expression for the torsional curvature. He tried to correct this in subsequent publications. In so doing, the torsional curvature was improperly identified. Friedmann also partially linear-ized the resultant transformation matrix while developing the nonlinear equations of motion in most of his publications. More discussion on these terms was presented in the cited reference 1.

Both Hodges and Friedmann in their publications combined the pretwist with the elastic twist of the blades. In the present development since the derivation of the nonlinear equations of motion involves finite rotations, the sequence of which is important, the pretwist together with the control inputs are introduced before the elastic deformations.

C. It is believed that prior researchers in rotory wing aeroelasticity, e.g., Daughaday, DuWaldt, Pizialli and others have in fact developed nonlinear terms you refer to.

A. I am aware of some of the earlier publications by Daughaday, DuWaldt, and Pizialli. In these publications, they have not addressed the nonlinear terms reported in the subject paper.
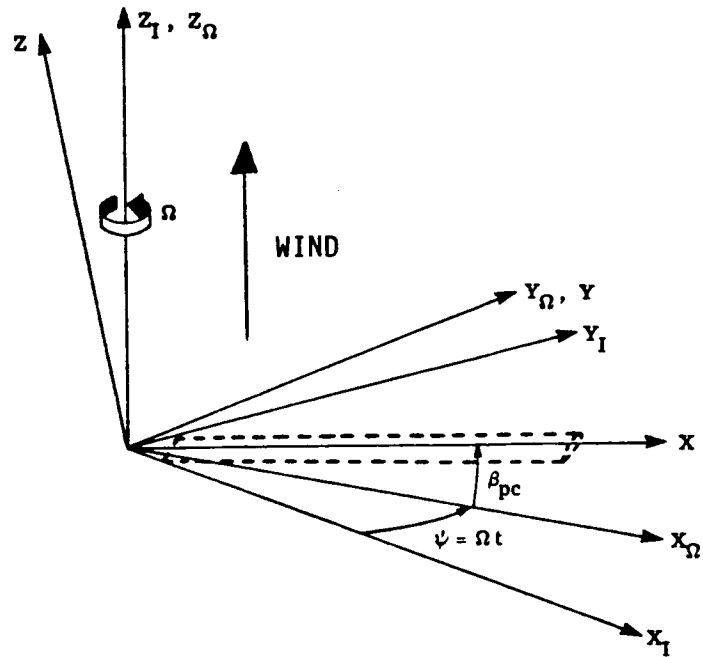
Figure 1. - Coordinate systems of undeformed blade. (Section pitch angle, Θ, not shown.)
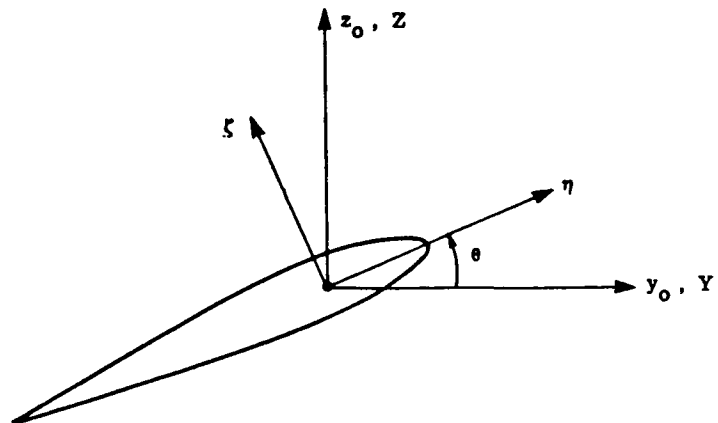

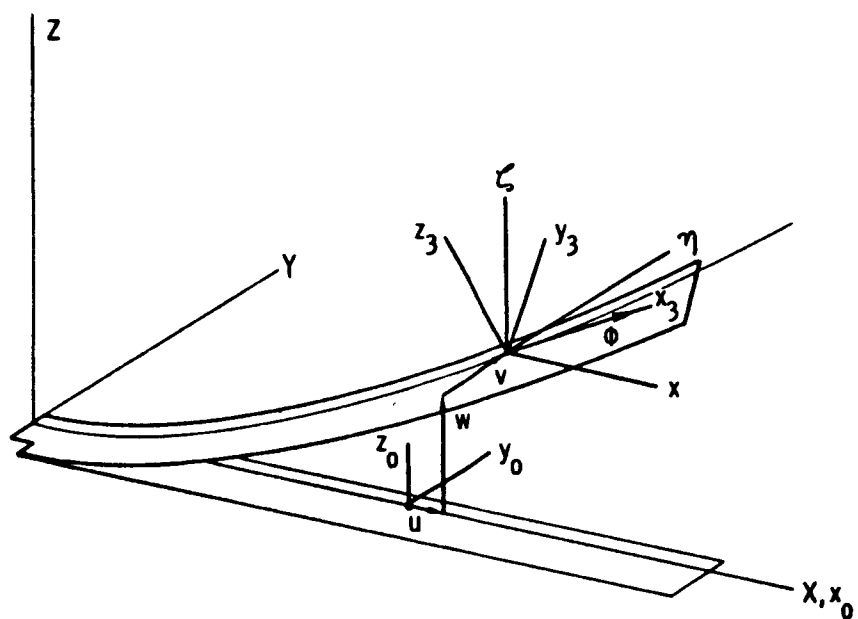Figure 2. - Coordinate systems of blade cross section.

Figure 3. - Schematic representation of undeformed and deformed blade. (Section pitch angle, Θ, not shown.)

69

FLOW FIELD ANALYSIS

William C. Cliff
and
M. Gary Verholek

Battelle Pacific Northwest Laboratories
Richland, Washington 99352

ABSTRACT

The average mean wind speed integrated over a disk is shown to be extremely close to the mean value of wind speed which would be measured at the center of a disk for most geometries in which a WECS (Wind Energy Conversion System) would operate. Field test results are presented which compare instantaneous records of wind speed integrated over a disk with the wind speed measured at the center of the disk. The wind field that a rotating element would experience is presented which has been synthesized from the outputs of an array of anemometers.

INTRODUCTION

At the present time, the Battelle PNL (Pacific Northwest Laboratories) are engaged in attempting to statistically characterize the nominal and extreme wind fields associated with flow over the disk of rotation of WECS systems. This area is presently being addressed experimentally through a field test program as well as by theoretical computations.

In many cases, the only measure of wind speed near a wind turbine may be a single anemometer located at hub height. Questions, with regard to how well wind speed measurements from this single anemometer represent the flow field over the disk of rotation of the wind turbine and how the measurements relate to the wind field a blade element would experience as it rotates, need to be resolved. It is the intent of this paper to examine these questions theoretically and through the use of field data collected from a set of anemometers arranged to describe the swept area of a wind turbine. (See Figure 1.)

MEAN WIND SPEED

In general, the mean wind profile in which a wind turbine operates (neutral atmospheric boundary layer) may be described as follows:

$$\overline{U}_z = \frac{u_*}{k} \ln z/z_0 \tag{1}$$

where $\overline{U}_z$ = the mean wind speed at height z ρ = fluid density

u_* = surface shear velocity = $\sqrt{\tau_w/\rho}$ z = height above grade level

τ_w = surface shear stress z_0 = surface roughness length

k = 0.4

The ratio of the mean wind speed averaged of a disk of rotation of radius R and hub height z_h, $\overline{U}_{z_h,R}$, to the mean wind speed at hub height, $\overline{U}_{z_h}$, could be expressed as:

$$\frac{\overline{U}_{z_h,R}}{\overline{U}_{z_h}} = \frac{2z_0}{\pi R \ln z/z_0} \int_{\frac{z_h - R}{z_0}}^{\frac{z_h + R}{z_0}} \left[\frac{R^2 - z_h^2 + 2z_h z_0 x - z_0^2 x^2}{R^2}\right]^{1/2} \ln x \, dx \quad (2)$$

Table 1 gives some example results using Equation (2) to solve for the ratio of the mean velocity averaged over the disk of rotation to the mean velocity measured at hub height for various blade radii, hub heights and surface roughness.

To estimate the ratio of the mean velocity averaged over the disk of rotation to the mean wind at hub height, the following formula may be used in lieu of Equation (2).

$$\frac{\overline{U}_{z_h,R}}{\overline{U}_{z_h}} \simeq \frac{1}{2R} \left[\frac{(z_h+R)\left[\ln\left(\frac{z_h+R}{z_0}\right) - 1\right] - (z_h-R)\left[\ln\left(\frac{z_h-R}{z_0}\right) - 1\right]}{\ln z_h/z_0}\right] \quad (3)$$

The results obtained from Equation (2) indicate that the average wind speed from a single anemometer at hub height will be representative of the average wind speed over the disk of rotation in almost all cases. However, the instantaneous wind speed measured at the hub will not represent the instantaneous average over the disk of rotation. Averaging over the disk of rotation will act as a low pass filter cutting off much of the high frequency content. The results of a field test program performed at Battelle PNL show the effect of spacial averaging over a disk. A schematic of the field test program is shown in Figure 1.

The field array consists of eight anemometer sets located on the circumference of a circle of radius 12.2 m (40 ft) and an anemometer set at the center of the circle and at a height of 24.4 m (80 ft). The instantaneous array average (simulating the average over a disk of rotation) was computed by arithmetically averaging the instantaneous output from the nine anemometer sets. A 15-second record showing both the array average and hub anemometer output is shown in Figure 2. The array average is much smoother than the single anemometer trace, as is expected. Spectral comparisons of the two traces also show the filtering effect of averaging over an area. That is, the spectral amplitude drops off at a quicker rate for the disk average than for the single anemometer record.

Using the anemometer array depicted in Figure 1, a wind record (simulating the wind field experienced at 12.2 m from the hub by a rotating blade) was synthesized by incrementally sampling the wind records from the anemometers around the circumference of the circle. Each 0.1 second, the wind record was sampled from the next anemometer output.

Thus, each 0.8 second, one complete revolution around the array had occurred. This simulates a rotation rate of 75 rpm. A 15-second synthesized wind record is shown in Figure 3 along with the wind trace taken from the hub anemometer at the same time. The synthesized wind trace shows principally the vertical profile of the wind (temperature measurements indicated neutral conditions).

DISCUSSION

Q. If wind data are available only from a hub-height anemometer, how can the full-disk wind flow field be estimated?

A. In general, the average value of the wind speed over the disk wind flow field is extremely close to the average value at the hub, as shown in Table 1. However, instantaneously, the two will be different. The average over the disk could be simulated by filtering the hub anemometer output with a first-order filter down 3 dB at a frequency of $\bar{U}/D$, where $\bar{U}$ is the mean velocity and D is the diameter of the system. Unfortunately, filtering processes are inherently time-averaging processes which, if used "on line" in a decision loop, have some negative features.

Q. How do the half-power frequency and turbulence factor change between a single anemometer and the total average of all anemometers? How does the energy in the 0.1- to 1-Hz range change by using the average of all anemometers rather than a single anemometer?

A. In most cases, the spacial averaging over the disk of rotation does not significantly decrease the total amount of energy in the spectrum; thus, the half-power point would not change significantly. The changes of the half-power frequency would have to be computed on a case-by-case basis. Obviously, a small disk does not have as large an averaging effect as a large disk.

The region of the spectra greatly affected by spacial averaging is the high-frequency region. For the atmosphere, this would include the range of 0.1 to 1 Hz, the region where most of the energy is lost. Thus, the region from 0.1 to 1 Hz would have significantly less energy when area-averaged over a disk commensurate with a large WECS. Again, the effect would be a function of disk size and height above ground level.

Battelle welcomes all comments and concerns which identify or assist in identifying important wind characteristics associated with WECS design.

1. Formal requests for assistance: Dr. Charles E. Elderkin, Program Manager
   (509) 946-2335

2. Informal discussion of wind characteristics for WECS design:
   Dr. William C. Cliff (509) 942-5066

Battelle, PNL
Department of Atmospheric Sciences
Richland, WA 99352

TABLE I. - RATIO OF MEAN VELOCITY AVERAGED OVER A DISK

OF ROTATION TO MEAN VELOCITY MEASURED

AT HUB HEIGHT

z_h,R	z_0 (meters)[a]			
(meters)	0.005	0.05	0.5	5.0
70:50	0.99	0.99	0.98	0.97
50:30	0.99	0.99	0.99	0.98
15:10	0.99	0.99	0.98	0.97

[a] The terrain features associated with various
surface roughnesses: 0.005 m = smooth
0.05 m = moderate
0.5 m = rough
5.0 m = extremely rough
(town)

74

INSTRUMENT ARRAY FOR
VERTICAL PLANE FIELD PROGRAM

GILL ANEMOMETERS   NO. 1-9
TEMPERATURE PROBES NO. 10-12
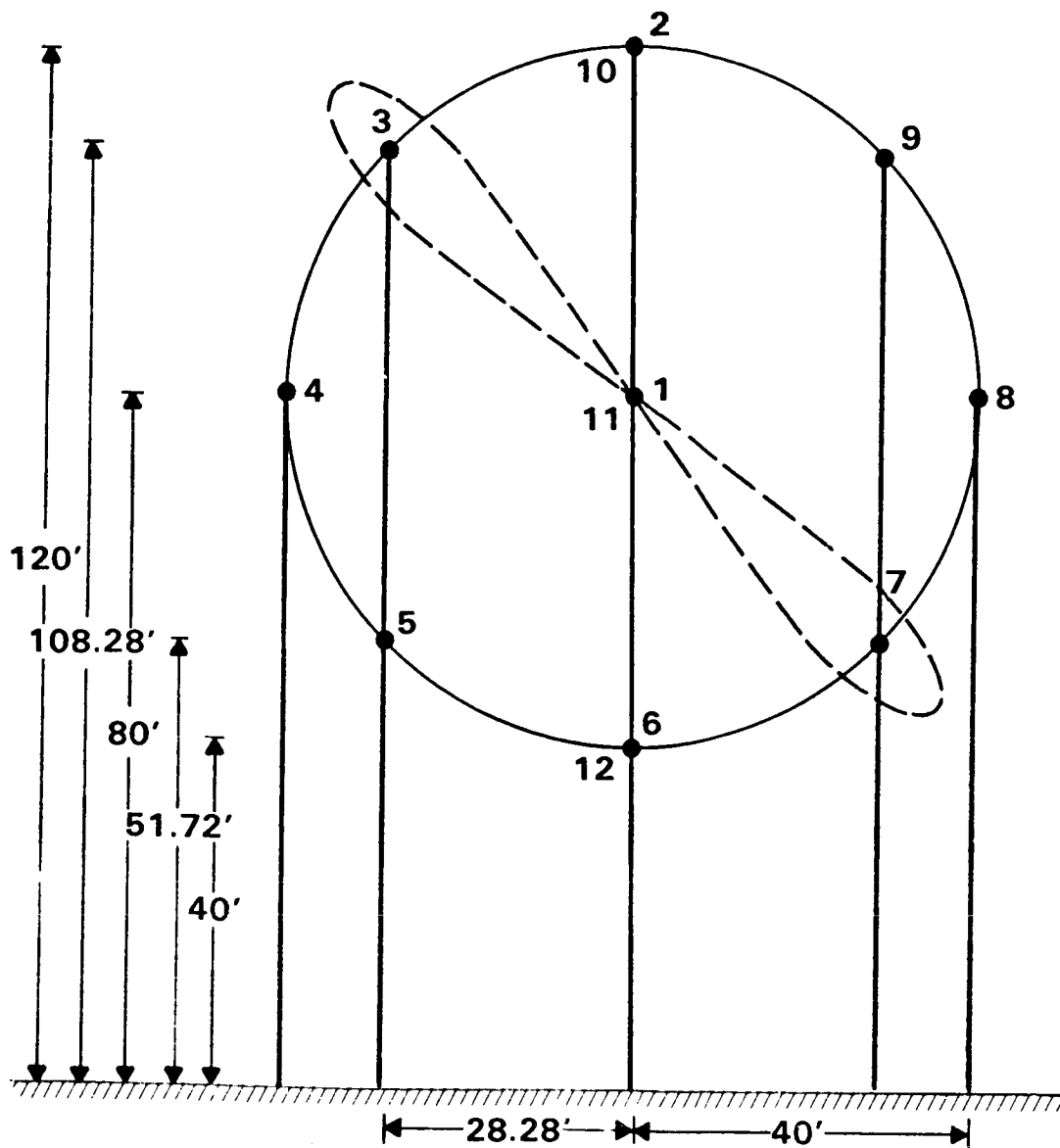
Figure 1. - Field test setup for vertical plane test.
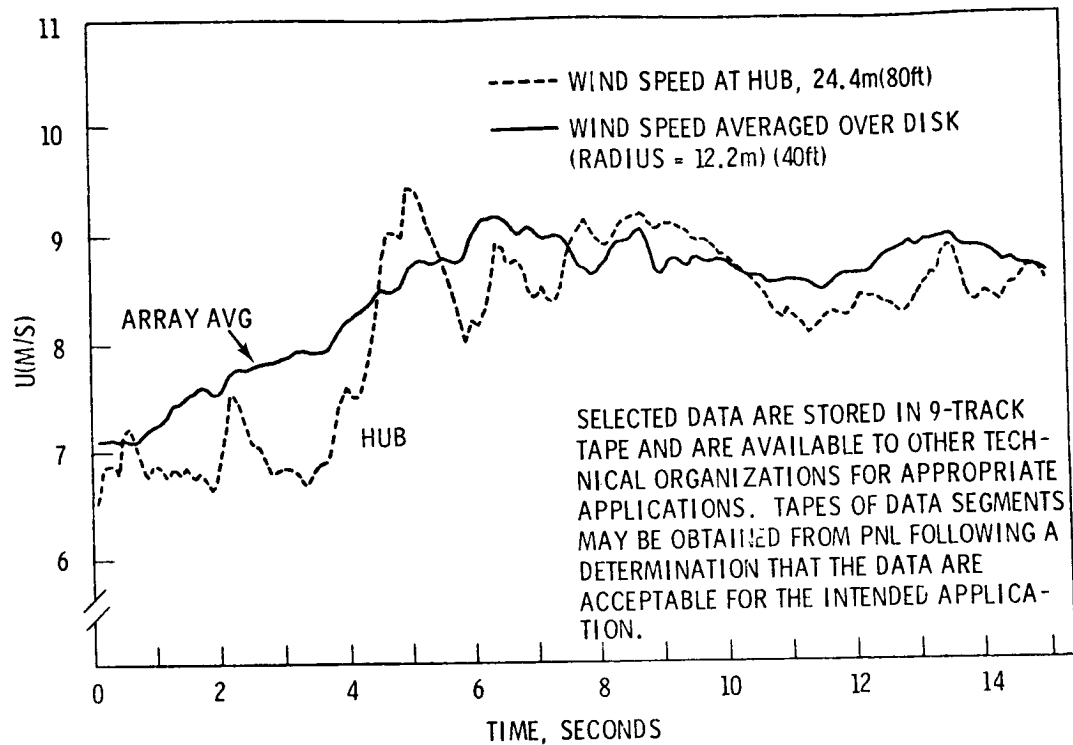
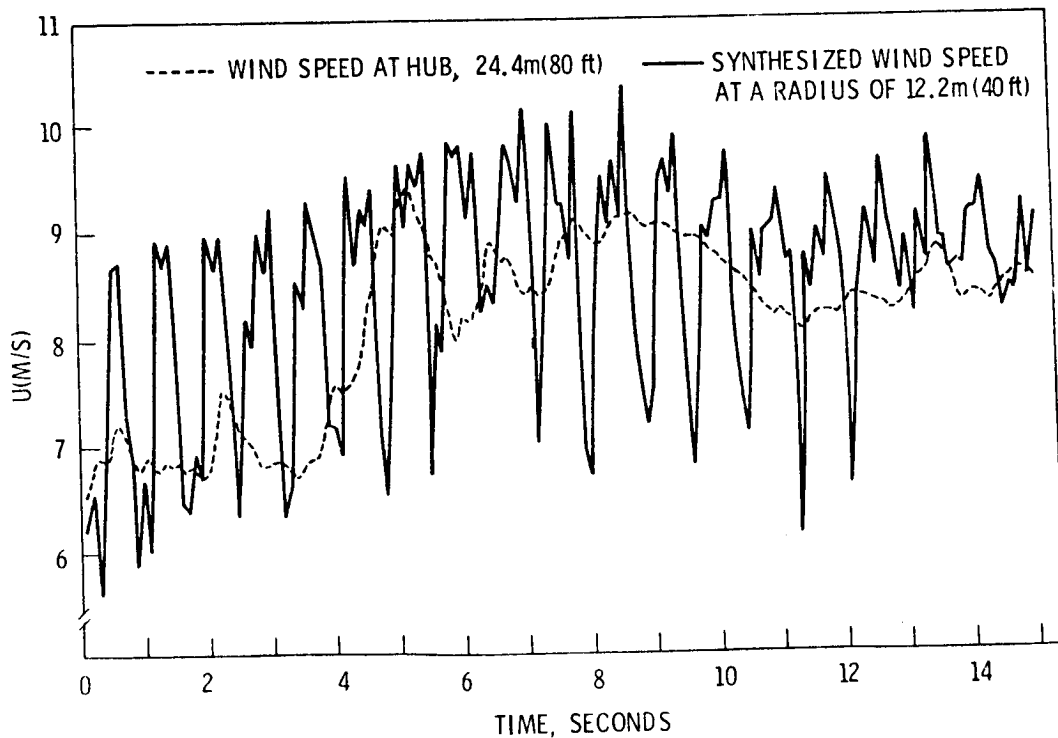Figure 2. - Wind speed at hub versus wind speed averaged over disk.

Figure 3. - Synthesized wind speed versus wind speed at hub.

76

FLUTTER OF DARRIEUS WIND TURBINE BLADES

Norman D. Ham
Department of Aeronautics and Astronautics
Massachusetts Institute of Technology
Cambridge, Mass. 02139

ABSTRACT

The testing of Darrieus wind turbines has indicated that under certain conditions, serious vibrations of the blades can occur, involving flatwise bending, torsion, and chordwise bending. It is the purpose of this paper to develop a theoretical method of predicting the aeroelastic stability of the coupled bending and torsional motion of such blades with a view to determining the cause of these vibrations and a means of suppressing them.

1.   Introduction

The troposkien type of vertical-axis wind turbine, Reference 1, embodies flexible curved blades connected at each end to the top and bottom of a vertical shaft which permits the blades to rotate about the vertical axis under the action of the wind. The curve of each blade is ideally that of a troposkien; i.e., the shape taken by a flexible cable of uniform density and cross section whose ends are attached to two points on a vertical axis, when it is spun at a constant angular velocity about the vertical axis. In this manner the bending stresses in the blades are eliminated.

The testing of such devices has indicated that under certain conditions, serious vibrations of the blades can occur, involving flatwise bending, torsion, and chordwise bending. It is the purpose of this report to develop a theoretical method of predicting the aeroelastic stability of the coupled bending and torsional motion of such blades with a view to determining the cause of these vibrations and a means of suppressing them. The present analysis is an extension of that of Reference 2.

2.   Flatwise Bending Vibration of the Ideal Troposkien

Consider the rotating troposkien-type rotor blade shown in Figure 1. The bending moment at x is given by

$$M(x) = \int_0^x \{[y_o+y(\xi)]\Omega^2 - \ddot{y}(\xi)\} \, m(\xi) \, (x-\xi) \, d\xi - H[y(o) - y(x)]$$

where

Ω = rotor rotational speed

$m(\xi)$ = rotor blade mass at ξ per unit of x-distance

H = blade tension force at mid-point between blade ends

Differentiating the bending moment equation twice with respect to x,

$$\frac{\partial^2 M(x)}{\partial x^2} = [y_o+y(x)] \, \Omega^2 m(x) - \ddot{y}(x) \, m(x) + H \frac{\partial^2 y}{\partial x^2}$$

From the theory of elasticity for the bending of slender beams,

$$M(x) = EI \frac{\partial^2 y}{\partial x^2}$$

Therefore

$$\frac{\partial^2 M(x)}{\partial x^2} = \frac{\partial^2}{\partial x^2} [EI \frac{\partial^2 y}{\partial x^2}]$$

Then the blade bending equation of motion is

$$\frac{\partial^2}{\partial x^2} [EI \frac{\partial^2 y}{\partial x^2}] - H \frac{\partial^2 y}{\partial x^2} - \Omega^2 m(x) \ (y_o + y) + m(x) \ddot{y} = 0 \qquad (1)$$

Note that $m(x) \ dx = m(s) \ ds$, where s = arc length along the blade, and $m(s) = m$, a constant. Then

$$m(x) = m \frac{ds}{dx} = m \ [1 + (\frac{dy}{dx})^2]^{1/2}$$

Equation (1) is the equation of the vibrating blade: the steady-state case is described and solved in Reference 1. For present purposes, consider the equation which results when it is assumed that $y = y(\theta)$:

$$\frac{\partial^2}{\partial \theta^2} [EI \frac{\partial^2 y}{\partial \theta^2} (\frac{\partial \theta}{\partial x})^2] \ (\frac{\partial \theta}{\partial x})^2 - H \frac{\partial^2 y}{\partial \theta^2} (\frac{\partial \theta}{\partial x})^2 - \Omega^2 m(\theta) \ [y_o + y(\theta)] + m(\theta) \ddot{y}(\theta) = 0 \qquad (2)$$

Let $y = \sum_{n=1}^{\infty} Y_n(\theta) \ g_n(t)$

Substituting into Equation (2), there results

$$\frac{\partial^2}{\partial \theta^2} [EI \sum_{n=1}^{\infty} \frac{\partial^2 Y_n}{\partial \theta^2} (\frac{\partial \theta}{\partial x})^2 g_n] \ (\frac{\partial \theta}{\partial x})^2$$

$$-H \sum_{n=1}^{\infty} \frac{\partial^2 Y_n}{\partial \theta^2} (\frac{\partial \theta}{\partial x})^2 g_n - \Omega^2 m \ [y_o + \sum_{n=1}^{\infty} Y_n g_n] + m \sum_{n=1}^{\infty} Y_n \ddot{g}_n = 0 \qquad (3)$$

Assume free vibration of the blade in the nth flatwise mode in a vacuum:

$$g_n = \bar{g}_n e^{i\omega_n t}$$

$$\ddot{g}_n = -\omega_n^2 \bar{g}_n e^{i\omega_n t} = -\omega_n^2 g_n$$

Substituting into the nth term of Equation (3), i.e., the equation for free vibrations in the nth mode,

$$\frac{\partial^2}{\partial\theta^2} \left[EI \frac{\partial^2 y_n}{\partial\theta^2} \left(\frac{\partial\theta}{\partial x}\right)^2 g_n \right] \left(\frac{\partial\theta}{\partial x}\right)^2 - H \frac{\partial^2 y_n}{\partial\theta^2} \left(\frac{\partial\theta}{\partial x}\right)^2 g_n - \Omega^2 m \left[y_0 + y_n g_n \right] = m \omega_n^2 y_n g_n$$

$$(4)$$

Then including all modes, substitute Equation (4) into Equation (3) to obtain

$$m \sum_{n=1}^{\infty} y_n \ddot{g}_n + m \sum_{n=1}^{\infty} \omega_n^2 y_n g_n = 0 \tag{5}$$

This is the equation for flatwise free vibration in a vacuum of the rotating ideal troposkien blade.

3. Flatwise Bending Vibration of the Approximate Troposkien

Reference 3 describes an approximation to the troposkien shape consisting of straight and circular-arc segments. In this instance, the origin of the axis system shown in Figure 1 is located at the center of the circular-arc segment, and the distance y_0 of the origin to the axis of rotation is determined by the geometry of the straight segments.

Reference 4 suggests the following approximate mode shapes for the flatwise vibration of non-rotating circular arcs of radius R with pinned ends:

$$y_n = R \sin \left(\frac{n\pi}{\alpha}\right)\theta \tag{6}$$

This expression was shown in Reference 2 to be an approximate solution to the eigenvalue equation describing the vibration of rotating circular arcs, for the case $\alpha = \pi$ and $y_0 = 0$.

79

The vibration frequencies are given by the expression

$$\omega_n^2 = \omega_{n_o}^2 + K_n \, \Omega^2 \tag{7}$$

where ω_{n_o} and K_n must be determined experimentally, or numerically by finite-element analysis. For the special case of Reference 2, $K_n = n^2 - 1$.

Then Equations (5), (6), (7) describe approximately the flatwise free bending vibration in a vacuum of the circular-arc segment of the rotating approximate troposkien blade.

4. Torsion/Chordwise Bending Vibration of the Approximate Troposkien

Reference 5 considers the torsion/chordwise bending vibration of non-rotating circular arcs. The forces due to rotation are shown in Figure 2. Adding these forces to the equations of Reference 5, in the nomenclature of the present analysis the torsion/chordwise bending equations become, for the circular-arc segment of the approximate troposkien blade,

$$z'^V - R\beta'' - k\,(z'' + R\beta'') = \frac{mR^4}{EI_2}\,(\ddot{z} - z\Omega^2 - 2\Omega\dot{y} - \frac{H}{mR^2}\,z'') \tag{8}$$

$$z'' - R\beta + k(R\beta'' + z'') = 0 \tag{9}$$

where $\beta(\theta)$ = blade torsional displacement

   $z(\theta)$ = blade chordwise bending displacement

   R = radius of circular arc

   k = GK/EI_2

   GK = torsional stiffness of blade section

   EI_2 = chordwise bending stiffness of blade section

   m = rotor blade mass per unit length of blade

Note that flatwise and torsion/chordwise bending are coupled dynamically only by the Coriolis forces $2\Omega\dot{y}m$ and $2\Omega\dot{z}m$.

Let $z = \sum_{n=1}^{\infty} z_n(\theta) \, f_n(t)$

$\beta = \sum_{n=1}^{\infty} \beta_n(\theta) \, f_n(t)$

Substituting into Equation (8), and neglecting the Coriolis coupling term at present, there results

$$\sum_{n=1}^{\infty} z_n^{'V} f_n - R \sum_{n=1}^{\infty} \beta_n^{''} f_n - k \left(\sum_{n=1}^{\infty} z_n^{''} f_n + R \sum_{n=1}^{\infty} \beta_n^{''} f_n \right)$$

$$= \frac{mR^4}{EI_2} \left(\sum_{n=1}^{\infty} z_n \ddot{f}_n - \Omega^2 \sum_{n=1}^{\infty} z_n f_n - \frac{H}{mR^2} \sum_{n=1}^{\infty} z_n^{''} f_n \right) \qquad (10)$$

Assume free vibration of the blade in the nth torsion/chordwise bending mode in a vacuum:

$$f_n = \bar{f}_n \, e^{i\bar{\omega}_n t}$$

$$\ddot{f}_n = -\omega_n^2 \, \bar{f}_n \, e^{i\bar{\omega}_n t} = -\bar{\omega}_n^2 \, f_n$$

Substituting into the nth term of Equation (10), i.e., the equation for free vibrations in the nth mode,

$$\frac{EI_2}{mR^4} \cdot [z_n^{'V} f_n - R\beta_n^{''} f_n - k(z_n^{''} f_n + R\beta_n^{''} f_n)] + \Omega^2 m \, z_n f_n + \frac{H}{R^2} z_n^{''} f_n$$

$$= -m \, z_n \, \omega_n^2 \, f_n \qquad (11)$$

Then including all modes, substitute Equation (11) into Equation (10) to obtain

$$m \sum_{n=1}^{\infty} z_n \ddot{f}_n + m \sum_{n=1}^{\infty} \bar{\omega}_n^2 z_n f_n = 0 \qquad (12)$$

This is the equation for torsion/chordwise free vibration in a vacuum of the rotating approximate troposkien blade, not including Coriolis coupling with flatwise vibration of the blade.

Reference 2 suggests the following approximate mode shapes for the torsion/chordwise bending vibration of non-rotating circular arcs for the case $\alpha = \pi$ and $y_o = 0$:

$$z_n = R \sin n\theta$$

$$\frac{\beta_n}{\bar{C}_n} = \sin n\theta$$

These expressions were shown in Reference 2 to be approximate solutions to the eigenvalue equation describing the vibration of rotating circular arcs. Note that they satisfy only the pinned-end boundary condition, and are therefore even more approximate for other end conditions, such as the elastic restraint of the curved segment by the straight segments of the approximate troposkien blade.

For the case $\alpha \neq \pi$, the following approximate mode shapes will be used, as for the flatwise modes:

$$z_n = R \sin \left(\frac{n\pi}{\alpha}\right)\theta \tag{13}$$

$$\frac{\beta_n}{\bar{C}_n} = \sin \left(\frac{n\pi}{\alpha}\right)\theta \tag{14}$$

The vibration frequencies are given by the expression

$$\bar{\omega}_n^2 = \bar{\omega}_{n_o}^2 + \bar{K}_n \Omega^2 \tag{15}$$

where $\bar{\omega}_{n_o}$ and $\bar{K}_n$ must be determined experimentally, or numerically by finite-element analysis. For the special case of Reference 2, $\bar{K}_n = n^2 - 1$.

Then Equations (12), (13), and (14) describe approximately the torsion/chordwise bending free vibration in a vacuum of the circular-arc segment of the rotating approximate troposkien blade.

Note that Equation (9) expresses the structural coupling between torsion and chordwise bending of the circular arc. Substitution of Equations (13) and (14) into Equation (9) yields the nth mode structural coupling coefficient for circular arcs having pinned ends,

$$C_n = \frac{R\beta_n}{z_n} = - \left(\frac{n\pi}{\alpha}\right)^2 \frac{1+k}{1+k\left(\frac{n\pi}{\alpha}\right)^2} \tag{16}$$

This approximate relation was investigated experimentally in Reference 6 and found to be valid for the troposkien blade with pinned ends for the case $n = 2$, if an effective value $\alpha_{eff} = 2.8$ is used to account for the flexibility of the straight segments of the blade.

For the case of clamped ends, the approximate nth mode structural coupling coefficient for circular arcs with clamped ends is shown in Reference 6 to be

$$C_n = \left[\frac{0.75}{\sin^2\left(\frac{n\pi}{\alpha}\right)\theta} - 2.25\right] \left(\frac{n\pi}{\alpha}\right)^2 \frac{1+k}{1+k\left(\frac{n\pi}{\alpha}\right)^2}$$

where the effective value $\alpha_{eff} = 2.8$ again applies.

Equation (16) is believed to be a reasonable approximation for the structural coupling coefficient of practical blade configurations in the absence of a more precise determination by finite element analysis of the blade.

5.   Blade Flutter Equations

Adding the Coriolis forces due to blade bending, and the blade aerodynamic lift force, as shown in Figures 2 and 3, Equations (5) and (12) become

$$\sum_{n=1}^{\infty} m \, y_n \, \ddot{g}_n + \sum_{n=1}^{\infty} m \, \omega_n^2 \, y_n \, q_n + \sum_{n=1}^{\infty} 2m\Omega \, z_n \, \dot{f}_n = \frac{1}{R} \frac{dL}{d\theta} \sin\delta \tag{17}$$

$$-\sum_{n=1}^{\infty} 2m\Omega \, y_n \, \dot{g}_n + \sum_{n=1}^{\infty} m \, z_n \, \ddot{f}_n + \sum_{n=1}^{\infty} m \, \bar{\omega}_n^2 \, z_n \, f_n = 0 \tag{18}$$

where chordwise aerodynamic forces are neglected.

Using Equations (6) and (13), multiplying Equations (17) and (18) by $R \sin(\frac{n\pi}{\alpha})\theta$, and integrating from 0 to α, the coupled equations of motion in the nth mode are obtained:

$$I_n \ddot{g}_n + I_n \omega_n^2 g_n + 2I_n \Omega \dot{f}_n = \int_0^\alpha \sin\delta \, \sin(\frac{n\pi}{\alpha})\theta \, \frac{dL}{d\theta} \, d\theta \qquad (19)$$

$$-2I_n \Omega \dot{g}_n + I_n \ddot{f}_n + I_n \bar{\omega}_n^2 f_n = 0 \qquad (20)$$

where $\quad I_n = \int_0^\alpha m \, R^2 \, \sin^2(\frac{n\pi}{\alpha})\theta \, d\theta$

and noting that $\quad \int_0^\alpha \sin(\frac{n\pi}{\alpha})\theta \, \sin(\frac{m\pi}{\alpha})\theta \, d\theta = 0$.

Following Reference 7 and Figure 3, the aerodynamic lift for the wind turbine rotating in <u>still</u> air at constant rotational speed Ω is

$$\frac{1}{R}\frac{dL}{d\theta} = -\frac{1}{8}\rho a c^2 \, \Omega y_1 \dot{\beta} - \frac{1}{2}\rho a c \Omega y_1 C(k) \, [\dot{y} \, \sin\delta + \Omega y_1 \beta + (0.5c - x_A)\dot{\beta}]$$

where ρ = air density

  a = blade section lift curve slope

  c = blade chord

  β = blade twist angle (postive nose down) (see Fig. 2)

  y_1 = outer blade undisturbed shape = $y_0 + R \sin\delta$

  C(k) = Theodorsen's lift deficiency function

  x_A = distance from section aerodynamic center to blade elastic

    axis, positive when A.C. is forward.

Neglecting the $\dot{\beta}$ terms since c << R, multiplying by $R \sin(\frac{n\pi}{\alpha})\theta$ and dividing $I_n \Omega^2$, there results

84

$$\frac{1}{I_n \Omega^2} \int_0^\pi \sin\delta \, \sin(\frac{n\pi}{\alpha})\theta \, \frac{dL}{d\theta} \, d\theta = - m_{\dot{g}}\dot{g}_n - m_\beta C_n f_n$$

where $C_n = \dfrac{R\beta_n}{z_n}$ as before.

Then

$$m_{\dot{g}} = \frac{\gamma}{2} \, \overline{C(k)} \, \frac{\int_0^\alpha (y_o/R + \sin\delta) \sin^2\delta \, \sin^2(\frac{n\pi}{\alpha})\theta \, d\theta}{\int_0^\alpha \sin^2(\frac{n\pi}{\alpha})\theta \, d\theta}$$

$$m_\beta = \frac{\gamma}{2} \, \overline{C(k)} \, \frac{\int_0^\alpha (y_o/R + \sin\delta)^2 \sin\delta \, \sin^2(\frac{n\pi}{\alpha})\theta \, d\theta}{\int_0^\alpha \sin^2(\frac{n\pi}{\alpha})\theta \, d\theta}$$

where $\gamma = \dfrac{\rho acR}{m}$

$\overline{C(k)}$ = typical value of $C(k)$ evaluated at $y_1 = y_o + R \sin\bar{\delta}$ (see Appendix),

and the contributions of modes other than the nth are neglected.

Dividing Equations (23) and (24) by $I_n \Omega^2$ and including the aerodynamic terms,

$$\frac{\ddot{g}_n}{\Omega^2} + m_{\dot{g}} \frac{\dot{g}_n}{\Omega} + \nu_n^2 g_n + 2\frac{\dot{f}_n}{\Omega} + m_\beta C_n f_n = 0 \tag{21}$$

$$- 2\frac{\dot{g}_n}{\Omega} + \frac{\ddot{f}_n}{\Omega^2} + \bar{\nu}_n^2 f_n = 0 \tag{22}$$

where $\nu_n = \dfrac{\omega_n}{\Omega} = [(\dfrac{\omega_{n_o}}{\Omega})^2 + K_n]^{1/2}$

$\bar{\nu}_n = \dfrac{\bar{\omega}_n}{\Omega} = [(\dfrac{\bar{\omega}_{n_o}}{\Omega})^2 + \bar{K}_n]^{1/2}$

These are the flutter equations for the wind turbine rotating in still air.

5.   Calculation of Flutter Boundaries

Assume the following solutions to Equations (21) and (22):

$$g_n = \bar{g}_n \, e^{\nu \Omega t} \tag{23}$$

$$f_n = \bar{f}_n \, e^{\nu \Omega t} \tag{24}$$

where $\nu = \dfrac{\sigma}{\Omega} + i \, \dfrac{\omega}{\Omega}$. Assume at present that $\overline{C(k)} = 1$.

Substitution of Equations (23) and (24) in Equations (21) and (22) results in two coupled homogeneous algebraic equations. For a solution to exist, the determinant of coefficients must vanish; i.e.,

$$\begin{vmatrix} (\nu^2 + m_g \nu + \nu_n^2) & (2\nu + m_\beta C_n) \\[2mm] -2\nu & [\nu^2 + \bar{\nu}_n^2] \end{vmatrix} = 0$$

Expanding the determinant yields the characteristic equation of the system:

$$A\nu^4 + B\nu^3 + C\nu^2 + D\nu + E = 0$$

where the coefficients are combinations of the system parameters. Then by Routh's criteria for system stability

$$A, \ B, \ C, \ D, \ E \geq 0 \tag{25}$$

and

$$BCD - AD^2 - B^2 E \geq 0 \tag{26}$$

It is now possible to determine the values of $\bar{\nu}_n^2$ required to satisfy conditions (25) and (26) for a given blade configuration. Since

$$\nu_n^2 = \left(\frac{\omega_{n_o}}{\Omega}\right)^2 + K_n$$

and
$$\bar{\nu}_n^2 = \left(\frac{\bar{\omega}_{n_o}}{\Omega}\right)^2 + \bar{K}_n$$

the values of rotational speed at which flutter or divergence will occur (Ω_F) are then specified for given non-rotating flatwise and torsional frequencies ω_{n_o} and $\bar{\omega}_{n_o}$.

In the present case, the characteristic equation is

$$\nu^4 + m_{\dot{g}}\nu^3 + (4 + \nu_n^2 + \bar{\nu}_n^2)\nu^2 + (m_{\dot{g}}\bar{\nu}_n^2 + 2m_\beta C_n)\nu + \nu_n^2 \bar{\nu}_n^2 = 0$$

Then conditions (25) and (26) determine the rotational speed at flutter, Ω_F.

Applying condition (25), flutter occurs when

$$\bar{\nu}_n^2 = -2\frac{m_\beta}{m_{\dot{g}}} C_n \tag{27}$$

Applying condition (26), flutter occurs when

$$\bar{\nu}_n^2 = \frac{2m_\beta^2 C_n^2 - 4m_\beta m_{\dot{g}} C_n - m_\beta m_{\dot{g}} C_n \nu_n^2}{2m_{\dot{g}}^2 - m_\beta m_{\dot{g}} C_n} \tag{28}$$

6.   Application to an Existing Blade

The theory developed above is now applied to the preliminary prediction of the flutter of the blades of the Sandia seventeen-meter wind turbine. For this turbine the parameters for the geometry of the circular arc portion of the blade are

$$y_o = 9.10 \text{ ft.}$$
$$R = 18.33 \text{ ft.}$$
$$\alpha = 2 \text{ rad.}$$

For this case it can be shown that $m_\beta \approx 1.575 m_{\dot{g}}$ Also from Equation (16) for $n = 2$, $k = .0512$, $\alpha_{eff} = 2.8$ (Ref. 6):

$$C_n = -4.2$$

87

Applying Equation (27), flutter occurs when

$$\bar{\nu}_n^2 = 13.2$$

From Reference (8), for the seventeen-meter blade,

$$\bar{\nu}_2^2 = (\frac{324}{\Omega_F})^2 + 7.70$$

Equating and solving the two expressions for $\bar{\nu}_2^2$,

$$\Omega_F = 138 \text{ rpm}$$

Applying Equation (28) flutter occurs when

$$\bar{\nu}_2^2 = 13.2 + 0.768 \, \nu_2^2$$

From Reference (8), for the seventeen-meter blade,

$$\nu_2^2 = (\frac{215}{\Omega_F})^2 + 6.76$$

Then
$$\bar{\nu}_2^2 = 18.4 + 0.768 \, (\frac{215}{\Omega_F})^2$$

Equating and solving the two expressions for $\bar{\nu}_2^2$,

$$\Omega_F = 80.4 \text{ rpm}$$

Here Equation (28) is evidently the critical case.

Final prediction of the flutter speed requires accurate determination of the structural coupling coefficient C_n by finite element analysis.

7.   Conclusions

(1) Coriolis forces provide the dominant coupling between flatwise bending and torsion/chordwise bending of the blade. (Also see Reference 2).

(2) Blade flatwise bending velocity and blade torsional displacement contribute the dominant aerodynamic forces acting on the blade.

(3) Accurate determination of the structural coupling between blade
torsion and blade chordwise bending is essential to blade flutter
prediction.

(4) The following parameters determine the rotational speed at flutter
for troposkien-type blades:

(a) blade geometry y_o, R, α (see Figure 1).

(b) blade torsion/chordwise bending structural coupling coefficient
C_2 for the second mode.

(c) blade rotating and non-rotating flatwise bending frequencies
ω_2 and ω_{2_o} for the second mode.

(d) blade rotating and non-rotating torsion/chordwise bending
frequencies $\bar{\omega}_2$ and $\bar{\omega}_{2_o}$ for the second mode.

REFERENCES

1. Blackwell, B.F. and Reis, G.E., "Blade Shape for a Troposkien Type of
Vertical-Axis Wind Turbine", Sandia Laboratories Report SAND 74-0154,
April 1974.

2. Ham, N.D., "Aeroelastic Analysis of the Troposkien-Type Wind Turbine",
Sandia Laboratories Report SAND 77-0026, April 1977.

3. Reis, G.E. and Blackwell, B.F., "Practical Approximations to a Troposkien
by Straight-Line and Circular-Arc Segments", Sandia Laboratories Report
SAND 74-0100, March 1975.

4. Den Hartog, J.P., "The Lowest Natural Frequency of Circular Arcs", Phil.
Mag. 5 (Series 7), 400, 1928.

5. Ojalvo, I.U., "Coupled Twist-Bending Vibrations of Incomplete Elastic
Rings", International Journal of Mechanical Sciences, 4, pp. 53-72, 1962.

6. Ham, N.D., "An Investigation of the Structural Coupling Coefficient and Torsional Frequency of Troposkien-Type Wind Turbine Blades with Application to Blade Flutter Prediction", Sandia Laboratories Report in preparation, 1977.

7. Miller, R.H. and Ellis, C.W., "Blade Vibration and Flutter", Journal of the American Helicopter Society, 1, 3, July 1956.

8. Barzda, J., Kaman Aerospace Corp., Bloomfield, Conn., unpublished communication.

DISCUSSION

Comment: I would like to reemphasize the significance of Professor Ham's conclusions that a) quarter-chord mass balancing of the turbine blades is unimportant with regard to flutter speed location, and b) increasing torsional stiffness is an effective method of increasing flutter speed. The impact of the first conclusion on design and fabrication of low cost blades is very favorable, and knowledge of the second conclusion is valuable to the designer. At the same time, I would like to de-emphasize the threat of encountering flutter in any particular blade design. Based on Professor Ham's analysis, blade property evaluation, field experience, and consultation with fabricators, it is relatively easy to design a blade that will not flutter.

Q: Do you agree with R. Reuter that it is relatively easy to design Darrieus blades which do not flutter in their operating regime?

A: Yes.

Q: Am I correct in presuming that the forced response to periodic stalling should also be independent of the chordwise c.g. of the blade sections, and also of the chordwise shear center?

A: Yes.

Q: What were your assumptions relative to the aerodynamics; was the free stream velocity zero? If not what of the resultant periodic coefficient?

A: In the analysis the free stream velocity was assumed to be zero. If this were not so, harmonic airloads would be generated and would cause a forced blade response at various integral multiples of rotor speed. However, in a linear analysis, this forced response is uncoupled with any self-excited motion such as flutter. Experimentally, model blade flutter occurred at the same rotor rotational speed whether or not there was an incident wind.
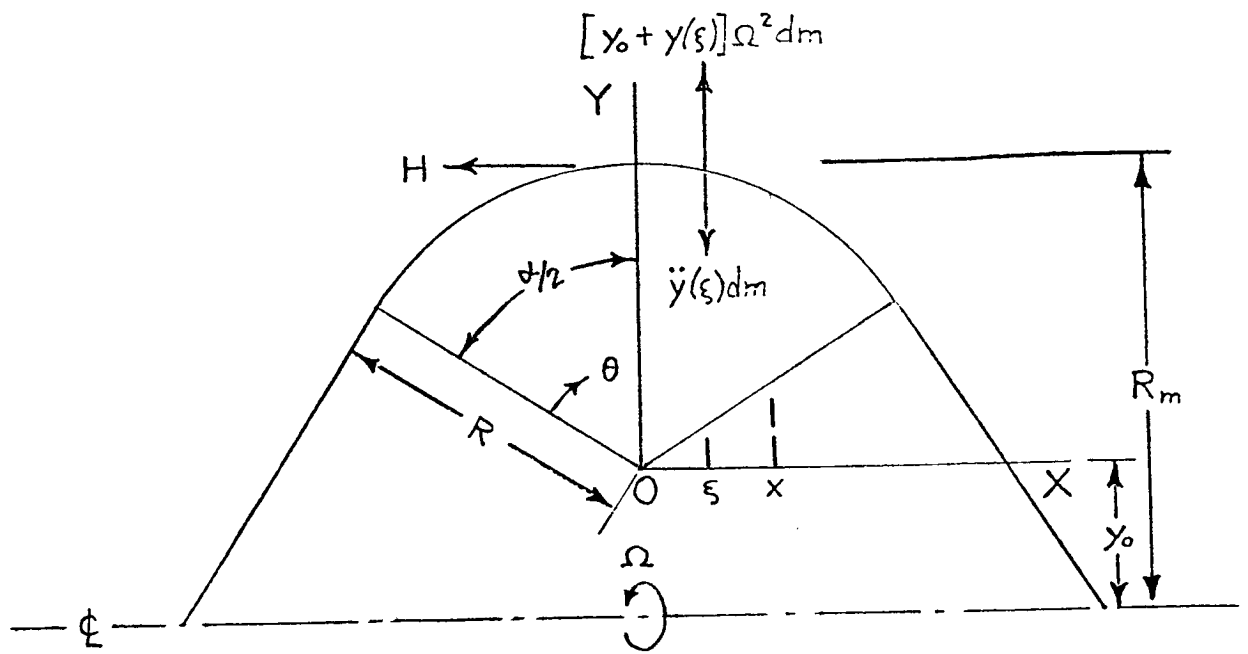
Figure 1. – Blade geometry.
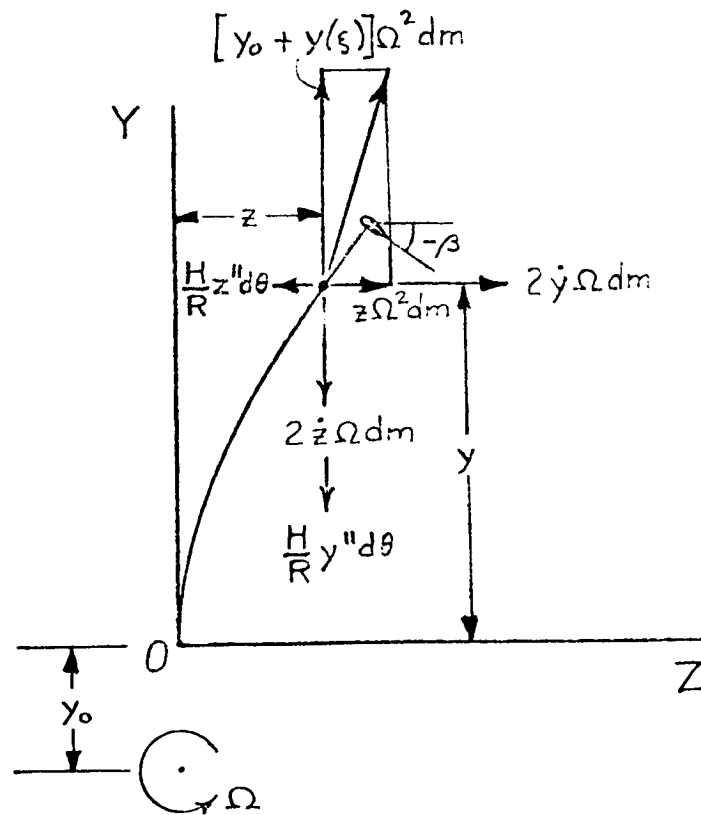
Figure 2. – Blade dynamics.

92
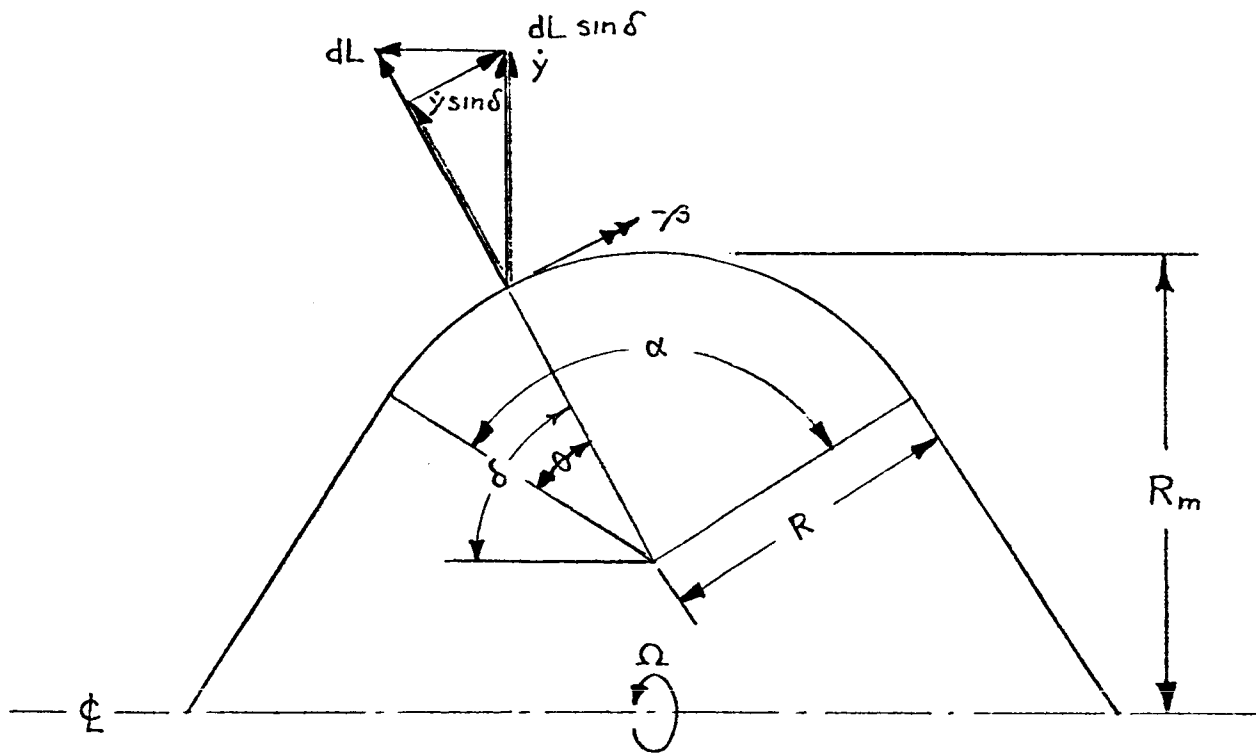
Figure 3. – Blade aerodynamics.

ANALYTICAL TESTING TECHNIQUES

Robert Jones

Kaman Aerospace Corporation
Bloomfield, Connecticut 06002

ABSTRACT

Structural Dynamic Analytical Testing Techniques can be a tool to determine the source of structural dynamic problems and the solution to these problems. Analytical testing techniques are based upon new and unique dynamic testing methods and analysis of test results. Thus, these methods apply primarily to constructed wind turbine systems. This paper gives a summary of these methods.

INTRODUCTION

Kaman Aerospace Corporation, for the past several years, has been doing research on structural dynamic analytical testing techniques. This research has been sponsored by the Army, NASA, and in-house, and has consisted of computer experiments, laboratory testing of a beam, laboratory testing of a helicopter dynamic model and full scale testing of an AH-1G helicopter. This research has led to new testing techniques that for helicopters, which can be applied to wind turbine systems, can eliminate moment shaking of the hub, allows for on-site checking of the test data, allows for the use of small shakers since near resonant testing is done, and allows for ease of shaker location. This research has also led to new methods of data analysis which can be used to predict system response from component testing, obtain equation of motion from test data, determine the best location of a structural change to improve the operating condition response, and determine the force and moment from the rotor. Although this research has been done primarily for helicopter testing, these techniques can be used in the development of wind turbine systems.

ANALYTICAL TESTING TECHNIQUES

Single Point Shaking

Single point shaking is a test technique that requires shaking the structure at a point of high response. For a helicopter, this could be at the nose or tail location as shown in Figure 1. For wind turbine systems, this would be near the top of the tower. However, it does not necessarily have to be at the point of force and moment input such as at the hub of the wind turbine system. As shown in Figure 1, the accelerometers and force must be recorded and analyzed to obtain the real and imaginary acceleration mobility. This data, then, can be analyzed to obtain the undamped natural frequencies, structural damping, and modal acceleration parameters. With these parameters

a complete mobility matrix can be obtained and response of the system determined as if shaken at any pick up location of the structure.

Figure 2a illustrates this, in that testing was done on a beam in which the transfer mobility at Station 25 was obtained by shaking at Station 72.5. Identification of the structure was made from data obtained with the force at Station 72.5. Figure 2b shows the transfer mobility at Station 25 for shaking at Station 72.5 and the identification of the structure was made from data obtained with the force at Station 0.5. It is seen from this figure that excellent correlation was obtained from the identification procedure, in that the system response was predicted from data obtained at another shake point. A complete mobility matrix was obtained by shaking at only one point.

This single point shaking simplifies the shaking procedure, in that small shakers can be used because data near resonance is required and a point of high response is required. Shaker location can be selected for convenience rather than the point of force input to the structure.

Force Determination

Data obtained from the shake test can be analyzed to predict system response from component testing, to determine the best location on a structure for an impedance change, to determine the equation of motion of the structure, and to determine the magnitudes of excitation forces and moments. All of these methods of analyzing the test data can be applied to wind turbine systems. However, this paper will concentrate on force determination.

One of the major problems in helicopter development and field maintainability is high level low frequency vibration. The source of these vibration problems is usually the force and moment input from the main rotor. However, the magnitude of these forces and moments are usually unknown. Therefore, research on force determination has been sponsored primarily by Applied Technology Laboratory, U. S. Army Research and Technology Laboratories (AVRADCOM). This research is presently being conducted on an Army furnished AH-1G helicopter.

The magnitudes of the forces and moments inputs to any structure can be calculated from the following relationship:

$$\{\ddot{y}\} = [\ddot{Y}] \quad \{f\}$$
$$N\times1 \quad N\times6 \quad 6\times1$$

where $\{\ddot{y}\}$ is the matrix of accelerations in the fuselage or structure which are measured with the system operating, $[\ddot{Y}]$ is the acceleration mobility matrix which is obtained in the shake test of the fuselage or tower, and $\{f\}$ is the three force and three moment hub excitation matrix. N is the number of locations of accelerometers in this fuselage or structure.

96

The procedure for force determination would then be to shake the structure and obtain the mobility matrix of the structure at the points of force input. Then obtain the acceleration response of the system under actual operating conditions. With these two results, the rotor forces and moments can be obtained.

For example, for the wind turbine system, the tower without the rotor as shown in Figure 3 should be shaken.

The tower can be shaken directly at the hub in the direction of the three forces and three moments and the required mobility matrix obtained directly or the tower can be shaken at a point of high response (single point shaking) and the mobility matrix constructed. The tower should be shaken without the rotor, since the forces and moments to be determined are those that would be acting at the rotor shaft and will include the inertia effects of the rotor.

The rotor of the wind turbine system should be shaken as a free-free system and the driving point acceleration mobility versus frequency obtained, as shown in Figure 4. From this data, the natural frequencies of the blade as a cantilever and as a free-free system can be obtained. The antiresonant frequencies of the real acceleration mobility are the cantilever modes and the natural frequencies of the acceleration mobility are the free-free natural frequencies of the system. For large wind turbine systems, in which rotor rpm is very low, the frequencies obtained in test will be essentially the frequencies of the rotor since centrifugal stiffening is negligible. Therefore, when installed on the system, the natural frequency of the rotor will be between the cantilever frequency and the free-free system since that cantilever frequency is for infinite hub impedance and the free-free frequency is for a zero hub impedance.

It must be remembered that the rotor mobility data is effectively in the rotating system. By converting this test data to fixed system test data and combining with the tower shake test data, complete system response can be obtained.

Therefore, by shaking the blade and tower in this manner, the forces and moments of the rotor can be obtained. Knowing these forces and moments will permit better correlation with rotor loads programs, as well as determine the problem areas in the rotor that are the source of large vibration in the tower structure.

Further, by shaking the tower and rotor by this procedure, the complete response versus frequency of the system can be determined and the magnitude and location of an impedance change on the structure to improve the response can be determined.

Also, if required, equations of motion of the system can be determined from the test results and correlated with the finite element model.

DISCUSSION

Q. When coupling rotor and tower, did you use two blades?

A. This is a suggested procedure for shake testing a wind turbine system. I have not combined test rotor test results with hub test results.

Q. Do you have a way of determining the collective edgewise mode including the on-line generator?

A. I have no way of determining that mode from test results. However, calculating the impedance of the on-line generator and combining with the test results of the rotor could give a good estimate of that mode.

Q. Would you not get (determine) the power coming from the rotor, to the nacelle independently of the characteristics of the rotor, i.e., independent of the number of blades, the periodic coefficients effects, etc.?

A. Force determination does not depend on the type of rotor system or number of blades. Therefore, the vibratory forces and moments would be obtained for any rotor system. Thinking of power as a steady term, the theory could be extended to include steady forces.

Q. Briefly explain how we would proceed if we wished to apply this technique to the Mod-0 WTG, for example?

A. I would remove the rotor and shake the tower using additional accelerometers, approximately thirty, and obtain mobility versus frequency for all these pickups and analyze this data to determine damping and natural frequencies and obtain hub mobility data to use for force determination.

I would shake the rotor as a free-free system and obtain driving point mobility versus frequency of the rotor and determine cantilever and free-free natural frequencies.

This data is now useful for either an upwind or downwind system. Reassemble the system, and obtaining acceleration data under actual operation, rotor forces and moments can be obtained.
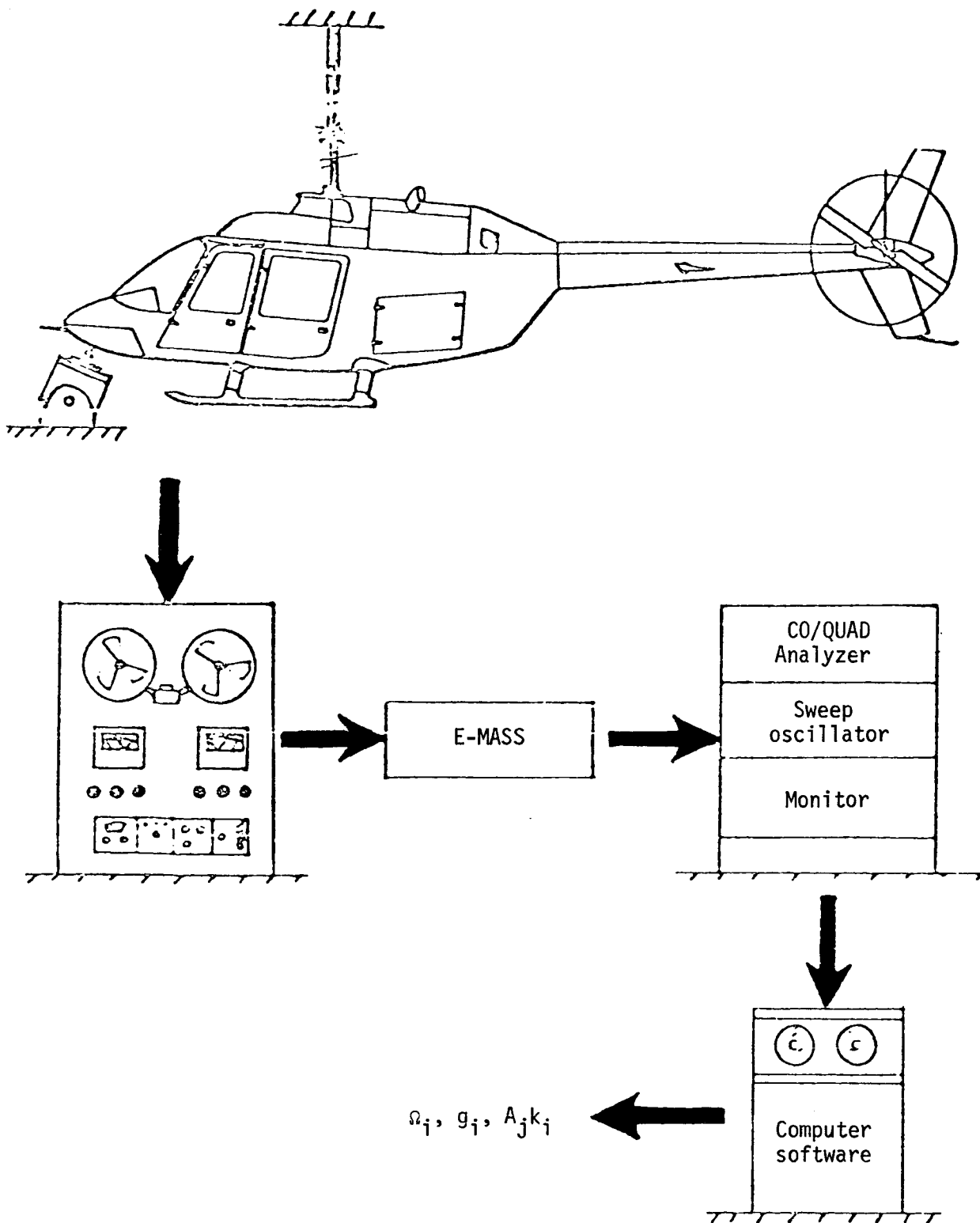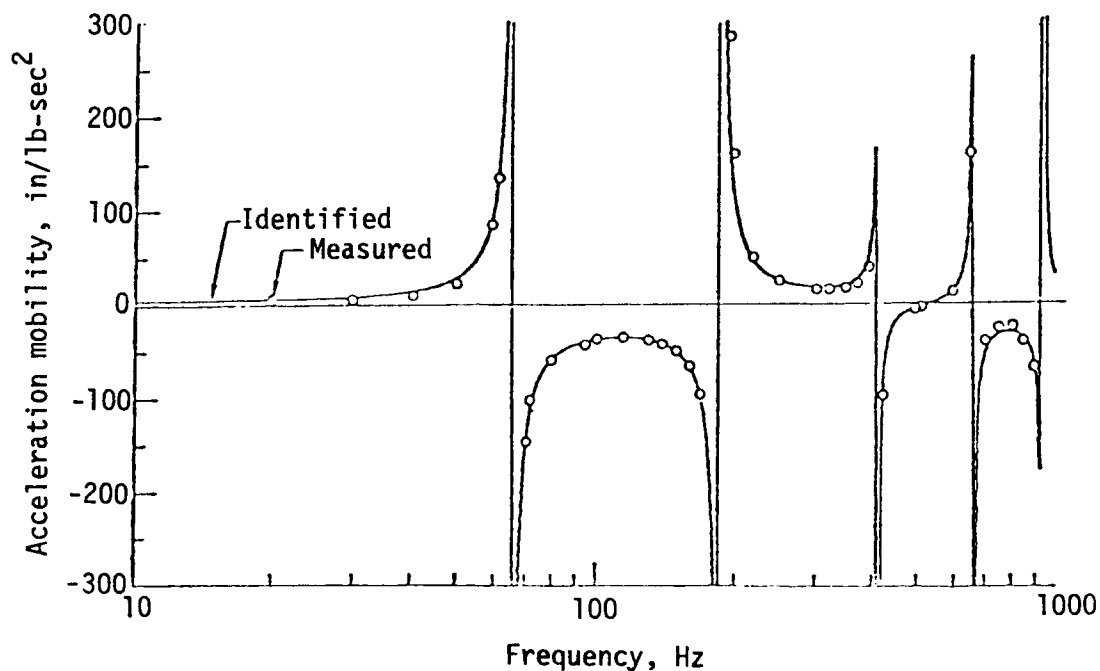
Figure 1. - Analytical testing.
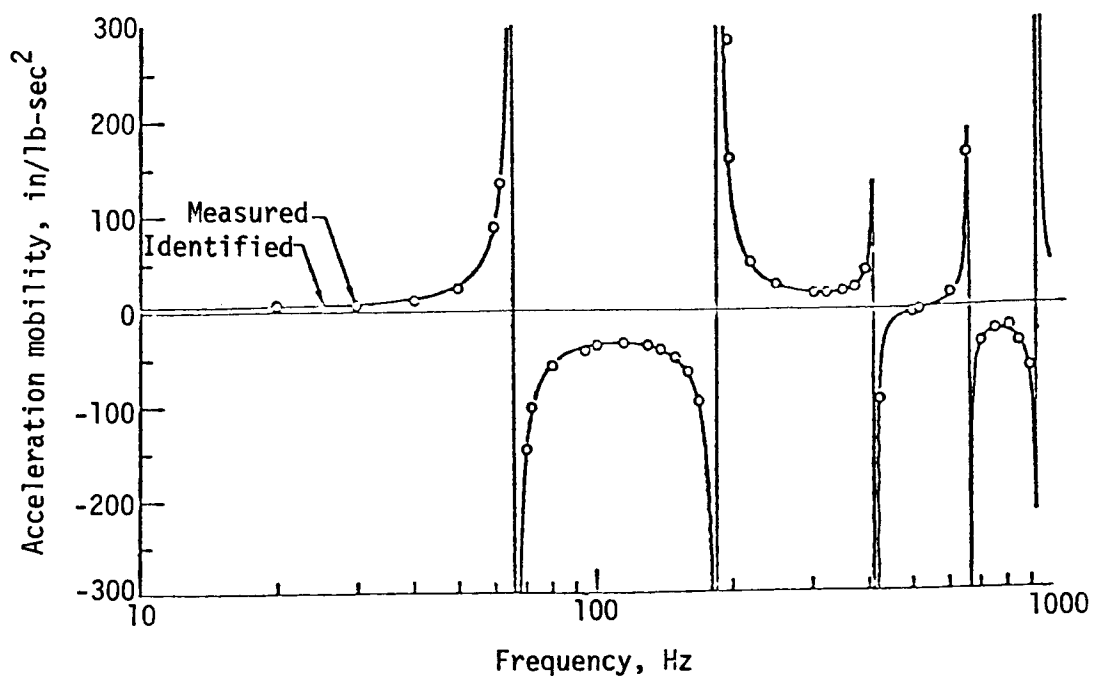
(a) Identification made from data obtained with force at 72.5-inch station.

(b) Identification made from data obtained with force at 0.5-inch station.

Figure 2. - Acceleration mobility for response at 25-inch station and force at 72.5-inch station.
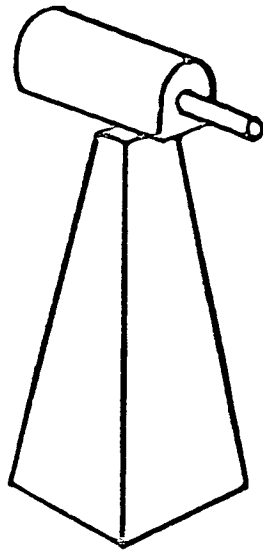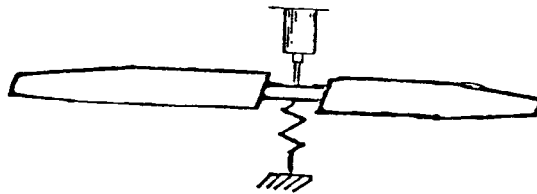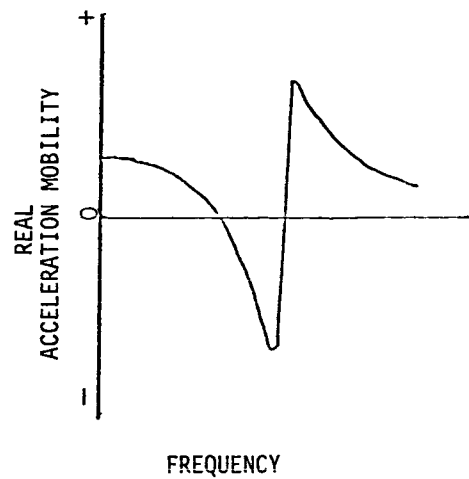
100

Figure 3. - Structural dynamic testing of
tower and rotor (mobility of tower
versus frequency).

(a) Test setup.

(b) Mobility.

Figure 4. - Rotor shake test.

INFLUENCE OF WIND TURBINE FOUNDATION

Suey T. Yee

National Aeronautics and Space Administration
Lewis Research Center
Cleveland, Ohio 44135

ABSTRACT

The 200 kw Mod-OA wind turbine was modeled using a 3 lumped mass-spring system for the superstructure and a rotational spring for the foundation and supporting soil. Natural frequencies were calculated using soil elastic moduli varying from 3000 to 22,400 p.s.i. The reduction in natural frequencies from the rigid foundation case ranged up to 20 percent.

INTRODUCTION

The foundation of the Mod-O wind turbine was designed for the static loads only (including wind). Caissons reaching down to hard shale support the tower. This allowed us to assume infinite rigidity of the system at the tower base in any natural frequency calculations. Subsequent field measurements taken on the tower verified the validity of this assumption.

When it was decided to upgrade the Mod-O to 200 kw and duplicate it at other sites, we were concerned about the design of the foundation for two reasons:

° The sites for the Mod-OA were unknown and thus the soil conditions were unknown.

° A computer program for a vibration systems analysis would not be ready for use in time for design.

MOD-OA FOUNDATIONS

We decided to make a parametric study of the Mod-OA foundation vibrations using the soil modulus as a variable. Dr. Paul Chang, et al. of Akron University made this study. Figures 1 to 5 summarize the significant features of this study, including the geometry of the structure, the mathematical model, and the primary results.

103

A square mat foundation for the tower was chosen for several reasons:

° The rocking mode is probably the dominant mode of tower-foundation vibration and large dimensions in plan view are optimum for resisting this type of vibration.

° Excavation and forming for the foundation are relatively simple. This is an important factor in remote areas.

° For a given cost you can probably get the largest concrete mass in a mat foundation which is of course advantageous for the vibration as well as the static loads.

° Since the foundation thickness is small and the plan dimensions are only slightly larger than the tower footprint, the use of the foundation could be universal; that is, wherever the tower could fit dimensionally, the foundation should also fit.

For the parametric study, the mathematic model consisted simply of a 3 lumped mass-spring system for the superstructure and a rotational spring for the soil. Calculation of the spring constant for the soil-springs was based on the theory for dynamic interaction between a rigid slab and an elastic half space. The fundamental rocking frequency was calculated for various soil moduli and the change in frequency from the base line frequency (i.e., completely rigid soil) was plotted against soil elastic modulus (Fig. 5). The mass-spring model was subsequently verified by finite analysis of the mat.

CONCLUSIONS

° For rigid soils (E > 20,000 p.s.i.), the effect of the soil on natural frequency is insignificant.

° For soft soils (E < 5,000 p.s.i.) the reduction of natural frequency can be 20% or more.

° The spring-mass model was accurate within 5 percent as compared to the finite element model.

° A systems analysis, which includes the foundation-soil, is required for Mod-OA towers with mat foundations placed on soft soils.

POTENTIAL AREAS OF FUTURE STUDY

° Foundation rocking coupled with vertical, sliding or twisting modes.

° Optimization of foundation types for various classes of wind turbines.

° Automatic design of foundations such that a minimum amount of soil information and design effort is required.

° Instrumentation of foundations to verify assumptions and math models.

° Effect of foundation-soil in earthquake analysis of wind turbines.

DISCUSSION

. Are there any building codes which apply to your foundation design?

. The only applicable code is the ACI code which gives allowable stresses for reinforced concrete design. I am not aware of any code that spells out how to analyze the structure for forces and stresses.
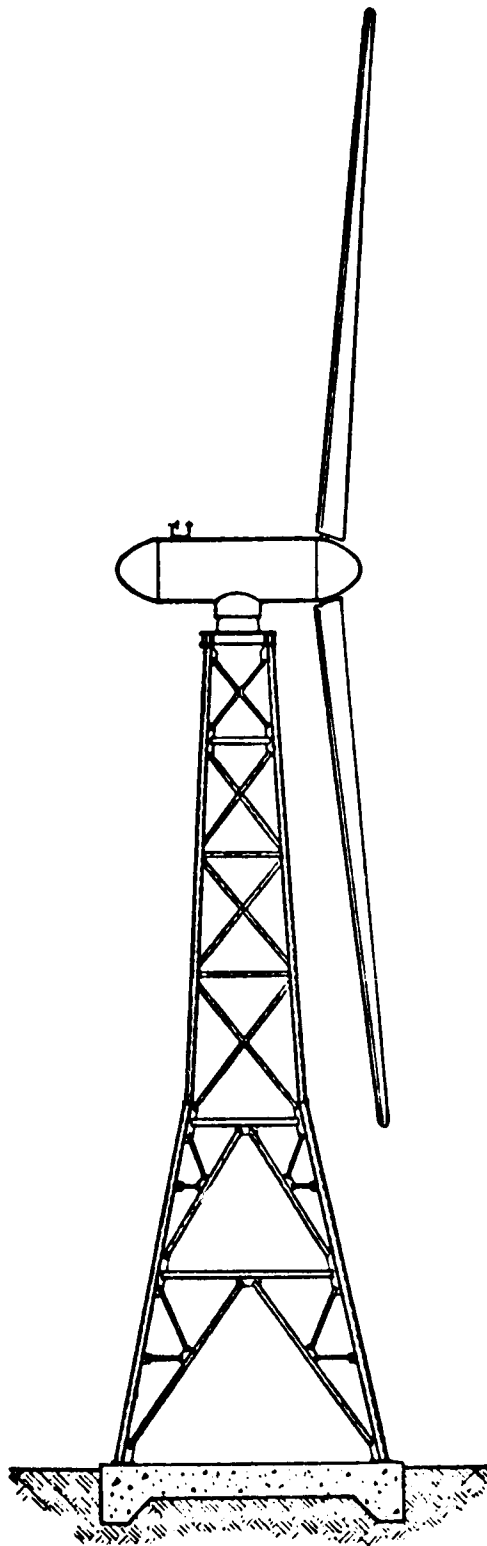
Figure 1. - Mod-OA wind turbine.
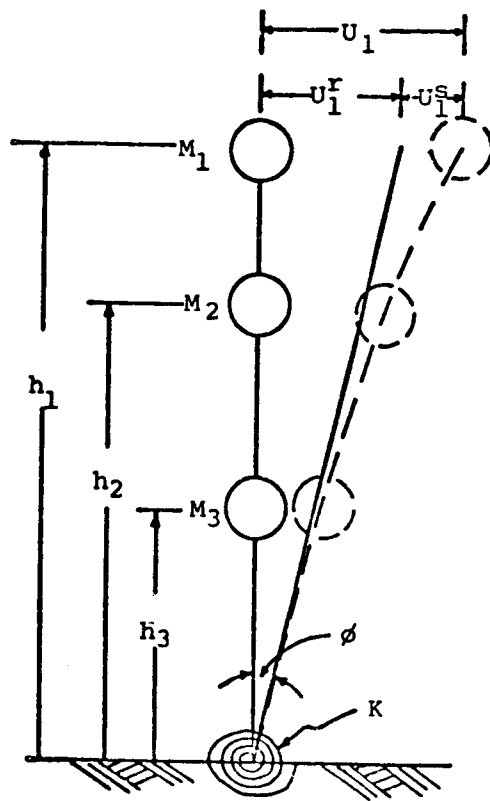
Figure 2. - A simple model.
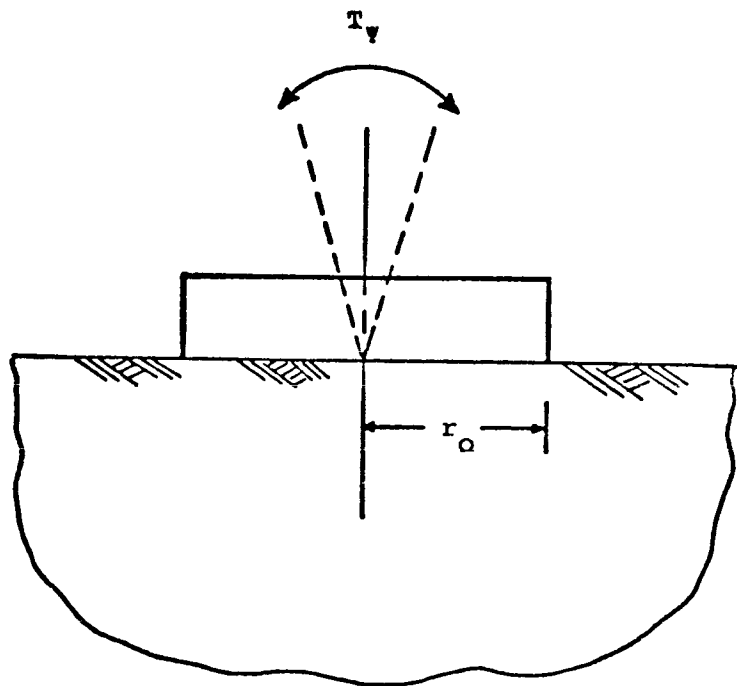
Figure 3. - Rocking of rigid footing on
elastic half space.

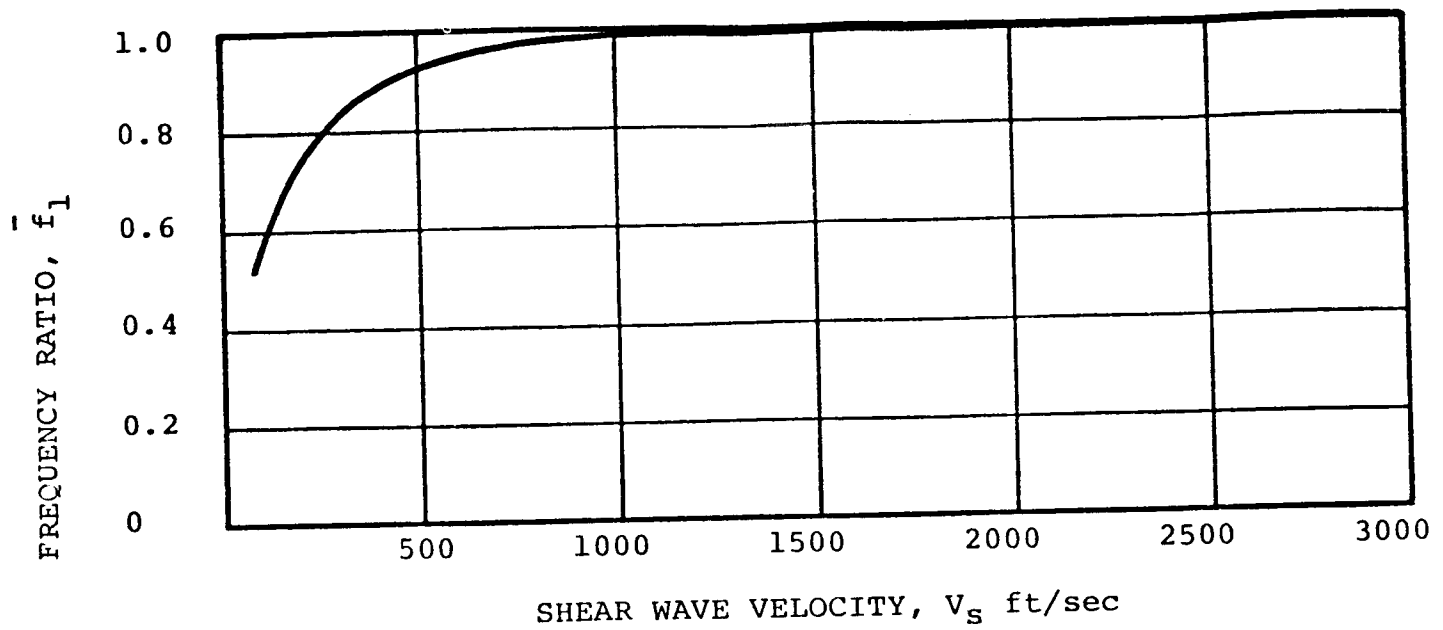$$\bar{f}_l = \frac{\text{First Natural Freq.(Non-rigid base)}}{\text{First Natural Freq.(Rigid base)}}$$
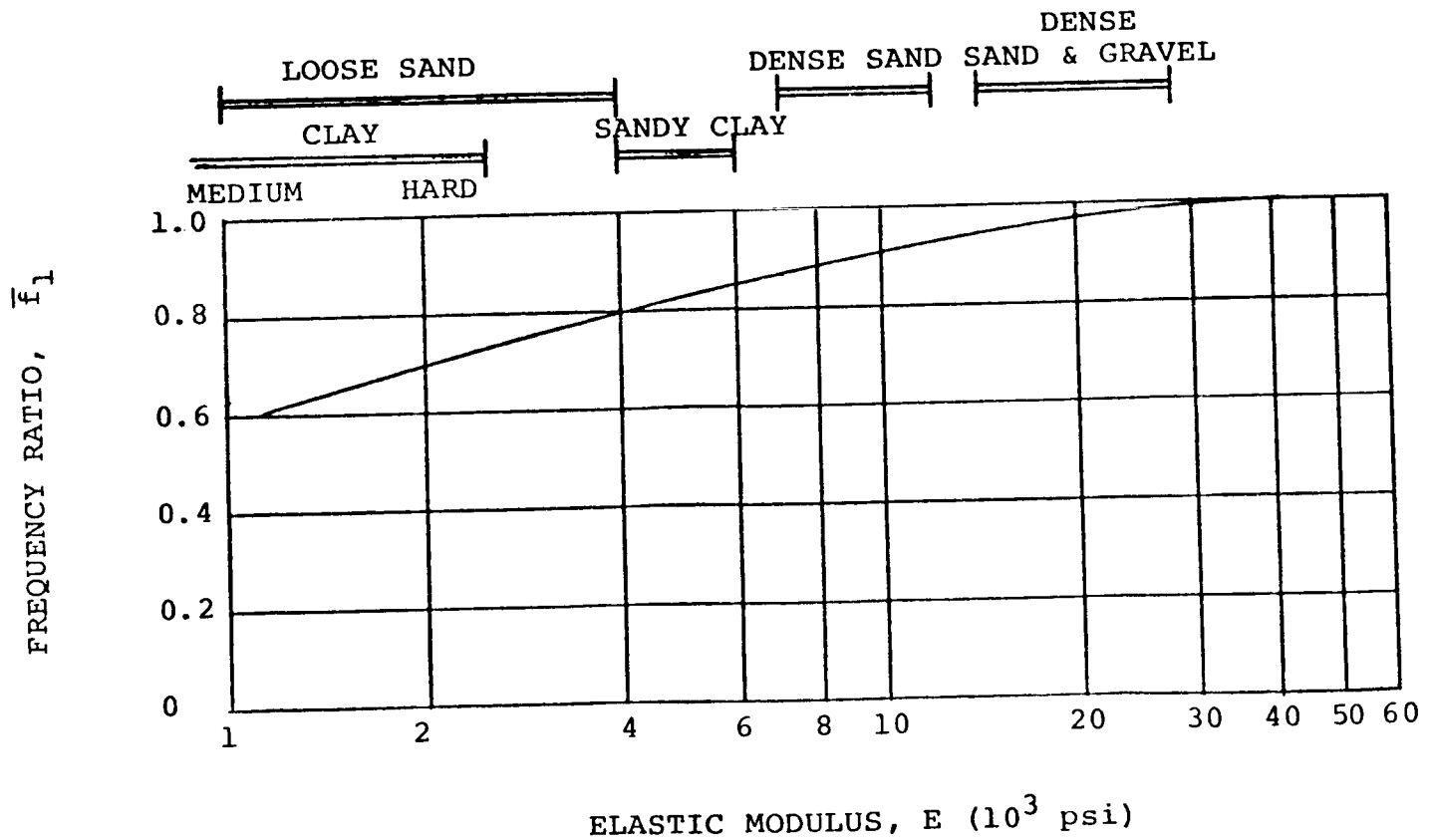
FREQUENCY RATIO, $\bar{f}_l$

SHEAR WAVE VELOCITY, V_s ft/sec

Figure 4. - Frequency ratio versus shear wave velocity.

FREQUENCY RATIO, $\bar{f}_l$

LOOSE SAND

CLAY

MEDIUM   HARD

SANDY CLAY

DENSE SAND

DENSE
SAND & GRAVEL

ELASTIC MODULUS, E (10^3 psi)

Figure 5. - Frequency ratio versus elastic modulus.

108

SUMMARY OF STATIC LOAD TEST OF THE MOD-0 BLADE

Dean R. Miller

National Aeronautics and Space Administration
Lewis Research Center
Cleveland, Ohio 44135

ABSTRACT

A static load test was performed on the spare Mod-0 windturbine blade to define load transfer at the root end of the blade, and to validate stress analysis of this particular type of blade construction (frame and stringer).

Analysis of the load transfer from the airfoil skin to the shank tube predicted a step change in spanwise stress in the airfoil skin at station 81.5 inches (STA 81.5). For flatwise bending a 40% reduction in spanwise stress was predicted, and for edgewise bending a 6% reduction. Experimental results verified the 40% reduction for flatwise bending, but indicated about a 30% reduction for edgewise bending.

The agreement between experimental and predicted results was quite good. For flatwise bending, the predictions were about 11% low between STA 81.5 and STA 120. Results for edgewise bending fell between predictions for the trailing edge skins cross-sectional area being 100% effective and 0% effective in carrying bending moment. The trailing edge skins appeared to be about 50% effective.

INTRODUCTION

A static load test was performed on the spare Mod-0 windturbine blade. The purpose of the test was twofold: (1) to evaluate load transfer at the root end of the blade between the airfoil skin and shank tube, and (2) to validate the stress analysis of this frame and stringer metal blade.

ANALYSIS OF LOAD TRANSFER

At the root end of the blade, bending moment is transferred to the shank tube by the action of a "shear couple" between two D-SPAR ribs (at stations 48 and 81.5 inches), and by means of 24 bolts connecting the shank tube to the D-SPAR rib at STA 81.5. Figure 1-A shows a cutaway view of the D-SPAR between STA 48 and STA 81.5. The rib at STA 81.5 has 24 bolts oriented radially around the shank tube.

A freebody diagram of the idealized airfoil is shown in Figure 1-B. The loads on the airfoil create a bending moment M_0. To maintain static equilibrium, the shank tube provides a reaction to this moment by applying a shear force "V" at each structural rib, thereby creating a "shear couple." The bolts in the rib at STA 81.5 also resist "M_0," by applying a redundant moment "M_1" to the airfoil. The term redundant is used because these bolts were primarily

intended to resist centrifugal loads on the airfoil, while the "shear couple" was assumed to transfer all the bending moment. However, a review of the above assumption, led to the suggestion that the bolts might actually be transferring a significant portion of the moment "M_0." As such, the redundant moment "M_1" was predicted to cause a step change in spanwise airfoil stress at STA 81.5. A maximum reduction in stress of 39% was predicted for flatwise bending, and a maximum of 6% for edgewise bending.

TEST APPARATUS

Figure 2 is a photo of the overall test set up. The blade was bolted to a test support stand. Loads were applied vertically (up and down) for four 90° orientations of the blade. These four orientations provided data for tension and compression of both the high pressure surface and the leading edge.

The blade was instrumented with strain gages to sense only spanwise strain. As shown in Figure 3, the gages were clustered about station 81.5 inches (STA 81.5) on the high pressure surface and on the leading edge.

TEST RESULTS

The results of the test are shown in Figures 4 and 5. In both figures, the ratio "σ/M" is plotted as a function of spanwise blade station. The ratio "σ/M" is the ratio of measured spanwise stress to the total bending moment (be that flatwise or edgewise). It is used because it provides a means of comparing stress levels at various spanwise locations along the blade, but still accounting for the different local cross-sectional properties.

Stress in the high pressure surface of the blade due to flatwise bending is shown in Figure 4. The solid dark line indicates the prediction, while the dashed line represents the experimental results. Locations of the D-SPAR ribs are shown by the "speckled" regions centered about STA 48 and STA 81.5.

As predicted there was about a 40% drop in airfoil stress across the rib at STA 81.5. Between STA 48 and STA 81.5, the experimental results agreed quite closely with the predicted behavior. Outboard of STA 81.5, the results were about 11% higher than the predictions. The little peak at STA 85.5 was attributed to some local bending effects of the airfoil skin over the D-SPAR rib at STA 81.5.

The leading edge stress due to edgewise bending are shown in Figure 5. Again, the solid dark lines indicate predicted results, while the dashed lines represent experimental results. There are two predicted lines: one which assumes none of the cross-sectional area of the trailing edge skin is effective in carrying bending moment (0%), and one which assumes all of the cross-sectional area is effective (100%).

The experimental data indicated about a 30% reduction in airfoil stress across the rib at STA 81.5. This was significantly more (24%) than predicted. For edgewise bending then, the shank tube bolts are actually carrying approximately 1/3 of the total bending moment.

In general, the data fell between the two predicted lines for 0% and 100% effective trailing edge skins. Attributing the peak at STA 87.5 to local bending of the airfoil over the D-SPAR rib, the data seem to indicate about a 50% effective trailing edge. Information from a previous static load test seemed to suggest that 50% was a good value for trailing edge effectiveness.

CONCLUSIONS

With regard to evaluating load transfer at the root end of the blade:

1. 40% of the flatwise bending moment in the airfoil was transferred to the shank tube thru the shank tube bolts.

2. 30% of the edgewise bending moment in the airfoil was transferred to the shank tube thru the shank tube bolts.

In general, the experimental results validated our predictions. The results indicated:

1. Spanwise stress in the airfoil due to flatwise bending moment was 11% above the predictions for stations beyond 81.5.

2. The cross-sectional area of the trailing edge skins was 50% effective in carrying edgewise bending moment.

REFERENCES

1. Timoshenko, S.; and Goodier, J. N.: Theory of Elasticity, 2nd Edition, McGraw Hill, 1951.

2. Cherritt, A. W.; and Gaidelis, J. A.: 100-kW Metal Windturbine Blade Basic Data, Loads and Stress Analysis, Report No. LR 27153, Lockheed California Company, 6-17-75.

3. Spera, D. A.: Structural Analysis of Wind Turbine Rotors for NSF-NASA Mod-O Wind Power System, NASA TMX-3198, March 1975.

DISCUSSION

Q. The outboard rib which was not designed to carry diaphragming type loads was found to be carrying 40% of the blade bending load as a diaphragming load. Doesn't this present a static or fatigue stress problem?

A. Fortunately, no. The rib was conservatively designed to carry a very high shear load and as a result, rib stresses remained below skin stresses even with the additional diaphragm load.

Q. Did you make any shear flow calculations?

A. Shear flow calculations were performed by the blade manufacturer and are contained in reference 2.

Q. Did you assess the strain at the trailing edge (roughly 50% span) to check for buckling?

A. Buckling was of the local panel type, rather than overall buckling of the trailing edge itself, and was observed both visually and through strain gage data.

COMMENT:
With regard to the effectivenss of trailing edge skins, an exact analysis of skin load transfer for airfoil shapes at skin endings is available. It was performed by Dr. Biot.
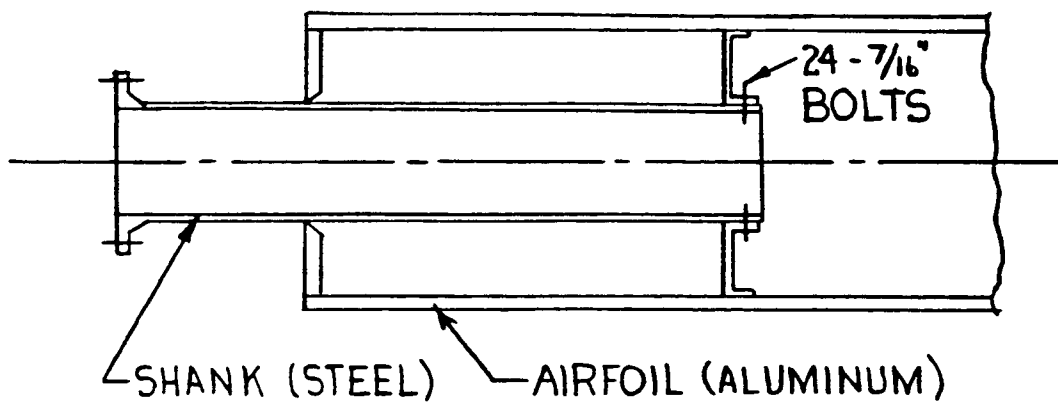
(a) Cutaway view of idealized blade.
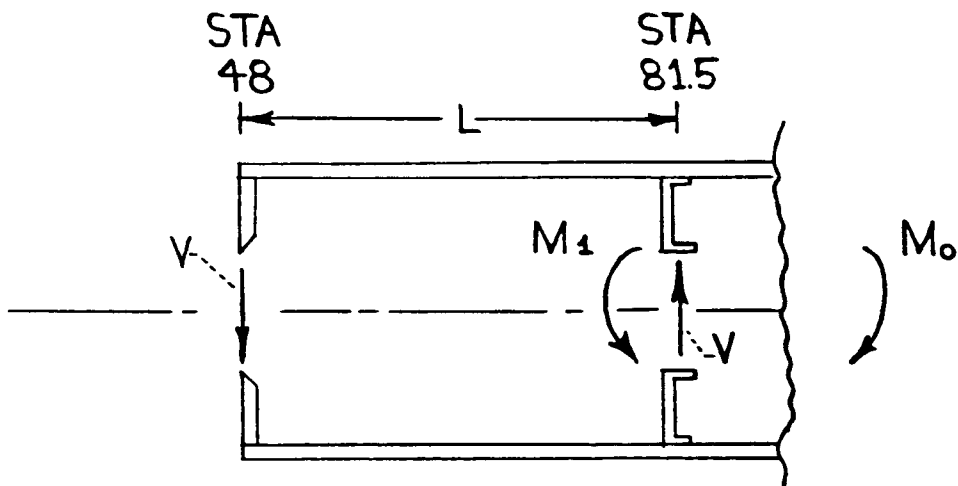
V ≡ SHEAR FORCE
Mo≡ BENDING MOMENT DUE TO BLADE LOADS
M₁≡ REDUNDANT MOMENT DUE TO
    SHANK BOLTS

(b) Free-body diagram of airfoil.

Figure 1. - Root end of Mod-0 wind turbine blade.

113
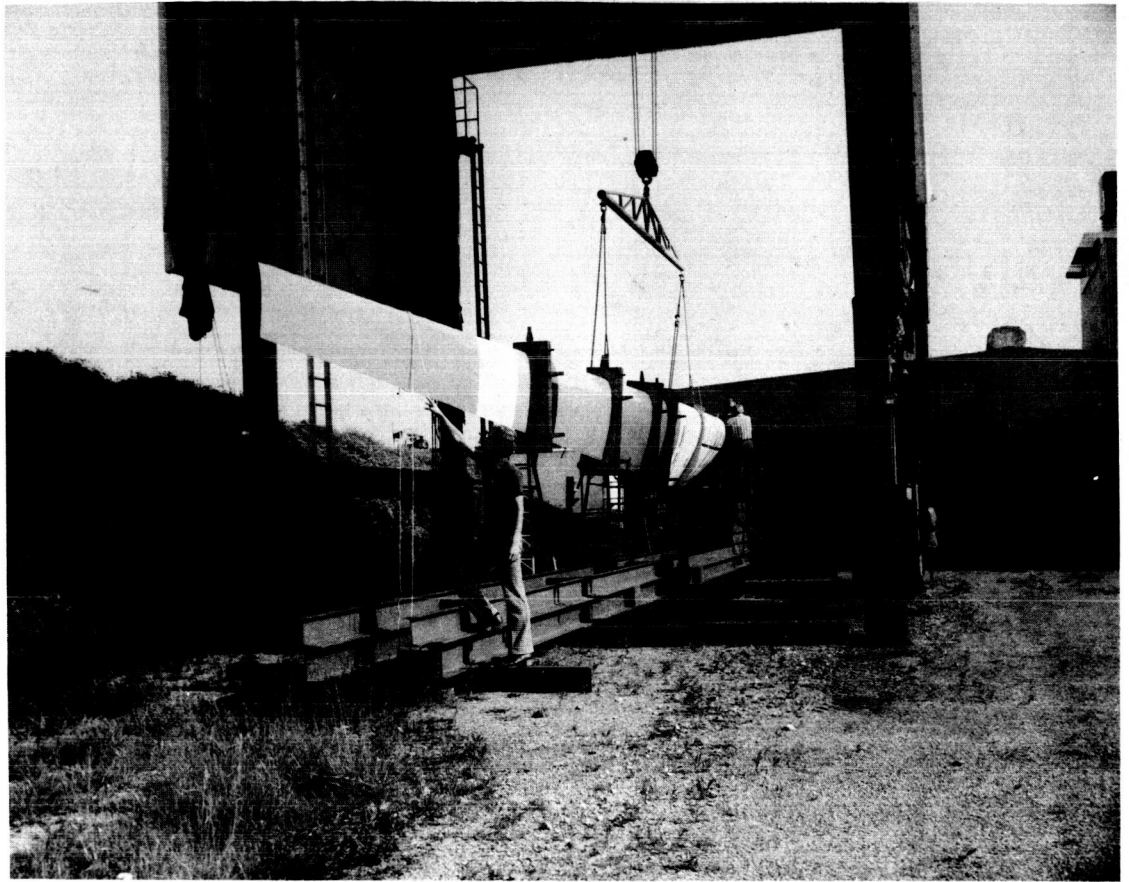
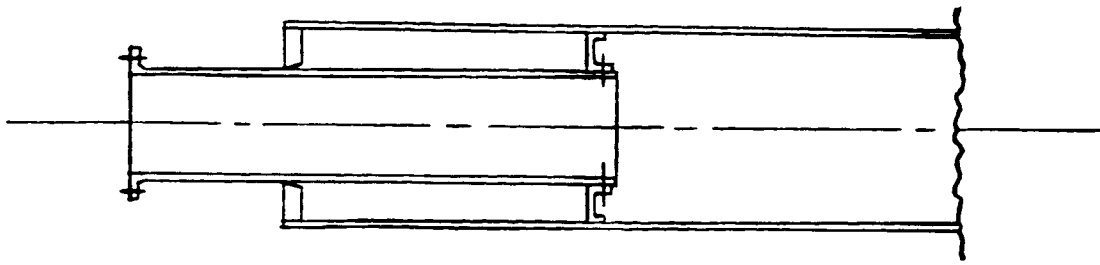Figure 2. – Test setup for static load test of Mod-0 blade.

H.P.

TRAILING
EDGE

HIGH PRESSURE SIDE

LEADING
EDGE GAGE

HIGH PRESSURE
SURFACE GAGE

STA
48

STA
81.5
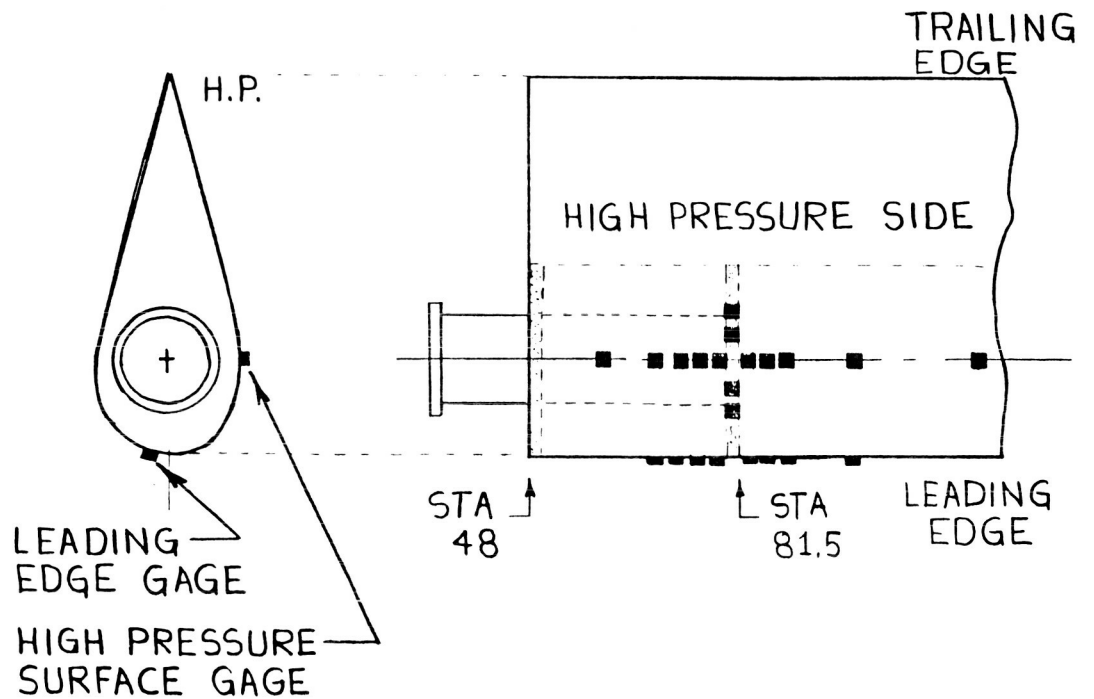
LEADING
EDGE

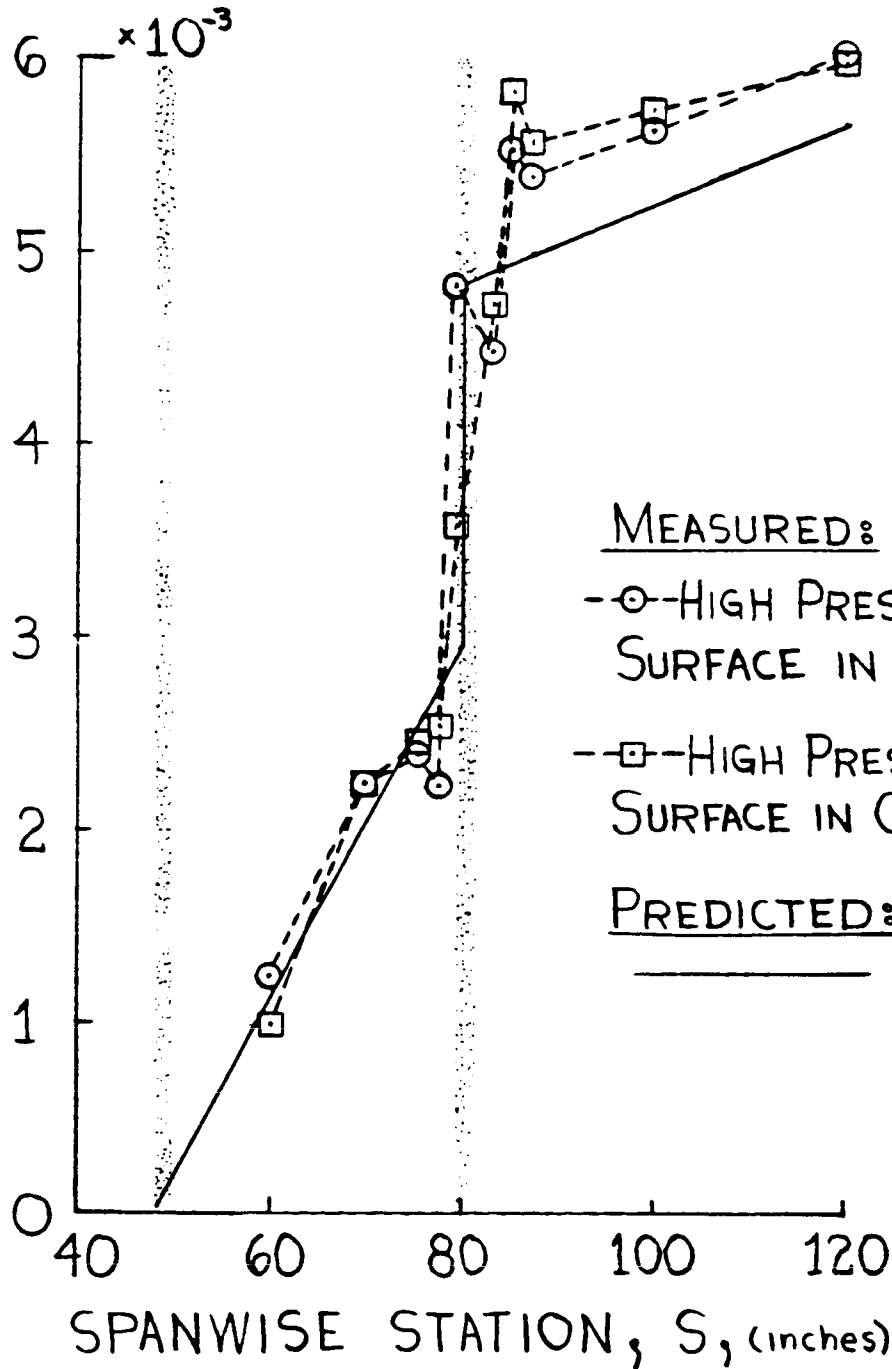Figure 3. – Strain-gage location on Mod-0 blade for static load test.
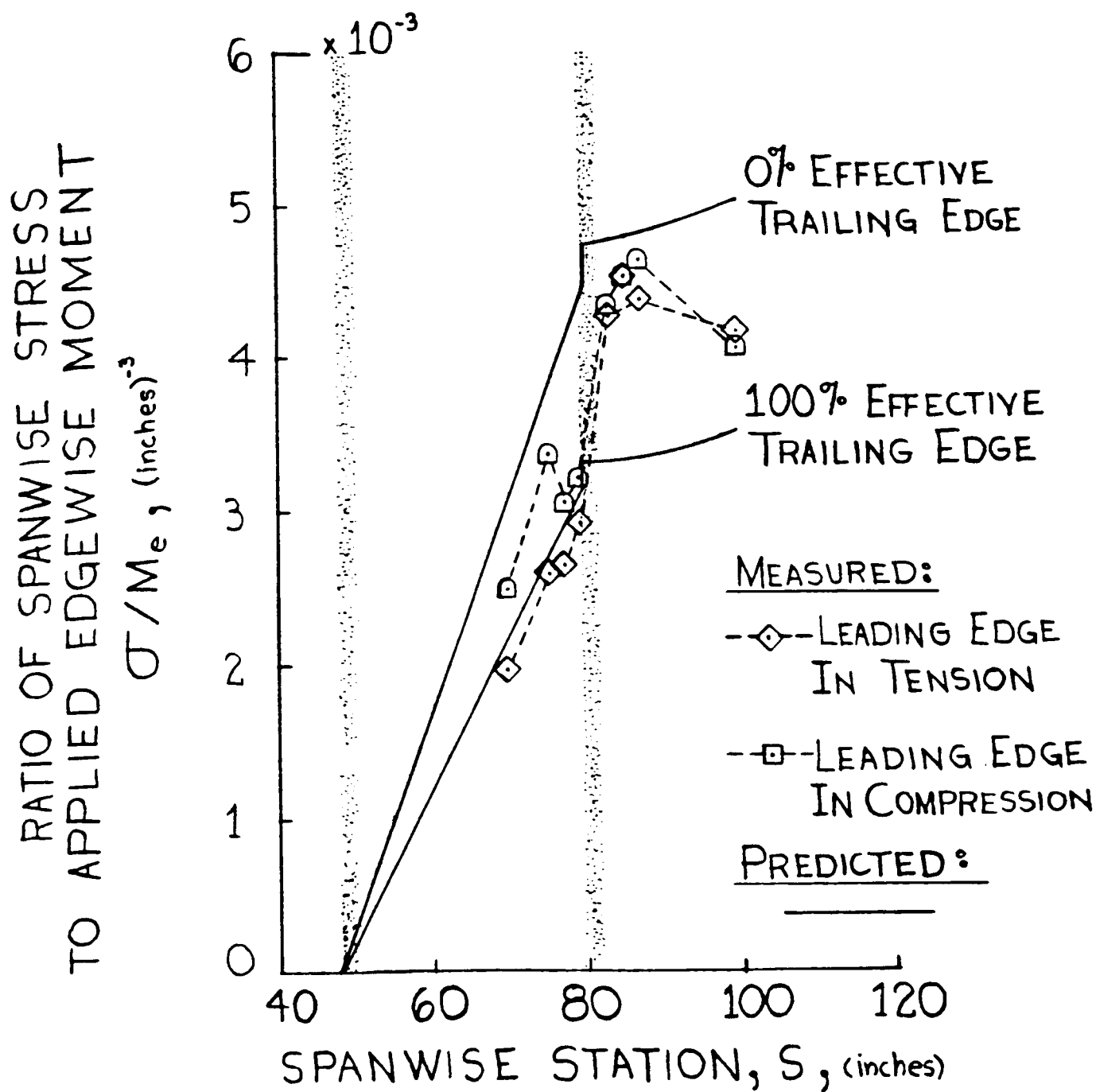
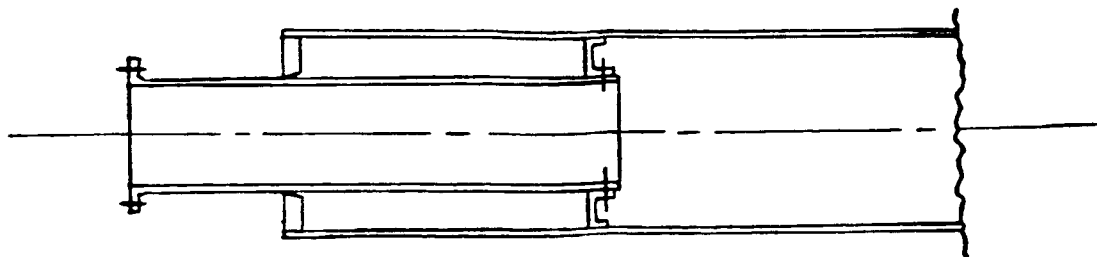Figure 4. - High-pressure surface stress.

Figure 5. - Leading-edge stress.

DOE/NASA MOD-0 100KW WIND TURBINE

TEST RESULTS

John C. Glasgow

National Aeronautics and Space Administration
Lewis Research Center
Cleveland, Ohio 44135

ABSTRACT

The Mod-0 100kW Wind Turbine was designed and fabricated by the NASA under the direction of the U.S. Department of Energy to assess technology requirements and engineering problems of large wind turbines. The machine became operational in October 1975 and has demonstrated successful operation at 40 rpm while producing power on resistive load bank and while synchronized with power grids. The Wind Turbine has also demonstrated the capability of automatic unattended operation, including startup, achieving synchronism, and shutdown as dictated by wind conditions. During the course of these operations, a wealth of engineering data has been generated. This paper presents some of this data which is associated with rotor and machine dynamics problems encountered and the machine modifications incorporated as a solution. These include high blade loads due to tower shadow, excessive nacelle yawing motion, and power oscillations. The results of efforts to correlate measured wind velocity with power output and wind turbine loads are also discussed.

INTRODUCTION

The Mod-0 100 kW Experimental Wind Turbine is a part of the National Wind Energy Program under the direction of the U.S. Department of Energy. The NASA Lewis Research Center has designed, built and erected this machine near Sandusky, Ohio and is currently testing it to obtain engineering data on large horizontal axis wind turbines.

The wind turbine described in reference 1 has a 125 foot diameter two bladed rotor which drives a 100 kW capacity synchronous generator through a step up gear box. The rotor is positioned downwind of a 100-foot steel truss tower as pictured in figure 1. The rotor is designed to operate at a constant speed of 40 rpm and it drives a 480 volt 60 Hz three phase generator at 1800 rpm. Rotor speed or output power level is maintained by controlling rotor blade pitch angle with an active feedback control system. The rotor, generator, transmission and associated equipment are mounted in a nacelle, figure 2, which can be yawed to align the rotor with the wind. Power, instrumentation and control connections to the ground are made through slip rings.

The turbine was designed to begin generating power in winds of 10 mph (at 100 ft) and produce 100 kW at a wind velocity of 18 mph. In winds above 18 mph, the generator continues to operate at 100 kW output by adjusting the pitch of the rotor to spill excess wind energy. When the wind velocity exceeds 30 mph the generator is taken out of synchronism with the power network, the blades

are feathered to bring the rotor to a halt and the machine is shut down to await the return of lower velocity winds.

Final assembly of the machine was completed in September 1975 and since that time successful operation of the wind turbine has been demonstrated for each of its design operating modes at 40 rpm; Manual operation on a resistive load and while synchronized to a large power grid and a simulated small power grid, and unattended automatic synchronization and operation on a large power grid.

In keeping with the primary objective of the Mod-0 program, a considerable amount of engineering data has been generated for use in the ongoing U.S. Wind Energy Program. On the Mod-0 project as with any research project, useful information is generated both from demonstrations of successful designs and operations and from designs which create engineering problems or unsuccessful operation. This paper discusses some of the engineering problems which pertain to rotor and machine dynamics and the design changes which have been incorporated to eliminate or reduce their undesirable effects. Also included is a short discussion on techniques which are being used to correlate wind turbine power output and loads with measured wind velocity.

Instrumentation

The Mod-0 research data system provides approximately 100 channels of information. This data is recorded on magnetic tape at the request of an operator or at specific time intervals. The data is processed off-line for analysis. Selected instruments are displayed on Brush recorders for real time monitoring and review. Most of the data presented in this paper is from the Brush recorders and the transducers which produced the data are listed below.

1. Nacelle wind velocity and yaw angle of nacelle relative to the wind.

2. Nacelle accelerations $\ddot{x}$, $\ddot{y}$, and $\ddot{z}$ at the rotor shaft bearing support nearest the rotor.

3. Rotor blade pitch angle.

4. Rotor blade bending moments, indicating flatwise (Mm) and inplane (Mn) bending at two stations along the blade span.

5. Rotor shaft torque (Mz) and bending moments (Mx) and (My).

6. Rotor speed and position.

7. Alternator output in kW.

8. Yaw drive shaft torque.

Figures 3 and 4 give a schematic representation of these measurements, their location on the wind turbine, and the sign convention of each.

TOWER SHADOW

Initial operations of the Mod-0 wind turbine at 40 rpm resulted in blade and low speed shaft loads which exceeded design loads by a considerable margin. These results were presented in reference 2. Review of the data indicated two factors to be the primary cause of the high loads (a) tower shadow or low velocity air flow immediately downwind of the tower which affected the downwind Mod-0 rotor, and (b) excessive nacelle yawing motion. Nacelle yawing motion is discussed in a later section; tower shadow is discussed below.

The flapwise bending load experienced by a Mod-0 rotor blade near the root is presented in figure 5. The moment increases negatively as the blade moves from behind the tower and reaches a maximum value at approximately 35° from the vertical down position indicating deflection toward the tower in response to the reduced air load in the tower shadow region. Also indicated in the figure are design values for this moment and a calculated value using a tower shadow value which would reproduce the measured loads.

After the initial Mod-0 40 rpm operation, wind tunnel tests were conducted to define the tower shadow for the Mod-0 tower in its original configuration and to evaluate various tower configurations designed to reduce tower shadow. The results of this investigation are reported in reference 3 and figures 6 and 7 show measured tower shadow values for the original Mod-0 with stairs and rails and for the tower with stairs and rails removed.

Based on the wind tunnel results the stairs were removed and Mod-0 operation at 40 rpm showed a marked reduction in flapwise bending loads as reported in reference 4 and shown in table 1. As indicated in the table, the flapwise bending moment for steady-state operation was reduced from 130,000 ft.lbs. to 70,000 ft.lbs. when the stairs were removed. While the load reduction attributable to reduced tower shadow was significant with respect to flapwise bending moment, very little improvement was seen in inplane moment and both flatwise and inplane moments remained high with respect to blade design load. Inplane bending moments have been observed to be affected more directly by lateral motion of the rotor which can be produced by lateral motion of the tower or by yawing of the nacelle. The major source of lateral motion at the rotor has been attributed to nacelle yawing which is discussed below.

Nacelle Yawing Motion

Data taken during early operation of the Mod-0 wind turbine at 40 rpm indicated high oscillatory torque loads on the low speed rotor shaft as the rotor speed varied between 37 and 40 rpm and the wind velocity indicated on the nacelle varied between 22 and 32 miles per hour. This data was presented and discussed in reference 2 and is shown in figure 8. When the data was first presented high drive train response indicated by the oscillatory load on the low speed shaft was attributed to a blade inplane mode being excited as the rotor speed varied between 38 and 42 rpm. Since that time it has been demonstrated that the primary cause of the conditions encountered in figure 8 was nacelle yawing motions which produces an oscillatory lateral motion at the

119

rotor. Tests were run in 1976 after the stairway was removed with a locked yaw mechanism. This locked the nacelle to the tower and increased the resonant frequency in yaw from approximately twice the rotor speed, 2P, to over 5 times the rotor speed as indicated in table 2. Comparison of data taken with and without the yaw drive locked indicated a reduced tendency for low speed shaft bending response with the yaw drive locked and reduced moments on the rotor blades and low speed drive shaft, which indicated a definite connection between nacelle yawing motion and the low speed shaft response.

Reducing tower shadow also had an effect in reducing the low speed shaft torque response at 4P as was indicated by the inability to reproduce the drive train torque response shown in figure 8b after the tower was modified to reduce tower shadow. Repeated attempts to reproduce the condition in winds of similar magnitude failed to excite the condition to the amplitudes originally encountered. This was true for both single yaw drive and locked yaw tests. Also, the rotor vertical motion as indicated in figure 8c, bearing "B" acceleration, $\ddot{Y}$, was reduced by an order of magnitude after the stairway was removed indicating a strong connection between vertical motion of the rotor or nacelle "nodding" and tower shadow.

After the test results for locked yaw were obtained a dual yaw drive and yaw brake were installed on the Mod-0 wind turbine. It was predicted that the dual yaw drive with a preload to remove free play would eliminate the problems associated with nacelle yawing motion. The single yaw drive permitted some free play and the drive system stiffness resulted in a nacelle yawing natural frequency approximately equal to twice the rotor speed. The dual yaw drive was designed to raise this frequency to 2.5 times the rotor speed, 2.5P, and decouple the machine in yaw. The yaw brake was added as a backup system which would provide capability for additional yaw restraint if this was required. The revised system is depicted in figure 2.

Tests with the dual yaw drive at 40 rpm indicated that more restraint was needed to prevent excessive nacelle yawing motions which resulted in high blade flapwise and inplane bending loads, low speed shaft bending loads and loads on the yaw drive mechanism. The yaw brake was used on subsequent operations and with the nacelle locked to the tower with a brake clamping pressure of 1500 psi, the frequency of occurrence of the high blade and shaft bending moments was greatly reduced.

The results of tests with the dual yaw drive and the yaw brake demonstrated the need for the yaw brake to keep machine loads within acceptable limits and the brake was incorporated as a part of the yaw control system. The yaw system was designed to provide a clamping pressure of 1500 psi on the yaw brake when the yaw drive motors were off and a drag pressure of 100 psi when the yaw motors were on to change nacelle azimuth.

Operations with this system proved to be unsatisfactory. High blade and shaft loads occurred frequently as the yaw brake clamping pressure was relieved to permit a nacelle azimuth change. This effect is depicted in figure 9 showing a rapid buildup in low speed shaft bending as the yaw brake is released. Yaw

brake release is indicated by activity on the yaw drive torque trace. Raising the yaw brake drag pressure from 100 psi to 300 psi reduced the undesirable effects resulting from brake release.

As stated above, locking the nacelle to the tower with the yaw brake reduced the frequency of occurrence of high blade and shaft loads. The yaw brake did not eliminate these high loads and a typical occurrence is indicated in figure 10 for load bank operation. In this figure the wind turbine is operating on the resistive load bank and electrical load has been removed and replaced in a period of approximately 30 seconds. Rotor motion has been reduced as indicated by the rotor bearing accelerations in figure 10a. However, as the wind velocity measured on the nacelle increases, rotor blade and low speed shaft loads increase above desirable levels (fig. 10b). A comparison of the rotor bearing accelerations with those of figure 8c clearly indicates that rotor motion has been greatly reduced, however, high blade and shaft loads continue to occur as wind velocity varies. The condition has been observed to be a transient response to variable wind speed rather than a condition which occurs at a particular wind velocity, and little correlation exists between low speed shaft bending and instantaneous nacelle wind velocity.

Future operations of the Mod-0 wind turbine will evaluate the potential of yaw brake as a yaw damper. In these tests, the preload will be removed from the dual yaw drive to permit some free play in yaw and a constant pressure will be applied to the yaw brake providing a constant restraint in yaw throughout the operation, yaw motors on or off. The yaw damping force can be varied by changing the yaw brake pressure and the effect of this variable on wind turbine response can be evaluated.

Power Oscillations During Synchronous Operation

Initial tests of the Mod-0 for synchronous operation were conducted at a 20 rpm rotor speed. This rotor speed was chosen because of the high loads encountered at 40 rpm with the single yaw drive, mentioned above. The blade loads and nacelle yawing response were reduced at 20 rpm and it permitted the operations to continue while the dual yaw drive and brake were being fabricated.

Obtaining synchronism with a large power grid or with a small diesel generator set presented no difficulty, the normal deviations from rotor speed set point being sufficient to provide enough variation in generator speed to permit synchronism with the aid of a commercially available synchronizer. Synchronization of the Mod-0 is discussed in detail in reference 5. However, once synchronous operation was obtained the rotor, drive train and generator experienced a high amplitude resonant response at 40 CPM or 2P, as indicated in figure 11.

The resonant response was identified as a first mode vibration of the drive train and rotor as described in reference 6 which predicts this mode to occur between 0.27 Hz and 0.62 Hz, or .8P to 1.86P (for 20 rpm operation) as the generator load is varied between 0 and 100 kW. The driving force for the mode is the tower shadow which creates a defect in rotor torque as each blade

passes behind the tower. The analytic value for this forcing function for 40 rpm operation is shown in figure 11. Synchronous operations were conducted at 26.3 rpm and 40 rpm and representative samples of the results are shown in figures 12 and 13. As shown by the figures, operation at 26.3 rpm did not relieve the resonant response observed at 20 rpm but the 40 rpm rotor speed improved the situation significantly. However, operation at 40 rpm still left a $\pm$15 to $\pm$20 kW power oscillation at 80 CPM or 2P.

To reduce the power oscillations, a fluid coupling was installed on the high speed shaft and was run at 20 and 40 rpm as shown in figure 2. The results are shown in figures 15 and 16. As indicated, a large reduction in power oscillations was achieved by the fluid coupling at 20 rpm and a somewhat less significant improvement is shown at 40 rpm. The 20 rpm test was run with a 4% slip at a 60 kW load and the 40 rpm test was run with a 2% slip at 100 kW load. The oscillations can be reduced still further by increasing the slip in the coupling.

The use of a fluid coupling in the drive train provided an additional benefit in permitting the use of larger amounts of proportional gain in the power control system. The power control system was highly unstable when proportional gain was used with a rigid drive train, but the fluid coupling removed the instability and proportional gain considerably improved control system response.

Correlation of Wind Turbine Response with Measured Wind Velocity

Since the beginning of Mod-0 operations, efforts have been under way to develop methods which can be used to describe wind turbine performance and load response as a function of wind velocity. As a result of these investigations, methods have been developed which permit the desired correlations of power versus wind speed and loads versus wind speed to be made. A report describing Mod-0 performance will be available in the near future and the method used to obtain this correlation is described briefly below. A method for describing loads versus wind speed is also presented along with some preliminary results using these methods.

Wind measurements for the Mod-0 wind turbine are taken at two locations, on the wind turbine nacelle and on a 195 foot meteorological tower located 650 southwest of the wind turbine as depicted in figure 17. Wind turbine response is measured in terms of alternator power output and load measuring instrumentation described previously.

The process of correlating wind turbine performance with measured wind speed is complicated somewhat by the method of wind measurement. Measurements made on the nacelle correlate well with wind turbine response but are subject to inaccuracies due to flow disturbances created by the rotor and the nacelle. Measurements taken on the meteorological tower are relatively free of flow disturbances but are hampered by the distance between the wind turbine and the tower. To account for these complications it was necessary to first obtain a relationship between nacelle wind speed and alternator power and then correct nacelle wind speed to an undisturbed value based on meteorological tower data taken over the same time period.

To obtain the relationship between alternator power output and nacelle wind speed, simultaneous measurements of power output and nacelle wind speed are taken over a broad speed range. A typical set of simultaneous data is shown in figure 18. These data are then sorted into 1 mph speed increments and a region averaged value is obtained for each speed range. The average values are then used to produce a power versus nacelle wind speed plot as shown in figure 19.

Wind speed measurements taken on the meteorological tower are curve fitted to obtain a wind speed at the nacelle height. Two minute averages of the nacelle wind speed and the derived meteorological tower wind speed are taken to smooth the data and the simultaneous averages are cross plotted to obtain a relationship between nacelle wind speed and free stream wind speed as shown in figure 20. The relationship thus derived permits the correction from nacelle wind speed to free stream wind speed to be made.

Analysis to describe Mod-0 performance using this method is presently underway and results will be published as they become available.

The method used in describing wind turbine loads is similar to that employed in describing performance. Fatigue is a primary concern in the design of wind turbines and cyclic loads are the major source of fatigue. Loads measured on Mod-0 are therefore described in terms of mean and cyclic values.

Loads data is first broken down into mean and cyclic values and the component parts along with the simultaneous wind speed are stored and sorted into wind speed ranges. The loads data contained in each wind speed range is then averaged and a standard deviation of the set is obtained. The results of limited samples of data processed in this manner is shown in figure 21 for rotor blade flatwise bending at station 40, near the blade root. The data indicates a trend increasing with increasing wind speed and provides a means of quantifying a highly variable set of data. A relatively small sample of data has been processed in this manner at this time but the results obtained thus far indicate that this approach is a good one for describing wind turbine loads and vibratory response.

REFERENCES

1. Puthoff, Richard L.: Fabrication and Assembly of the ERDA/NASA 100 kW Experimental Wind Turbine. NASA TM X-3390, 1976.

2. Glasgow, J. C.; Linscott, B. S.: Early Operation Experience on the ERDA/NASA 100 kW Wind Turbine. NASA TM X-71601.

3. Savino, J. M. and Wagner, L. H.: Wind Tunnel Measurements of the Tower Shadow on Models of the ERDA/NASA 100 kW Wind Turbine Tower. NASA TM X-73548, 1976.

4. Linscott, B. S.; Glasgow, J. C.; Anderson, W. D. and Donham, R. E.: Experimental Data and Theoretical Analysis of an Operating 100 kW Wind Turbine. Proceedings of the 12th Intersociety Energy Conversion Engineering Conference, Aug. 1977.

5. Gilbert, Leonard J.: Synchronization of the DOE/NASA 100 kW Wind Turbine Generator With a Large Utility Network. NASA TM-73861.

6. Sullivan, T. L., Miller, D. R. and Spera, D. A.: Drive Train Normal Modes Analysis for the ERDA/NASA 100 kW Wind Turbine Generator, NASA TM-73718, 1977.

DISCUSSION

Q. In view of the blade flapwise bending response and low speed shaft bending phasing, it would appear a teetered rotor would reduce 2P yawing motion. Why did NASA drop teetered hub?

A. Early in the Mod-0 program a teetered rotor was considered to relieve tower shadow problems. The idea was not pursued when Mod-1 studies indicated that teetering was not worth the added cost and complexity.

Q. Could you elaborate on the interesting observation made that damping the yaw drive tends to eliminate the 4P torsional oscillations of the low speed shaft?

A. Increasing yaw stiffness did not remove the 4P torsional drive train oscillations. They can be seen on figure 10b with the yaw brake applied. However, after the stairs were removed to reduce tower shadow the condition depicted in figure 8b could not be reproduced at any significant magnitude. Yaw stiffness did not seem to have as much effect on the condition as reduced tower shadow.

Q. Where should you measure the wind speed on which you base your performance?

A. As a first choice, I would prefer a point 1 rotor diameter upwind of the rotor at hub height.

Q. Do you use an average of the wind velocity cubed?

A. Harold Neustadter: No, at constant rotor speed power is linear with wind speed and averaging is performed on velocity to the first power.

Q. Don't you think that the yaw drive stiffness has been worked to the point that the tower has now been made the critical tuning problem?

A. I would have to agree with your statement insofar as we have tested a flexible, 2P yaw drive, a 2.5P yaw drive and a locked yaw mechanism at 5P in yaw. The locked yaw was the best of the three in terms of rotor loads but I do not feel that additional yaw stiffness will improve matters. We feel that damping may offer the best solution and plan tests for the near future using the yaw brake as a damping device.

Q. What was the magnitude of the actual tower shadow before and after the stairs were taken out of the Mod-0 tower?

A. Tower shadow was never measured on the wind turbine. Wind tunnel test results indicate velocity reductions near 100% for certain conditions with stairs in place. Maximum velocity reductions were reduced to about 40% with the stairs removed.

Q. Would a three bladed rotor help the "yaw" motion problem?

A. Yes, I feel that it would.

Q. Have you made a comparison of power output solely with an upwind anemometer?

A. Yes, these correlations are currently being investigated and will be reported in the near future.

Q. Do you impose a time delay between the anemometer data from the upwind meteorological tower and the power output? Time delay to correspond to transit time of wind and transfer through WECS to produce power.

A. We have seen some improvement in the meteorological tower-vs-nacelle wind speed correlation when the data from the two sites are time-shifted and a correlation calculated. The correlation coefficient increases from .4 to .7. However, this has negligible effect on the 2-minute averaged results.

Q. Rather than comparing instantaneous power output vs. instantaneous point wind data with the results of steady-state theory, shouldn't an effort be used to derive a dynamic system transfer function from data measured over time?

A. I think a system of the type you describe will develop as wind energy develops further. There are some shortcomings with the technique we have developed at Lewis but it appears to be satisfactory for our purposes at this point in time.

TABLE 1. - COMPARISON OF BLADE LOADS WITH AND WITHOUT
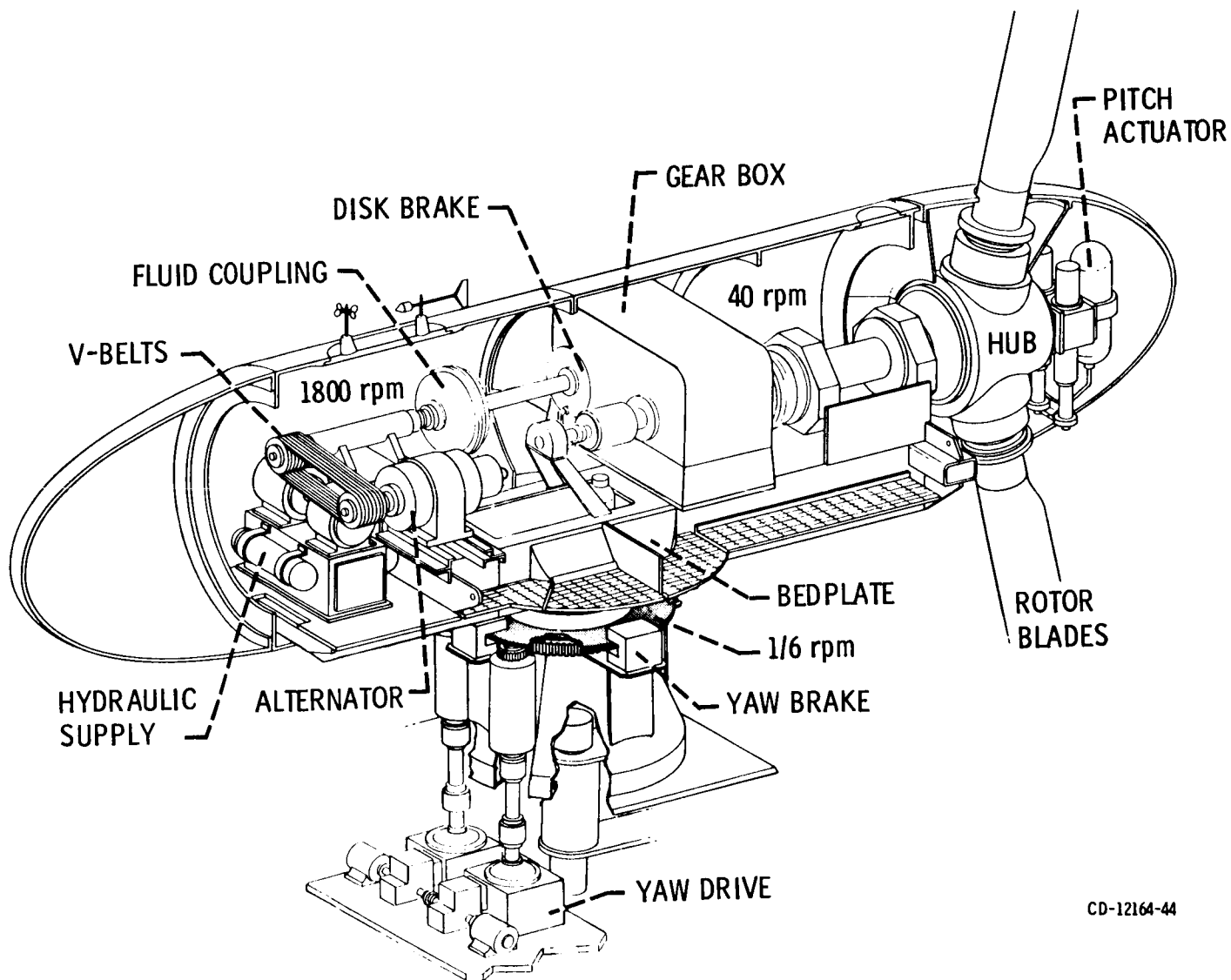STAIRWAY FOR STEADY STATE OPERATION

| CONFIGURATION | BLADE BENDING MOMENT AT STA 40   (FT-LBS) | |
	FLAPWISE PEAK TO PEAK	INPLANE PEAK TO PEAK
WITH STAIRS	130,000	108,000
WITHOUT STAIRS	70,000	103,000
DESIGN	58,000	75,000

TABLE 2. - MOD-O WIND TURBINE NACELLE YAWING RESONANT FREQUENCIES

SINGLE YAW DRIVE	1.2 - 1.4 Hz	2P
DUAL YAW DRIVE	1.7 Hz	2.5P
LOCKED YAW (PREDOMINANT LATERAL MOTION)	2.2 Hz	3.3P
LOCKED YAW (TORSION)	3.4 Hz	5.1P

Figure 1. - Mod-0 100-kW wind turbine.

PITCH
ACTUATOR

GEAR BOX

DISK BRAKE

FLUID COUPLING

40 rpm

V-BELTS

HUB

1800 rpm

BEDPLATE

ROTOR
BLADES

1/6 rpm

HYDRAULIC
SUPPLY

ALTERNATOR

YAW BRAKE

YAW DRIVE

CD-12164-44

Figure 2. - Cutaway drawing of Mod-0 wind turbine nacelle interior.
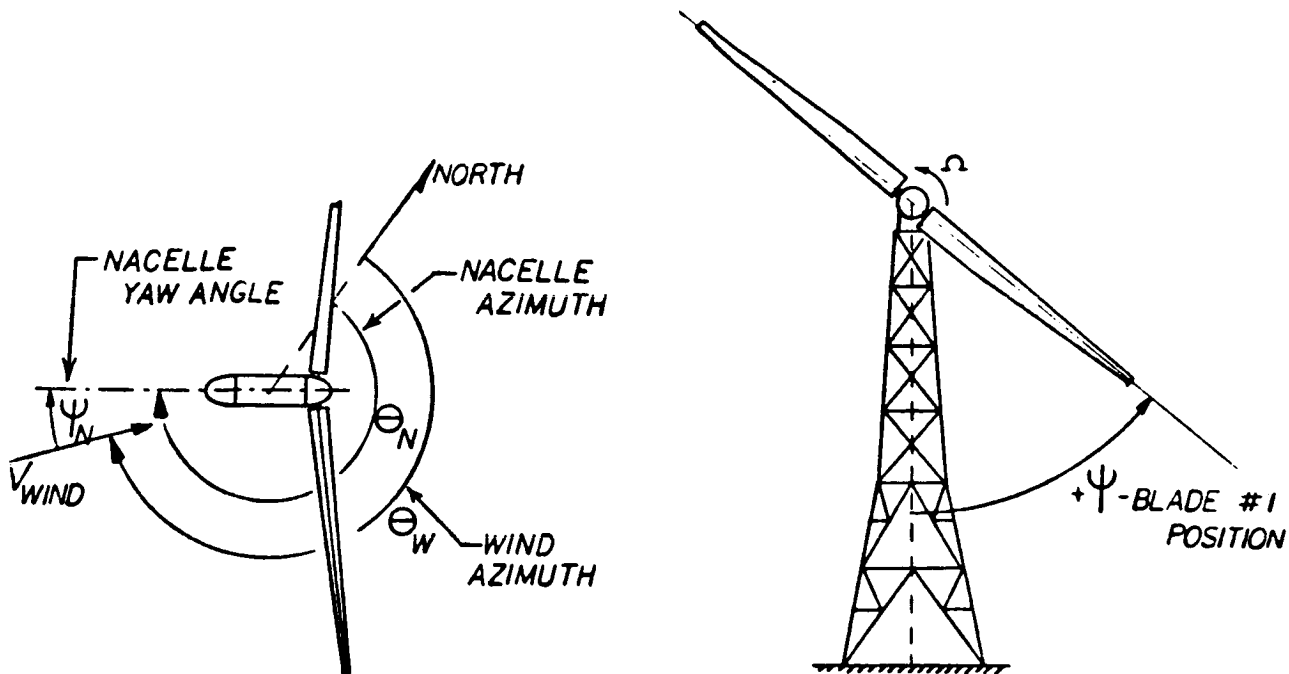
Figure 3. - Instrumentation sign convention.
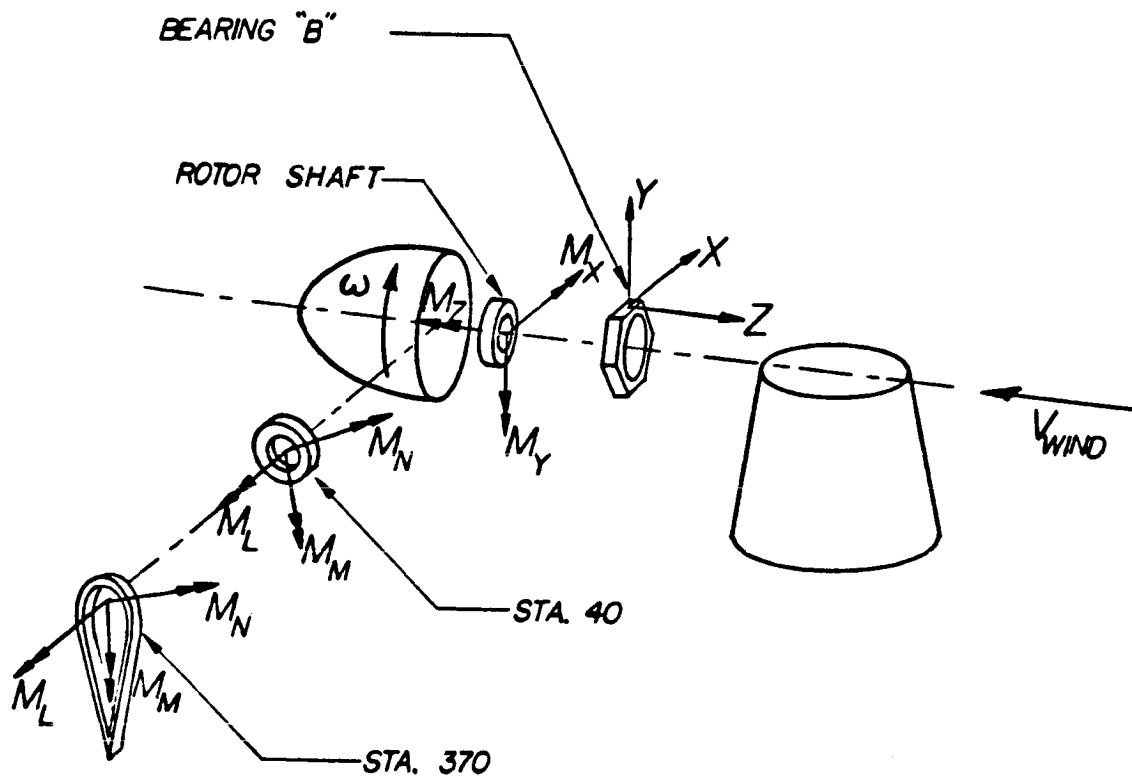
Figure 4. - Instrumentation sign convention.
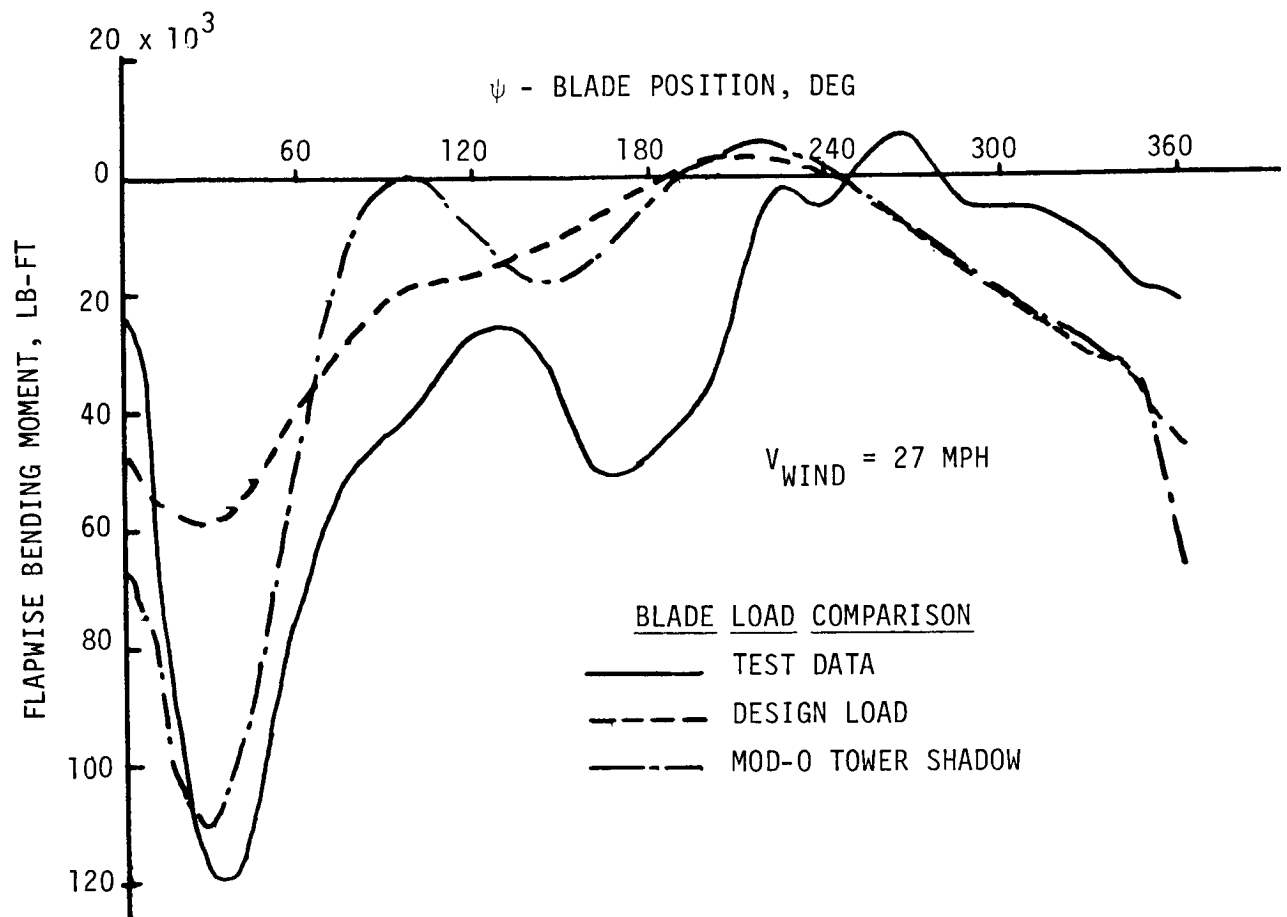
Figure 5. - Blade root flapwise bending with stairs - 40-rpm operation.
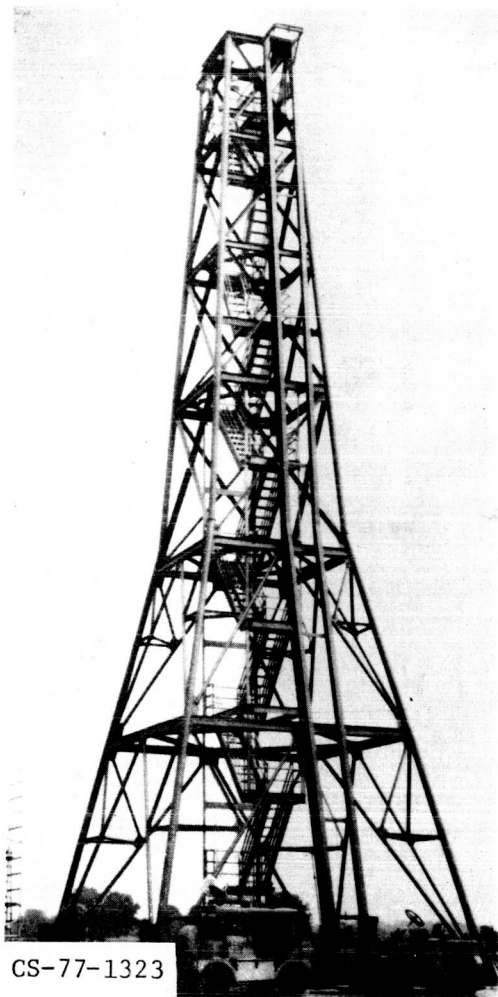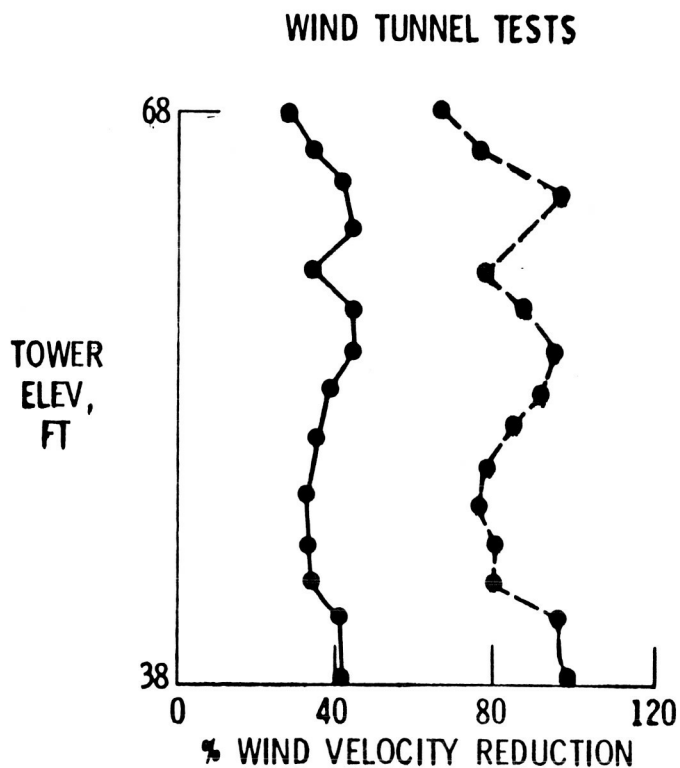
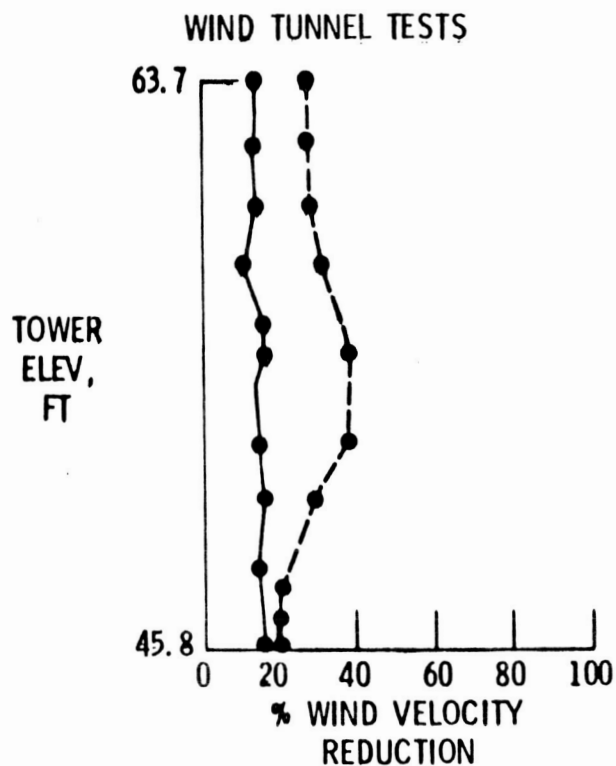Figure 6. - Mod-0 tower wind velocity reduction - with stairs and rails.
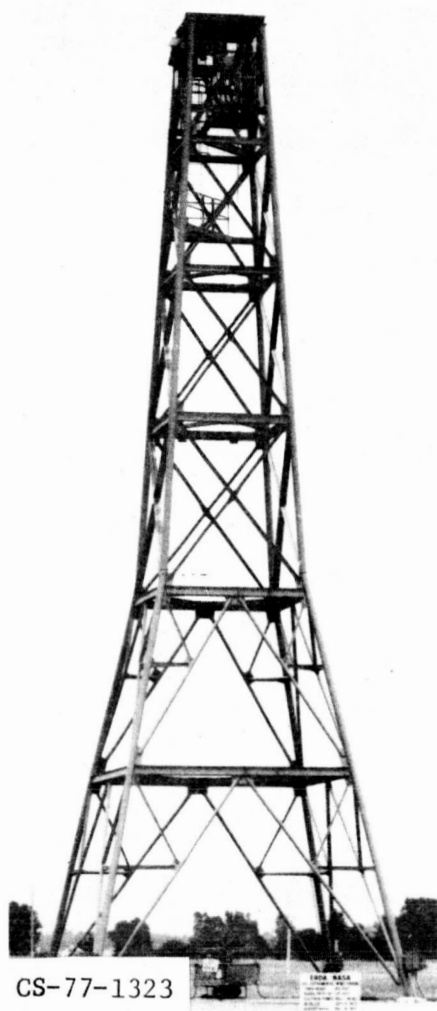
131

Figure 7. - Mod-0 tower wind velocity reduction with stairs and rails removed.
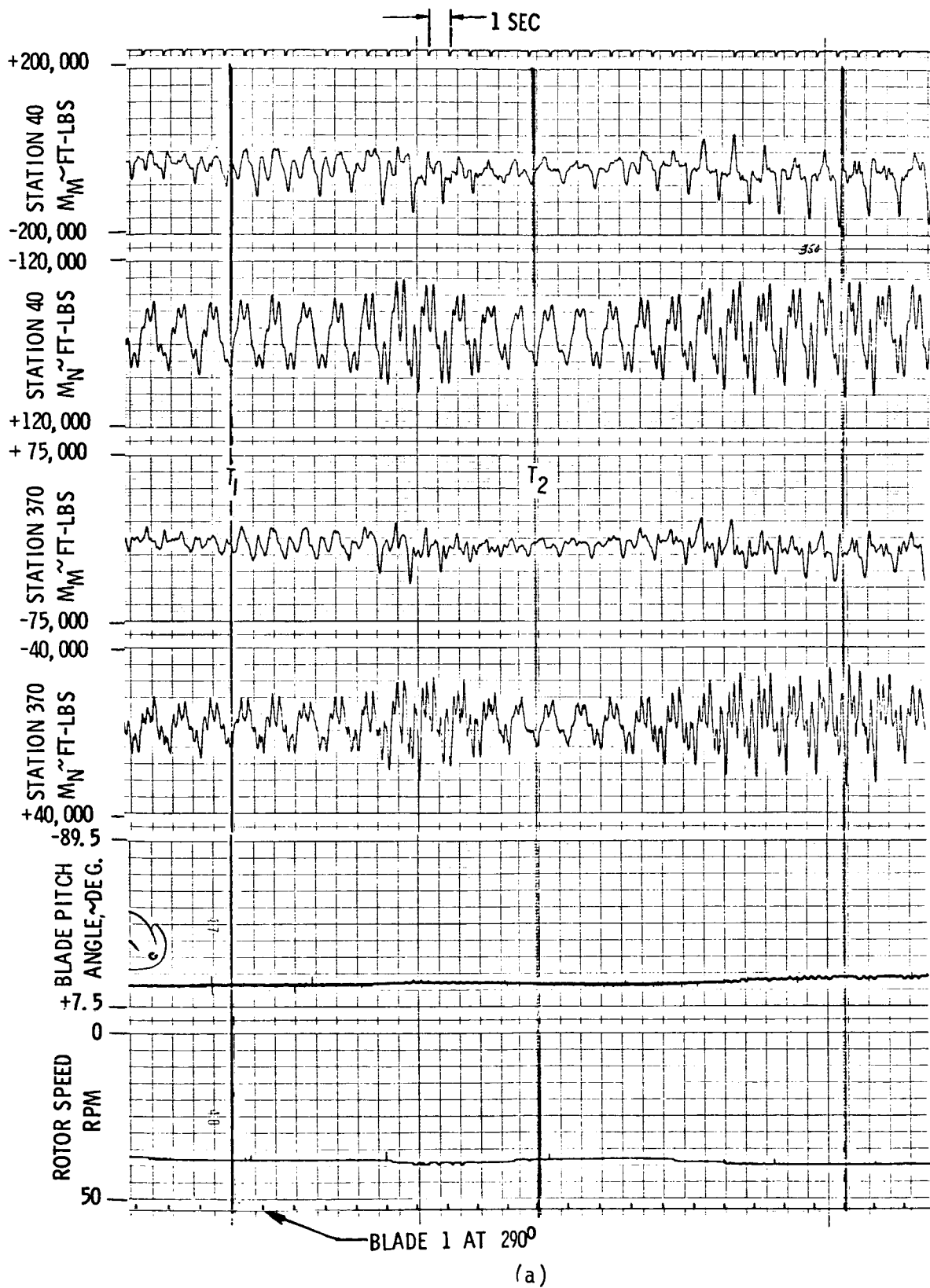
Figure 8. - Gust response with shaft oscillation.

Figure 8. - Continued.
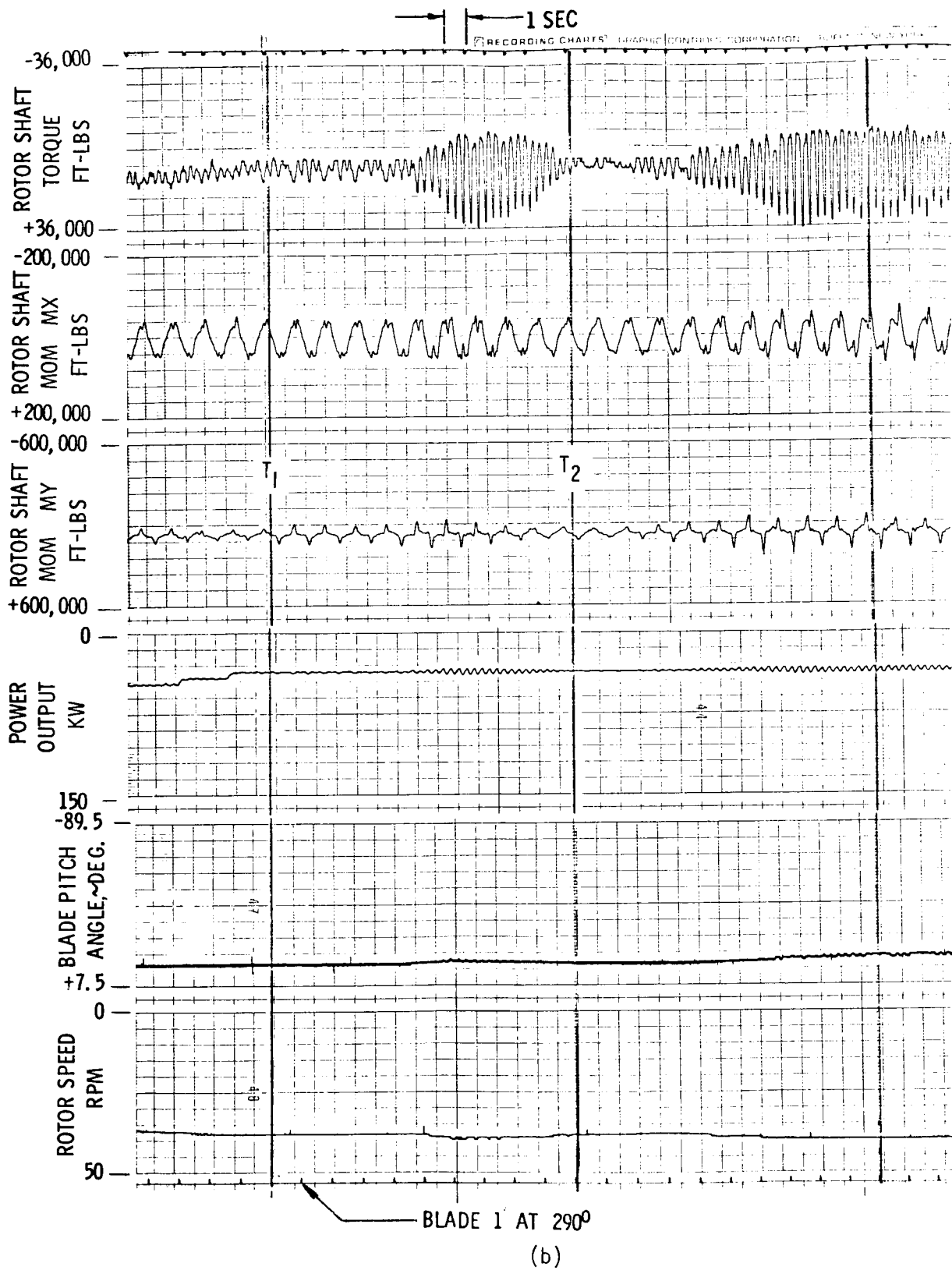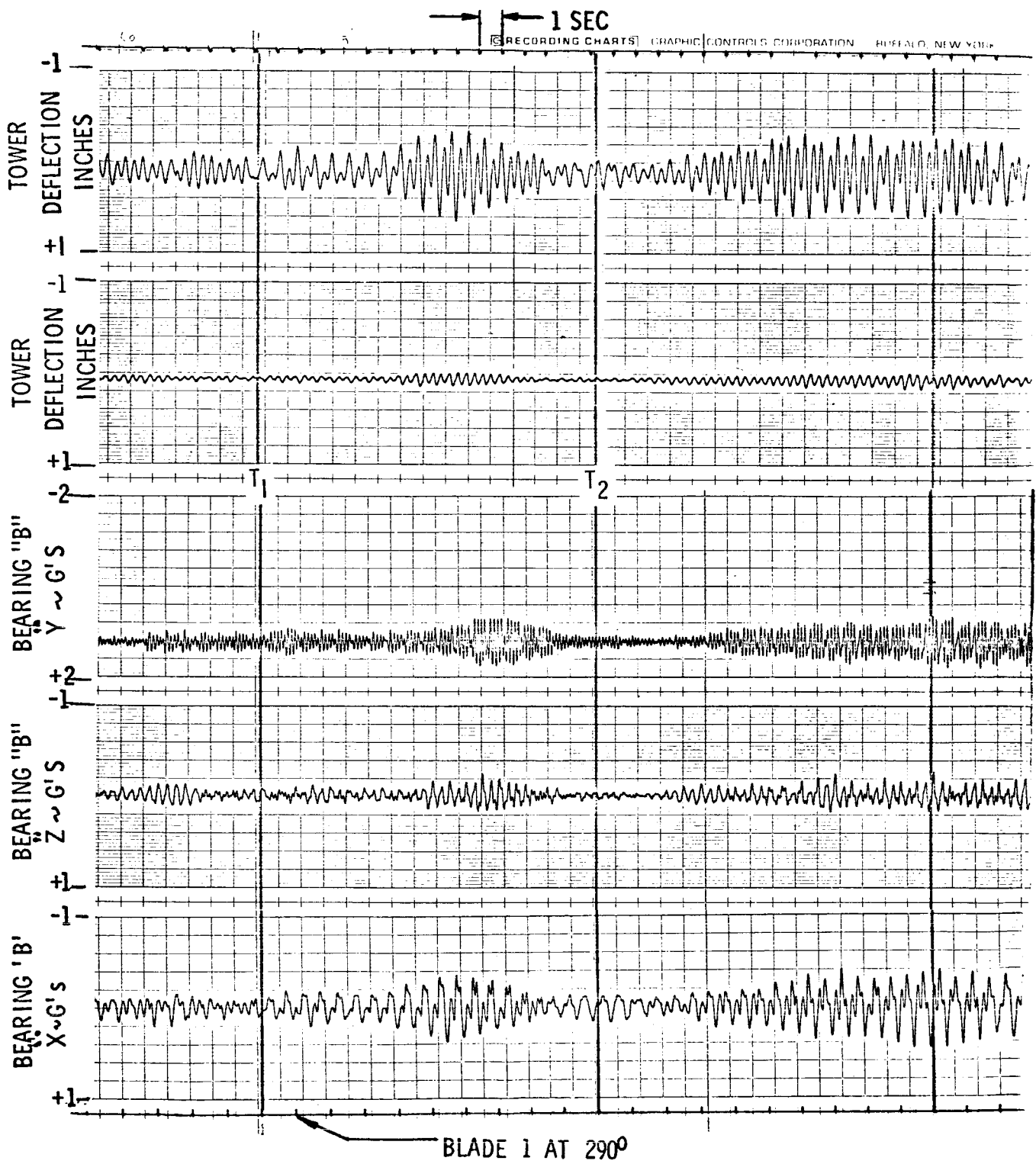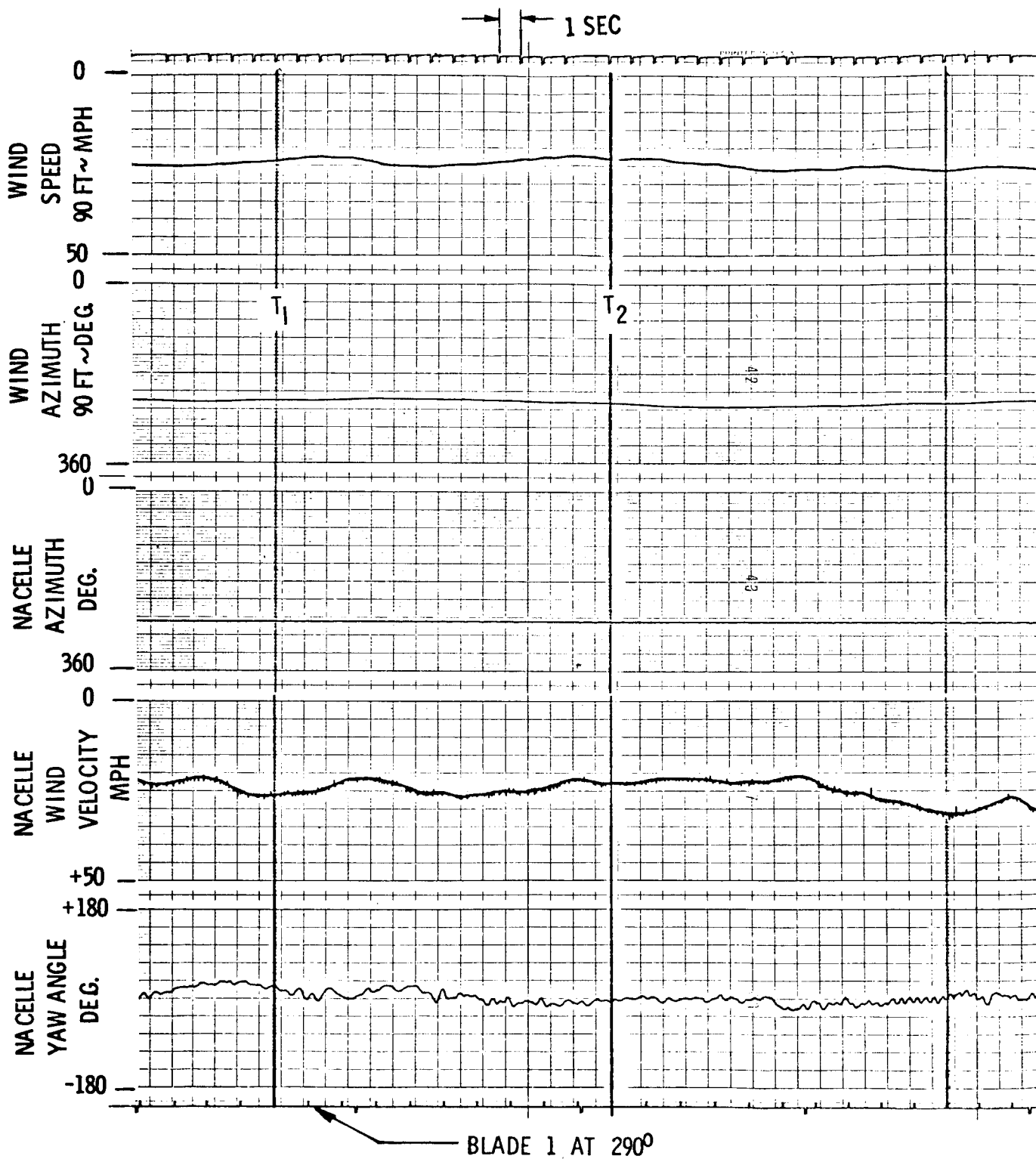
134

(c)

Figure 8. - Continued.

135

BLADE 1 AT 290°

(d)

Figure 8. – Concluded.

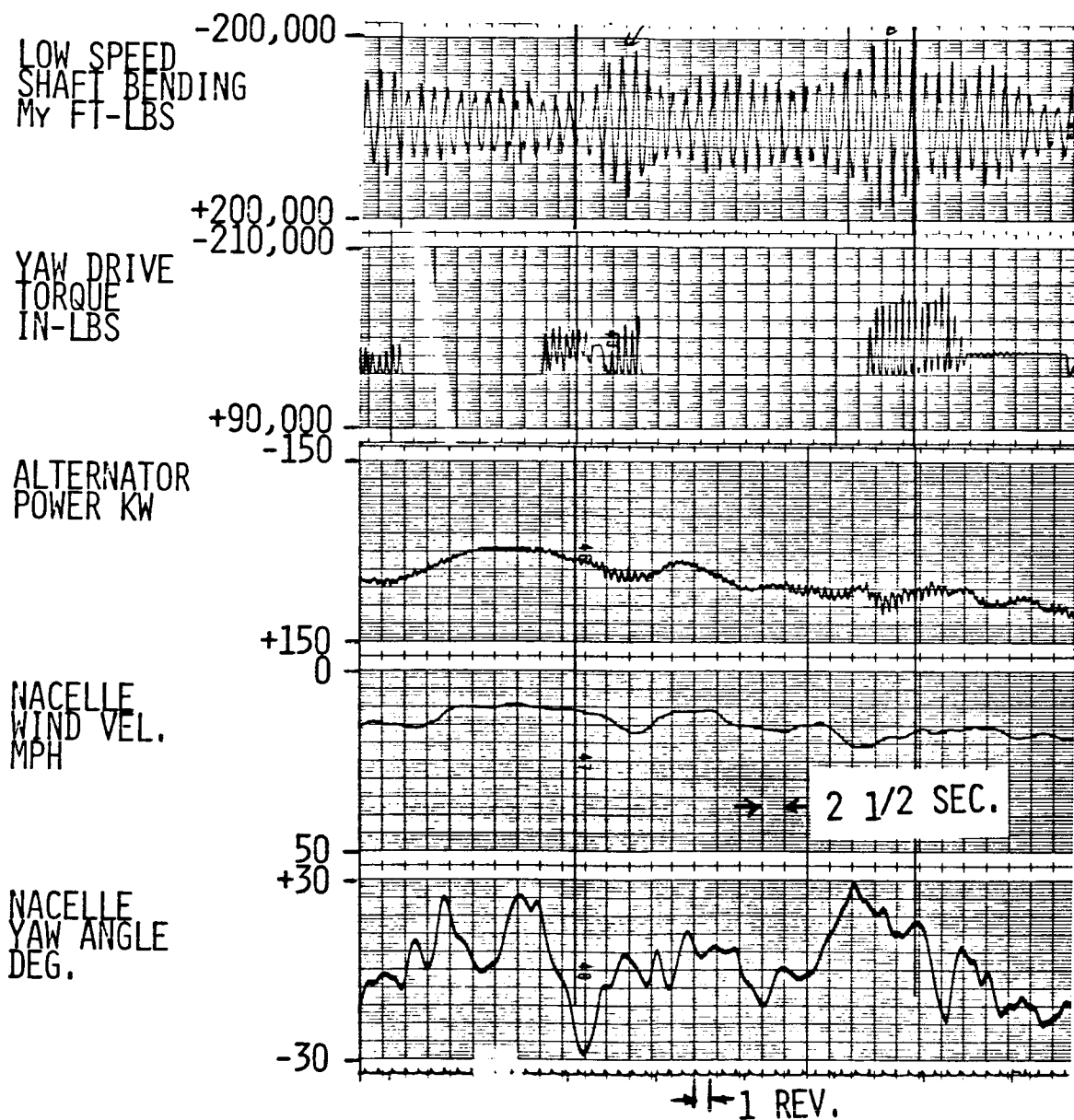Figure 9. - Low-speed shaft bending with yaw brake release.

137

Figure 10. - 40-rpm Load bank operation with yaw brake.

ALTERNATOR POWER - KW

ROTOR BEARING ACCEL - $\ddot{Y}$ G'S

ROTOR BEARING ACCEL - $\ddot{Z}$ G'S

ROTOR BEARING ACCEL - $\ddot{X}$ G'S

NACELLE WIND VELOCITY MPH

NACELLE YAW ANGLE DEG

(a)

138

BLADE FLAPWISE BENDING STA. 40 FT-LBS

BLADE INPLANE BENDING STA. 40 FT-LBS

LOW SPEED SHAFT TORQUE FT-LBS

LOW SPEED SHAFT BENDING MY - FT-LBS

NACELLE WIND VELOCITY MPH

NACELLE YAW ANGLE DEG

(b)

Figure 10. – Concluded.

STA 40 BLADE
FLAPWISE BENDING,
ft-lb

200 000

-200 000
-120 000

STA 40 BLADE
INPLANE BENDING,
ft-lb

120 000
-36 000

LOW SPEED
SHAFT TORQUE,
ft-lb

36 000
-75

ALT POWER OUTPUT,
kW

75
0

CURRENT,
A

200

Figure 11. - 20-rpm Synchronous operation - 60-kW
set point.

140

BLADE FLAPWISE BENDING, ft-lb — 200 000 / -200 000

STA 40 BLADE INPLANE BENDING, ft-lb — -120 000 / 120 000

LOW SPEED SHAFT TORQUE, ft-lb — -36 000 / 36 000

ALT POWER OUTPUT, kW — -75 / 75

CURRENT, A — 0 / 200
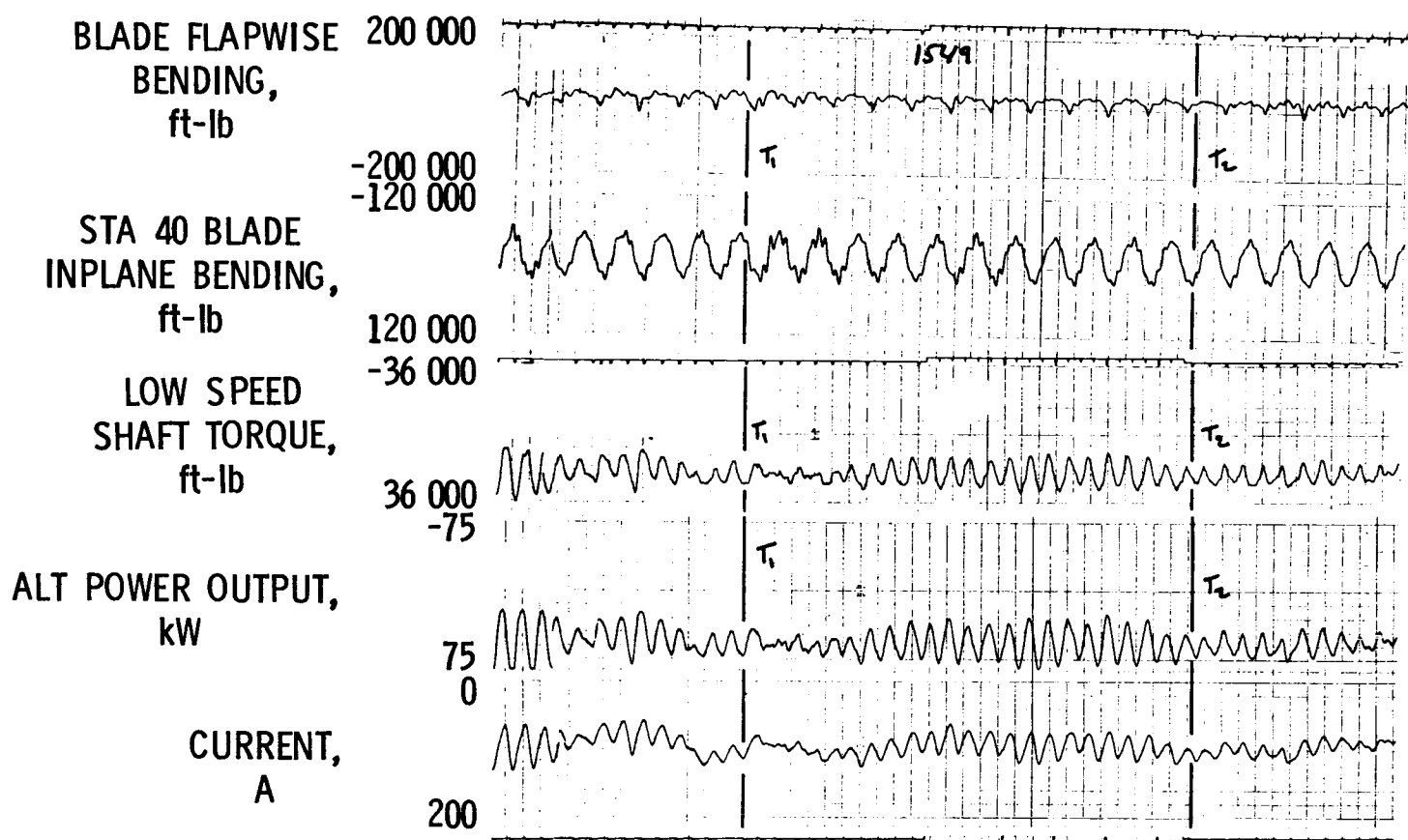
Figure 12. - 26.3-rpm Synchronous operation - 60-kW set point.

STA 40 BLADE FLAT
WISE BENDING,
ft-lb

STA 40 BLADE
INPLANE BENDING,
ft-lb

LOW SPEED
SHAFT TORQUE,
M_z - ft-lb

ALT POWER OUTPUT,
kW

CURRENT,
A

200 000

-200 000
-120 000

120 000

-36 000

36 000
-150
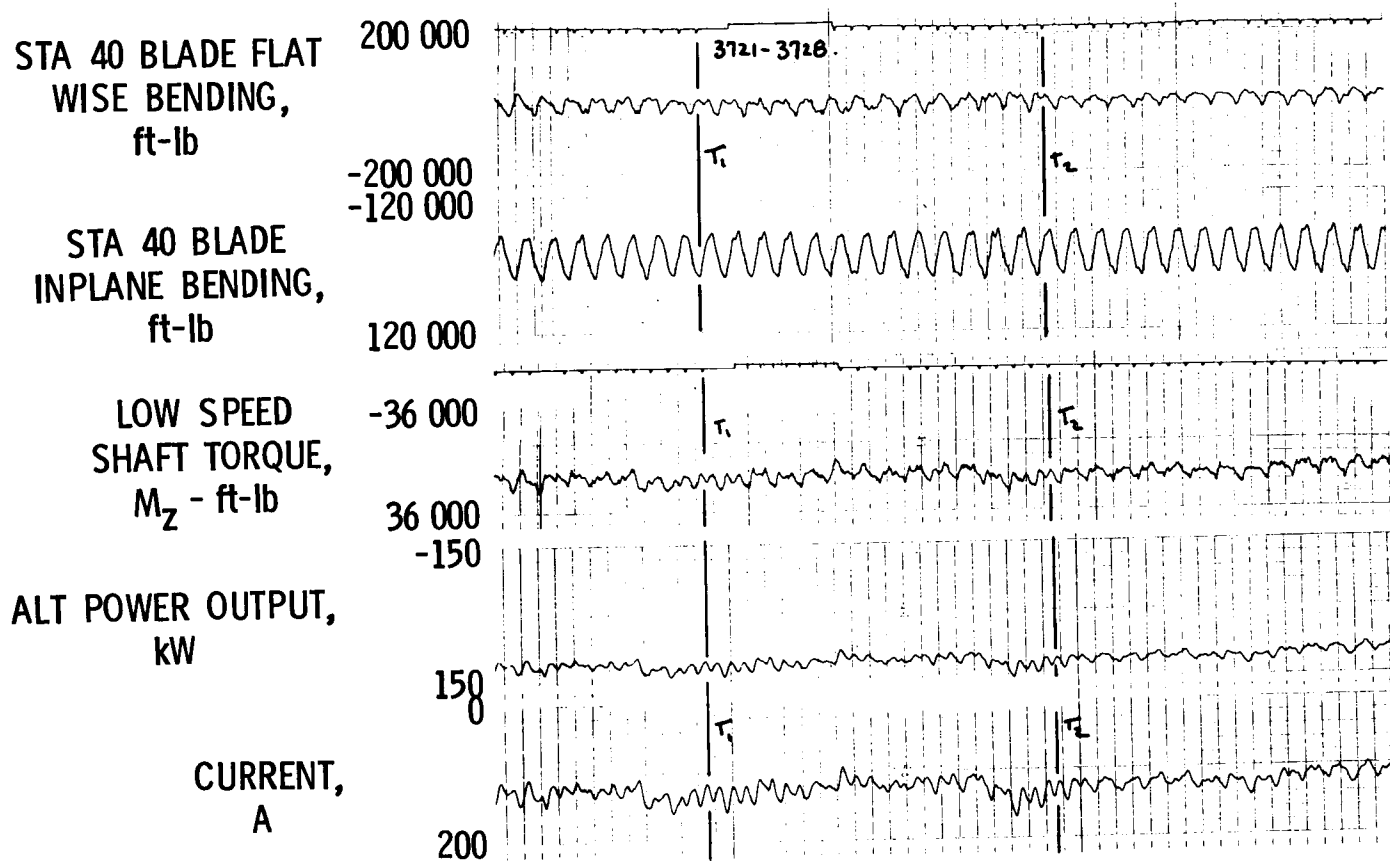
150
0

200

Figure 13. - 40-rpm Synchronous operation - 100-kW
set point.

142
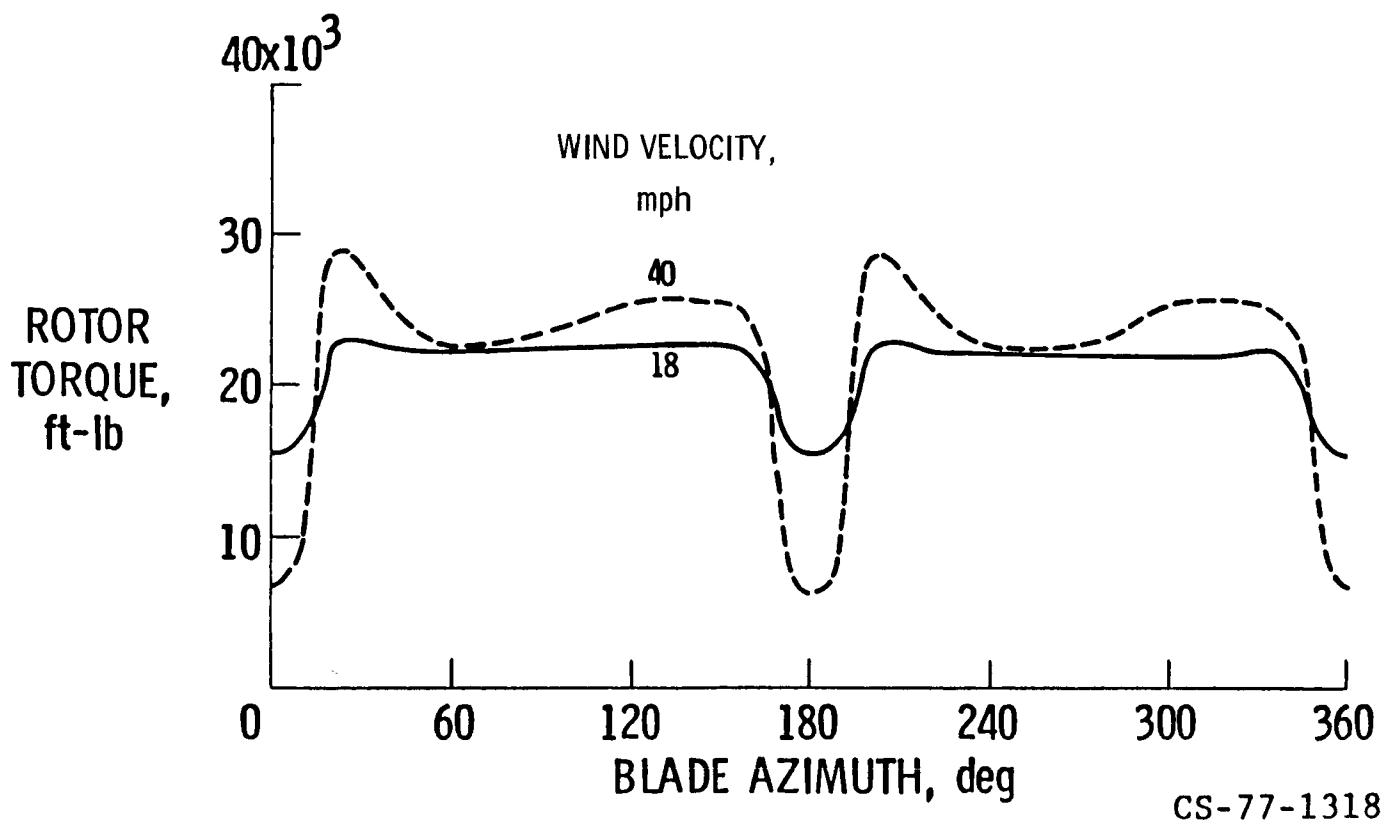
Figure 14. - Mod-0 rotor torque versus blade azimuth at 40 rpm.

CS-77-1318

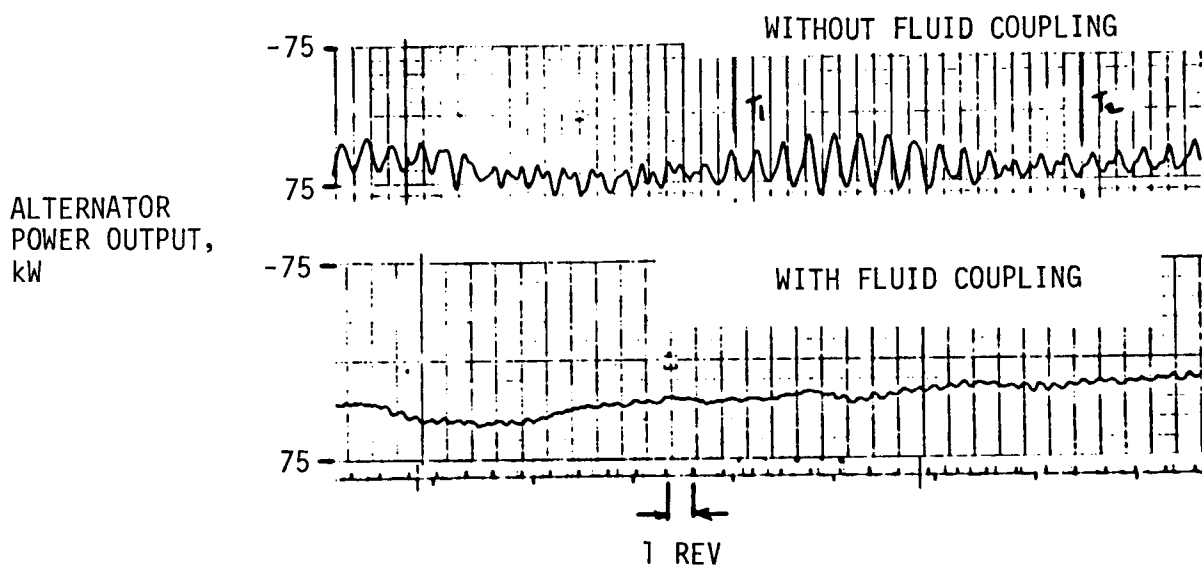ALTERNATOR
POWER OUTPUT,
kW

Figure 15. - Power oscillations with and without fluid coupling at 20 rpm.

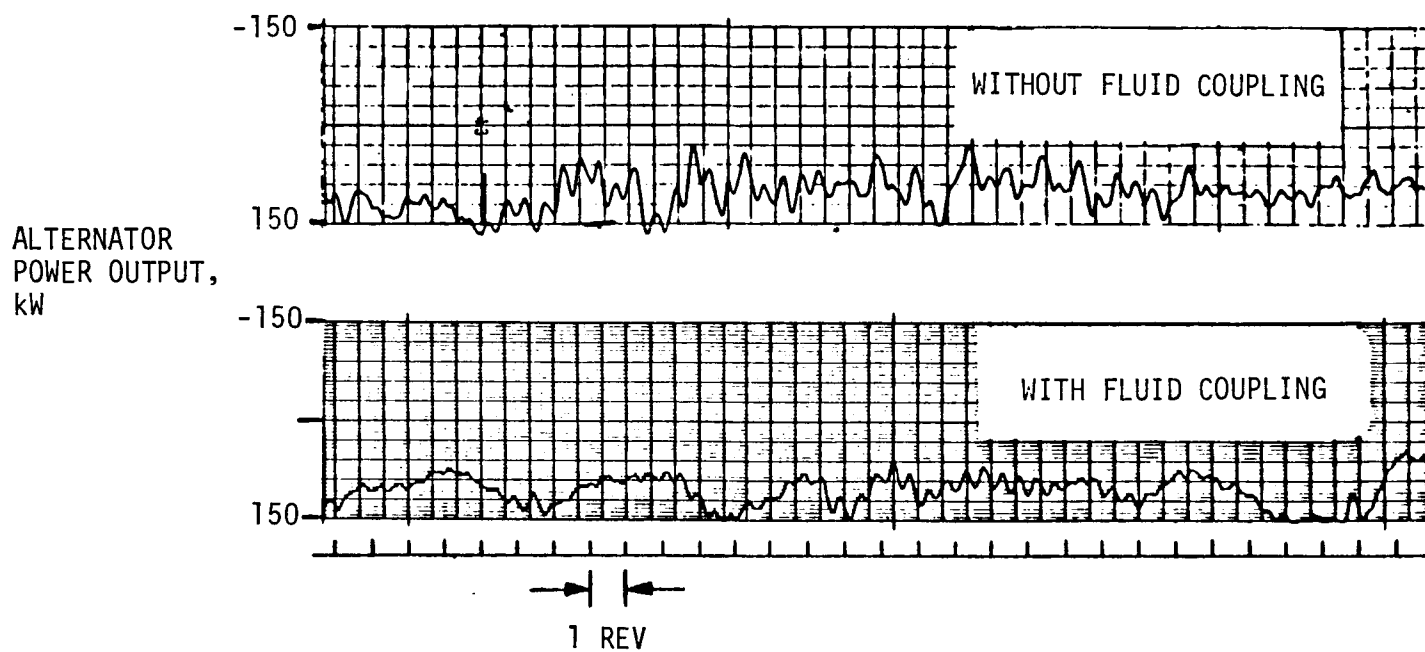Figure 16. - Power oscillations with and without fluid
coupling at 40 rpm.

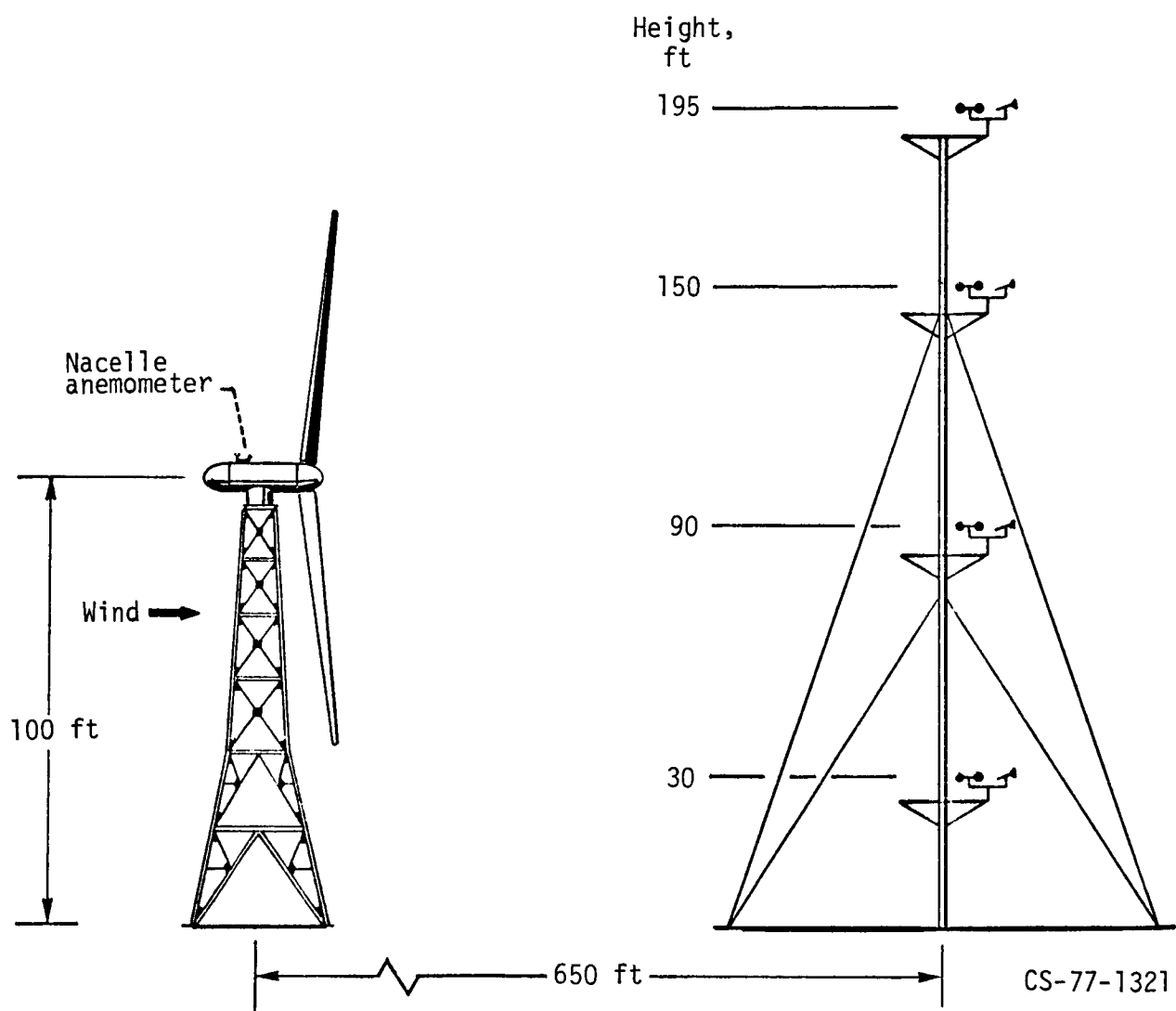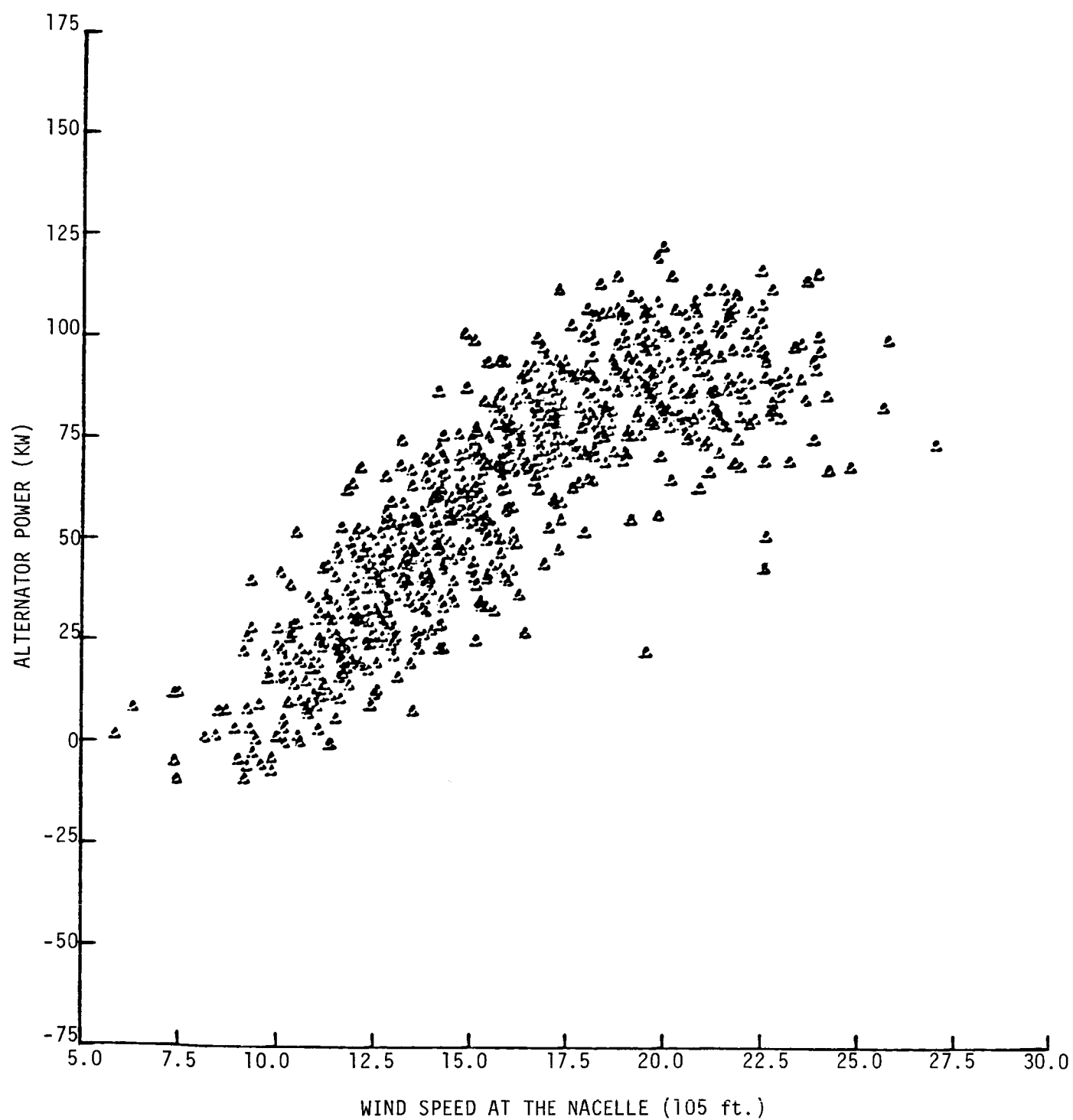Figure 17. - Mod-0 wind turbine and meteorological tower.

Figure 18. - Alternator power output versus nacelle wind speed - simultaneous measurements.
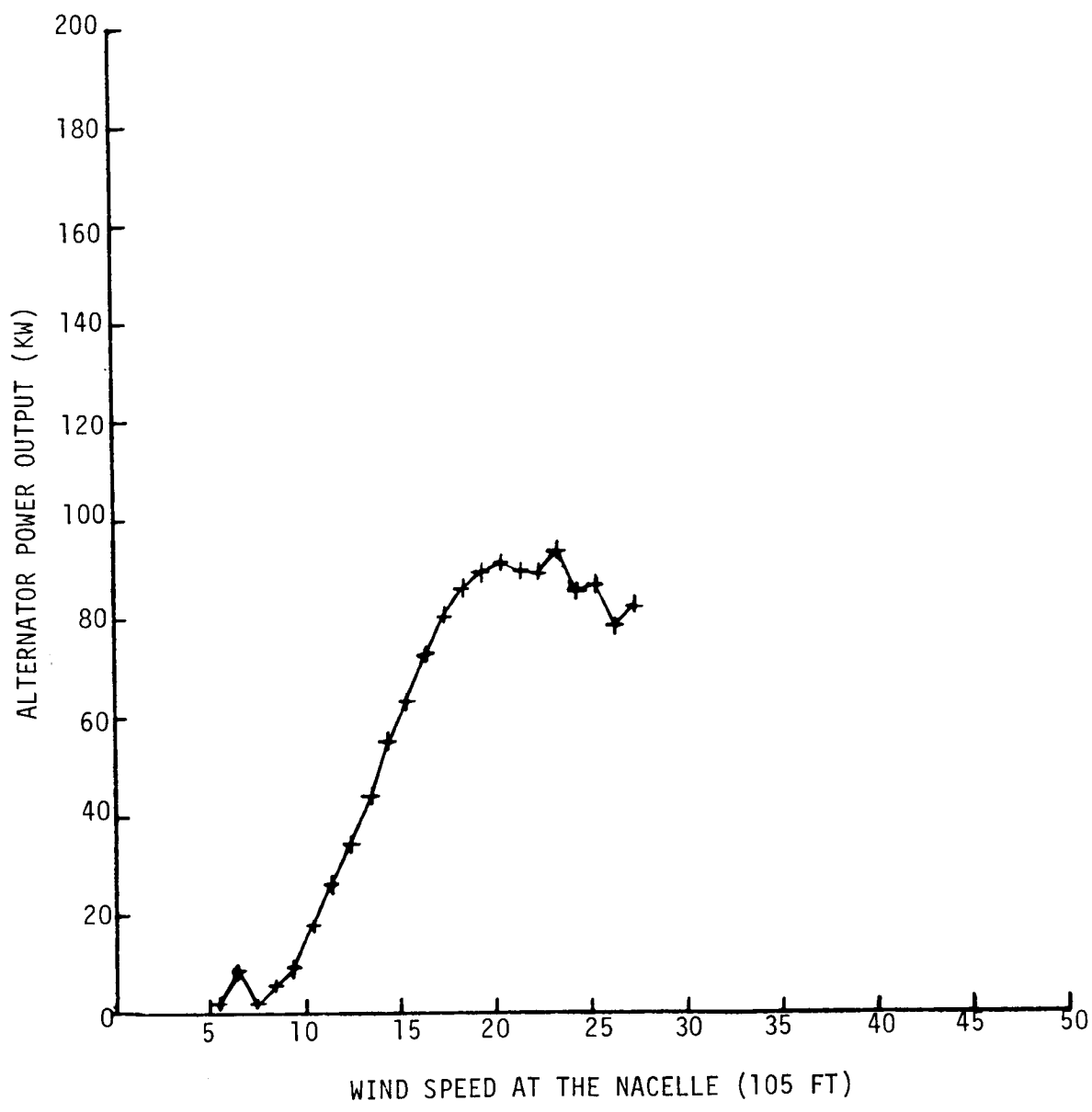
147

Figure 19. - Region-averaged alternator power output versus nacelle wind speed.
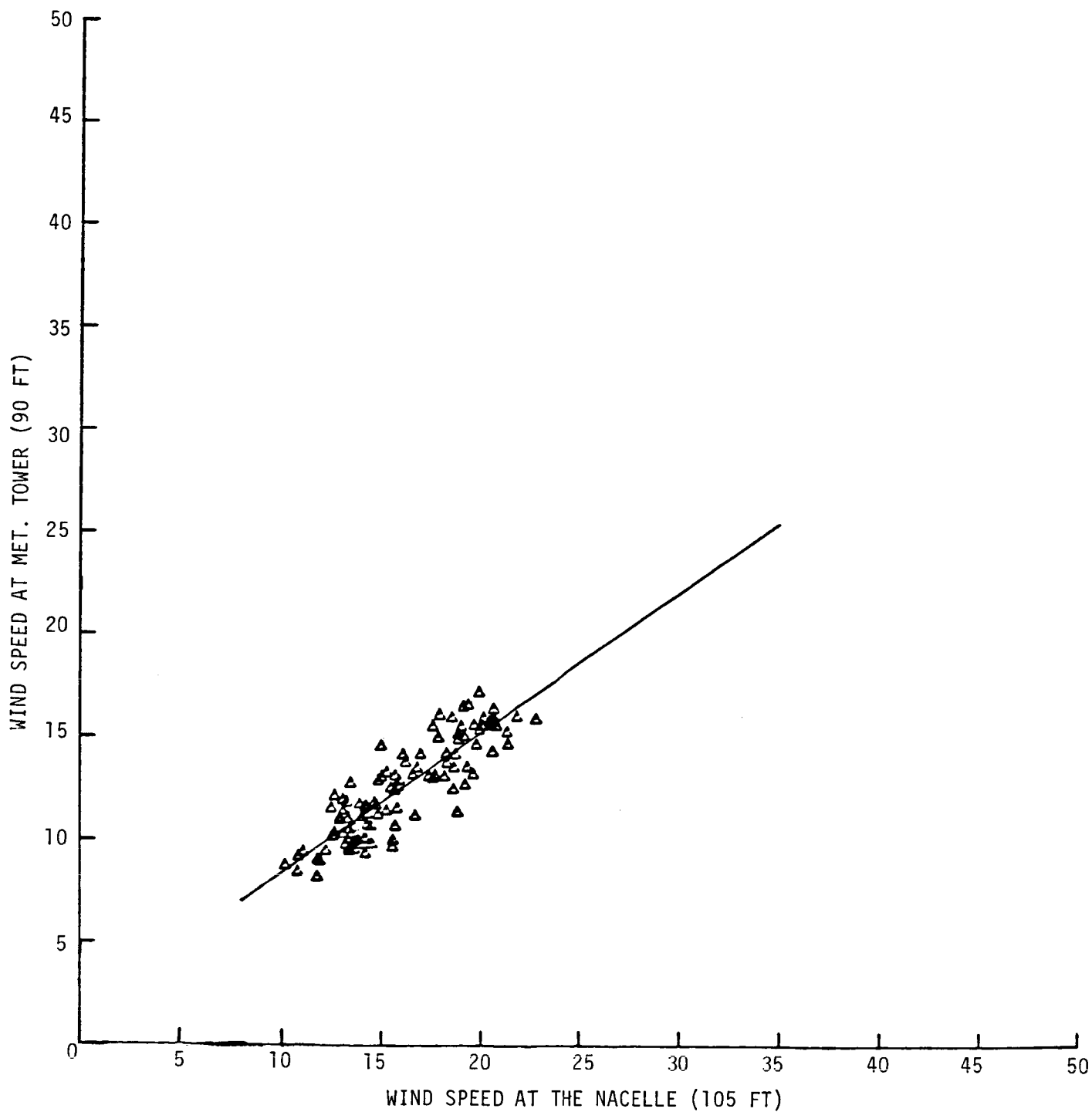
148

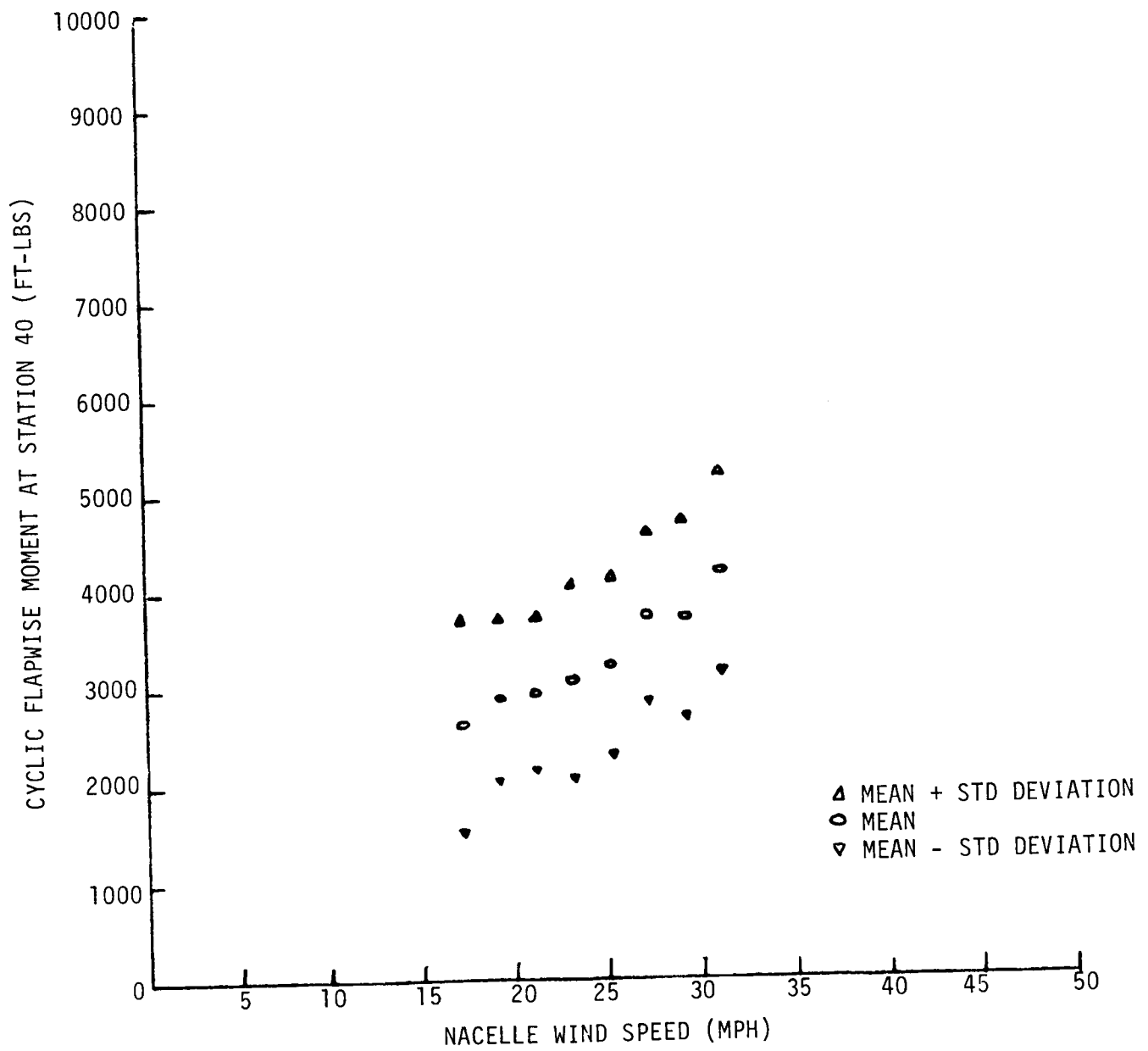Figure 20. - Meteorological tower wind speed versus nacelle wind speed - 2-minute averages.

Figure 21. - Mod-0 cyclic loads versus nacelle wind speed - flatwise moment, station 40.

POWER OSCILLATION OF THE

MOD-O WIND TURBINE

Robert C. Seidel

National Aeronautics and Space Administration
Lewis Research Center
Cleveland, Ohio 44135

ABSTRACT

The Mod-O power has noise components with varying frequency patterns.
Magnitudes reach more than forty percent power at the frequency of
twice per rotor revolution. Analysis of a simple torsional model of
the power train predicts less than half the observed magnitude and
does not explain the shifting frequencies of the noise patterns.

INTRODUCTION

The 60 cycle electrical power generated by the Mod-O wind turbine
generator has been relatively noisy. For perfect power the large
blades must rotate uniformly despite local wind patterns and power
train resonances. An error of only 0.1 degree in rotor position can
vary the power by about 20 percent. In the following, a model of the
power train is analyzed in the frequency and time domains to under-
stand its behavior, and results are compared with Mod-O data.

MODEL DESCRIPTION

A block diagram of the power train as represented by torsional springs,
dampers, and inertial masses is shown in figure 1. Each blade is a
single inertia with one dimension of freedom, (cordwise) lag. There
are no multi-dimensional degrees of freedom which have importance in
helicopter rotor studies. To admit such interactions here would
greatly complicate the simple analysis performed.

A typical torque pattern expected from the blades was known from a
separate aerodynamic computer code. This torque pattern served as an
input to the power train model for a time response analysis. The
aerodynamic program assumed a rigid but rotating hub and no blade lag
dynamics. To a first approximation the power train model supplies the
missing dynamics to the aerodynamics code.

RESULTS

Analytical

The rotor torque from the aerodynamic code is plotted in figure 2. As each blade swings behind the tower, more than 60 percent of the rotor torque is momentarily lost. Also plotted in figure 2 are the generator electrical torque responses to the rotor torque input. Data are shown for three high speed shaft configurations - a steel shaft, an elastomeric shaft, and a 2.3 percent slip coupling. The three responses have a similar oscillation pattern. The basic two per revolution oscillation (2P) is about 14 percent and there is a noticeable 4P component.

The system frequency responses are plotted in figure 3 for the three high speed shaft configurations. The responses at the even harmonics of rotor frequency, 2P, 4P, etc., are of special interest because at these frequencies the rotor torque input (of figure 2) has content. At these harmonics, the responses are similar, which is why the time responses of figure 2 are similar. The harmonic with the most spread is the 2P harmonic for which the slip coupling response is about half the steel shaft response.

Experimental

A sample trace of Mod-0 power and wind speed data is shown in figure 4. Two power variation examples are circled - a (general low frequency) control problem and a 2P oscillation. The control system contains a wind speed input which can directly command pitch changes. The peak to near 150 percent in power occurred when the measured wind speed dropped (but apparently not the true rotor average wind) and the blade pitched for more power. The 2P oscillation, the other variation circled, has a maximum amplitude of about 40 percent. It differs from the model analysis in two basic respects. First, the response can hold a 4P or a 2P pattern for periods of time of about 10 seconds. Second, the 40 percent maximum 2P oscillation is more than twice that predicted by the analysis. Evidently a significant 2P input is missing from the model analysis. To further our understanding, we plan to frequency response test the Mod-0 using the rotor pitch angle as the input and are also following results from a more complicated aerodynamics computer code from a contract effort.

DISCUSSION

Q. Please explain the idea you have for testing the dynamics by commanding harmonic collective pitch, in the field.

A. We plan to oscillate the pitch about a degree with a sinusoidal sweep frequency signal. The input would be on top of the control signal required to keep the synchronous power about constant and on line. Data reduction is to be off line from signals recorded on tape. The analyzer is expected to lock on to the signal and not the tower shadow.

Q. What frequency response capabilities can you get with Mod-O actuator to induce torque variations for running experimental frequency response of the drive train? This data can also be used to optimize control transfer function.

A. Experimental frequency response data is most desired to better validate the model dynamics. The pitch servo has about a 1.5 cps bandwidth. Care will be taken to avoid extended running at large amplitude to not deplete the hydraulic pressure in the pitch servo accumulator.

Q. Where would you add more inertia in the drive train to avoid the 2P bloom?

A. The power train is supposedly not near a 2P resonance. The bloom, however, does look like the response of a low damped resonance. The planned experimental frequency response test should help separate effects here. The most effective place for adding inertia, if deemed advisable for moving the _first_ mode, is probably on any shaft rotating at (or above) the generator speed.

Q. Where does the second resonance come from?

A. A normal modes analysis (with no blade degree of freedom) has shown the second mode to be primarily across the effective generator spring. The model frequency is quite sensitive to the blade degree of freedom, however. For example, the second mode natural frequency is nominally 3.50 cps for a blade natural frequency of 2.47 cps. If the blade spring constant is halved, the second mode frequency drops about 30 percent to 2.51 cps.

Q. What was the generator model?

A. It was a third order "voltage behind subtransient reactance" dynamic synchronous machine model connected to an infinite bus.

Q. What kind of excitation control was used for the alternator?

A. The Mod-0 has a slow VARS control which was simply modelled as a constant set to obtain the desired .8 power factor.

Q. How were numerical values for stiffness and damping properties obtained for the shafts, pulleys, and speed changers between the rotor and the generator?

A. The generator model is effectively the weakest stiffness element and the maximum damping element. Mechanical shaft stiffness values were calculated from geometry and material properties. The manufacturer's values for the Falk coupling were used. The external damping parameters were estimates based on a 75 percent efficiency and internal damping parameters were estimates to achieve at least about .05 damping ratios for the higher order modes.
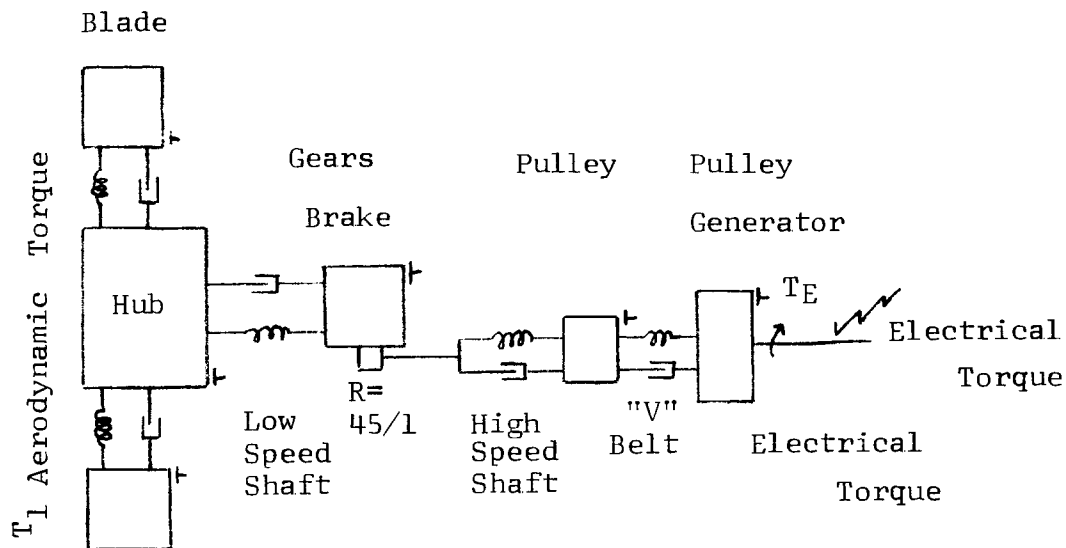
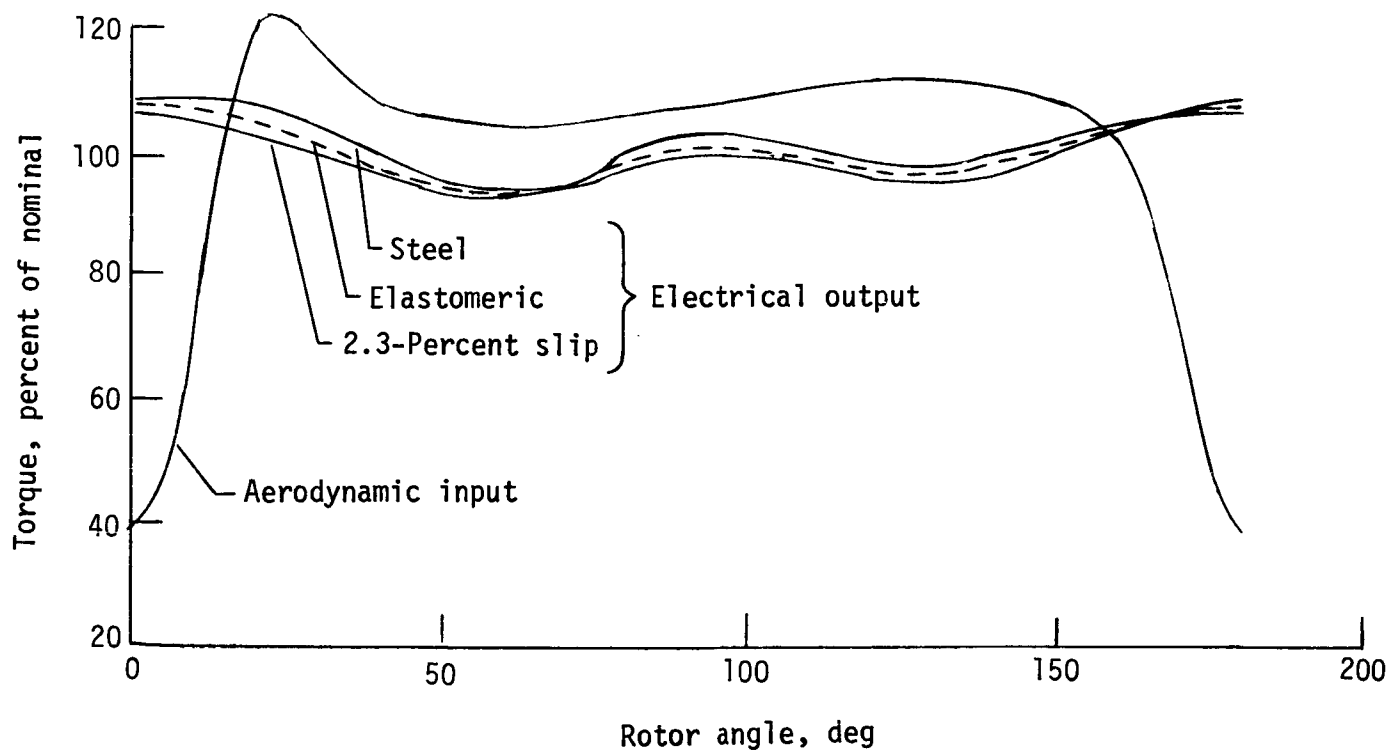Figure 1. - Block diagram of mechanical elements in power train.

Figure 2. - Output response comparisons of three high-speed
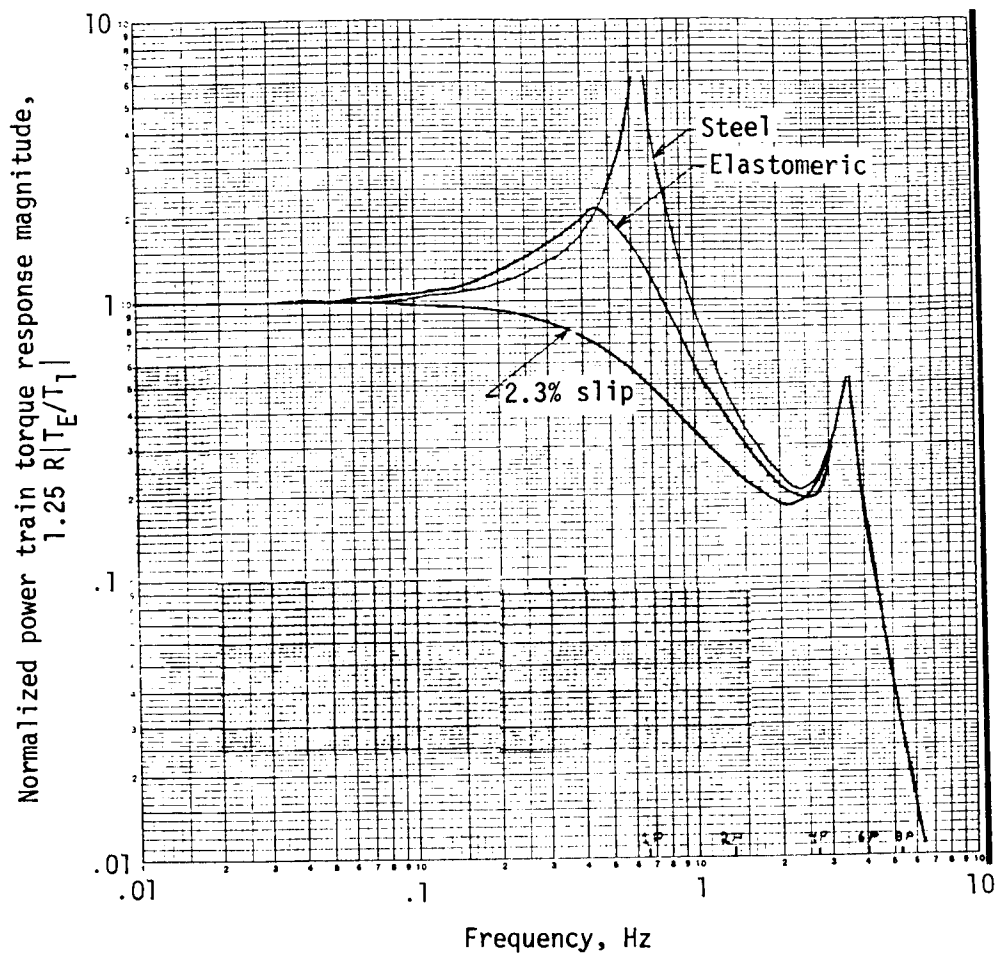shaft configurations to the same input.

Figure 3. - Power train frequency response magnitude
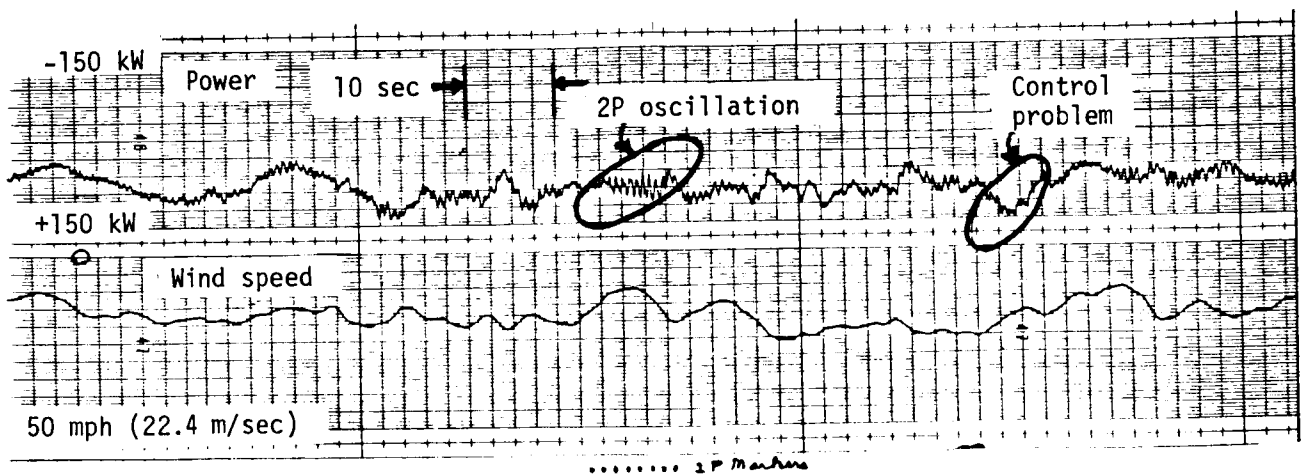comparisons for three high-speed shaft config-
urations.

Figure 4. - 2.3-Percent slip coupling with feed forward control, recorded
on 10/8/77.

DRIVE TRAIN DYNAMIC ANALYSIS

Nicholas Giansante

Kaman Aerospace Corporation
Bloomfield, Connecticut 06002

ABSTRACT

A method for parametric variations in drive train dynamic analysis is described. The method models the individual components of a drive system, forms the appropriate system interface coordinates and calculates the system dynamic response at particular frequencies. Application of the method for prediction of the dynamic response characteristics of a helicopter transmission and a comparison of results with test data is also included.

INTRODUCTION

Substructure methods using impedance techniques are a convenient and economical means for dynamic analysis of wind turbine drive trains. Response characteristics of a complex structure, such as a wind turbine drive system, may be effectively evaluated using the technique described herein. The method models the individual components comprising a complex system, forms the appropriate interface coordinates and predicts the total system dynamic response at particular frequencies of interest.

The method has two important features. The first of these relates to reduction in degrees of freedom. Analysis of each basic component is performed with as many degrees of freedom required to accurately predict the motion at the coordinates and frequencies of interest. When the resulting analytical model is used, however, the number of degrees of freedom may be drastically reduced and must include only the following: (1) those which interface other components such as gear mesh line of action coordinates, coupling coordinates and bearing support coordinates, (2) coordinates at which structural modifications are to be included, (3) coordinates at which a force is applied, and (4) coordinates at which dynamic response is desired.

This reduction in the number of coordinates is performed only once at each frequency of interest with no loss in the validity of the analytical model, regardless of the extent of the reduction.

The second important feature relates to the ease with which structural changes may be implemented. Structural modifications such as local mass or stiffness changes, the addition of springs or dampers between components, addition of vibration absorbers and changes in boundary conditions may be cost effectively modeled.

THEORETICAL BASIS

A linear structure may be represented in the frequency domain as a finite element model using an impedance formulation in terms of the mass, stiffness and damping matrices.

The relationship between the applied force and the structural response is

$$Zy = f \qquad (2)$$

where y is a vector representing the response, either displacements or rotations, Z is the impedance matrix, and f is a vector denoting the excitation, either force or moment. Except for an undamped system at resonance or for $\omega = 0$, Z will not be a singular matrix. Thus

$$y = Z^{-1}f = Yf \qquad (3)$$

where Y is referred to as the mobility matrix and may be determined by inversion of the impedance matrix. Elements of the mobility matrix are not amenable to analytical modeling, however, they have physical significance and are measurable quantities representing the deflection at a coordinate due to a unit force applied at that or some other point. Since each element may be directly measured on the actual structure, they are independent of the number and location of the other degrees of freedom.

The criterion for a valid impedance matrix is that the elements of its inverse correctly represent the true response characteristics of the structure. Thus, a direct method of obtaining a valid reduced impedance matrix is as follows: (1) perform a structural analysis using conventional methods to obtain a valid, full size, impedance matrix, $Z(\omega)$, at each frequency of interest, (2) invert $Z(\omega)$ to obtain a valid full size mobility matrix $Y(\omega)$, (3) select elements from $Y(\omega)$ corresponding to the coordinates to be retained, which form a new reduced mobility matrix, $Y_R(\omega)$, (4) finally, the reduced impedance matrix is formed by inversion of $Y_R(\omega)$:

$$Z_R(\omega) = Y_R^{-1}(\omega) \qquad (4)$$

The reduced impedance matrix $Z_R(\omega)$ is valid only at the frequency at which it was formed. There is no special interpretation of $Z_{R(\omega)}$ in terms of mass stiffness and damping matrices. The physical system represented by $Z_{R(\omega)}$, at the frequency ω, behaves precisely as the system under study (Ref 1).

The reason for specifically obtaining the impedance matrix of the reduced system is that the impedance matrix of a complex structure may be obtained by adding the impedance matrices of the separate components at coordinates where the deflections are common. If Z_a, Z_b, Z_s are partitioned impedance matrices of subsystem a, b and the complete system, respectively,

and ($\hat{\underline{}}$) refers to interface coordinates, ($\hat{}$) refers to noninterface coordinates and ($^-$) refers to coupling between interface and noninterface coordinates, then

$$Z_s = \begin{bmatrix} \hat{Z}_a & \overline{Z}_a & 0 \\ \hat{\overline{Z}}_a & \overline{Z}_a + \overline{Z}_b & \hat{\overline{Z}}_b \\ 0 & \hat{Z}_b^T & \hat{Z}_b \end{bmatrix}$$

(5a)

and $Y_s = Z_s^{-1}$.

(5b)

There are several considerations involved in the practical application of this analysis technique as follows: (1) the substructures must be modeled as if they were unrestrained at the interface coordinates, (2) it is not important how the reduced mobilities are computed as long as they are valid, (3) the number of reduced coordinates must not be so large that matrix inversions are prohibitive, (4) local impedance changes due to addition of spring-mass systems or boundary condition changes are simply added to the reduced component impedances, (5) addition of impedance matrices must be performed at corresponding elements representing deflections or rotations in the same direction, (6) the impedance of spring-damper devices separating system components must be added to one of the substructures prior to synthesis.

SYSTEM OVERVIEW

A computer program was developed to implement the analytical technique. The computer program automatically and conveniently performs the coordinate reductions, coordinate transformations, addition of impedance changes, impedance matrix addition for subsystems and determination of the mobility matrix of the combined system. The program has the ability to accommodate structural modifications including local mass, stiffness or damping changes, addition of springs and/or dampers between components, addition of vibration absorbers and changes in boundary conditions without performing new and costly analyses for each change. Figure 1 presents a schematic of the computer program. Impedance matrices of the various components comprising the structure are formed at the frequencies of interest and stored, with appropriate identification, in the common data bank. Component modifications are performed as desired and the modified impedance matrices with appropriate identification are optionally stored in the data bank or used in the current analysis. The original component impedance matrices are retained in the data bank.

The methodology and associated computer program has the capability to modify the characteristics of any dynamic component as follows:

1. Add Structural Damping

Structural damping may be added in the form igK, where K is simply the component impedance matrix at zero frequency which is stored in the data bank. Thus, the component impedance matrix with the addition of structural damping at a particular frequency of interest, ω, is

$$Z_{Mod}(\omega) = Z_{Orig}(\omega) + ig\, Z_{Orig}(\omega = 0) \tag{6}$$

where g is the structural damping coefficient.

2. Addition of Vibration Absorber or Lumped Mass

The modification of the component impedance matrix due to vibration absorbers attached at particular coordinates involves a change in both the real and imaginary components of the impedance matrix yielding

$$Z_{Mod}(i,i) = \frac{\{[(1 - \frac{\omega}{\Omega})^2] + 4(\frac{\omega}{\Omega})^2\}\,\omega^2 m}{[1 - (\frac{\omega}{\Omega})^2]^2 + 4\xi^2} + i\,\frac{2(\frac{\omega}{\Omega})^3 \xi\omega^2 m}{[1 - (\frac{\omega}{\Omega})^2]^2 + 4\xi^2} + Z_{Orig}(i,i) \tag{7}$$

For the addition of a lumped mass the impedance change becomes

$$Z_{Mod}(i,i) = -\omega^2 m + Z_{Orig}(i,i) \tag{8}$$

In the above equations, ω is the frequency of excitation and Ω, m and ξ are the undamped natural frequency, the mass and the damping ratio, respectively, of the vibration absorber. This change is made in the original impedance matrix to the diagonal element corresponding to the point at which the vibration or lumped mass is attached.

3. Addition of Spring-Damper in Series

Since the addition of a parallel spring-damper system at a coordinate generates a coordinate at the free end of the system, an additional row and column are included in the modified impedance matrix. If k is the spring rate and c the damping rate of the system, the modified impedance matrix becomes

$$Z_{Mod} = \begin{bmatrix} & \vdots & & & 0 \\ \cdots & (Z_{Orig} + k + i\ c) & \cdots & & (k + i\ c) \\ & \vdots & & & \vdots \\ & \vdots & & & \vdots \\ \hline \cdots 0 \cdots (k + i\ c) & \cdots \cdots & 0 \cdots & & (k + i\ c) \end{bmatrix} \qquad (9)$$

<div align="center">Attachment Coordinate   Additional Column</div>

<div align="center">Additional Row</div>

4. Addition of Spring-Damper to Ground

In this situation the modified impedance matrix is simply the original impedance matrix with each diagonal element altered by the spring-damper system impedance:

$$Z_{Mod}(i,i) = Z_{Orig}(i,i) + k + i\ c \qquad (10)$$

5. Coordinate Transformation

Any linear transformation of coordinates may be effected. Rotations, sign changes and combinations of rotation and translation are common applications. Transformation of local coordinates into the global system for component synthesis is a typical application. Additionally, transformation of coordinates on interfacing components to conform to the direction of the line of action of a gear mesh may be implemented. If the transformation matrix is defined as T, the impedance matrix for the transformed coordinates becomes

$$Z_{Mod} = T^T Z_{Orig} T^1 \qquad (11)$$

6. Coordinate Reduction

Coordinate reduction must be performed on the mobility matrix since the elements of this matrix have individual physical significance. Thus, to accomplish a coordinate reduction the impedance matrix for a component must be retrieved from the data bank and inverted to yield the mobility matrix. The coordinates to be eliminated are removed from the mobility matrix and the resulting matrix inverted to form the desired reduced impedance matrix.

$$Y_{Orig} = Z_{Orig}^{1}; \qquad Y_{Mod} = (Y_{Orig})_{Reduced}; \qquad Z_{Reduced} = Y_{Mod} \qquad (12)$$

APPLICATION

The method was successfully applied in a vibration study of a helicopter transmission shown schematically in Figure 2 (Ref 2). The configuration was appropriate to a substructure type analysis satisfying the requirements of a small number of components and a small number of excitation frequencies. The transmission case and each of the shafts were treated as substructures with interfaces at the bearings and gear meshes and which could be reduced to an analytical model with a small number of coordinates. The study included such effects as bearing stiffness, mass and stiffness changes in the shafts, case damping, case vibration absorbers and mounting characteristics.

To validate the dynamic substructure analysis method, analytically derived vibration characteristics were compared to simulated operational test data for a Kaman SH-2D helicopter main transmission. Acceleration response of the transmission case, measured normal to the surface, at fourteen selected points was compared to the respective analytically obtained response. Figure 3 presents a comparison of measured and predicted case surface accelerations in peak g's for excitation applied at the planetary system fundamental frequency of 348 Hz at 80% rotor rpm and a torque loading of 9120 in-lb.

WIND TURBINE APPLICATION

The method may be cost effectively applied in wind turbine drive train dynamic analyses. A typical wind turbine power system, including a torsional isolation system is presented in Figure 4. Using the rotor, torsional isolation system, gearbox and generator impedance matrices the torque response at the generator may be determined. Thus, parametric studies may be easily conducted to evaluate the effect of torsional isolation system, gearbox modifications and generator structural characteristics on the generator output.

CONCLUSIONS

1. An analytical method and associated computer program have been developed which have application in the dynamic analysis of a linear complex structure and modifications of it at a small number of discrete frequencies.

2. The method has been successfully demonstrated in the dynamic analysis of a helicopter main transmission where the components consisted of a gearbox case, the shafts and gears and a planetary system.

3. The method has application in the dynamic analyses of wind turbine drive systems.

REFERENCES

1. Berman, A., "Vibration Analysis of Structural Systems Using Virtual Substructures", The Shock and Vibration Bulletin 43, NRL, Washington, D.C., June 1973.

2. Bowes, M. A., "Development and Evaluation of a Method for Predicting the Vibration and Noise Characteristics of Helicopter Transmissions", AHS Paper No. 77.33-76, American Helicopter Society 33rd Annual National Forum, Washington, D.C., May 1977.

3. Berman, A., Flannelly, W. G., "Theory of Incomplete Models of Dynamic Structures", AIAA Journal, Volume 9, August 1971, pp 1481-1487.

DISCUSSION

Q. Are there problems with inversions if experimental data are used?

A. Information loss can be significant when developing an analytical model from experimental data. Information loss in inversion can be minimized if the ratio of extreme eigenvalues which characterize the structure is minimized. One approach is to form several models, each valid over a limited frequency band, within the complete frequency spectrum. An alternate technique is to use the method of incomplete models of dynamic structures (Ref 3) which combines analytical and test data to yield a model which is valid for the points of interest over a limited frequency range.

Q. Does provision exist in planetary gearing for torsional damping?

A. Torsional damping can be introduced in the planetary gear mesh by adding structural damping at gear mesh coordinates.
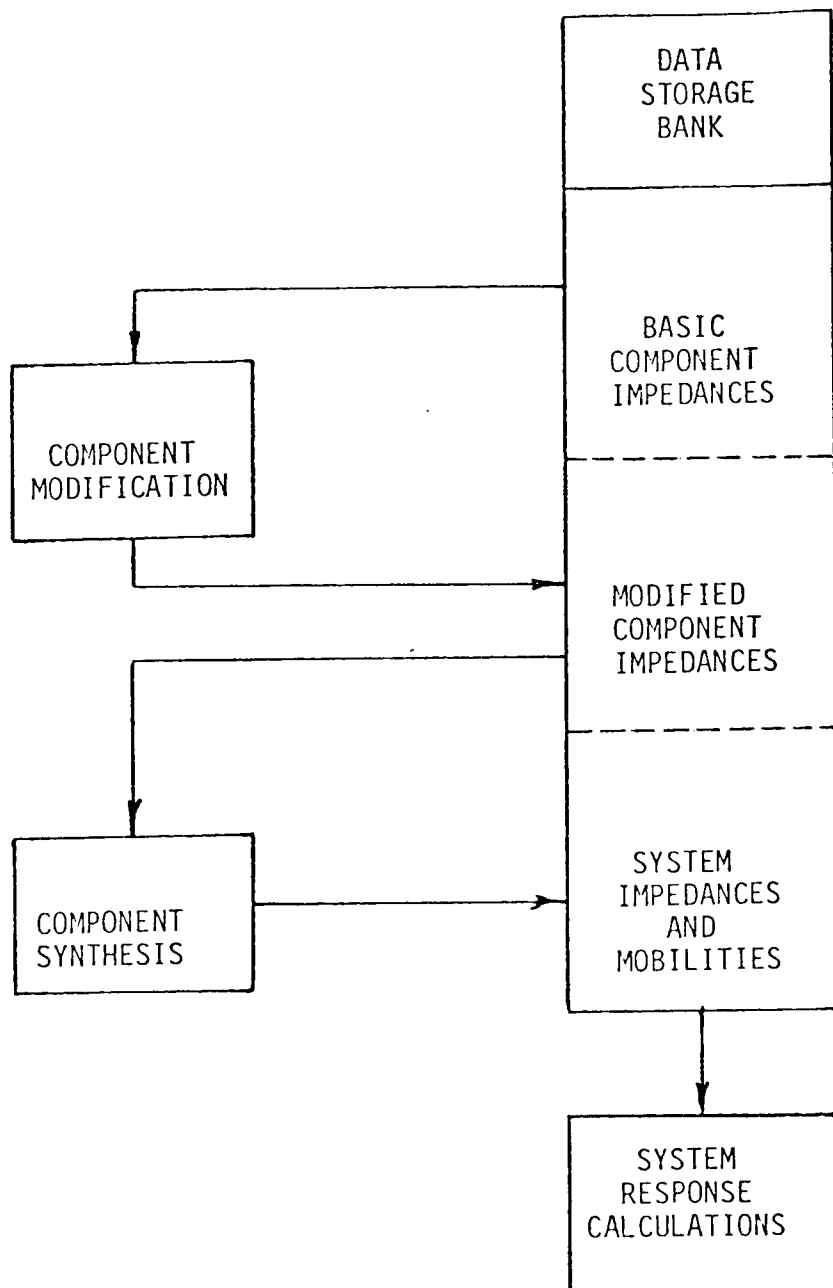
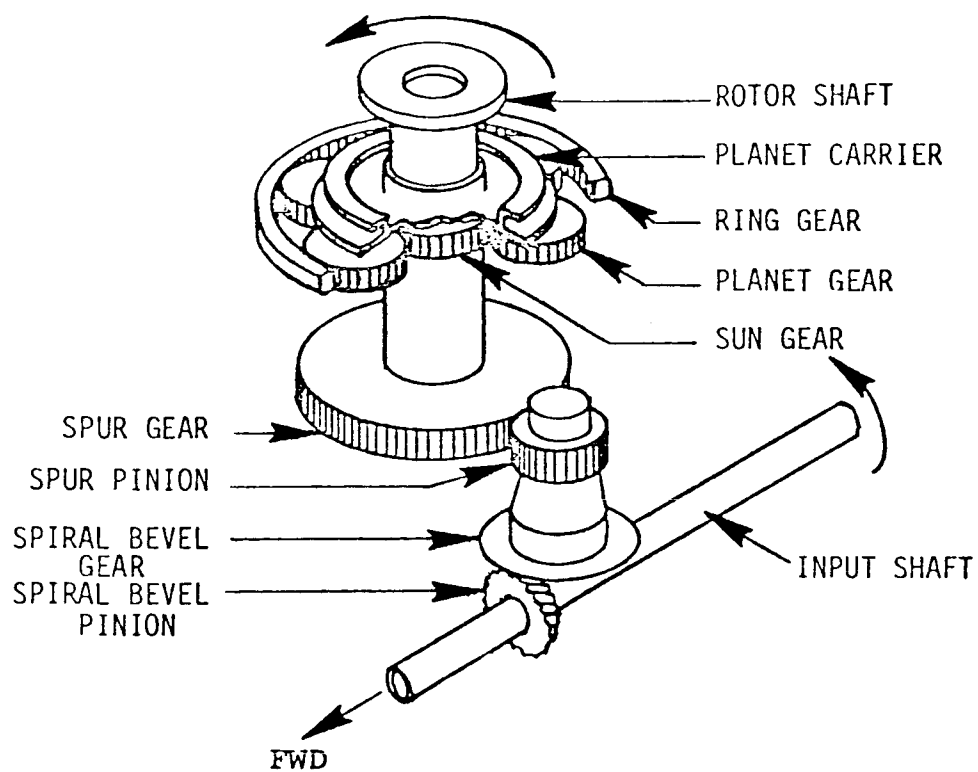Figure 1. - Schematic of computer program.
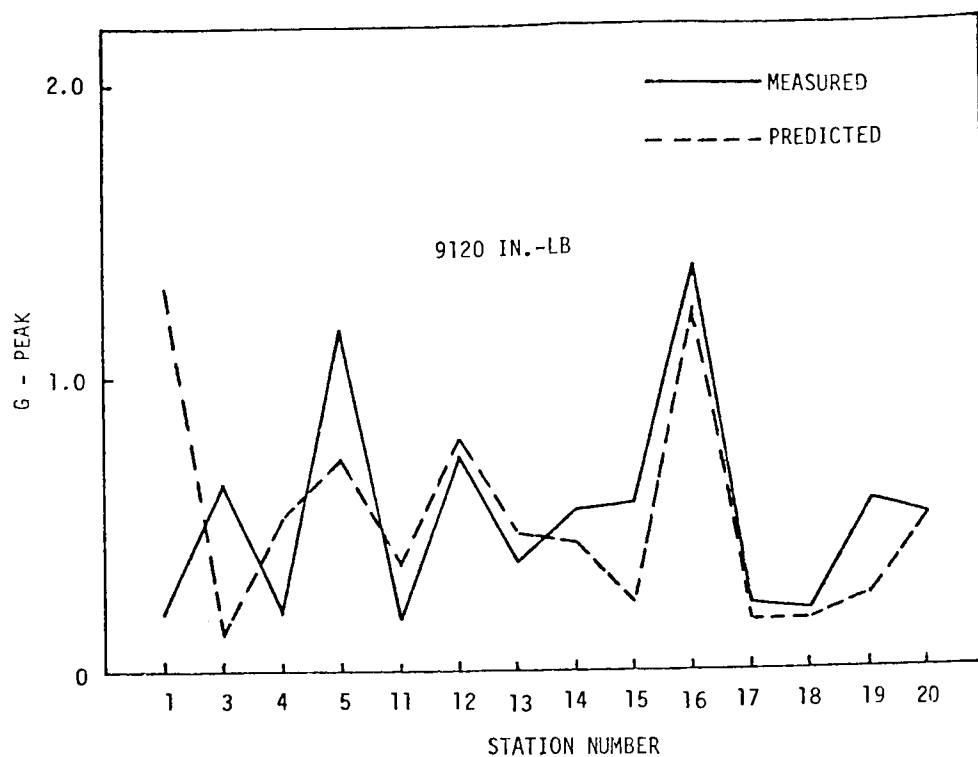
Figure 2. – Schematic of SH2 main transmission.

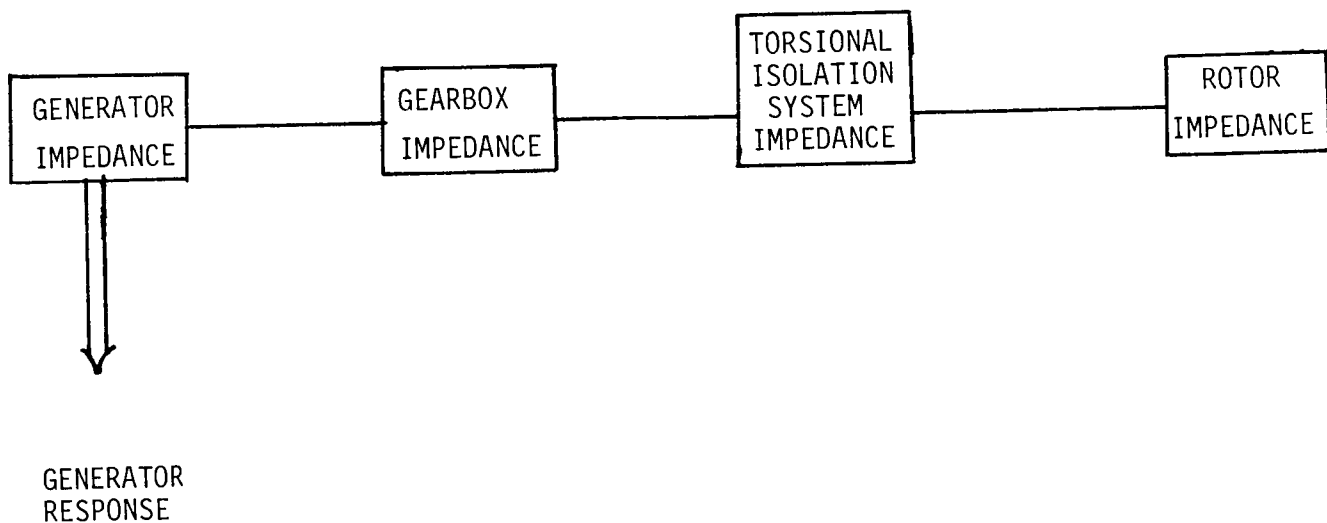Figure 3. - Measured versus predicted case acceleration
for 348-Hz excitation.

Figure 4. - Schematic of wind turbine power system.

MOD-1 WIND TURBINE GENERATOR ANALYSIS

Robert S. Barton

General Electric Company
Valley Forge Space Center
Philadelphia, Pa.   19101

ABSTRACT

A general summary of the MOD-1 Wind Turbine Generator control system and simulation is presented. Mechanical and speed stabilization control means to add drive train damping are mentioned and MOD-1 simulation results showing the effects of speed stabilization are displayed.

INTRODUCTION

This is an overview of the MOD-1 Wind Turbine Generator dynamic simulation performance characteristics and control. The MOD-1, designed by the General Electric Company, Space Division, Advanced Energy Programs, will be installed at a site near Boone, North Carolina. Under NASA Lewis Research Center direction, the design is a horizontal axis, constant speed system for a mean wind regime of 8 meters per second (18 mph) and rated at 2000 KW electrical at 11 meters per second (24.5 mph) at sea level.

Figure 1 shows the system which has a two-bladed, 200 foot downwind rotor. A step-up gearbox transfers rotor power to a synchronous generator housed in a nacelle which is supported by a truss type tower. Generation is at 4160 volts and the design provided for connection to the utility grid at a nominal 12-47 KV distribution level. The overall design is similar to the MOD-0A system but an order of magnitude larger in rating.

DRIVE TRAIN

Power flow in the drive train shown in Figures 2 and 4, is from the blades, into the rotor hub, through a low-speed shaft with gear coupling ends into the gearbox, then through a torque limiting coupling and high-speed shaft to the generator. System inertia at the rotor is just above 2 million lb.-ft.-second squared.

Drive train frequencies, exclusive of blade responses, can be represented with a three-inertia system for phenomenon in the wind frequency range. The rotor, gearbox, and generator are the reference inertias with stiffness and damping elements between the rotor and gearbox representing the low-speed shaft and similar elements between the gearbox and generator representing the gearbox and high-speed shaft flexibilities.

167

Generator air gap torque applied to the generator inertia when on-line has stiffness and damping characteristics relative to the electrical grid synchronous reference, as well as an active torque contribution due to excitation system influence. The design range of operating power and effective impedance to the utility grid reference make the apparent stiffness of the air gap vary over a three to one range which results in drive train frequency migration.

MOD-1 on-line fundamental drive train frequency is less than 1 per rev over the entire range and the second drive train torsional frequency is above 4 per rev. This places them outside the dominant 1 to 4 per rev excitation and blade response from wind shear and tower shadow. Shaft speed is 35 rpm.

DYNAMIC CONTROL

The dynamic control system on MOD-1 has two effective means of control. One input controls blade power gain by full span pitch control. The second input controls excitation or rotating magnetic field strength on the salient pole synchronous generator. Figure 3 shows the basic control loops of the system.

Inputs to the control system are wind speed via multiple sensors, rotor speed, generator speed, generator voltage, real power, and reactive power.

During start up and off-line rated speed operation blade power gain is closed loop controlled from generator speed. During on-line operation, blade power gain is closed loop controlled from generator power with wind speed feed forward augmentation. The excitation system on-line is closed loop controlled from voltage, speed, and reactive power. By modulating excitation with a speed derived stabilization signal, increased damping is provided at the drive train fundamental frequency.

Start up and shut down sequencing, yaw control, alarm monitoring, operator interface and general signal and command information are provided by means of a distributed processor system. System control and monitoring may be performed on site or remotely.

MECHANICAL STABILIZATION

The MOD-0 systems are utilizing fluid couplings in the drive train to obtain near critical damping at the drive train fundamental with a few percent speed difference, or slip. Implementation of a similar device on an order of magnitude larger MOD-1 system, while analytically sound, is a cost, size, and loss dissipation problem when the major benefit, more damping, can be provided via an active excitation control in a more cost effective manner.

In the same vein, a squirrel cage induction generator in the megawatt class has the slip mechanical characteristic to provide damping but is less efficient and removes the control opportunity of an excitation system. Torque control must be upgraded to provide the same electrical system performance as a synchronous machine or a loss in voltage excursion control must be accepted.

168

SPEED STABILIZATION

Inputs to synchronous generator excitation systems to improve power transfer stability margins have been used on large power systems for some time. Reference 1 is one of the early papers on the technique. Signals derived from shaft speed and output power have been used to modulate the excitation system to improve the apparent damping of the generator mechanical system.

Limitations exist in the frequency response of an excitation system that determine whether stabilization techniques will be effective at the desired frequency. For example, an attempt, reported in Reference 2, was made to decrease the 2 per rev response on MOD-0 with less than encouraging results. A careful analysis of each system and suitable compensation of the control signal must be provided for optimum effect.

On the MOD-1 system, a shaft speed signal, suitably compensated, is utilized to vary excitation and improve the effective damping of the fundamental on-line drive train torsional frequency. This frequency is relatively stable over the power range of operation because the mechanical stiffness elements are relatively "soft" and the variable generator stiffness thus has less influence on the fundamental.

The unstabilized fundamental is around 2.4 radians per second or 0.7 per rev with an unstabilized damping of around 5 percent of critical. These numbers vary slightly with the voltage regulator gain settings, power level, and electrical system effective impedance and voltage. The speed stabilization system improves the MOD-1 damping to a respectable 25 percent in the results following.

SIMULATION MODEL

Since the MOD-1 system is not yet built, the characteristics presented are based on analytical frequency and time domain studies using the general model shown in Figure 3. In addition to the drive train previously noted, blade and electrical dynamics are carried as well as detail modelling of the torque and excitation control systems. Figure 4 shows the basic drive train mechanical model.

Simulation for time domain results on the MOD-1 system is implemented on a hybrid computer system. The mix of small time constants in the controls and low frequency mechanical responses plus the desire to examine long time response to filtered random noise "wind" make this analytical tool superior to the conventional digital numerical integration approach. Digital techniques are utilized for frequency domain analysis. Hybrid output is on 24 channels of pen recorder with 16 channels on fixed variables. Table 1 shows the fixed output variables used.

In the limited scope of this presentation, only the damping augmentation performance provided by the MOD-1 speed stabilizer will be shown.

First, the system response to a step initial deflection condition will be shown with the excitation system closed loop but without wind input or torque control. Figure 5a shows the case without the stabilizer. Time scale is one second per division and amplitude scales are indicated. The high frequency oscillation superimposed on the fundamental is a gearbox inertia mode. The fundamental is 2.4 radians per second at 5% damping ratio.

Figure 5b illustrates the excitation system response to a 1.5% step change in on-line voltage reference. The MOD-1 solid state voltage regulator is capable of negative field forcing and is set for about 15% damping ratio oscillatory behavior.

In Figure 6a, the same initial condition as in 5a is applied but with the stabilizer circuit closed loop. The damping has increased to a respectable 25 percent of critical at the fundamental. No improvement is observed or expected at higher frequencies of oscillation as the stabilizer loop is keyed to a single frequency. Figure 6b illustrates the response to a step change in on-line voltage reference with the stabilizer. Note that there is a penalty to pay for the stabilizer, a slight increase in excitation system oscillation which will contribute to increased voltage variation.

Figure 7 shows the effect of steady wind forcing the system, with response to tower shadow and wind shear continuous excitation clearly showing up in mechanical and electrical system response. System response to two steps, down and up, in voltage reference are shown. The steady state peak to peak terminal voltage excursion is less than 1.0 percent, will be reduced with suitable compensation and will be less at a critical load bus. This magnitude is within acceptable utility standards at the frequency of occurance.

CONCLUSIONS

The technique of stabilization by utilizing the excitation system capabilities of synchronous generators is shown to be an effective means of increasing the damping of the fundamental torsional frequency of megawatt class horizontal axis wind turbines and is being applied for that purpose on the MOD-1 system.

REFERENCES

1. Demello, F. P. and Concordia, C., Concepts of Synchronous Machine Stability as Affected by Excitation Control, IEEE Transactions, Vol. PAS-88 No. 4, pp 316-328, 1969.

2. Gebben, V. D., Investigation of Excitation Control For Wind Turbine Stability, ERDA/NASA/1028-77/3, NASA TM-73745, August, 1977.

DISCUSSION

Q. Were systems with and without wind feed forward tried? MOD-0 test data shows both good and bad results.

A. MOD-1 simulation has used wind feed forward in an idealized manner with good results. The idealization incorporates sensor and mechanism time constants but assumes that the wind sensed for control purposes is the same as the wind producing rotor torque with suitable time shift to accommodate upwind sensor mounting.

MOD-1 has hardware to sense the wind field with more than one sensor where MOD-0 uses a single sensor. If the sensed wind for control is not representative of the wind field producing rotor torque, ambivalent results can be expected. Further work is indicated in the implementation of an inexpensive means of large area wind sensing for wind turbine control.

Q. What was the technical tradeoff concerning selection of a synchronous generator with active excitation control versus an induction generator?

A. Basically, an induction generator was rejected for MOD-1 because of excessive voltage dips due to wind gusts when connected by reasonable distribution system connection impedances. Performance simulation runs had twice the voltage dip with induction than with synchronous for the same effective pitch control gain and wind disturbance. Also, the MOD-1 specification called for a synchronous machine.

The MOD-1 synchronous with speed stabilizer provides comparable on-line drivetrain torsional frequency damping with that resulting from an induction generator without the loss in efficiency. This type of machine decision tends to be site oriented and such factors as very small connection impedance, faster response blade power gain control, and smaller machine rating may contribute to a different conclusion for a different application.

Q. Is the blade pitch control loop inactive in damping the system as you have modeled it?

No, closed loop pitch control increases system stability and improves drivetrain damping. The results showing speed stabilizer and excitation system performance to step inputs were run with open loop pitch control and no wind disturbance in order to better illustrate the main topic.

171

TABLE 1. - MOD-1 HYBRID SIMULATION FIXED OUTPUT VARIABLES

V_w	Wind at Nacelle Centerline
V_wB1	Wind on Blade 1 including shear and tower shadow affects
$\triangle T_{B1}$	Aerodynamic torque on Blade 1 - Variational
$\triangle \phi_{B1}$	Blade degree of freedom response - Variational
$\triangle \phi_{LS}$	Rotor to gearbox response - Variational
$\triangle \phi_{HS}$	Gearbox to generator response - Variational
$\triangle T_E$	Air gap torque - Variational
β	Pitch angle at .75 blade radius
EFD	Generator field voltage
V_r	Voltage regulator output voltage
$\triangle E_T$	Generator terminal voltage - Variational
Cos γ	Generator power angle to infinite bus voltage
$\triangle W_g$	Generator speed - Variational
$\triangle W_r$	Rotor speed - Variational
P_e	Real Power
Q_e	Reactive Power

200 FT.

STEP-UP
TRANSFORMER

CONTROL
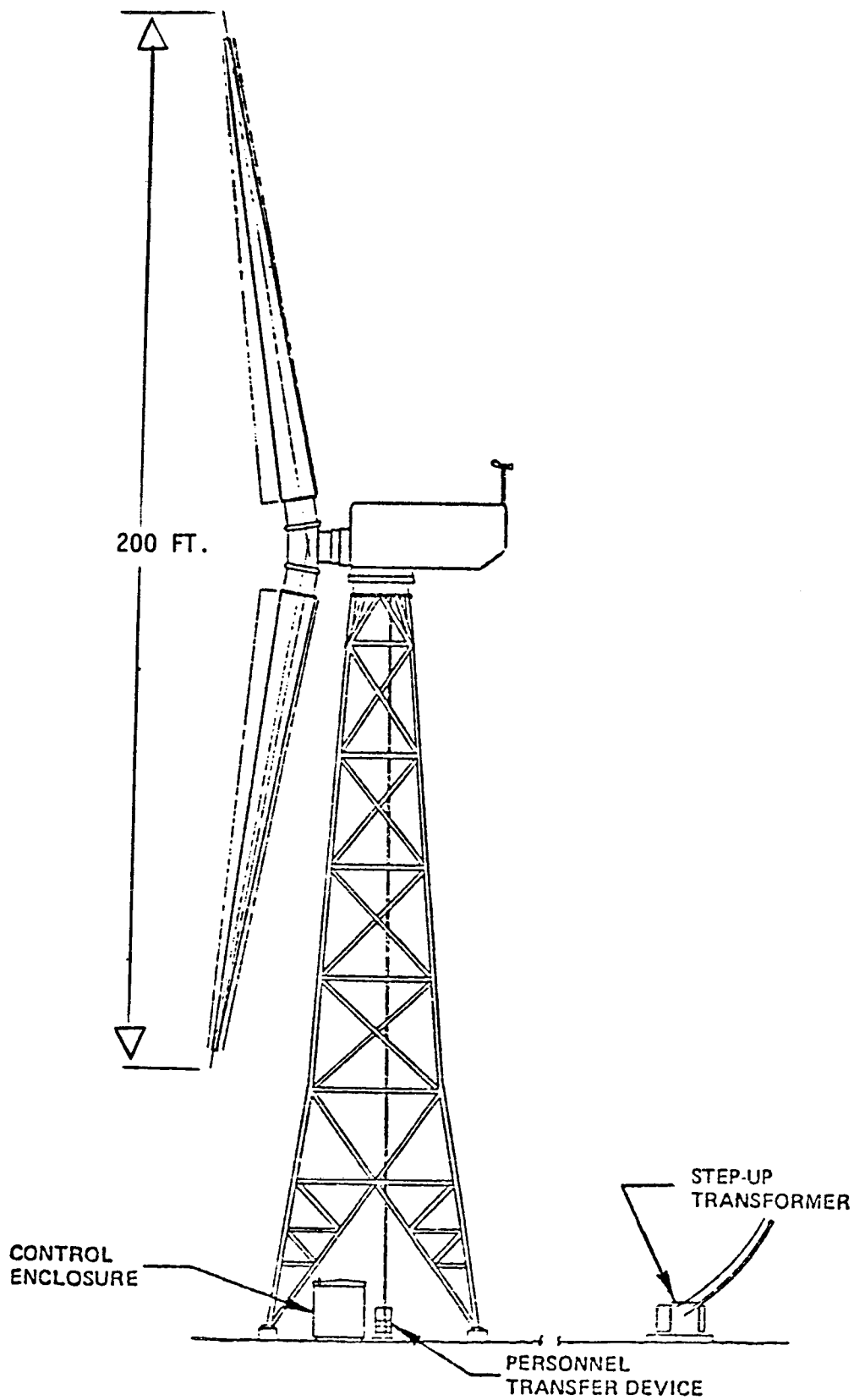ENCLOSURE

PERSONNEL
TRANSFER DEVICE

Figure 1. - Mod-1 wind turbine generator.
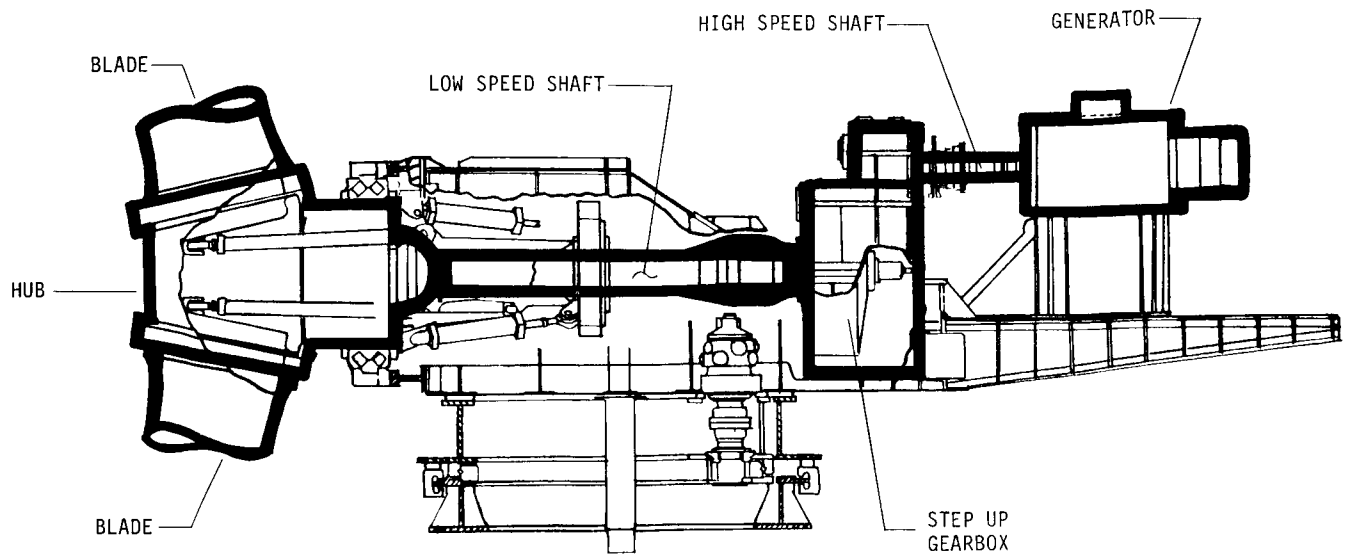
Figure 2. - Drive train power flow.
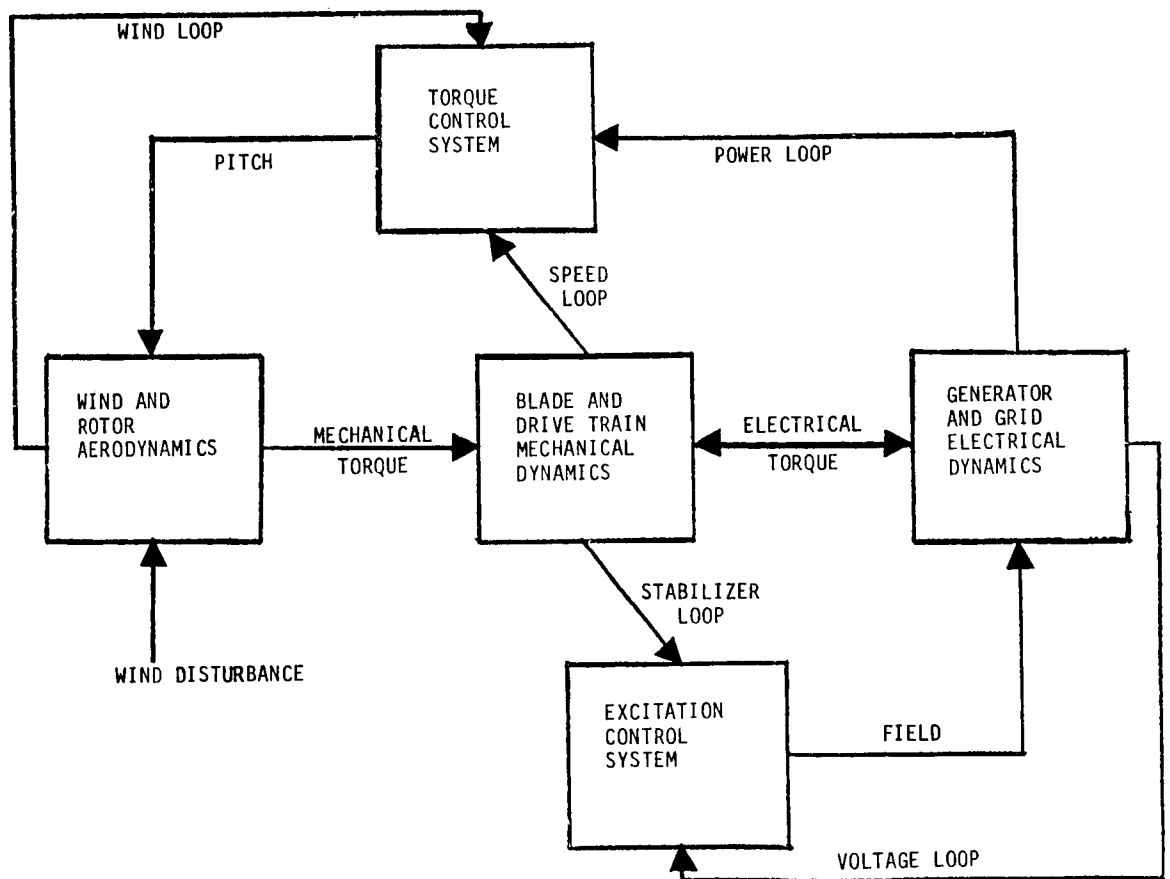
Figure 3. - Simulation block diagram.

174

Figure 4. - Drive train model.
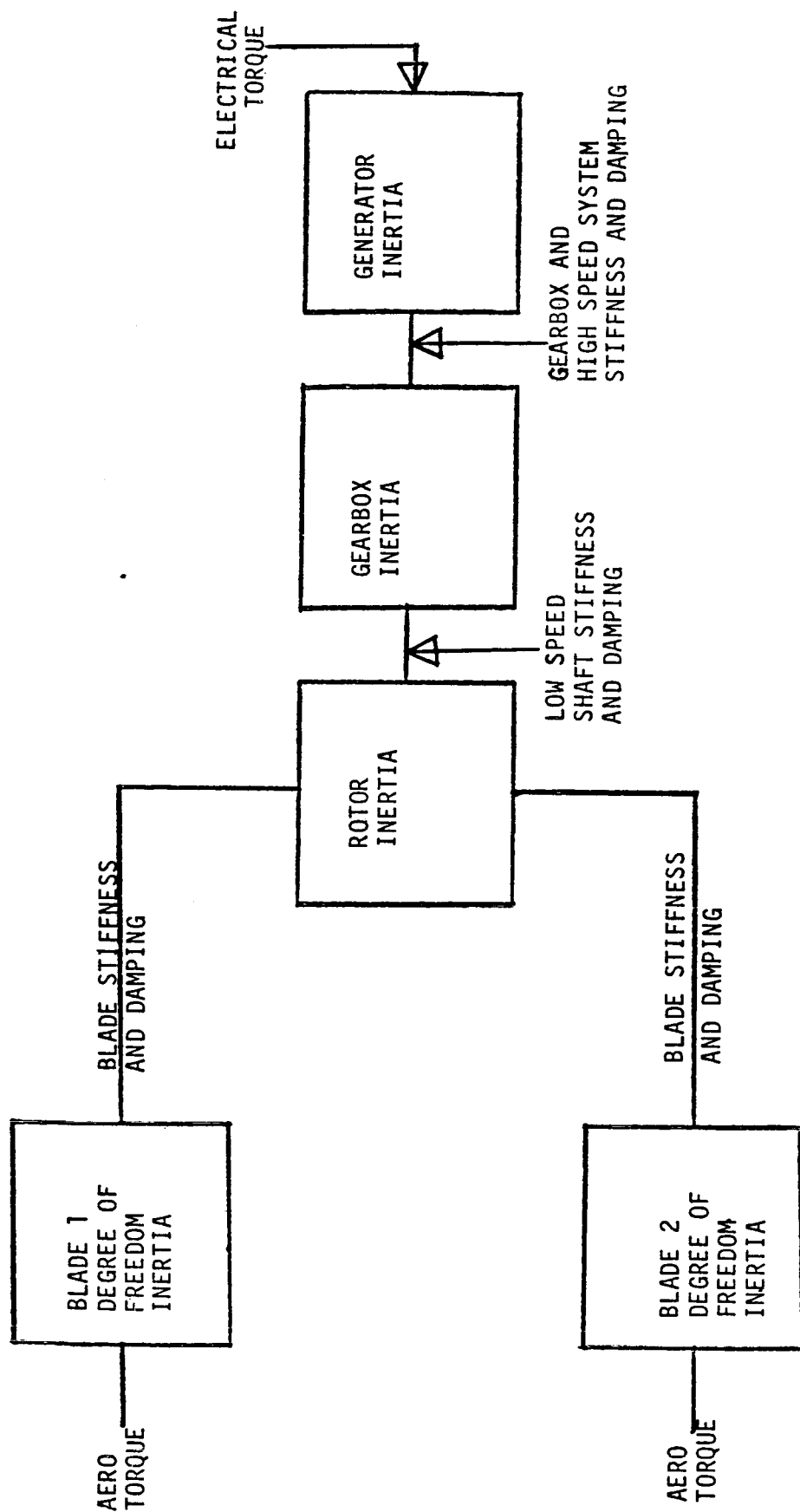
175

Figure 5.

Figure 6.

177

ΔØLS
.01 rad/line

ΔØHS
.001 rad/line

ΔTE
.02 pu/line

SECONDS

EFD
.2 pu/line

Vr
1 pu/line

ΔET
.0625%/line

Cos δ
.05/line
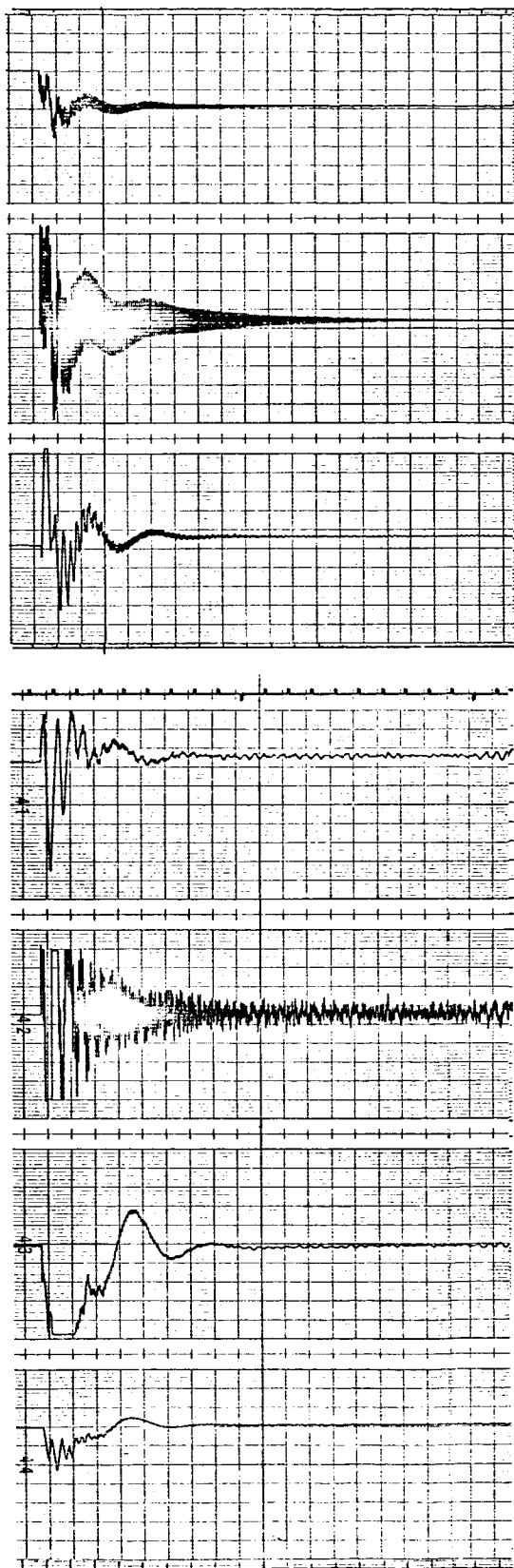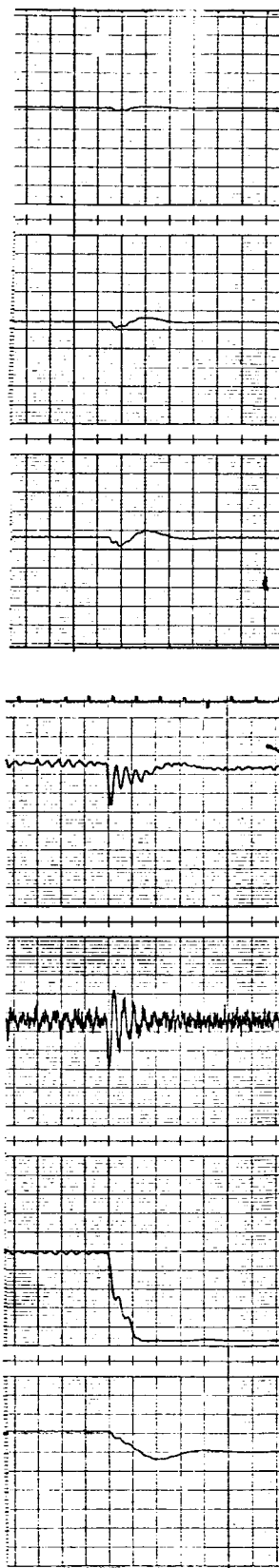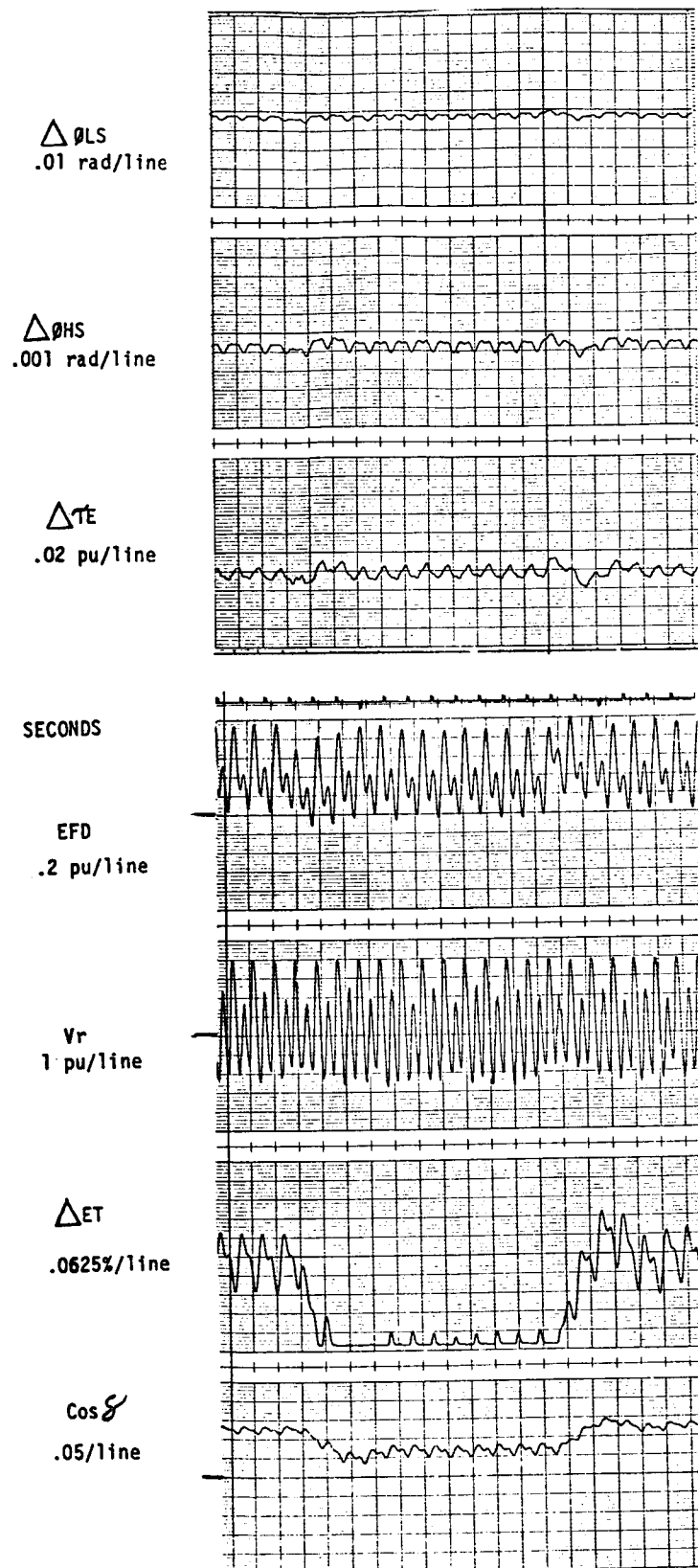
Figure 7.

METHODS OF ATTENUATING WIND TURBINE AC GENERATOR

OUTPUT VARIATIONS

Harold Gold

National Aeronautics and Space Administration
Lewis Research Center
Cleveland, Ohio 44135

ABSTRACT

Wind speed variation, tower blockage and structural and inertial fac-
tors produce unsteady torque in wind turbines. Methods for modifying
the turbine torque so that steady torque is delivered to the coupled
AC generator are discussed. The method that may evolve will be
influenced by the power use that develops and the trade-offs of cost,
weight and complexity.

INTRODUCTION

The production of AC power at substantially constant level by a wind
turbine driven synchronous generator has not yet been achieved.
Improvements in blade angle response and torsional damping appear to
be steps that will lead to significantly reduced power distortion
from wind velocity variation; but the as yet unexplained and prob-
ably characteristic persistance of the 2P tower shadow effect
observed on Mod 0 may be more difficult to attenuate. A number of
methods of attenuating the tower shadow effect have been tried or
have been proposed. A review and discussion of a number of these
methods will be given herein. The methods included are listed in
Table I.

WIND DISTURBANCE

Direct wind disturbance was analyzed in reference 1, where a damped
compliant shaft was found to be effective for attenuating gust distur-
bances. The effect of a finite capacity network was not evaluated
and the shadow effect was not considered.

Some experience with the feed-forward concept has been obtained on
Mod 0, where it has been found to be partially effective. The Mod 0
system could very likely be improved by faster pitch operation and
wind velocity signal averaging.

TOWER SHADOW/STRUCTURAL DISTURBANCE

The compliant shaft with a combination of mechanical and generator induced damping as the means of attenuating the 2P tower shadow effect is being planned for Mod 1 and Mod 2. There is an uncertainty about the effectiveness of this approach because Mod 0 data show a considerably greater 2P disturbance than is predicted by the present spring-mass models. The feasibility of obtaining adequate damping through generator damping windings and exciter manipulation remains to be demonstrated, and much the same can be said for a satisfactory mechanical-torsional damper.

The slip coupling was used on the Smith-Putnam wind turbine, but definitive data is not available. Operation on Mod 0 has shown that a two percent slip furnishes sufficient damping to completely suppress the first generator-torsion resonant peak. However, the coupling does not suppress the power dip at 2P because the coupling is neither an energy storage or active device. Power loss in steady state is an added disadvantage of the slip coupling.

Two torsion dampers that do not cause a power loss in steady state are shown in Figure 1. The elastomeric shaft is made up of coaxial, tubular segments that are bonded together by an elastomeric compound. A model has been built and is awaiting test on Mod 0. Bench tests of this model show very high compliance and substantial damping.

The second configuration shown in Figure 1 is currently in use on engine mounted aircraft generators. The compliance is provided by the spring steel quill, and the clutch type flanges provide the damping.

If a wind turbine generator that produces substantial power variation is coupled to a large power facility, it looks to the line as a noisy consuming device, but the line impedance may be so low that the effect is not seen. However, oscillatory stresses on the wind turbine structure, which are principally the result of line synchronization, are not attenuated.

A small parallel generator can provide an effectively low parallel impedance, provided the governing of the prime mover is sufficiently responsive. This result was reported in reference 2.

Direct mechanical power insertion or extraction can be accomplished through the planetary differential. A system of this type has been in use on aircraft gas turbine driven generators for over a decade. A schematic drawing of this gearing is shown in Figure 2. In this configuration, the wind turbine drives the planet carrier, the ring gear

drives the generator and the sun gear is held or driven by the auxiliary motor. At design conditions the motor speed is zero, and the motor runs in either direction, the direction depending on the existence of either a power excess or deficiency. The power capacity of the motor can therefore be set at the maximum expected wind turbine power variation or about 20 percent of the generator power.

On the aircraft system the motor is hydraulic and is supplied by a variable displacement, engine driven pump. The engine also drives the planet carrier. The motor compensates for a steady state speed variation of approximately $\pm$ 25 percent. In the wind turbine case there is no steady state power requirement. For this reason and because efficiency is less important, the motor could be supplied by a servovalve instead of a variable displacement pump. The aircraft system parallels AC generators through a phase-lock loop. Phase lock could be applied to the wind turbine mechanical power insertion system.

The planetary transmission can also be used to provide a very low compliance and damped shaft. For this function, the sun gear is held from rotating by a lever arm that is restrained by a spring and a dashpot, or by a torsion spring and a rotary dashpot. The spring and dashpot do not rotate and therefore a very wide range of spring constants and damping coefficients can be incorporated.

The system employed on aircraft utilizes the planetary because it provides a system of considerably higher efficiency than a full hydraulic drive system. Efficiency is not as important in the wind turbine case, and therefore a full hydraulic drive can be considered. A full hydrostatic drive system was reviewed by a proposer on Mod 2. It was not proposed mainly because the variable displacement pump of sufficient size was not in production, but its development was considered to be technically feasible.

The power level presently being considered for low cost, fixed pitch wind turbines is well within the range of available hydraulic pumps and motors. A hydrostatic drive comprising a turbine driven variable displacement pump operating in a constant pressure control mode and driving a fixed displacement generator drive motor has many important technical capabilities for this application. AC power of very constant level could be produced even in the presence of the large torque variations that will accompany fixed pitch, synchronous operation.

There is a multiplicity of possible pump, motor and gear configuration, and therefore the optimum cost, weight, complexity and performance trade-offs will require a detailed study.

Complete decoupling of the power line from the wind turbine can be accomplished through the use of a D.C. generator and a D.C. to AC converter. The conversion could be accomplished through a motor-generator set or through a solid state device. The wind turbine has certain desirable characteristics with this system, but motor-generator set is costly, and the solid state converter is susceptable to noise generation.

CONCLUSIONS

It is currently feasible to consider direct hydrostatic drives, connected to the turbine through a gear box, for power levels up to 200 kw, and hydrostatic-planetary drives up to 1000 kw. AC power of high quality could be produced by wind turbines through the development of these systems. The broad use of wind turbine AC power may depend on the quality of the power. The configuration of direct or augmented drive that evolves will be shaped by the power use that develops and the trade-offs of cost, weight and complexity.

REFERENCES

1. Johnson, Craig C.; and Smith, Richard T.:   Dynamics of Wind Generators on Electric Utility Networks.   IEEE Trans on Aerospace and Electronic Systems, VOL AES-12 No. 4, July 1976.

2. Hannett, L. N.; and Undrill, J. M.:   Wind Turbine-Generator Power and Speed Control.   Progress Report No. 2, Power Technologies, Inc.   Report No. R-36-77, July 1977.

DISCUSSION

Q. Why the need for damping when in the compliant drive system the effect is to decouple the oscillating rotor loads from the generator, particularly at power conditions below rated?

A. Damping in the compliant shaft attenuates ringing during gusts and provides a stabilizing factor under closed loop power control through pitch variation. The correct amount of damping in the compliant shaft will moderate power oscillation at all power levels.

Q. Would not a tuned passive restraint of the planetary sun gear system be satisfactory?

A.   The practicality of a tuned passive restraint should be experiment-
     ally evaluated. It can be expected to smooth out the 2 P power
     oscillation; however, the benefits under rapid changing wind speeds
     would be much less than that of an active restraint.

Q.   Is the approximately 10% power loss associated with a direct hydrau-
     lic drive an acceptable price to pay for "clean" power?

A.   In combination with a planetary drive, the maximum hydrostatic
     transmission load will be less than 20% of the generator power, and
     the average load will be approximately 5%, giving a power loss of
     approximately 1/2%.

TABLE I. - ATTENUATION METHODS

I   Wind Disturbance

Damped compliant shaft

Wind feed forward

II   Tower shadow/structural disturbance

Compliant shaft + ⎡Mechanical damping
                  ⎣Generator damping

Slip coupling

Auxiliary power insertion ⎡Low impedance line
                          ⎢Constant speed - parallel generator
                          ⎣Differential gearing

Hydraulic power generation + AC drive

D C   generation + AC conversion ⎡Rotary
                                 ⎣Solid state

184
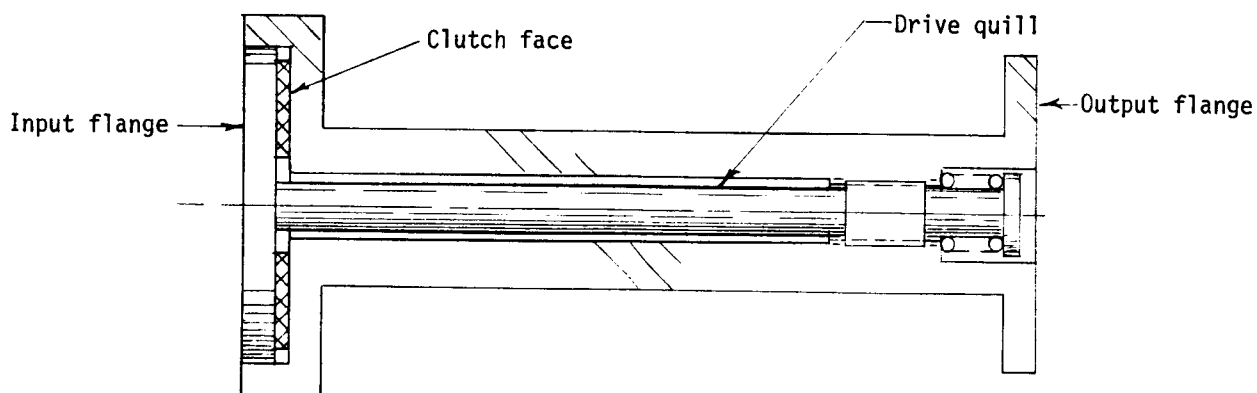
Aircraft-generator-type torsion damper
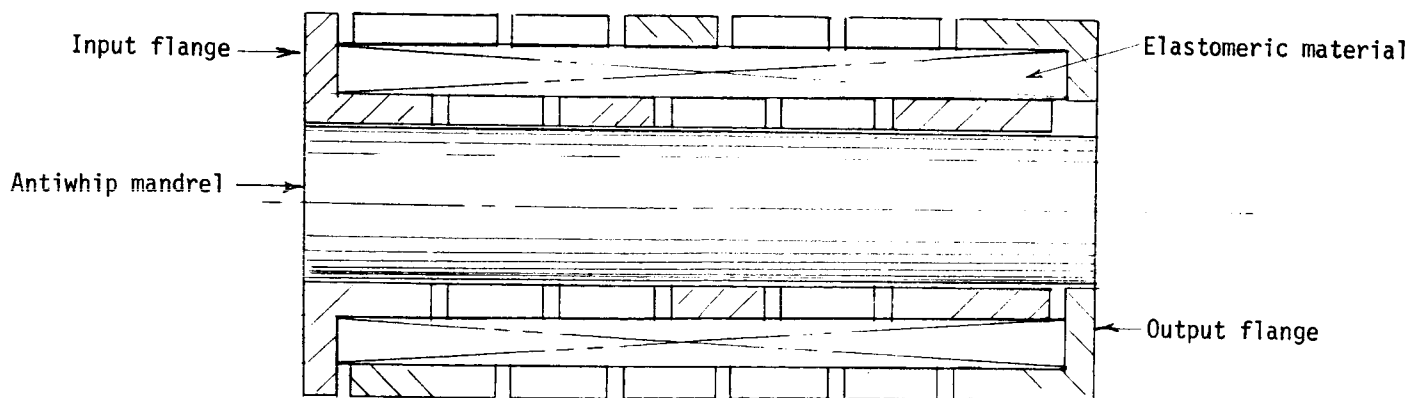
Elastomeric shaft

Figure 1. - Dynamic torsion dampers.

185

Figure 2. - Power insertion through planetary differential gearing.

DYNAMICS OF DRIVE SYSTEMS FOR WIND ENERGY CONVERSION

Manuel Martinez-Sanchez

Massachusetts Institute of Technology
Cambridge, MA 02139

ABSTRACT

Calculations are performed to determine the dynamic effects of mechanical power transmission from the nacelle of a horizontal axis wind machine to the ground or to an intermediate level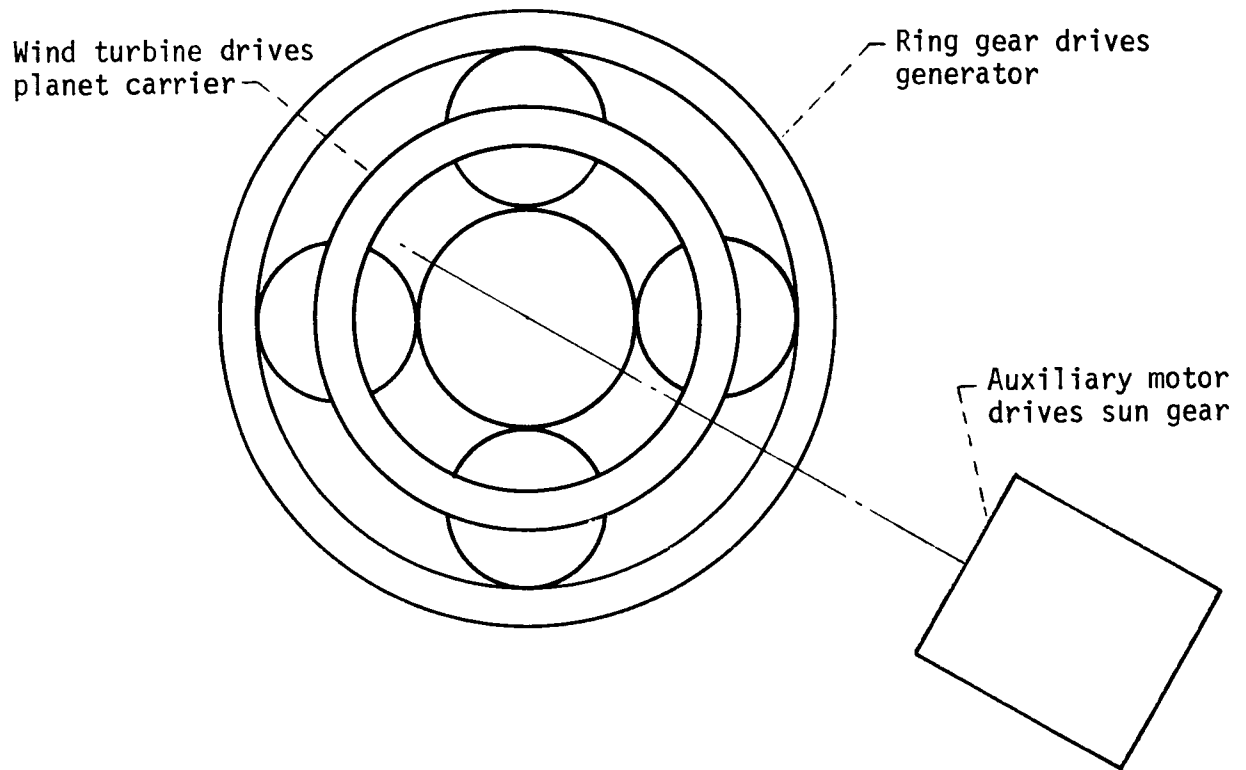. It is found that resonances are likely at 2 or 4/REV, but they occur at low power only, and seem easily correctable. Large reductions are found in the harmonic torque inputs to the generator at powers near rated.

Introduction

Due to the large weight of the gear-up and generation equipment in horizontal-axis wind turbines, there have been suggestions that it might be desirable to transmit the power mechanically to the base of the tower, where electrical conversion would then take place. Although hydraulic transmission involving a controllable pump-motor pair is a possibility, considerations of pump mass and efficiency at low rpm, as well as long term reliability, indicated that mechanical transmissions are to be preferred. Of these, only the concepts involving a long vertical shaft will be considered here (chain belt drives might be lighter, but would require more servicing).

A decision on the most desirable location for the conversion equipment can only be based on a design and cost study which accounts for the accompanying modifications of nacelle and tower design. We are presently conducting such a study, and this paper will focus on the drive train dynamic implications of the choice of configuration.

Cases Studied

Figure 1 gives in schematic form the three configurations selected as representative of the range of possible arrangements. Case 1 is the standard (all aloft) configuration. Case 2 involves transmission of low speed, high torque power through a 90° bevel gear all the way down to the speed increaser and generator on the ground. In Case 3 the gearbox is aloft, and only high speed, low torque power is transmitted to the generator on the ground. Intermediate cases, with the equipment mounted halfway down the tower were also considered for cases 2 and 3.

Model Description

For purposes of dynamic analysis, a three-mass system was assumed. The inertias are those of the rotor blades plus hub, the gearbox and the generator rotor respectively (shaft inertias are neglected). The stiffnesses are those

of the connecting shafts, modified in the case of the blades and the generator as described below.

The physical parameters (sizes, masses, stiffnesses) corresponding to a given configuration, rated power and mean wind speed were determined using a combination of ab-initio calculations and judicious extrapolations from the more detailed designs reported in Refs. 1, 2, and 3. The low speed shaft was assumed hollow, with internal-to-external diameter ratio of 0.54, and it was dimensioned for both torsion and bending. The high speed shafts were taken to be solid. In all cases, allowance was made for extended fatigue life.

The generator was assumed to be a 4-pole synchronous alternator, controlled for constant power angle, and hence its equivalent torsional stiffness was varied in proportion to $V^3 c_p$ $(V/\Omega R)$, where c_p is the power coefficient. No other non-linear elements were assumed.

The rotor blades were represented by its polar moment of inertia relative to the shaft, (taken to scale like $R^5 \cdot V^2_{WIND}$) and by an equivalent stiffness due to their "S-mode" lag bending. This stiffness was obtained from estimated in-plane natural frequencies, together with the blade inertias. The two blade stiffnesses were added together, and the inverse of this sum was added to the input shaft stiffness.

For calculational purposes all angular deflections, stiffnesses and intertias were reduced to the high speed side of the speed changer.

Discussion of Results

Most of the work centered on the sizes of 500 and 1500 KW, very similar in characteristics to those described in Ref. 2. Figures 2 and 3 show the variation of the drive train natural frequencies with generated power. Five cases are included for each size, namely, conventional nacelle (Case 1), long slow shaft (C2, sh = 1), intermediate slow shaft (C2, sh = 0.5), long fast shaft (C3, sh = 1), and intermediate fast shaft (C3, sh = 0.5). Only the two lowest modes are included, since the third mode has very high natural frequencies. The mode shapes for some of the cases are depicted in Fig. 4, where the deflections are normalized by the one with maximum value, and are reduced to the high speed side. Therefore, the actual deflection of the rotor disc can be obtained by dividing the amount shown by the gear ratio (of the order of 60). Mode I, with the lowest frequency, is a collective oscillation of all inertias (but mostly the rotor) resisted by the generator field and the low speed shaft. In Mode II the rotor is nearly fixed, and the other inertias oscillate against generator and slow shaft again. As discussed for instance in Ref. 4, rotational excitations arising from stationary disturbance sources can only have frequencies at even multiples of the rotation frequency. From Figs. 2 and 3 we can see that, from this point of view the standard designs (C1) are safe, since neither 2/REV nor 4/REV or even 6/REV disturbances will excite modes I or II at any power. The lowest frequency (Mode I) is below 2/REV, while the next frequency (Mode II) is at about 6/REV. The longer shafts of cases C2 and C3 have the effect of depressing both natural frequencies, with the result that mode II now becomes resonant at some intermediate power level (at 4/REV for case C3, and both at 4/REV and 2/REV for case C2). Notice that even for the full length high torque shaft, a very large stiffness reduction would still be needed to bring all of Mode II

188

below 2/REV. This can be artificially provided by a flexible coupling, but the point is that shaft lengthening by itself is not an effective way to achieve dynamic decoupling.

This point is further emphasized in Figs. 5 and 6, which show (for the 500 KW case) torque transmissivities from the rotor disc to the generator input shaft, namely, the ratio of torque amplitudes for harmonic excitations at 2/REV (Fig. 5) and 4/REV (Fig. 6). At relatively high powers, near rated, the long shafts do achieve large reductions in the torque transmissivity, especially at 2/REV. However, this is achieved at the cost of resonances in the range below 200 KW of power. The sharpness of these resonances suggests however that with modest amounts of damping, combined with deliberate avoidance of prolonged synchronous operation at those low power levels, these resonances may not pose a fundamental obstacle.

Conclusions

(1) Long transmission shafts to ground can lead to 2 or 4/REV drive train resonances at low power levels.

(2) They do reduce greatly the harmonic torque inputs to the generator at near rated power.

References

1. "Drive Train Normal Mode Analysis for the ERDA/NASA 100 KW Wind Turbine Generator," T.L. Sullivan, D.R. Miller and D.A. Spera (NASA/Lewis) NASA TM-73718, July 1977.

2. "Design Study of Wind Turbines 50KW to 3000 KW for Electric Utility Applications, Analysis and Design," G.E., Report #NASA CR134935 February 1976.

3. "Design Study of Wind Turbines 50 KW to 3000 KW for Electric Utility Applications, Analysis and Design," Kaman Aerospace Corp., NASA Report #CR-134937, February 1976.

4. "Rotor/Generator Isolation for Wid Turbines," by L.P. Mirandy presented at AIAA-ASME 18th Structures, Structural Dynamics and Materials Conf., San Diego, CA, March 21-23, 1977.

DISCUSSION

Q. Would you comment on the accuracy of your results if you include long shaft bending modes and possible feeding of energy for torsional DOF's to bending ones (as in classical Den Hartog or Ker Wilson)?

A. The accuracy of the torsional vibration calculations is not affected by bending, provided whirling resonances are avoided. In principle, this can be done by providing intermediate bearings so that the critical shaft frequencies are raised above the shaft turning frequency. For Case 2 (long low speed shaft), a single intermediate bearing accomplishes this

(especially if the shaft is made hollow). For Case 3 (long high speed shaft) operation below the first critical speed would require one bearing every 1.6 m of shaft roughly; but since lateral loads are not involved, it should be feasible to operate, say, between the second and third criticals, which implies spacings of about 4 m between bearings (or about 10 of them).

Q. Physically how would you propose a damper for the long shaft?

A. What is of interest is to damp out the generator shaft oscillations. Notice that the possible resonant conditions at 2P, 4P, etc. all affect the second mode of the drive, which involves largely generator osciallations, with little participation of the massive rotor blades. Therefore any method of introducing damping at or near the alternator should prove effective. As an example, one can estimate that for our Case 2 (long slow shaft), generator damping to the tune of 0.2 of critical (based on the isolated alternator) is sufficient to reduce the peak response at the 2P resonance to less than ±3 electrical degrees for rotor torque inputs equal to rated torque.
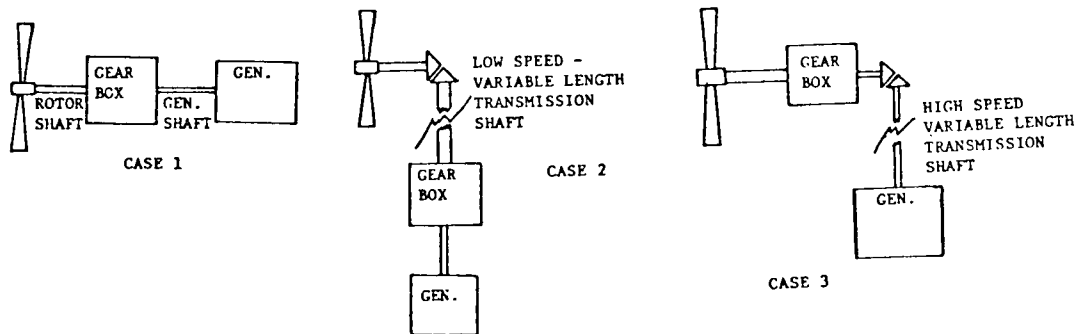

Figure 1.
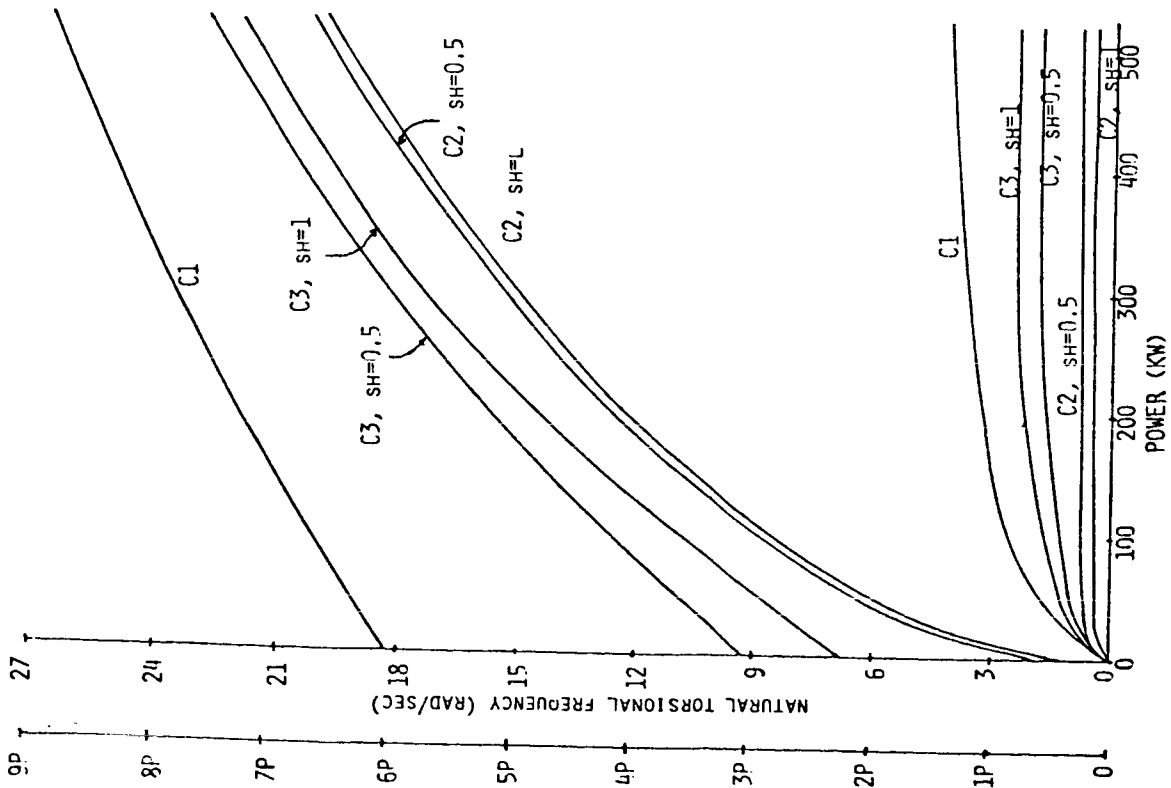
Figure 3.

Figure 2.

191

Figure 4.
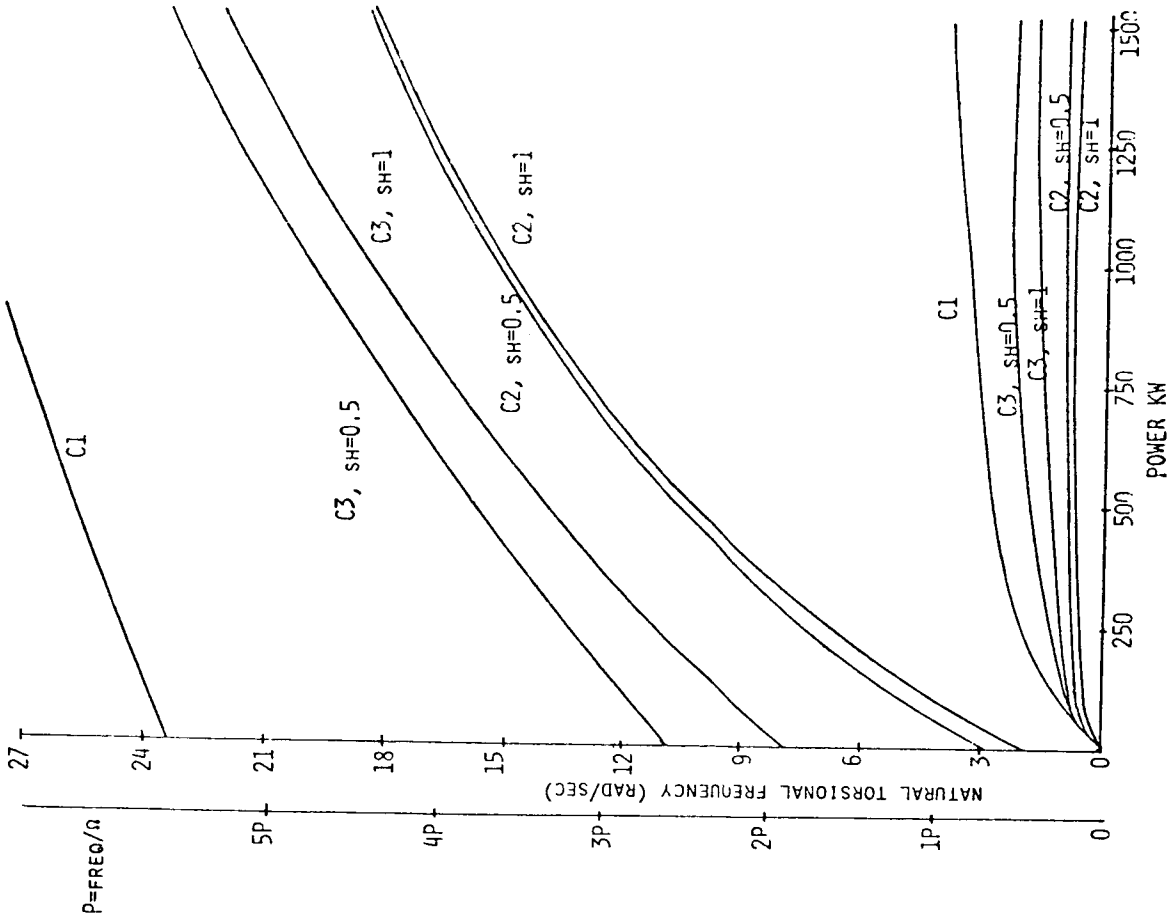
TORQUE TRANSMISSIVITY
AT 4 PER REV

C2

C3

C1

C3

C1

C3

C2

C3

P(KN)

Figure 6.

TORQUE TRANSMISSIVITY AT
2 PER REV

P(KN)

C2

C3

C2

C1

C3

C1

C2

TO ~0.6

Figure 5.

TORQUE IN GEN, SHAFT/ROTOR TORQUE
FOR EQUIV, (UNREDUCED) SYSTEM
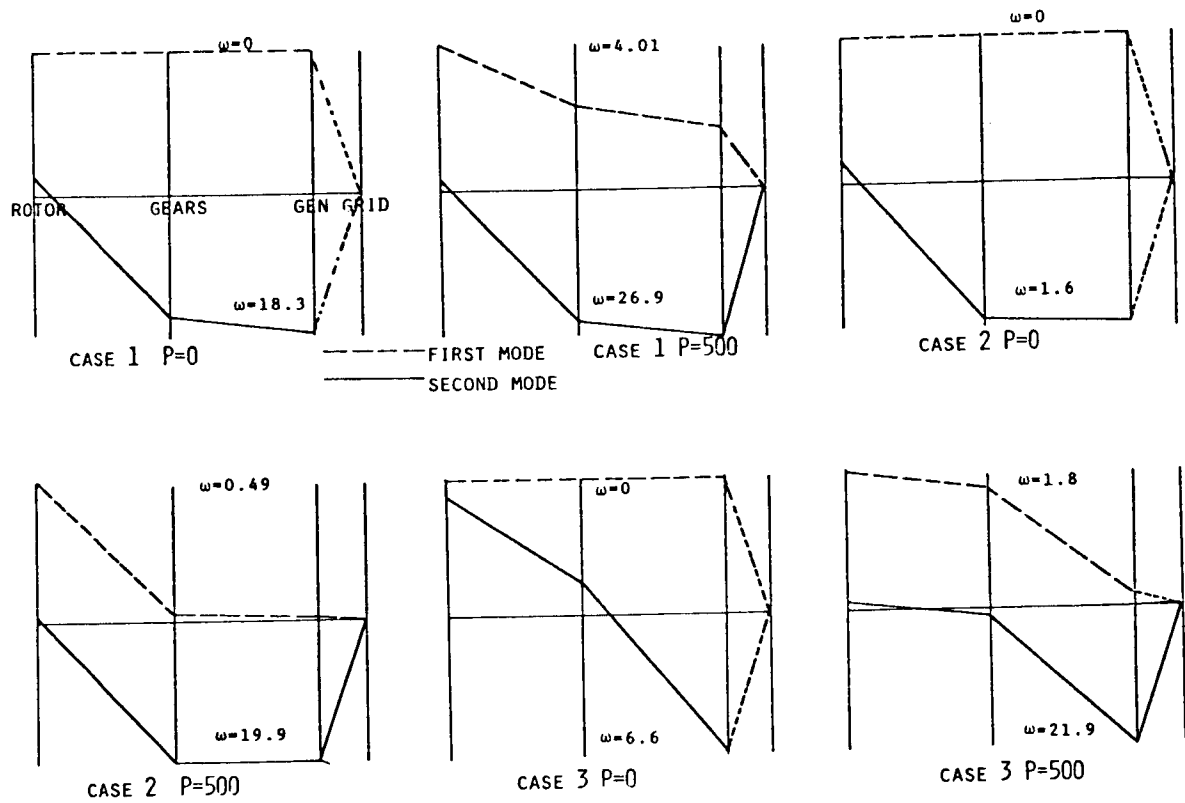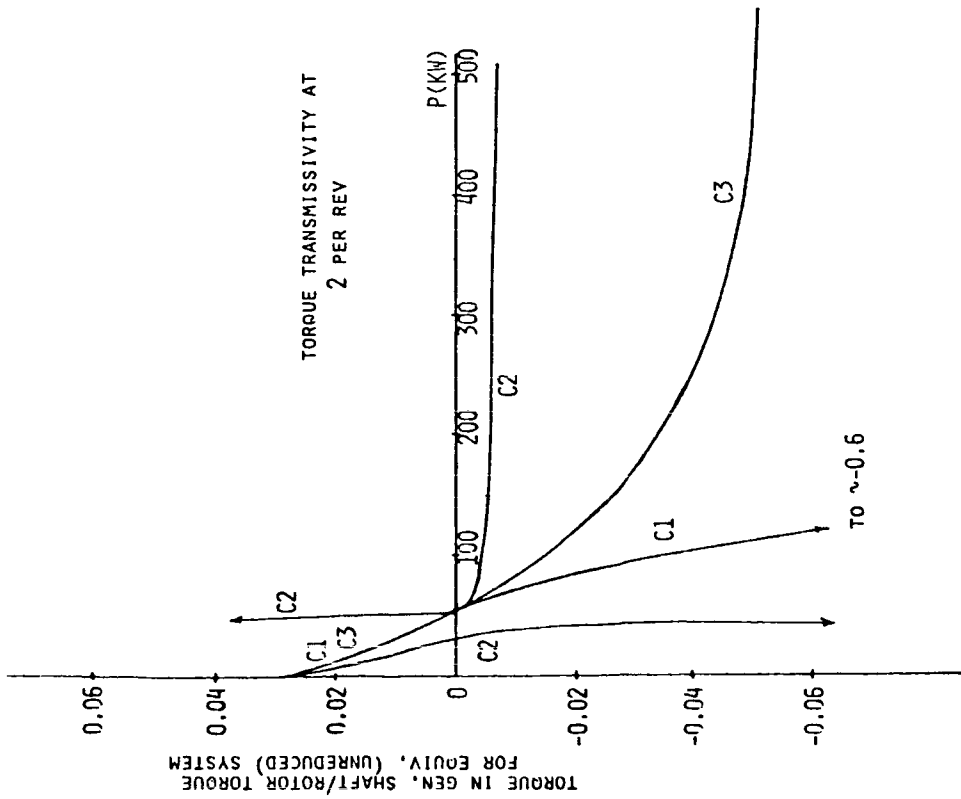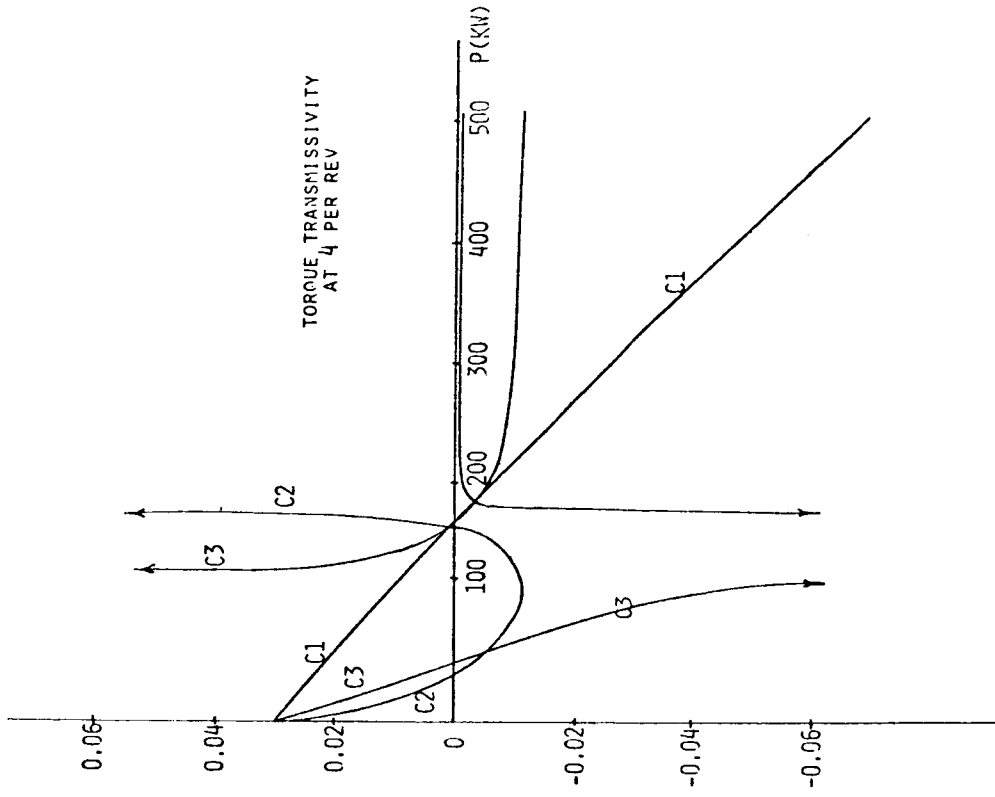
SOME ALTERNATIVE DYNAMIC DESIGN CONFIGURATIONS

FOR LARGE HORIZONTAL AXIS WECS

Kurt H. Hohenemser

Washington University, St. Louis, Missouri 63130

Abstract

The present US development effort toward large horizontal axis WECS concentrates on the configuration with two rigid blades with collective pitch variation and a yaw gear drive. Alternative configurations without yaw gear drive are considered where the rotor is either self-centering or where the yaw angle is controlled by blade cyclic pitch inputs. A preliminary evaluation of the dynamic characteristics for these alternative design configurations is presented.

List of Symbols

a	lift slope
c	blade chord at .7R station
$\overline{C}_M$	$= M/\rho\pi R^3 (\Omega R)^2 a\sigma$ yaw moment coefficient
$\overline{C}_{M\dot{\chi}}$	$= \partial\overline{C}_M/\partial\dot{\chi}$ partial derivative with respect to $\dot{\chi}$
$\overline{C}_{M\mu}$	$= \partial\overline{C}_M/\partial\mu$ partial derivative with respect to μ
I_N	nacelle moment of inertia about yaw axis
I_b	blade moment of inertia about rotor center
I_R	average rotor moment of inertia about yaw axis, 2 blades: $I_R = I_b$, 3 blades $I_R = (3/2)I_b$

List of Symbols (cont')

M	yawing moment
N	number of blades per rotor
P	non-dimensional blade natural flap frequency when rotating, frequency unit Ω
R	rotor radius
T	$= \Omega R/V$ tip speed ratio
t	non-dimensional time, unit $1/\Omega$
$\dot{V}$	wind velocity
γ	$= \rho c a R^4/I_b$ blade Lock number
Θ_o	collective pitch
Θ_c	cyclic pitch
μ	$= V\chi/\Omega R$ non-dimensional velocity in rotor plane from yaw angle χ (small χ assumed)
ρ	air density
σ	$= Nc/\pi R$ rotor solidity ratio
χ	yaw angle, defined in Fig. 8
Ω	angular rotor speed

Introduction

The MOD-0 wind turbine has initially experienced dynamic difficulties with the yaw gear drive that had to be considerably stiffened by adopting a dual drive system (reference 1). The yaw gear system stiffness requirements will be even harder to satisfy for larger WECS. It thus seems appropriate to look into some alternative dynamic design configurations that are less demanding of the yaw gear drive or that can possibly do without this drive. A very cursory examination of the economic potential of wind electric power shows that even relatively small first cost or maintenance cost savings may mushroom into billions of dollars. If wind power captures 10% of the future yearly US investments in electric power plants we will have investments in WECS in the order of 2 billion dollars per year or 20 billion dollars per decade. Before embarking on such a large capital program we better make sure that we have not overlooked alternative WECS designs with possibly lower initial and/or life cycle costs. A very rough outline of some such alternatives will be given here.

Eight Pairs of Alternatives

Table 1 shows 8 pairs of alternatives for horizontal axis WECS configurations. The first five are conventional classifications and are listed for example in reference 2. Another important alternative - two or more blades per rotor - is not included in Table 1 since we will mainly discuss here two-bladed wind turbines. Mast and nacelle dynamic loads and vibrations can be reduced by adopting more than 2 blades and, in the long run, the selection of a 3 or 4 bladed wind turbine may pay off despite the greater first cost. In rotor craft, 2-bladed rotors are limited to smaller sizes and all large helicopters are 3 or more bladed. There are, however reasons for this preference that may not apply to wind turbines.

The alternatives 6 to 8 are unconventional. Cyclic pitch is today a standard requirement for rotorcraft and in the following we will discuss its potential application to wind turbines. Gearless yawing is of course a feature of most small WECS that have an upwind rotor and a vane downwind of the mast. For large systems the vane size would become rather awkward and vanes have been replaced by yaw gears. What is meant here in Table 1 is vaneless _and_ gearless yawing. This can be achieved either by a downwind turbine that has self-centering characteristics, called here rotor self-yawing, or by cyclic pitch controlled yawing. The first feature was tested by Saab-Scania on their 75 KW wind turbine, see reference 3. It was also suggested by Boeing-Vertol, see reference 4.

A recent interesting study is concerned with the first 3 pairs of alternatives in Table 1, see reference 2. For the case of 2 rigid blades with variable collective pitch 3 combinations of the alternatives 1 to 3 were looked at:

1. rotor downwind, rotor axis tilted 12°, blades radial

2. rotor downwind, rotor axis level, blades coned 12°

3. rotor upwind, rotor axis tilted 12°, blades radial

Loads for blade root bending, hub bending and hub torque in selected load cases have been determined for a 200 ft diameter wind turbine. The first two configurations have about the same hub bending moments and torques, while the third configuration shows largely reduced hub loads, particularly in the hub torque. The reason is the mast wind shadow for the downwind configuration assumed to reduce the inflow velocity by 22% over 30° azimuth angle, see reference 1 for a substantiation of these assumptions.

The alternative 4, hinged or rigid blades, is treated for a 2 bladed wind turbine in reference 5. A teetering hinge entirely relieves the nacelle of gyroscopic and aerodynamic hub moments, though the effects on the blades are less pronounced, since they receive a large portion of their bending moments both flapwise and chordwise from gravity, the more so, the larger the turbine. Thus the main effect of a teetering hinge is to alleviate nacelle and mast loads and vibrations. In particular, the yaw gear drive is relieved of loads when a teetering hinge is adopted. Thus the overall weight and cost of the system may well be smaller with teetering hinge than without. The rather successful Allgaier-Hütter wind turbine that operated between 1958 and 1967 in Stötten, F.R. Germany, had a teetering hinge that allowed ± 7° teetering, limited by elastic stops. The unconventional pairs of alternatives 6 to 8 are the main topic of this paper.

Five Alternative Configurations

Table 2 shows for the 8 alternatives of Table 1 the columns 1 or 2 applicable to 3 actual large WECS and to 2 configurations without yaw gear drive. The 3 actual large WECS began to operate in 1940, 1958 and 1975 and they have in most respects the same features. Differences exist only with respect to alternatives 2 and 4; level or tilted rotor axis, hinged or rigid blades. Actually there is a difference not shown in Table 2, since the Smith-Putnam wind turbine had a hinge for each blade, while the Allgaier-Hütter turbine had only one teetering hinge.

The two rigid blade configurations without yaw gear drive in the 4th and 5th row of Table 2 are first; a self-yawing rotor, located downwind of the mast, with variable collective pitch and fixed or possibly variable cyclic pitch, second; a rotor that is yawed by cyclic pitch inputs, located either downwind or upwind of the mast with fixed or possibly variable collective pitch. The selection of rigid blades is believed to be necessary for wind turbines without yaw gear drive, otherwise the centering capability for the first configuration or the cyclic pitch effectiveness for the second configuration would be inadequate. One principle reason for having a teetering hinge - load alleviation for the yaw gear drive - does not apply any way to self-yawing turbines. An auxiliary yaw gear drive for the initial start-up period may be used as in the Saab-Scania 75 KW wind turbine, reference 3, though proper yawing by natural rotor moments appears to be possible and may be preferable.

Self-Yawing

Before knowing that Saab-Scania had built and begun testing a self-yawing wind turbine, a preliminary study was made at Washington University to determine both analytically and with a small wind tunnel model the self-yawing charac-teristics of a wind milling rotor. The analysis was made with the method of reference 6, which assumes the blades to be rigid in bending and flexibly hinged at the rotor center. This assumption usually gives good approximations for the aerodynamic blade root bending moments. The blades were assumed to be of constant chord and untwisted, as were those of the wind tunnel model. The analysis is of the linear type, omitting blade stall or large angle effects and omitting effects of non-uniform or dynamic inflow. The nacelle inertia moment is negligible as compared to gyroscopic or aerodynamic rotor moments. Also the forces in the plane of the rotor have a moment about the yaw axis that is negligible as compared to the rotor hub moments. These assumptions made for the analysis are valid for the MOD-0 turbine (see for example reference 7) and also for the wind tunnel model.

Under the foregoing assumptions the pitching and hub moment coefficients depend only on two rotor parameters; the non-dimensional blade Lock number $\gamma = a\rho cR^4/I_b$ (which relates the airloads to the blade inertia), and the non-dimensional flapping frequency P. The moment coefficients depend further on two operational parameters; the blade pitch setting Θ and the non-dimensional velocity in the rotor plane when yawed by the angle χ assumed to be small

$$\mu = V\chi/\Omega R \qquad (1)$$

One can show that rotor self-yawing is governed by the first order differential equation

$$\dot{\chi} \; \overline{C}_{M\dot{\chi}} + (\chi V/\Omega R)\overline{C}_{M\mu} = 0 \tag{2}$$

If we have initially a yaw angle χ_0, this equation gives an exponential decay to $\chi = 0$ with a time constant

$$\tau = (\overline{C}_{M\dot{\chi}}/\overline{C}_{M\mu})\Omega R/V \tag{3}$$

The derivative $\overline{C}_{M\dot{\chi}}$ is independent of blade setting, while $\overline{C}_{M\mu}$ increases with the average angle of attack of the blade. For typical operating conditions the time constant is 10 to 30 turbine revolution periods. During start-up at low $\Omega R/V$ the time constant is much shorter.

The theory briefly outlined here was used to determine for a given yaw angle the reduction of the hub moment at the instant when the yaw restraint is released. The yawing moment then goes to zero, but the pitching moment is not zero. The total hub moment reduction factor depends only on γ and P as shown in Fig. 1. It is seen that in the region of P = 2.5 typical of a configuration like MOD-0 (reference 7) the hub moment reduction factor is about .6. When P is reduced to a value of about 1.4, the hub moment reduction factor is below .2.

The reduction in hub moment or blade root bending from self-yawing is even more impressive for a system described in reference 4 from which Fig. 2 is taken. The much larger hub moment reduction despite very stiff blades with P > 2.5 is obtained by feeding the hub pitching moment into a cyclic pitch control system, apparently in a way related to that developed by Lockheed for their Advanced Mechanical Control System (AMCS), see reference 8. Such feedback system is effective in canceling hub-moments for rigid blades, and its application looks promising for large self-yawing wind turbines with 2 rigid blades. As stated in reference 4, the feedback system not only reduces blade root moments to almost zero but also removes a yaw position instability that was encountered beyond the operating condition characterized in Fig. 2 by the trough of the cantilever system curve at 37 mph wind velocity. One must keep in mind, however, that the nacelle angular acceleration moment must give rise in a two bladed rotor to a vibratory hub moment with an amplitude equal to the angular acceleration moment. This is the reason why the vibratory blade root moment for self-yawing is not quite zero, except where the cantilever system produces zero

restoring moment, see Fig. 2 at V = 37 mph. Fig. 2 is the
result of a computation. The system has not as yet been
tried even in a wind tunnel model.

When discussing reference 4 with its author the following
facts were learned that are not evident from the reference:
First, the curves shown in Fig. 2 are vibration amplitudes,
consisting mainly of the first harmonics. If these first
harmonics were plotted instead, the curves beyond 37 mph
would cross the horizontal axis and be negative at higher
wind speed. The explanation is that with decreasing
collective pitch angle to keep the rotor speed constant at
increasing wind speed, a reverse inflow pattern develops in
the blade tip region that is responsible for the yaw position
instability. Second, the blade coning angle was assumed to
be zero when computing the conditions of Fig. 2. With
increasing coning angle the trough in the cantilever system
curve and the associated onset of instability will move to
higher wind speeds.

At Washington University a small two bladed auto-rotating
self-yawing wind tunnel model has been tested as shown in
Fig. 3. The rotor diameter is 400 mm, the test section is
square with 610 mm sides. The rigid blades are attached by
flexures to the hub. The blades are untwisted and have a
constant chord of 25 mm. The blade flap frequency without
rotation is 13 cps, the blade Lock number is 4.5. The rotor
has a high blade solidity ratio of .08. The "nacelle",
consisting of a massive shaft of 20 mm diameter and a pulley
at the bottom, has in relation to the blades more yaw inertia
than the MOD-0 nacelle.

The "nacelle" could be deflected in yaw by hand using
the pulley below the lower wall of the wind tunnel test
section. When yawed about 20 to 30 degrees, the pulley was
released and the nacelle moved to its equilibrium position
that in all cases except one was close to the alignment
position of rotor and tunnel axis. The time to center
agreed roughly with Eq. (2). The rotor speed was measured
with a stroboscope, the tunnel speed with a pitot static
probe. The blade pitch angle θ_0 could only be varied in
between runs. $\theta_0 = 90°$ corresponds to the feathered position
of the blades, $\theta_0 = 0$ to their in-plane position. As θ_0 is
lowered the rotor speed at a given tunnel speed picks up and
the non-dimensional flap frequency P becomes lower.

Fig. 4 shows the test results as plots of θ_0 and $\Omega R/V$
vs. P. Two tunnel speeds are shown; 4.6 and 8.2 m/s. The
unstable condition, where the rotor would not center but
rather go to a 40° yawed position, occurred for the higher

tunnel speed, however not at the highest $\Omega R/V$. Above the critical $\Omega R/V$ the rotor centered again. The unstable condition probably occurs in a range of collective pitch angles rather than for a specific angle which was missed because only rather large steps in collective pitch were made.

The instability occurred only at the higher tunnel speed, not at the lower tunnel speed with equal θ_0 and $\Omega R/V$. The likely explanation of this phenomenon is the difference in coning angle between aerodynamically similar conditions. As the tunnel speed is lowered together with the rotor speed, the blades become relatively stiffer as indicated by the higher non-dimensional flap frequency P. The negative increment of coning angle in the reversed tip flow region is now smaller and the rotor centers at exactly the same θ_0 and $\Omega R/V$ that lead to non-centering at the higher tunnel speed. If this explanation is correct, a higher P-value and or pre-coning should eliminate the non centering region for 8.2 m/s tunnel speed. It appears that Saab-Scania have as yet not encountered a non-centering region despite operation up to 35 mph wind velocity.

Tests were also conducted with the stopped rotor. When the feathered blades were horizontal the nacelle did not show a centering tendency beyond $\pm$ 70° from the center position. However, when the feathered blades were inclined by about 20° from horizontal, centering occurred from every yawed position except for a small dead range at 180° yaw angle. Thus it may not be necessary to have an auxiliary yaw gear drive for start-up of the wind turbine, if the blades are parked in a position that is inclined somewhat from horizontal.

In summary, it can be said of the self-yawing configuration that it looks promising from the point of view of avoiding for rigid blades a heavy yaw gear drive together with its control system. Without cyclic pitch inputs the vibratory hub moments are reduced somewhat but are still quite high for a 2 bladed rotor of the MOD-0 type. Cyclic pitch inputs can be used to reduce the vibratory hub moments to near zero. The question then is, whether or not a teetering hinge in combination with a light yaw gear drive is not a simpler and cheaper solution to the problem of alleviating the vibratory hub moments of the rigid blades. The regions of centering instability can probably be removed by blade preconing, they can also be removed by cyclic pitch feedback. The development of such a feedback system can be a demanding and time consuming task judging from the experience at Lockheed. The ultimate success is, however, beyond a doubt.

Yawing by Cyclic Pitch Control

While in the previous section cyclic pitch was considered as an auxiliary input from a feedback system, we will now discuss the possibility of cyclic pitch as the main yaw control mechanism for a large wind turbine. All previously discussed configurations are based on propeller technology and require a variation of the collective pitch angle over a range of approximately 90°. In contrast, cyclic pitch control for yawing is based on helicopter rotor technology. Cyclic pitch application allows the rotor to be rapidly positioned at any desired yaw angle without encountering large hub moments.

One may question the wisdom of utilizing helicopter technology for wind turbines with their much longer expected life times. Actually the number of lifetime load cycles for a large wind turbine is not much different from that for a helicopter. For example, a 4-bladed helicopter rotor with 300 rpm rotor speed and 10,000 hours operational life has the same number of main load cycles as a large 2-bladed wind turbine with 30 rpm and 200,000 hours operational life, namely 720 million. Thus the dynamic design considerations for rotorcraft and for large wind turbines should not be different, and much of the dynamic design experience gained in 40 years of rotorcraft design should be applicable to large wind turbines.

Helicopter type blade pitch controls require no gears as found in propeller hubs but merely blade pitch arms, rotating axial links and a mechanism to transmit the rotating control loads to non-rotating actuators. This mechanism avoids the rotating hydraulic seals which have a tendency to leak. In helicopters collective and cyclic pitch ranges are usually about 12°, which is more than enough to operate a wind turbine.

Fig. 5 shows the collective pitch θ_0 versus tip speed ratio $T = \Omega R/V$ at rated rotor speed of the MOD-0 wind turbine for the entire power range from zero to rated power. These curves have been transcribed as well as possible from data in references 9 and 10. The range of collective pitch required between syndronization wind speed and cut-off wind speed is from zero to less than 10°. The remaining range up to 90° is merely used for parking the turbine in the feathered position. A cyclic pitch controlled turbine would be parked edgewise to the wind as is done for most small WECS. A position close to edgewise could also be used for start-up and shut down similar to the autogiros of the twenties that used to taxi around the airport to start the wind milling rotor. Since the large WECS are to deliver power into a net, start-up with net power is also convenient same as for the non-self starting vertical axis large WECS.

A particularly simple cyclic control system is possible if the wind turbine is designed for fixed collective pitch operation. Fig. 6 shows one of many examples for such a system as a schematic planview of the shaft S, the power take-off P and the cyclic pitch control system, when the blades B are in a horizontal position. A rotating flexure F allows sideways motions parallel to the blade axes but it is stiff in the plane perpendicular to these axes. At the aft end of the flexure and connected to it by a bearing is a non-rotating lug L that can be horizontally displaced by a rod R with the help of an also non-rotating linear actuator A that can respond to signals representing errors in either yaw angle, rpm, or torque or power. The sideways displacement of the rod R causes a cyclic pitch change of the blades. The mechanism is very simple and rugged both compared to the conventional helicopter pitch controls and to the pitch controls employed in the first three WECS listed in Table 2. There are no gears in the hub and no bearings that are axially loaded, since the centrifugal force of the 2 blades B is balanced, so that the bearings which connect the blades with the shaft experience mainly radial forces. The cyclic blade rotations are quite small, at most about $\pm 6°$, so that bearings can be of the elastomeric type without any gliding or rolling surfaces. The control actuator is non-rotating thus avoiding the difficulties of rotating hydraulic seals.

In some large WECS an emergency feathering system is employed in case of failure of the primary pitch change system. One can question the wisdom of such an added complication. In rotorcraft it is customary to use for the blade pitch variation single hydraulic actuators with dual pistons driven by two independent hydraulic circuits. The same arrangement would seem to be appropriate also for WECS. If the oil pressure is one system drops below a critical point the WECS would be shut down with the help of the second hydraulic system. Fig. 6 shows only one cyclic pitch control for yaw. For rotor pitching a second cyclic pitch control could be used in order to keep the hub moment in rotor pitch small. It is also possible that a second cyclic pitch control may be unnecessary if the yaw control is properly phased.

For a fixed collective pitch rotor the question is how to protect one self against over speeding or over torquing. When cyclic pitch is used for yawing this can readily be achieved by turning the rotor out of the wind. Fig. 7 shows a computed yaw rate response to a unit cyclic pitch input assuming a blade Lock number of $\gamma = 8$, a blade flap frequency of $P = 1.5$, and a ratio of nacelle over rotor inertia of $I_N/I_R = 1.7$ which applies to the MOD-0, except that γ and P are actually higher, leading to even faster rates of yaw and lower time constants. The first curve from the left represents

the time lag from nacelle inertia, if the rotor were to
respond instantaneously to a cyclic pitch input. The
second curve includes the delay from rotor dynamics. The
curves were computed with the method of reference 11.

The asymptotic yaw rate is .73°/time unit per degree of
cyclic pitch input. The time constant is about 1.7 time
units. For the MOD-0 with 40 rpm the time unit is 1.5/2π =
.24 seconds. Assuming 6° cyclic pitch range, one would
obtain for the MOD-0 case an asymptotic yaw rate of
.73·6/.24 = 18° per second, with a time lag of about .4
seconds. This must be compared to the one or two degrees
per second yaw rate usually assumed for the gear drive of
large WECS. The high rate of yaw from cyclic pitch does
not cause high hub moments since the gyroscopic moments are
balanced by aerodynamic moments. A hub moment is required
in order to accelerate the nacelle, and in a two-bladed
rotor it will cause 2 per rev. vibratory amplitudes of the
same magnitude. One can easily compute that these hub
moments will be moderate.

At 18° per second a complete turning out of the wind of
the rotor by 90° would take 5 seconds, which is even shorter
than the 8 seconds for emergency feathering of the MOD-0.
The preceding estimates ignore the centering moment expressed
by the second term of the left hand side of Eq. 2. This
centering moment is, however, small as compared to the power
of a cyclic pitch control system with 6° cyclic pitch amplitude.

Fig. 8 shows in the same form as Fig. 6 the relations
between tip speed ratio T (or MPH for MOD-0) and yaw angle χ
for rated rotor speed and a range of power between zero and
rated power. The definition of χ is given in the graph. The
rotor plane is perpendicular to the wind direction for χ = 0,
and edgewise to the wind direction for χ = 90°. The graphs
have been estimated from reference 12. One should realize
how similar the curves of Fig. 8 are to those of Fig. 5.

In reference 13, Fig. 8d a condition of the MOD-0 system
is described where the nacelle wind velocity varied from a
mean of 25 mph by ± 5 mph and where the nacelle yaw angle
varied by ± 10°, both with a period of about 8 seconds. This
condition caused for the then MOD-0 configuration substantial
over-loading of various components. From Fig. 8 it is seen
that at most ± 20° yaw angle variation would compensate for
the variable wind velocity and wind direction if rated power
were to be kept constant. With 18° per second of maximum yaw
rate, such a compensation should be achievable with only a
small variation in power or torque.

For operation of the WECS as part of a large electric network one might select a procedure indicated in Fig. 8 by the heavy lines with the arrows. After start-up, the cyclic pitch control would be operated by the rotor speed error. Synchronization would occur at near zero power and about 40° yaw angle. After synchronization the cyclic pitch control would be operated by the yaw angle, which could be either zero or more than zero as shown in Fig. 8. The latter setting has the advantage of obtaining a less steep slope of the yaw angle vs. wind speed curve for rated power.

After the wind speed for rated power is reached, cyclic pitch control would be operated by the signal representing the torque error from rated torque. At cut-off wind speed the load would be disconnected and the cyclic pitch control would revert again to operation by the signal representing rotor speed error, possibly from less than rated rotor speed. The rotor could be kept turning up to the highest wind speeds and turbulence without encountering dangerous loads.

Rotor speed control by cyclic pitch has been used in the McDonnell-Army XV-1 convertaplane and tested on the ground and in the air during hundreds of hours down to tip speed ratios of one, see reference 14. The system was simple, rugged and very well behaved. The speed governor was a fifty dollar commercial product. The rotor speed error was very small even in gusty weather and during maneuvers of the rotorcraft. There is no doubt that automatic rotor speed and torque control by cyclic pitch is feasible for WECS and should represent no more than the usual development problems for a new application of a tested system.

Though both upwind and downwind rotor location could be used with cyclic pitch control for yaw, it is likely that the downwind location would prove more attractive because of its more compact design. The mast wind shadow problem will be largely alleviated since first harmonic blade moments are cancelled by the cyclic pitch inputs, though higher harmonics from mast wind shadow will persist. For parking, start-up, and shut-down, provisions must be made to allow positioning of the wind turbine at a yaw angle of 90° or less when non rotating. Preferably this should be achieved by proper aerodynamic shaping of the nacelle, possibly using a small drag plate opposite to the rotor to balance the rotor drag. The blades themselves for all but horizontal positioning produce a weather-vaning effect that tends to keep the rotor at 90° yaw angle. The rotor brake would probably be designed to stop the blades in an azimuth position favorable for start-up. If positioning of the rotor for start-up by natural wind effects should prove to be too cumbersome, an auxiliary low torque yaw drive and/or start-up with net or storage power could be used.

A major advantage of the WECS previously described is that the blades are never exposed to flatwise gravitational bending moments. These moments lead even for non-rotating helicopter blades to critical stresses. For the much larger diameters of wind turbines, these flatwise gravitational moments are even more significant and have led to blade designs with very thick root sections and very high flapwise natural blade frequencies. With non-feathering wind turbine blades, whether they are fixed in collective pitch or have a small collective pitch range of about 10° for speed and torque control (Fig. 5), gravitational loads are essentially edgewise to the blades, which thus can be built with much thinner root sections. Substantial reductions in blade weight and cost and improvements in aerodynamic performance can be expected when adopting a non-feathering system.

In summary, the use of cyclic pitch control for yawing large WECS with rigid blades looks promising. Collective pitch variation could either be completely eliminated or limited to a small range of about 10°. In either case the blades will be much lighter and aerodynamically better, since flatwise gravitational loads remain small. The rotor need not be stopped at winds above cut-off velocity but could be kept in autorotation at constant rotor speed without high blade loads. The principle of rpm or torque control by cyclic pitch has been successfully tested on a rotorcraft, so that the transfer of this technology to WECS will involve no major problems or uncertainties.

Conclusion

The rigid propeller technology presently pursued for the large WECS program appears to the writer as a step in the wrong direction. Lifting rotor technology appears to promise superior, simpler and cheaper solutions probably by a wide margin. Published arguments like those in reference 15 in favor of the rigid propeller solution are quite unconvincing and also contain errors of fact. The gist of these arguments are that by adopting systems that were designed 20 and 40 years ago by very small groups of engineers, a low risk of failure is achieved. This is a poor argument for laying the technical foundations of a possible multi billion dollar industry. We should try to find the best solution on the basis of present know-how and present related technologies. This takes careful comparative studies and a fresh look at the overall problem before making quantum jumps in WECS size. It is hoped that the preceding comments will lead to such a fresh look. The best solution may not be among the alternatives discussed here.

References

1. Spera, D.A., Janetzke, D.C. and Richards, T.R., "Dynamic Blade Loading in the ERDA-NASA 100 KW and 200 KW Wind Turbines", American Wind Energy Spring Conference, Boulder, Colorado, May 1977.

2. Spera, D.A. and Janetzke, D.C., "Effects of Rotor Location, Coning and Tilt on Critical Loads in Large Wind Turbines", Proposed for publication.

3. Gustavsson, B., "75 KW Test Plant Operation, Results and Findings", Third Biennial Conference on WECS, Washington D.C., September 1977.

4. Doman, G.S., "Dynamic Structural Characteristics of Rotors for WECS", Third Biennial Conference on WECS, Washington, D.C., September 1977.

5. Spera, D.A., "Structural Analysis of Wind Turbine Rotors for NSF-NASA Mod-O Wind Power System", NASA TMX-3198, 1975.

6. Peters, D.A. and Ormiston, R.A., "Flapping Response Characteristics of Hingeless Rotor Blades by a Generalized Harmonic Balance Method", NASA TN D-7856, February 1975.

7. Linscott, B.S., Shapton, W.R., Brown, D., "Tower and Rotor Blade Vibration Test Results for a 100-KW Wind Turbine", NASA TM X-3426, October 1976.

8. Pothhast, A.J. and Kerr, A.W., "Rotor Moment Control with Flap-Moment Feedback", Journal of the American Helicopter Society, Vol. 20, No. 2, pp. 34-44, April 1975.

9. Gilbert, L.J., "A 100 KW Experimental Wind Turbine: Simulation of Starting, Overspeed, and Shutdown Characteristics", NASA TMX-71864,

10. Hwang, H.H. and Gilbert, L.J., "Synchronization of the ERDA-NASA 100 KW Wind Turbine Generator with Large Utility Networks", NASA TMX-73613, March 1977.

11. Hohenemser, K.H. and Yin, S.K., "On the Use of First Order Rotor Dynamics in Multiblade Coordinates", 30th Annual Forum American Helicopter Society, Washington, D.C., May 1974, Preprint No. 831.

12. Gessow, A. and Tapscott, R.J., "Tables and Charts for Estimating Stall Effects on Lifting Rotor Characteristics", NASA TN D-243, May 1960.

13. Glasgow, J.C. and Linscott, B.S., "Early Operation Experience on the ERDA-NASA 100 KW Wind Turbine", NASA TM X-71601, September 1976.

14. Head, R.E., "Evaluation of some Flight Safety Aspects of the Single-Engine, Unloaded Rotor Winged Helicopter", Journal of the American Helicopter Society Vol. 4 No. 4, pp. 4-10, October 1959.

15. General Electric Company, "Design Study of Wind Turbines 50 KW to 3000 KW for Electric Utility A Application, Analysis and Design", NASA CR 134935, February 1976

Notes to paper by Kurt H. Hohenemser

1. Since writing the preceding paper the author learned from Professor D. E. Cromack that the University of Massachusetts 25 KW self-yawing wind turbine has been tested up to about 40 mph wind velocity without encountering the instability reported here for the wind tunnel model. The turbine has 3 blades with substantial built-in coning angle, which is probably the reason why it is self-centering up to at least 40 mph. The Grumman Windstream II turbine is also self-yawing, has 2 blades, but according to Mr. Stoddard has not been fully tested at high wind velocity.

2. As Mr. Doman pointed out to the author, the description of Fig. 2 contains an error. The vibratory blade root bending moment shown for the floating nacelle does not include the nacelle angular acceleration. Rather, the moment shown in Fig. 2 occurs when the nacelle is yawed by 20 degrees with the help of a cyclic pitch control system that trims first harmonic flatwise blade moments to zero. The moment contains only higher harmonics. When accelerating the nacelle first harmonic blade bending moments will occur.

DISCUSSION

Q. Your slide showed instability a function of blade pitch. Do you know if
    you experienced blade stall at this condition?

A. I doubt it that blade stall was involved. The instability did not occur
    with the same blade pitch and the same tip speed ratio at lower wind
    speed, when the blade angle of attack was the same.

TABLE 1. - EIGHT PAIRS OF ALTERNATIVES

		1	2
1	ROTOR	UPWIND	DOWNWIND
2	ROTOR AXIS	LEVEL	TILTED
3	BLADE AXES	CONED	RADIAL
4	BLADES	HINGED	RIGID
5	COLLECTIVE PITCH	VARIABLE	FIXED
6	CYCLIC PITCH	VARIABLE	FIXED
7	YAWING	GEAR	GEARLESS
8	GEARLESS YAWING BY	SELF-YAWING	CYCLIC PITCH

TABLE 2. - FIVE CONFIGURATIONS

	1	2	3	4	5	6	7	8
SMITH-PUTNAM 1940	2	2	1	1	1	2	1	-
ALLGAIER-HUTTER 1958	2	2	1	1	1	2	1	-
NASA 1975	2	1	1	2	1	2	1	-
SELF-YAWING	2	-	-	2	1	1 or 2	2	1
CYCLIC PITCH YAWING	1 or 2	-	-	2	1 or 2	1	2	2

211
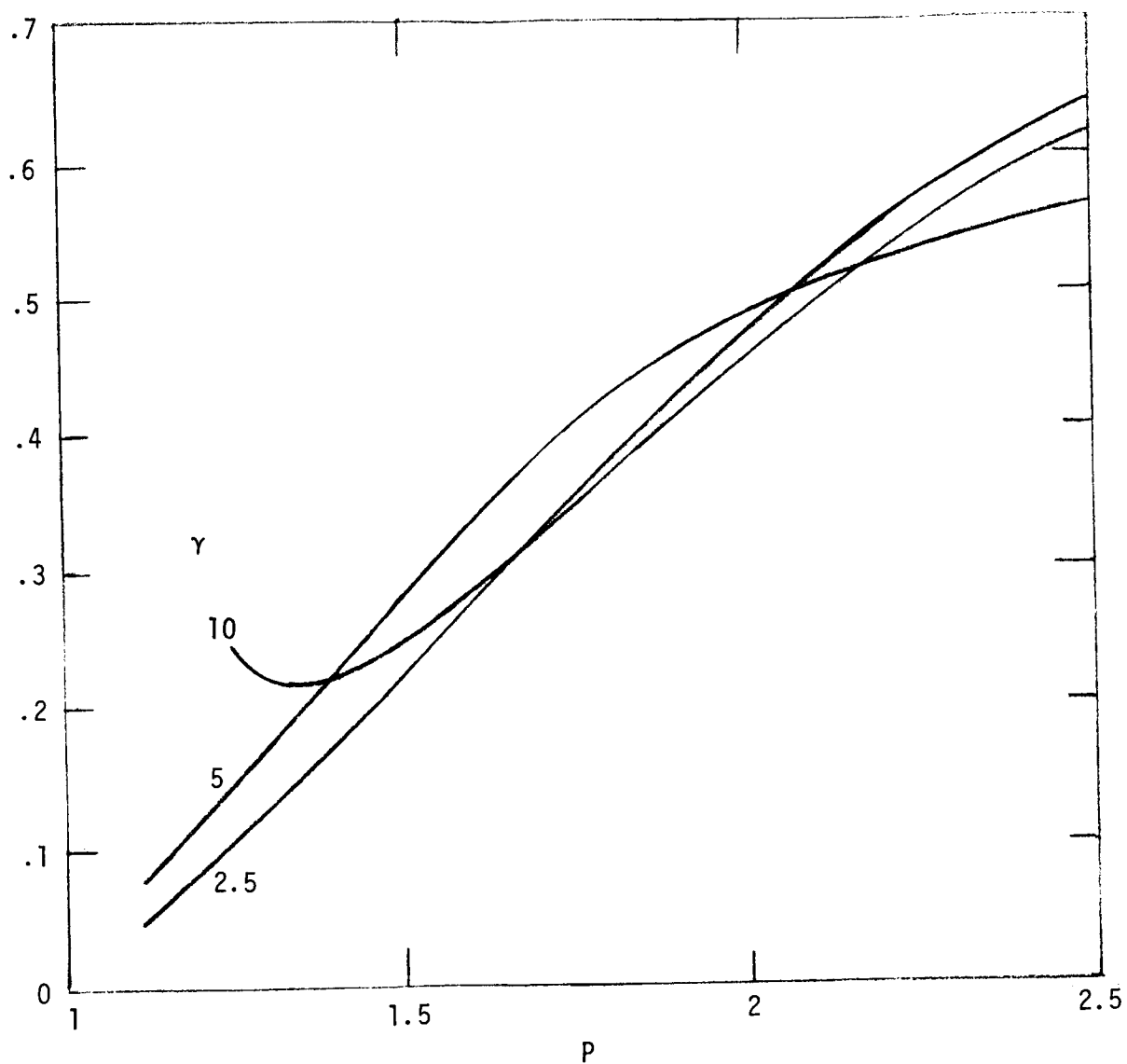
Figure 1. - Hub moment reduction factor from gearless yaw control versus nondimensional flap frequency P.
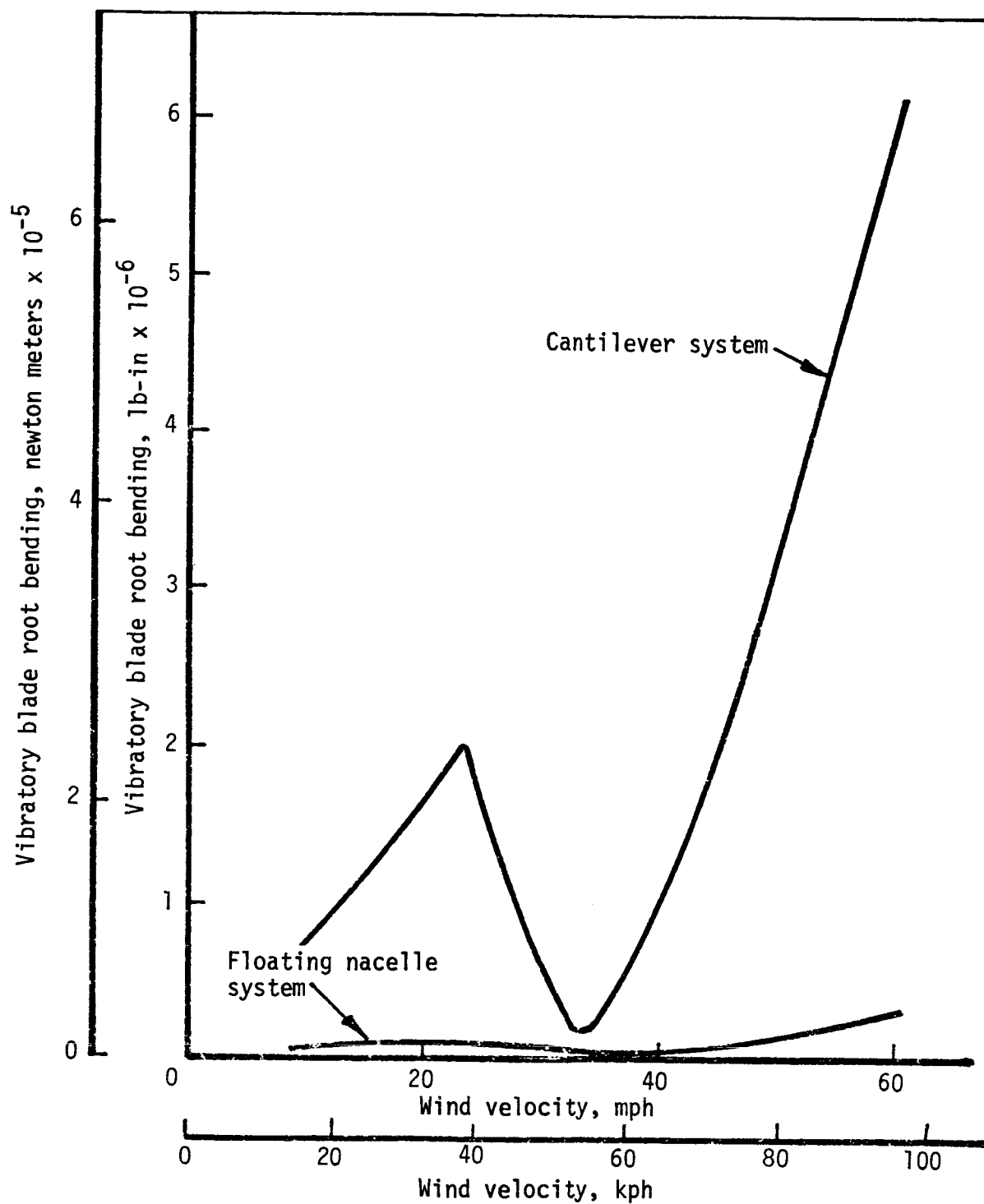
Figure 2. - Vibratory blade root moment versus wind velocity for
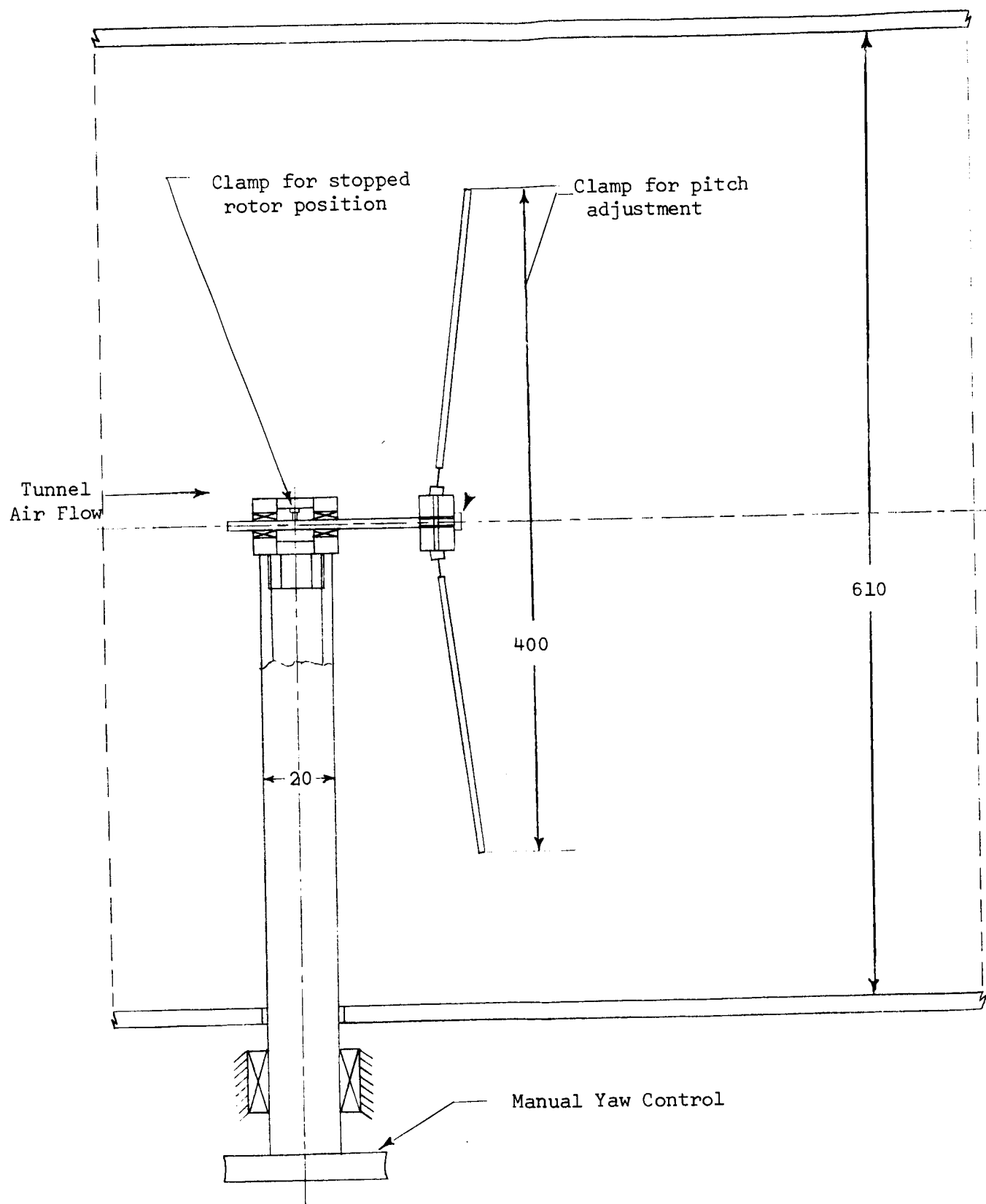two systems at 20° yaw angle.

Figure 3. - Schematic side view of self-yawing, windmilling model rotor in wind tunnel.
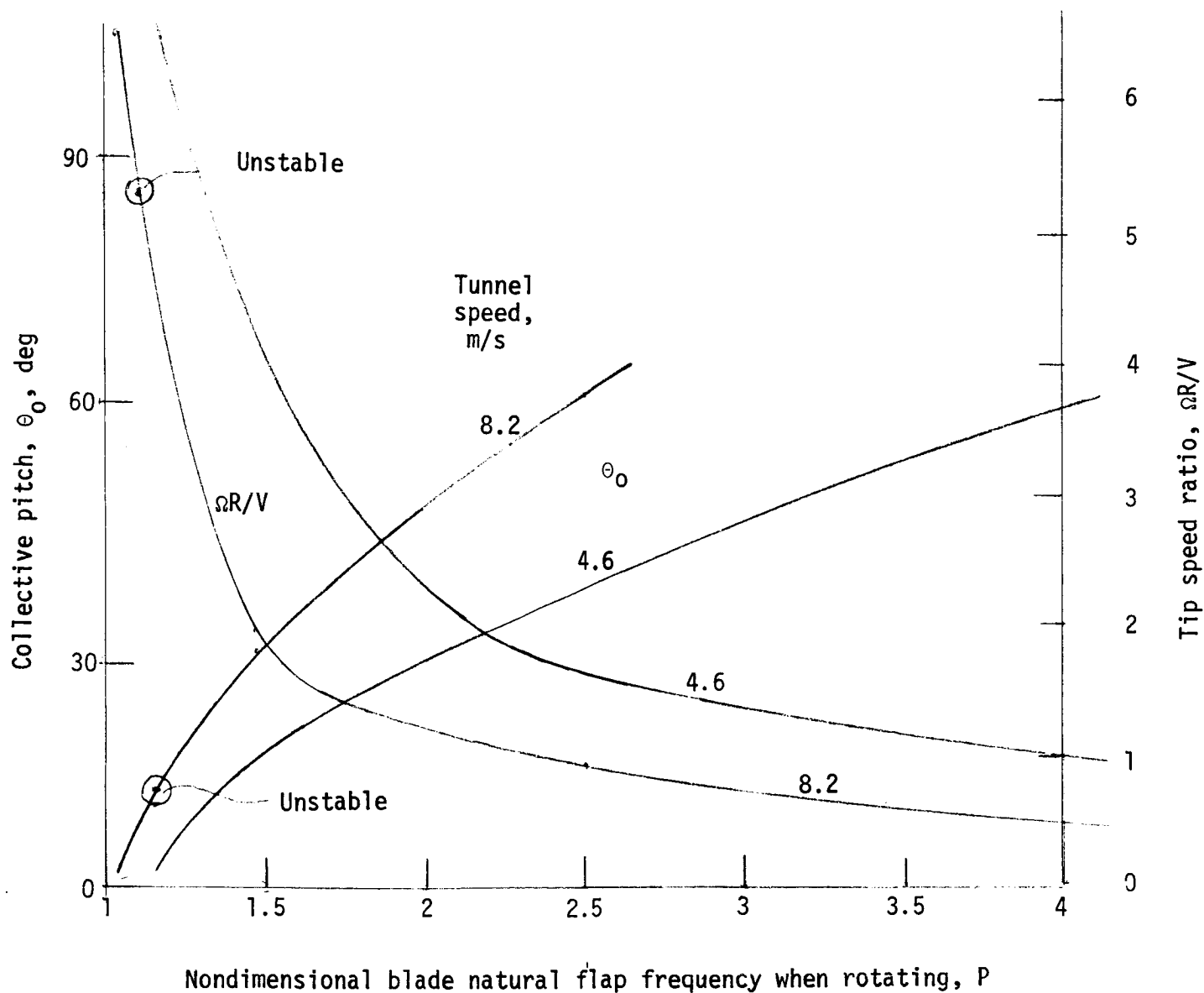
214

Figure 4. - Blade pitch setting Θ_0 and tip speed ratio $\Omega R/V$ versus nondimensional blade flapping frequency P when rotating.
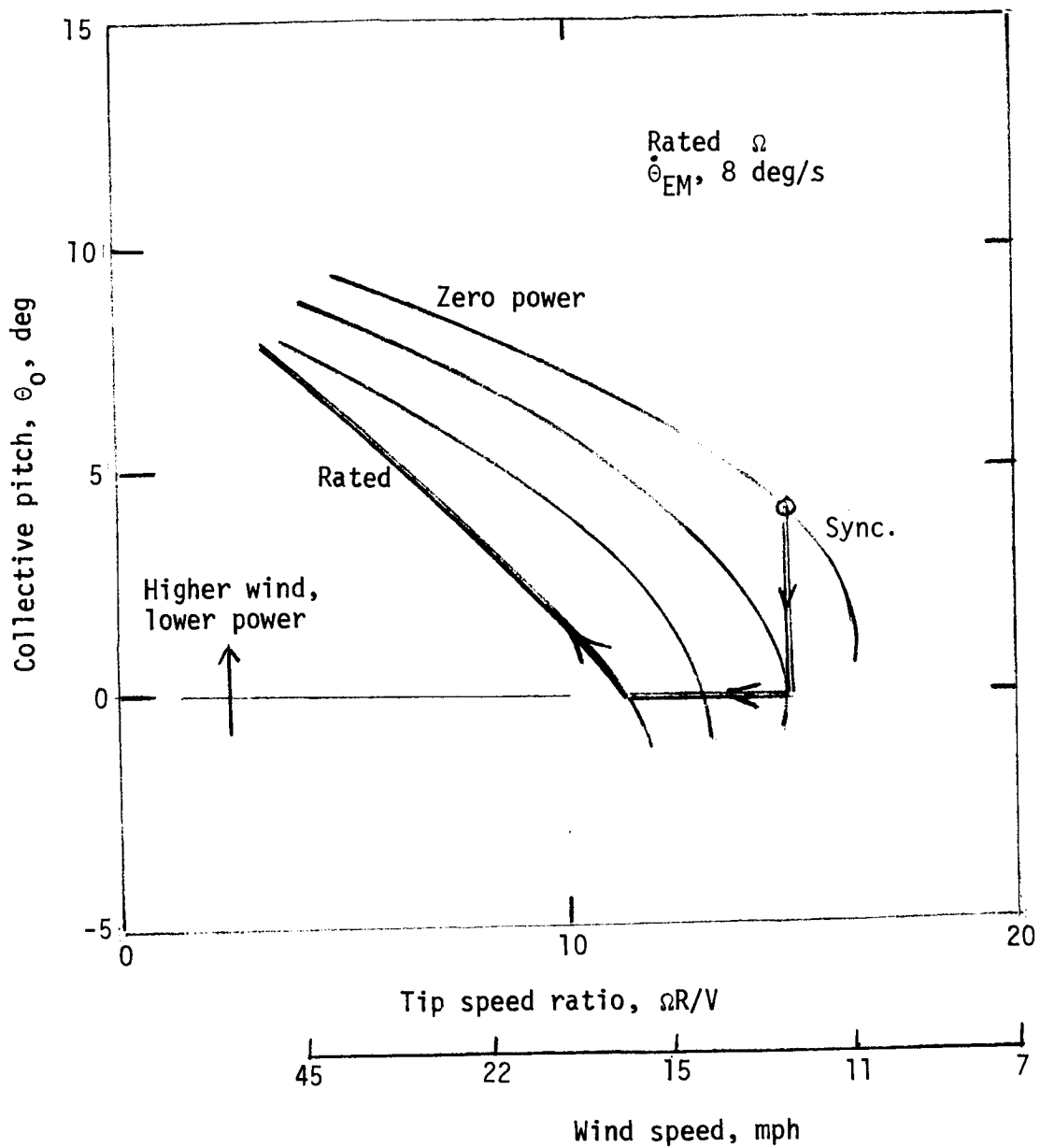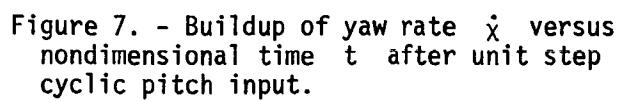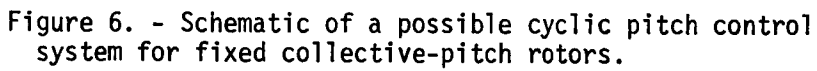
Figure 5. - Collective blade pitch angle Θ_0 versus tip speed ratio $T = \Omega R/V$ (or mph) at various power settings for rated tip speed. (MOD-0.)

Figure 6. - Schematic of a possible cyclic pitch control
system for fixed collective-pitch rotors.

Figure 7. - Buildup of yaw rate $\dot{\chi}$ versus
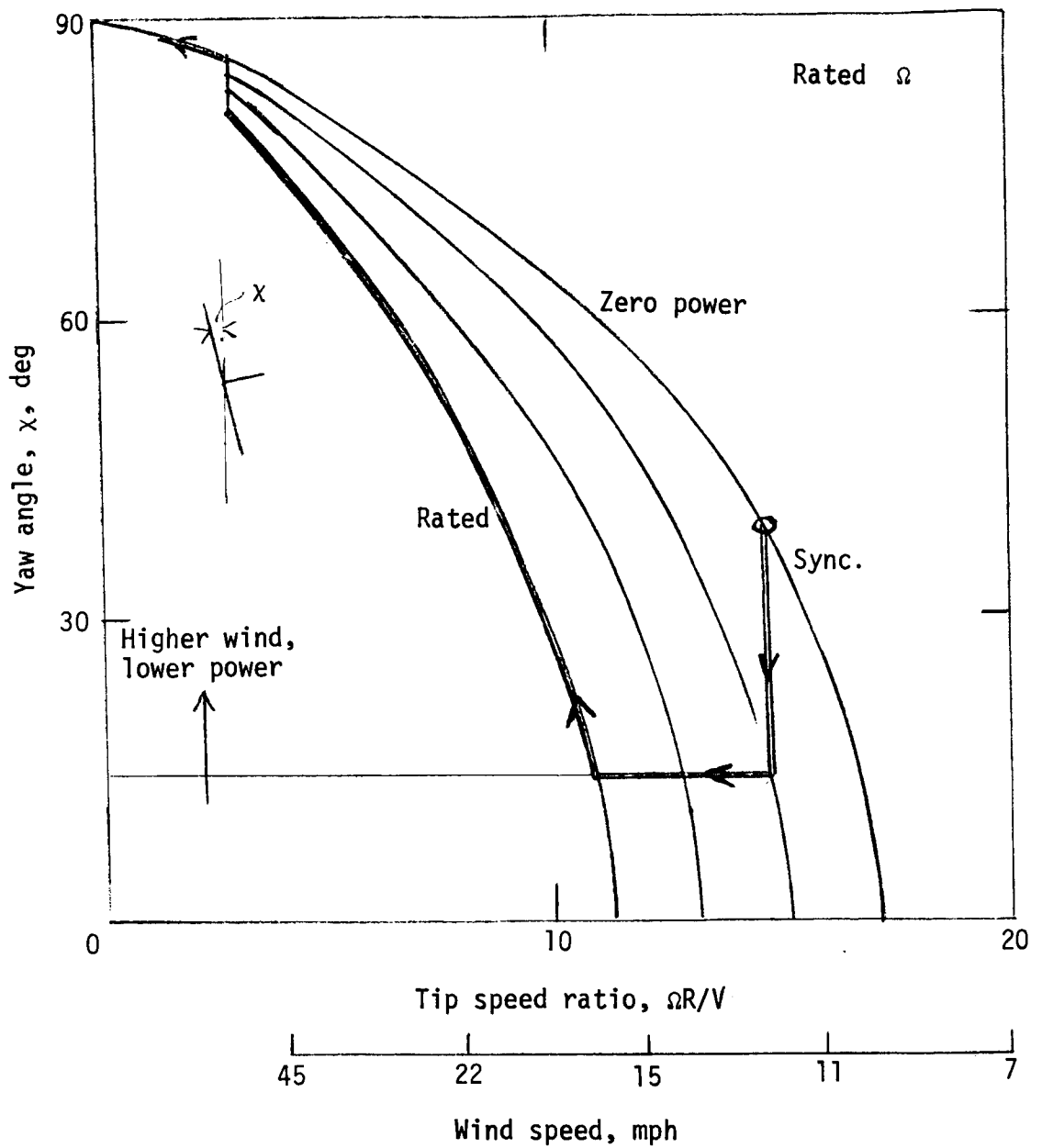nondimensional time t after unit step
cyclic pitch input.

Figure 8. - Yaw angle χ versus tip speed ratio $T = \Omega R/V$ at various power settings for rated tip speed (mph scale for MOD-0).

FATIGUE LOAD SPECTRA FOR UPWIND

AND DOWNWIND ROTORS

John S. Andrews
Chief Technical Staff - MOD-2 WTS

Boeing Engineering and Construction
Seattle, Washington   98124

ABSTRACT

Effect of both alternating and mean load on the fatigue life of an upwind and downwind MOD-2 wind turbine system is presented. It was shown that the fatigue damage varies as the product of the stress range cubed and the maximum stress. Hence, the alternating flapwise load caused by tower shadow and wind gradient is an important factor in determining rotor blade life.

INTRODUCTION

The baseline MOD-2 wind turbine system is a downwind, cantilevered, zero precone rotor approximately 300 feet in diameter which will generate approximately 2500 KW. Boeing is presently in the configuration concept design phase of the program. The aim of this paper is to show the effect of both the alternating and mean load parameters on the fatigue life of an upwind and downwind MOD-2 rotor.

LOAD AND FATIGUE ANALYSIS DISCUSSION

The fatigue design goal is to operate thirty years in a given wind/gust spectrum with a safe life design concept, and yet meet minimum energy cost goal. Safe life design means that the maximum operating loads will be below the endurance limit. However, allowance for .5 percent of the total applied cyclic loads can be above this limit. These loads are the infrequent occurring cyclic loads (approximately 5,000 - 10,000 cycles).

The fatigue environment is composed of a wind spectrum, Figure 1, for any site which is independent of rotor orientation with respect to tower and some gust spectrum shown in Figure 2. This gust spectrum defines the load distribution relative to a nominal load, M_0, for a specific wind speed and is applied to the alternating load only. Figures 1 and 2 can be combined into a load exceedance curve of the form shown in Figure 3. There will be a number of these spectra for each given wind speed such that the total of the accumulative cycles will equal 2.11×10^8 cycles equivalent to 30 years of life. An upwind and downwind rotor will have different load exceedance plots.

The load time history of the flapwise bending moment at a spanwise blade station of $r/R = .385$ and at 52 mph for an upwind and a downwind rotor is shown in Figure 4. These are preliminary loads for MOD-2 due to a 30 degree tower

shadow notch, wind gradient, and a 20 degree yaw wind. The C-60 computer program was used to establish these loads which would only allow input of the velocity reduction due to tower shadow in 15 degree azimuth increments which is quite conservative for the MOD-2 tower. For reference, the rotor blade is straight down at 180 degree azimuth. These flapwise alternating loads change with wind speed as shown in Figure 5. It can be seen that the tower shadow as represented has a large effect on the downwind rotor. The upwind and downwind steady state flapwise bending moment does not change much with wind speed as shown in Figure 6.

Now the question becomes, how do these loads relate to fatigue damage? Fatigue damage varies as the product of the stress range cubed and the maximum stress. The importance of this relationship with cut off wind speed is shown in Figure 7. An initial allowable stress for MOD-2 was established to be equal to the MOD-1 which was predicated on allowing .5 percent stress cycles to exceed the crack propagation threshold. The non-dimensional damage for the MOD-1 is shown in Figure 7 for comparison. A damage curve for the MOD-2 downwind rotor shown in Figure 7 indicates 4 percent exceedance of the crack propagation threshold. The reason for this is that the MOD-2 has a greater operating wind speed range between rated wind speed and cut off wind speed i.e., alternating loads are higher with a lower mean. Therefore, to meet the same fatigue criteria, the MOD-2 allowable would have to be reduced as shown in Figure 7 and spectrum testing would be required to establish the allowable since stress levels exceed the crack propagation threshold. Also noted in Figure 7 is the weight reduction available in an upwind rotor blade at this station based on the loads derived with this specified tower shadow and fatigue criteria.

CONCLUSIONS

The following conclusions were drawn from this study:

1. No direct linear relationship between alternating load and life.

2. Damage varies as the cube of alternating stress while it varies as maximum stress to the first power.

3. Damage will vary linearly with coning (max stress effect only).

4. Upwind rotor can produce dramatic reduction in damage depending on tower configuration.

5. Spectrum type fatigue test mandatory to establish allowables.

6. Fracture mechanics theory is to be an integral part of the fatigue test program to minimize number of specimens tested and to correlate with existing data.

DISCUSSION

Q. Why do you conclude that alternating loads have no direct effect on life?

A. Direct means linear and damage varies as the cube of the alternating loads.

Q. Have you looked at stresses at blade radii other than .385 radius?

A. Yes. The full radial stress distribution has been examined and this is one of the critical stations selected for this presentation.

Q. Is the repeated loads design going to be carried out primarily by the fracture-mechanics methodology now being used for USAF aircraft?

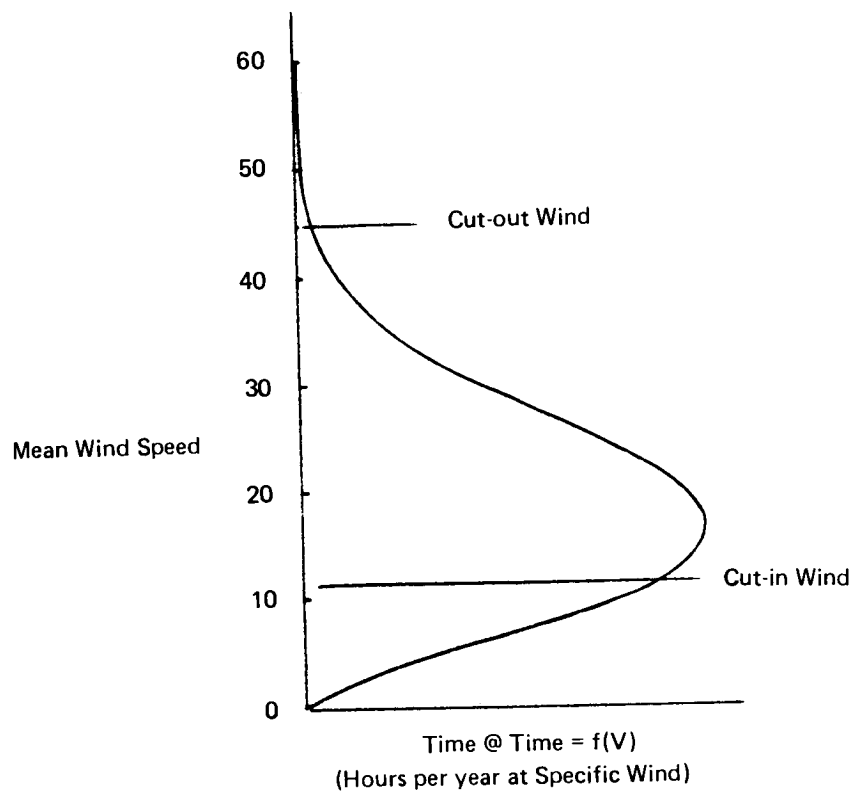A. Yes, as this is our standard practice at The Boeing Company.

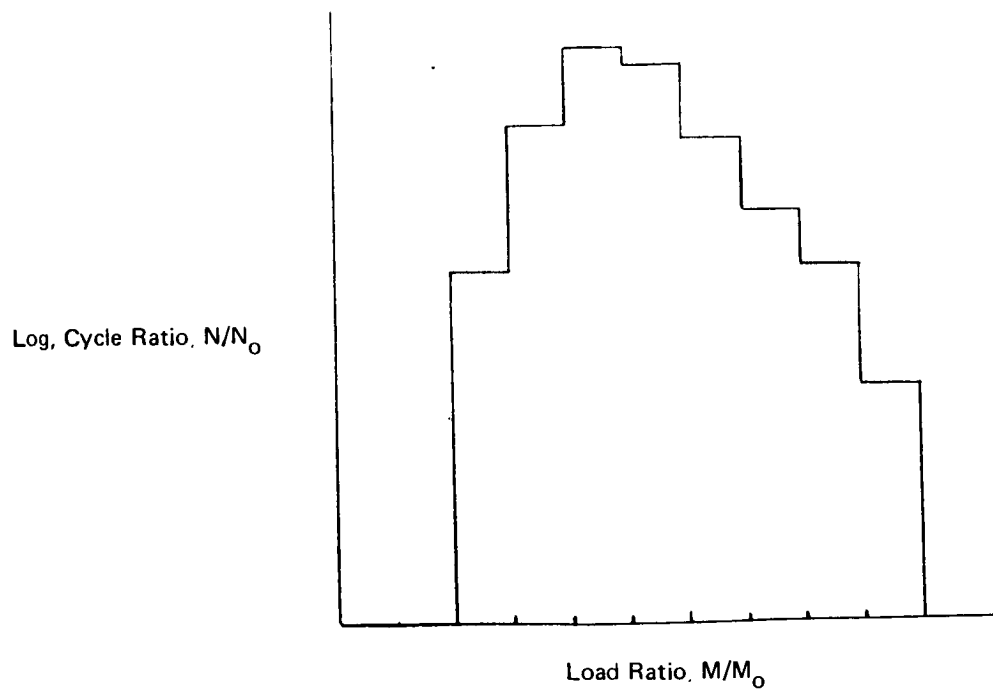Figure 1. - Wind spectrum - upwind and downwind rotor.
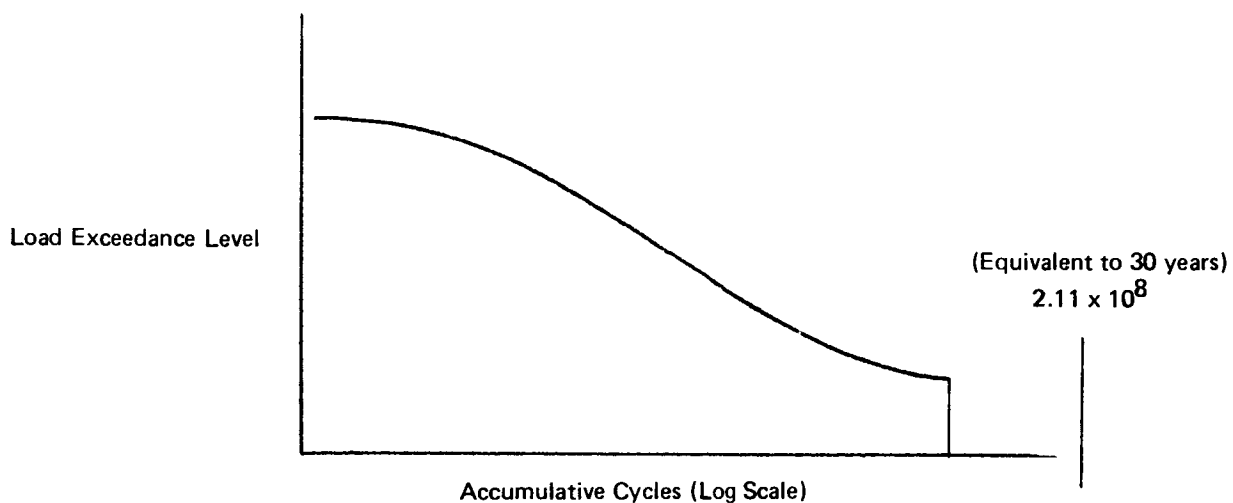

Figure 2. - Gust spectrum.

Figure 3. - Load spectrum for given wind speed.

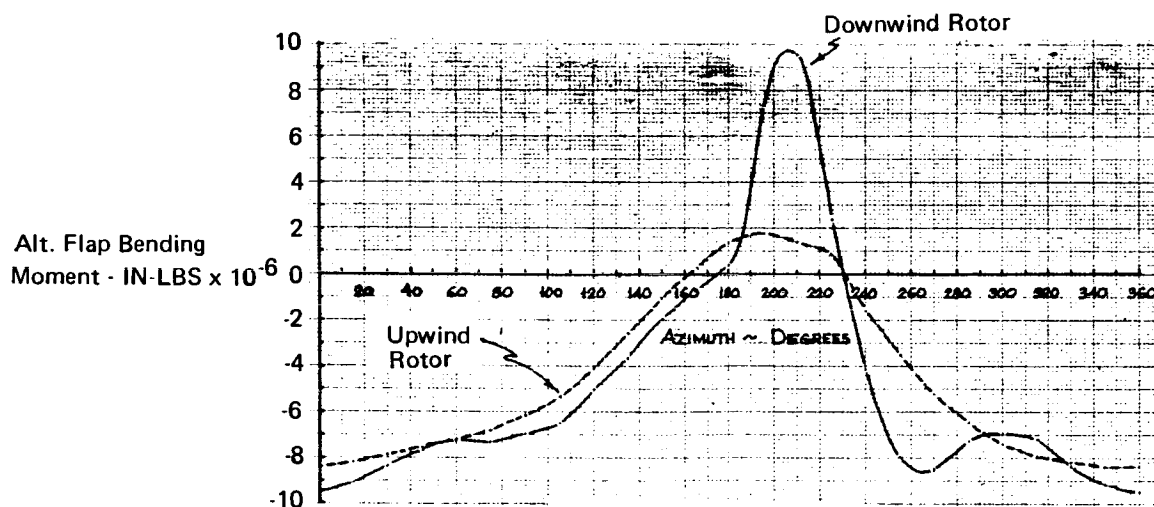Figure 4. - Alt. flap bending moment at 52 mph
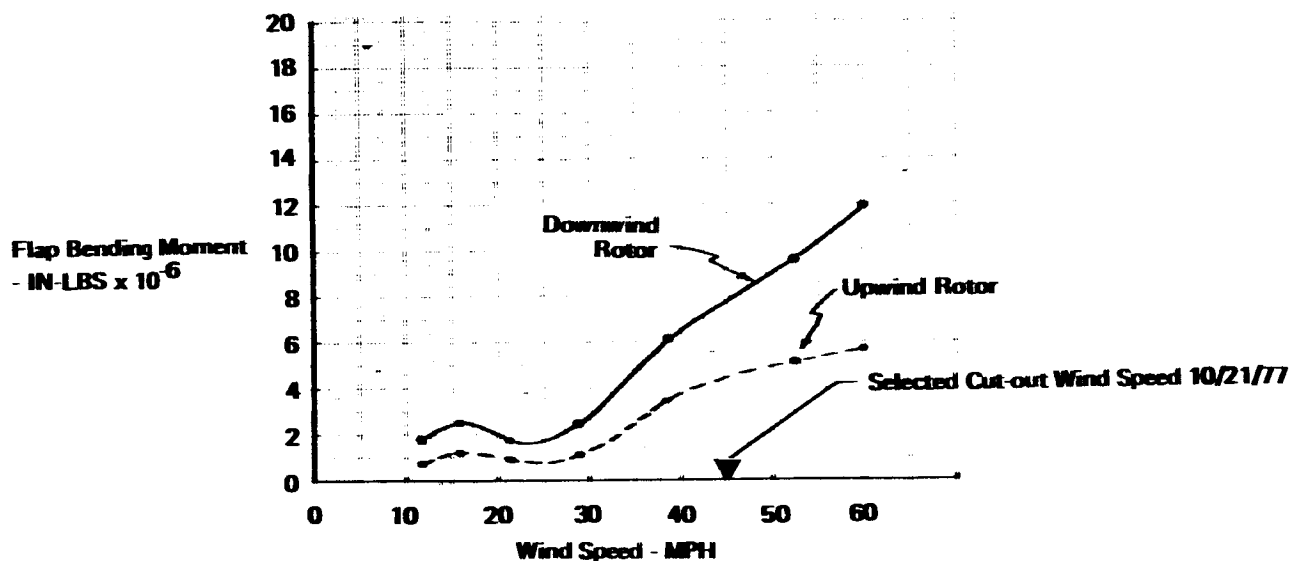and blade station r/R of 0.385.

223

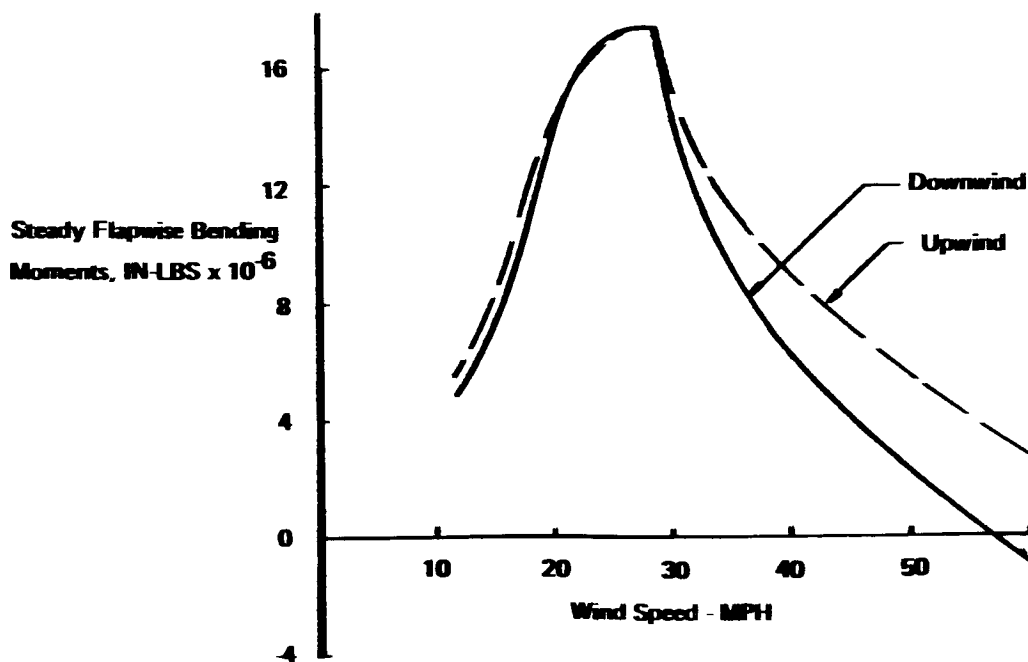Figure 5. - Flap bending moment at blade station r/R of 0.385.

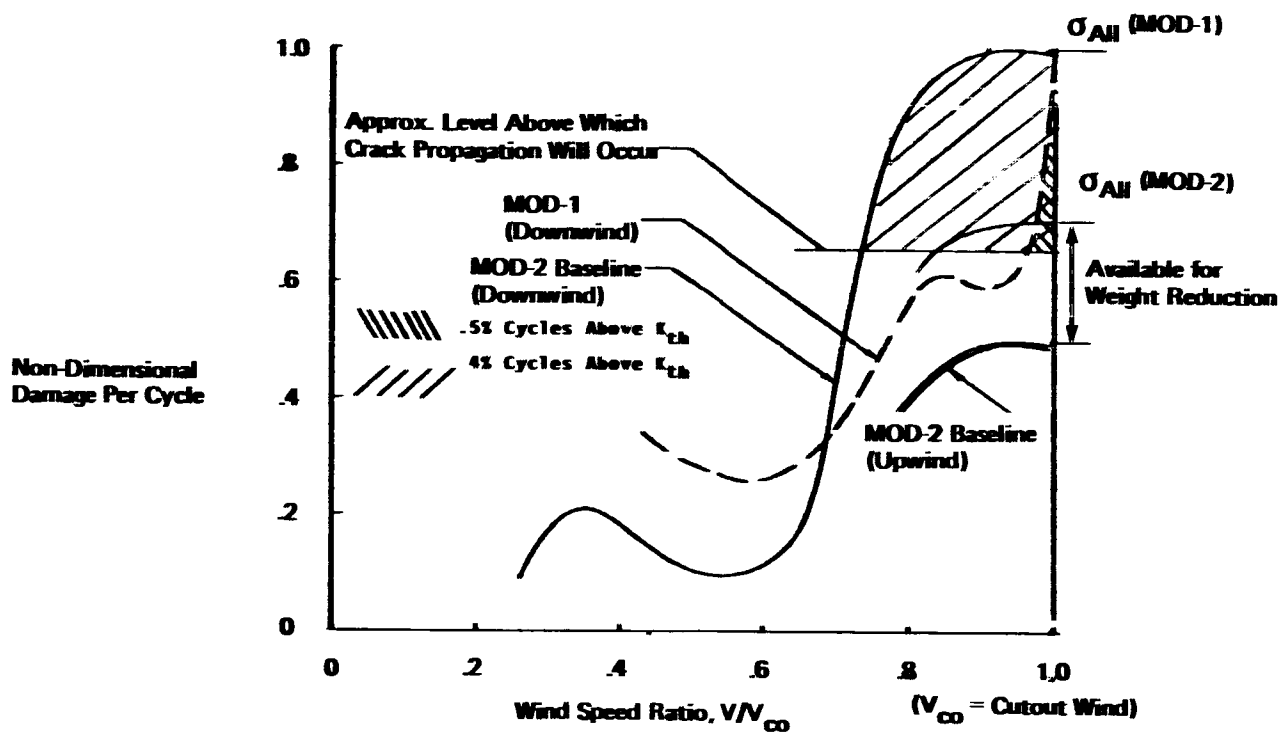Figure 6. - Steady flapwise bending moments at blade station r/R of 0.385 - upwind and downwind conditions.

224

Figure 7. – Effect of wind direction on fatigue

damage – damage cycle $\propto (\Delta\sigma)^3 \left(\frac{\Delta\sigma}{2} + \sigma_m\right)$.

EFFECTS OF ROTOR LOCATION, CONING, AND TILT ON CRITICAL

LOADS IN LARGE WIND TURBINES

D. A. Spera and D. C. Janetzke

National Aeronautics and Space Administration
Lewis Research Center
Cleveland, Ohio 44135

ABSTRACT

Three large (1500 kW) horizontal rotor configurations were analyzed to determine the effects on dynamic loads of upwind and downwind rotor locations, coned and radial blade positions, and tilted and horizontal rotor axis positions. Loads were calculated for a range of wind velocities at three locations in the structure: the blade shank, the hub shaft, and the yaw drive. Blade axis coning and rotor axis tilt were found to have minor effects on loads. However, locating the rotor upwind of the tower significantly reduced loads at all locations analyzed. Details of this study are presented in Reference 1.

INTRODUCTION

Many different rotor configurations have been proposed for large, horizontal-axis wind turbines, and several have been tested for varying periods of time. Generally, these configurations can be classified according to the following six factors:

1. Rotor location with respect to the tower -- upwind/downwind
2. Rotor axis inclination -- level/tilted
3. Blade axis inclination -- coned/radial
4. Number of blades -- two/three or more
5. Blade root attachment -- cantilevered/hinged
6. Blade pitch angle -- variable/fixed

No consensus now exists as to the rotor configuration preferred for generating electricity at low cost with high reliability. A systematic evaluation of all rotor configuration factors is required before such a consensus becomes possible.

The purpose of this study is to evaluate the effect on critical wind turbine loads of the first three factors listed above: rotor location, rotor axis inclination, and blade axis inclination. The remaining factors were fixed as follows: two blades, cantilevered root attachments, and variable pitch angles. An earlier study of this type (Ref. 1) investigated the effects which hinged and cantilevered blade root attachments could have on rotor loads. These studies are based on the assumption that factors which reduce critical loads can also reduce plant costs and increase reliability. In this study as in Reference 2, dynamic blade loads were calculated using the MOSTAB-WT computer

code. The accuracy of the load analysis methods used in this study has been verified using actual wind turbine test data (Ref. 3).

ROTOR CONFIGURATIONS ANALYZED

Rotor A in Figure 1 is the baseline configuration to which the other rotors are compared. In Rotor B, blade coning is removed, the blade axes are radial, and the rotor axis is tilted 12° to provide the same tower clearance as Rotor A. The downwind location of the rotor is maintained for Rotor B. Rotor C is the same as Rotor B except that its location is upwind of the tower. In this study critical loads were calculated at the following three locations which are shown in Figure 1: The blade shank, the hub shaft, and the yaw drive.

BLADE SHANK LOADS

The effect of rotor configuration on flatwise moments in the blade shank region is shown in Figure 2. In this figure the cyclic component of flatwise moment is plotted versus the steady component, for various wind speeds. Looking first at the results for Rotor A (the baseline configuration), it can be seen that a significant steady bending moment is present at all wind speeds. Large cyclic and large steady load occur simultaneously at cut-out wind speed in Rotor A.

Turning now to Rotor B, the absence of coning causes the steady moment load to change sign. Cyclic moments are almost unchanged compared to Rotor A because the rotor is still downwind of the tower. Small increases in cyclic aerodynamic load caused by tilting the rotor are offset by decreases in cyclic gravity load obtained by removing coning. In Rotor B, large cyclic moments at cut-out occur simultaneously with small steady moments, unlike Rotor A. Thus, while flatwise moments in Rotor A reach a maximum of 1,740,000 lb-ft at cut-out (cyclic plus steady), the maximum moment in Rotor B is only 816,000 lb-ft at the same wind speed.

For Rotor C, steady loads are approximately the same as for Rotor B, because both have radial blades. However, cyclic flatwise moments are significantly lower in Rotor C bacause of the minimal shadow effect upwind of the tower.

To further simplify the load comparison, the steady moment load can be eliminated by assuming a "constant fatigue life" line as shown in Figure 2. The slope of this line is taken as 0.2. At the cut-out wind speed the equivalent cyclic flatwise moments for Rotors A, B, and C are $\pm$ 850,000, $\pm$ 670,000, and $\pm$ 460,000 pound-feet, respectively. Therefore, changes in rotor configuration can significantly lower flatwise cyclic blade loads.

Table I shows estimates of the edgewise bending moments in the blade shanks for the three rotors studied. Most of the load reduction in Rotors B and C results from the assumed reductions in blade weight. In general, Rotor B edgewise moments were not significantly lower than those in Rotor A, whereas Rotor C moments were reduced 20 to 27 percent.

HUB SHAFT AND YAW DRIVE

Hub shaft bending loads are largest about an axis perpendicular to the rotor and blade axes. Moments about this axis are the sum of the flatwise bending moments at the roots of both blades. Figure 3 shows cycles of hub bending moments $M_{y,h}$ calculated for the three rotor configurations at the cut-out wind speed of 52 mph. The moments for downwind rotors, A and B, exhibit sharp peaks at blade azimuths of 40 and 220 degrees. This is a result of the tower shadow response of each blade. These sharp peaks are absent in the upwind rotor, C. Cyclic moments for Rotors A, B, and C are ± 1,420,000, ± 1,297,000, and ± 805,000 lb-ft, respectively. This, removing coning and tilting the downwind rotors has little effect on hub shaft bending. However, location of the rotor upwind reduces the hub shaft bending loads by 40%.

Figure 4 illustrates the variability which can be present in the torque output of rotors in large wind turbines. The shaft torques produced by Rotors A and B show characteristic troughs which occur each time a blade enters the tower's shadow and loses aerodynamic lift. This produces cyclic torques of ± 114,000 and ± 125,000 lb-ft for Rotors A and B, respectively, at a wind speed of 52 mph. Rotor C produces a much smoother torque, verying only ± 28,800 lb-ft, which is less than ± 10% of the shaft working torque.

Yaw drive torques for the three rotor configurations are shown in Figure 5 for a wind speed of 52 mph. Rotors A and B exhibit similar maximum torques, which are 811,000 and 717,000 lb-ft, respectively. The torque for Rotor C is reduced considerably below these values, to a maximum absolute value of 420,000 lb-ft.

SUMMARY OF RESULTS

A summary of the results of this study is given in Table II. Loads for Rotor B do not differ significantly from those for Rotor A except in flatwise bending in the blade shank. The maximum flatwise bending load which occurs in Rotor B at a wind speed of 29 mph is almost 30 percent less than the maximum for Rotor A which occurs at a wind speed of 52 mph. This indicates that the 12° cone angle in Rotor A is excessive, since it increases rather than decreases the maximum flatwise moment present in Rotor B with radial (unconed) blades.

The cyclic flatwise moment in Rotor B is approximately 20% less than than for Rotor A. This is primarily the result of adjusting the actual cyclic moments to account for steady moments. The actual cyclic moments are approximately equal for the two rotors.

As shown in Table II, all loads in Rotor C were significantly less than equivalent loads in Rotor A. This can be attributed primarily to the upwind rotor location for Rotor C. Blade shank bending loads were reduced by 25 to almost 50 percent. Hub shaft bending moments were reduced almost 40 percent. Of particular importance is the reduction in cyclic hub torque. Cyclic torques in Rotor C were only one-fourth those in Rotor A at a wind speed of 52 mph. Moreover, at the rated wind speed of 29 mph this ratio was only one-eighth. Yaw drive torques for Rotor C were 30% to 40% less than those for Rotor A.

CONCLUSIONS

1. Coning and tilt have little effect on critical loads in either the blades, the hub, or the yaw drive, provided the angles are not excessive.

2. Coning of blades to reduce loads is unnecessary, though coning might be used to provide tower clearance for a downwind rotor.

3. Rotor location (upwind or downwind of the tower) has a significant effect on blade, hub, and yaw drive loads for rotors with cantilever blade attachments.

4. Locating the rotor upwind of the tower can reduce cyclic shaft torques by 75% to 90% and other critical moment loads by 25% to almost 50%, compared with a downwind rotor location. Thus, an upwind rotor location is potentially very advantageous in terms of both reliability and cost.

REFERENCES

1. Spera, D. A., and Janetzke, D. C.: Effects of Rotor Locating, Coning, and Tilt on Critical Loads in Large Wind Turbines. Wind Technology Journal, Vol. 1, No. 2, 1977, pp. 5-10.

2. Spera, D. A.: Structural Analysis of Wind Turbine Rotors for NSF-NASA Mod-0 Wind Power System. NASA TM X-3198, 1975.

3. Spera, D. A.; Janetzke, D. C.; and Richards, T. R.: Dynamic Blade Loading in the ERDA-NASA 100 kW and 200 kW Wind Turbines. Presented at American Wind Energy Spring Conference, 1977. (To be published.)

DISCUSSION

Q. What confidence do you place in these results, considering the fact that they were obtained with MOSTAB-WT which has only one degree of freedom?

A. We consider MOSTAB-WT and -WTE to be excellent tools for "back-to-back" comparisons in which parameters are varied but the general system remains constant. This is the case here.

Q. Have you looked at blade loads near eight-tenths span?

A. Yes. Loads outboard follow the same trend as the shank loads reported here.

Q. Was a spring constant used in your calculations to represent the drive train?

A. No. MOSTAB-WT enforces a constant shaft speed, which is equivalent to a drive train with infinite impedance.

Q. Was a tower shadow effect used for the upwind rotor?

A. Yes. A truss tower was assumed in which the upwind shadow was 10% of the downwind shadow.

Q. If you could take out the first harmonic of the tower shadow effect, how would the upwind versus downwind comparison look?

A. The load most directly affected would be cyclic flatwise bending of the blades. The difference in this load between the upwind and the downwind configurations would be reduced about 50%.

TABLE I. - ESTIMATES OF EDGEWISE BENDING LOADS IN BLADE SHANKS

[Nominal wind speed, 52 mph; power, 1500 kW.]

Rotor	Blade Weight, lb	Shank edgewise moment, $M_{z,b}$, lb-ft				
		Cyclic, $\delta M_{z,b}$			Steady, $\overline{M}_{z,b}$	Max
		Gravity	Coupled[a]	Total		
A	12,000	260,000	158,000	418,000	175,000	593,000
B	10,700	232,000	156,000	388,000	175,000	563,000
C	9,300	201,000	96,000	297,000	175,000	472,000

(a) 25% of cyclic flatwise moment

TABLE II. - RATIO OF MOMENT LOADS IN ROTORS B AND C TO LOADS IN ROTOR A

[Nominal wind speed, 52 mph; power, 1500 kW.]

Moment Load, M		M_B/M_A		M_C/M_A	
		Max	Cyclic[a]	Max	Cyclic[a]
Blade shank bending	Flatwise	0.73[b]	0.79	0.75[b]	0.54
	Edgewise	0.95	0.93	0.80	0.73
Hub shaft	Bending	0.91	0.91	0.57	0.57
	Torque	1.14	1.10	0.97	0.25[c]
Yaw drive torque		1.13	1.00	0.58	0.71

(a) Adjusted to zero steady load, except hub torque

(b) Max at V_0 = mph for rotors B and C
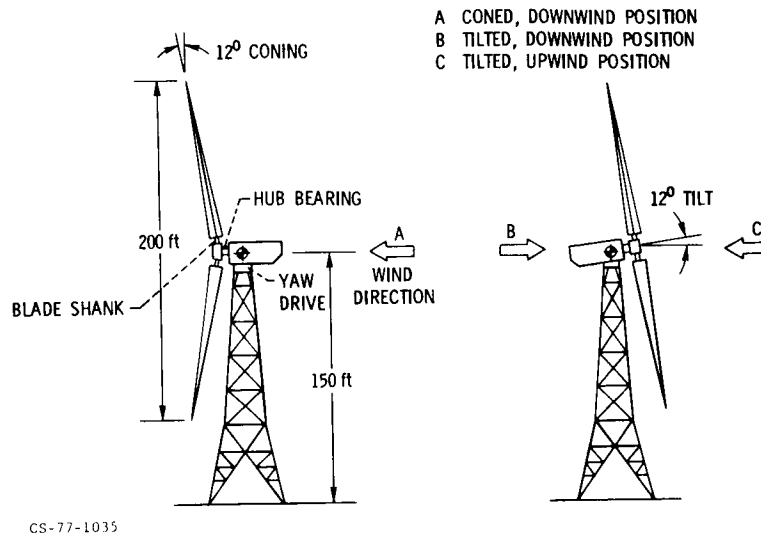
(c) 0.12 for V_0 = 29 mph

Figure 1. - Rotor configurations analyzed, which
are designed to produce 1500 kW at a nominal
wind speed of 29 mph.

Figure 2. - Calculated variation of flatwise
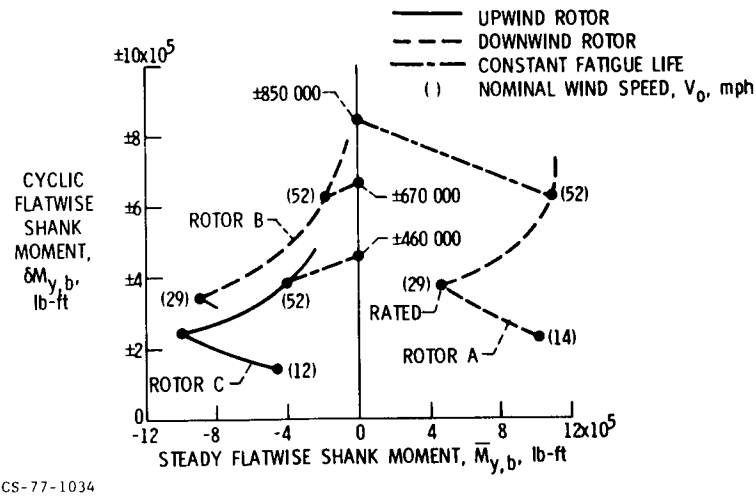blade shank loads with wind speed and
rotor configuration (blades pitched for
rated power, V_o > 29 mph).

234
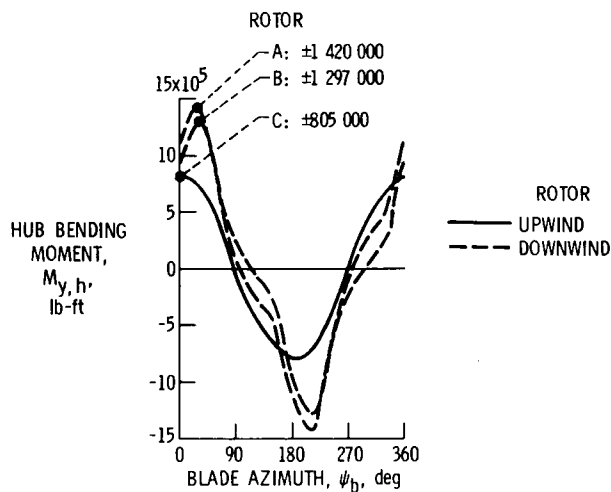
Figure 3. - Calculated variation of hub
bending moment with blade azimuth and
rotor configuration (wind speed,
52 mph; power, 1500 kW).
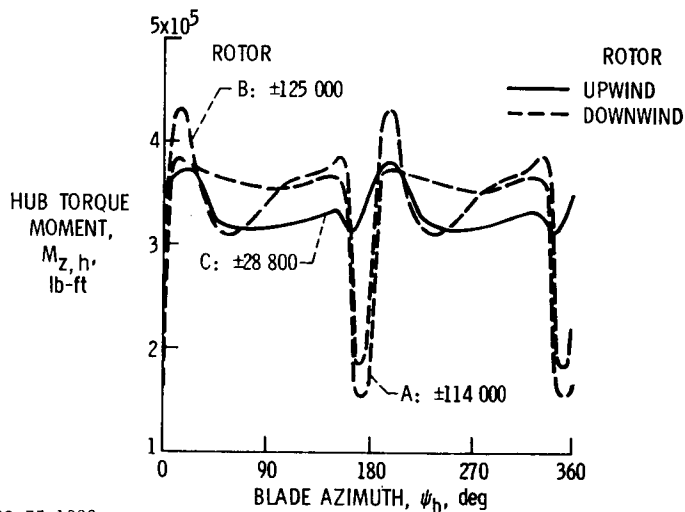
Figure 4. - Calculated variation of hub
torque with blade azimuth and rotor
configuration (wind speed, 52 mph;
power, 1500 kW).

235

Figure 5. - Calculated variation of yaw
drive torque with blade azimuth and
rotor configuration (wind speed,
52 mph; power, 1500 kW).

COMPARISON OF BLADE LOADS OF FIXED

AND FREE YAWING WIND TURBINES

Marvin C. Cheney and Richard L. Bielawa

United Technologies Research Center
East Hartford, CT 06108

ABSTRACT

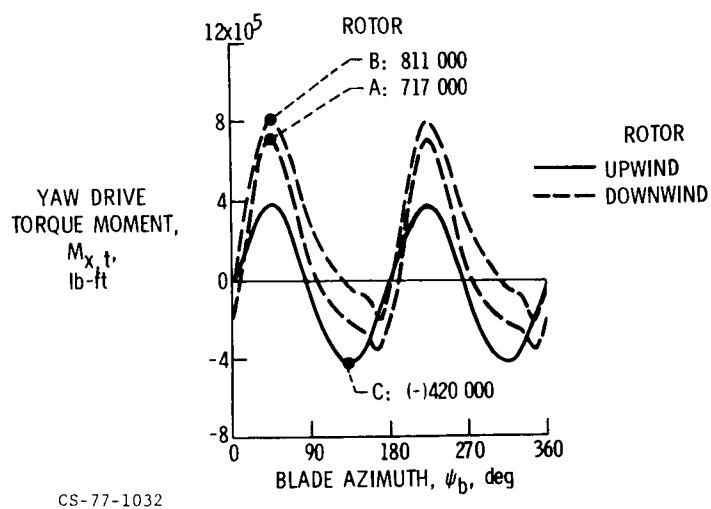The UTRC Self Regulating Composite Bearingless Wind Turbine utilizes an automatic pitch control concept and a completely unrestrained yawing degree of freedom. Aerodynamic moments caused by skewed flow provide the control to align the wind turbine with the wind. Model tests have demonstrated the feasibility of the concept and analytical studies have shown the free system to experience lower blade loads compared to the fixed system.

INTRODUCTION

Many of the early windmills were free in yaw and were controlled through an aerodynamic vane or "rudder". These rudders not only directed the rotor into the wind but also served to shut the system down when they were positioned in the same plane as the rotor. The concept was simple and it worked. Modern wind turbines, many times more efficient than their ancestors, have often been designed to be fixed in yaw and mechanically controlled when realignment is required. The purpose of this paper is to make a brief comparison of the blade loads in free and fixed modes of operation for the wind turbine developed by the United Technologies Research Center (UTRC). This wind energy system has been developed under two ERDA contracts, Refs. 1 and 2, and will continue under a recently awarded contract from Rockwell International.

Analytical Results

The moments experienced by a wind turbine, in addition to those related to gravity, are primarily aerodynamic and gyroscopic. Ignoring the effects of wind shear and coning, aerodynamic moments can only originate from nonaxial wind velocities. Under such conditions there exist advancing and retreating blades which produce different lifts resulting in a steady rotor moment. Figure 1 is a schematic of a wind turbine showing the moments experienced when the wind velocity is skewed by an angle, ψ, and the turbine is yawing at a rate, $\dot{\phi}$. Using the right hand rule, the moments are depicted by the vectors M_A and M_G, where the subscripts denote aerodynamic and gyroscopic. When a yaw rate is imposed by an external agent, such as a yaw motor, it

produces the following gyroscopic moment:

$$M_G = I\Omega\dot{\phi}$$

where I is the moment of inertia of the rotor and Ω is the rotational speed. The aerodynamic moment can be approximated by the following equation:

$$M_A = KV_w^2 \sin\psi$$

where K is a constant containing blade area, radius, and air density. The total rotor moment is then:

$$M_R = M_G - M_A = I\Omega\dot{\phi} - KV_w^2 \sin\psi$$

Under conditions when V_w is small and the system is being mechanically yawed, the moment reduces to:

$$M_R = I\Omega\dot{\phi}$$

For the free system, the initial rotor moment resulting from the skewed flow is only the aerodynamic moment.

$$M_{R_0} = M_A$$

The system responds to this moment and yaws at a rate proportional to this moment,

$$\dot{\phi} = \frac{M_A}{I\Omega} \text{ or } M_A = I\Omega\dot{\phi}$$

however the gyroscopic moment produced by this yaw rate is, as before:

$$M_G = I\Omega\dot{\phi}$$

Thus, $$M_R = M_G - M_A = 0$$

The resulting rotor moment is therefore always eliminated under steady yawing conditions for the free yawing system. The system requiring imposed yaw would always experience moments except at the one time during the maneuver when the gyroscopic moment equals the aerodynamic moment.

The UTRC F762 computer program was used to compare blade stresses under various yaw conditions at a wind speed of 22 mph. The F762 program is a multiblade, movable hub aeroelastic analysis which models general wind turbine configurations and in particular the UTRC wind turbine concept. Three conditions were investigated at a wind speed of 22 mph with an initial wind direction of 30 deg off axis. The cases were: a fixed system without a yaw degree of freedom, a free yaw system, and finally the case where a prescribed yaw rate is imposed externally. The results of these computer runs are

238

presented in Figs. 2 to 4. Figures 2 and 3 show the flatwise and edgewise stresses for the fixed and free yawing systems. The stresses are shown to be generally lower by a factor of 1/2 for the free system. The vibratory stresses in the free yaw case would eventually go to zero as the system aligns with the wind. This would occur in this case in approximately 5 seconds.

The stress characteristics for the condition where a prescribed yaw rate is imposed on the rotor are shown in Fig. 4. The large 1P stress is attributed primarily to the gyroscopic moment which exists as long as the yaw rate is maintained.

Experimental Results

Tests conducted under an ERDA contract, Ref. 1, included conditions where a model wind turbine was allowed to yaw freely under the influence of a skewed wind velocity. The model had blades with relatively low flatwise stiffness in comparison to other blades, such as the Mod 0 blades. Sample results of these experiments are shown in Fig. 5 where the yaw angle and blade stress time histories are presented following the release of a wind tunnel model from a preset angle of -30 deg. Initial vibratory stresses are high due to the aerodynamic moment created by the skewed flow, however the stresses are quickly reduced as the rotor responds. The final yaw angle and resulting stresses are due to the tower shadow.

CONCLUSIONS

1. A free yawing wind turbine does not generate large unbalanced gyroscopic and/or aerodynamic moments as compared to a wind turbine fixed in yaw or having a fixed yaw rate.

2. A free yawing wind turbine having relatively low flatwise stiffness blades inherently adjusts to wind direction changes.

REFERENCES

1. Cheney, M. C. and P. A. M. Spierings: Self Regulating Composite Bearingless Wind Turbine. ERDA Report COO/2614-76/1, Sept. 1976.

2. Spierings, P. A. M. and M. C. Cheney: Design of a Self-Regulating Composite Bearingless Wind Turbine. ERDA Report COO/4150-77/8, August 1977 (to be published).

Q. How would a free-yaw system respond to a wind direction changing ± 20
degrees, as has been observed at Plum Brook?

A. A free yawing system will continue to try to correct for wind direction
changes, however the rate of correction is inversely proportional to
the rotor inertia and rotational speed which would result in a lag.
If the wind direction is continuously changing from + 20 deg to - 20 deg
then the turbine would oscillate at some lower angle however I wouldn't
expect the power output to be very much affected.

Q. In the rotor start up mode, when the nacelle was at large yaw angle
did you notice any instabilities such as those mentioned by K. Hohenemser
- i.e. any tendency to yaw toward the upwind direction?

A. We noticed no such instability when starting from zero rpm at any
yaw angle. We did see a tendency for the 4-bladed fixed pitch system to
oscillate about a yaw angle of about 45 deg if the turbine was manually
positioned at that angle while rotating. However, recent tests with a
2-bladed rotor, using the UTRC pendulum control concept, showed no
tendency for the rotor to experience this type of yaw instability.

Q. Since your wind tunnel model was operated at nearly zero torque (i.e.
freewheeling) your induced velocity profile may not be representative of
a loaded wind generator (i.e. way down into windmill brake). Do you
have plans to extract power and to assess the effect of α distribution
when loaded?

A. Our model was not operated at zero torque at all conditions. We extracted
power for a limited number of runs but the purpose of the test was to
explore the dynamic characteristics of the pendulum control system and
this could be done most cost effectively by eliminating the power aspect.
Also, friction losses were relatively high since the alternator was ex-
cessively large for this size model.

Induced velocity is not directly dependent on power extraction. The
induced velocity is only a function of the circulation of the bound vor-
ticity on the blade and the shed vorticity in the wake. The vorticity
in turn is a function of the blade geometry, tip speed, airfoil
characteristics, and wind speed.

We are not planning additional model tests for the purpose of measuring
performance, however our performance analysis which we use to predict
power characteristics simulates the vorticity and the resulting induced
velocity to a high degree of accuracy under all loading conditions.
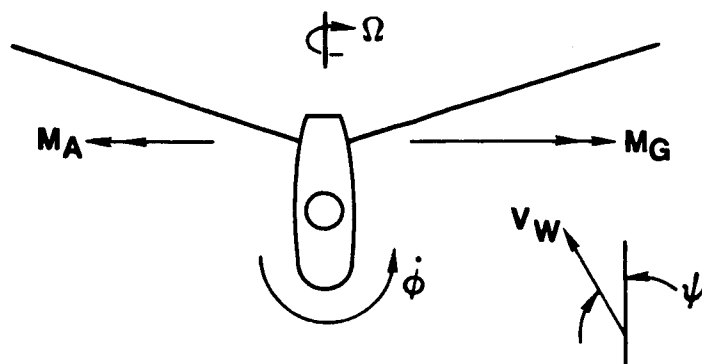
Figure 1. - Schematic of wind turbine yaw moments.

$V_W = 22$ mph, $\Omega R = 300$ fps

R = 20 ft $\bar{r} = 0.05$

$\psi_o = 30$ deg
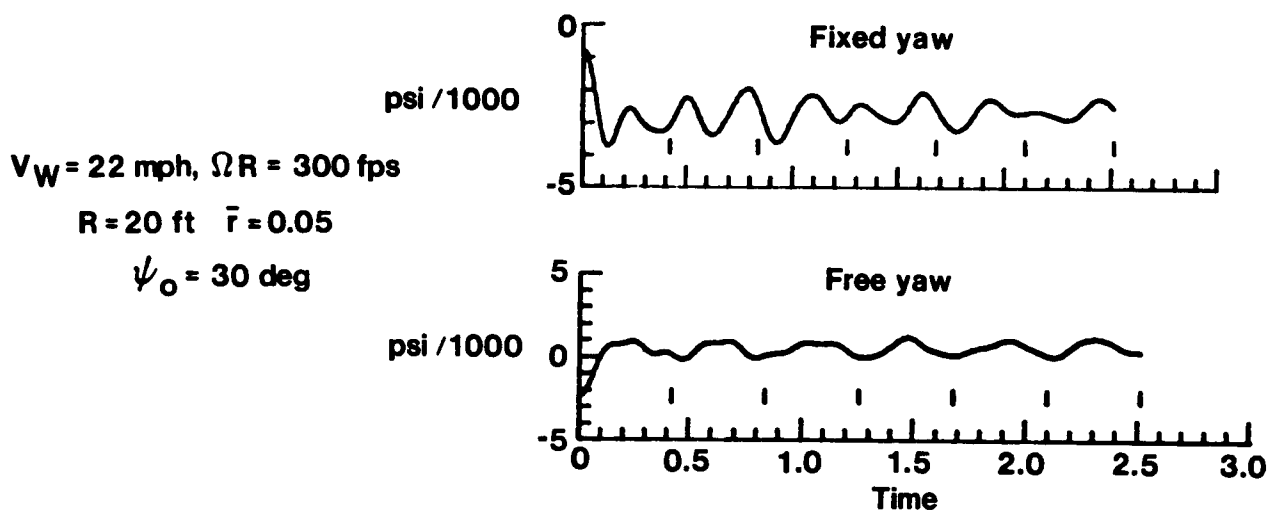
Figure 2. - Blade flatwise stress comparison.

$V_W = 22$ mph, $\Omega R = 300$ fps

R = 20 ft $\bar{r} = 0.05$

$\psi_o = 30$ deg
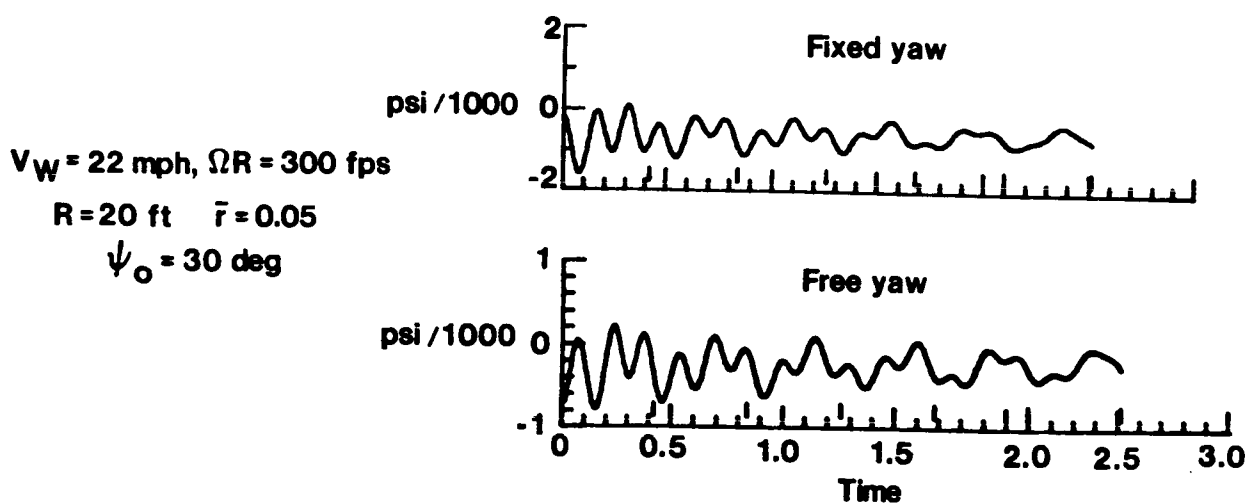
Figure 3. - Blade edgewise stress comparison.

241

V_W = 22 mph ΩR = 300 fps

R = 20 ft $\bar{r}$ = 0.05

$\dot{\phi}$ = 6 deg / sec.

Flatwise stress

Psi / 1000

Edgewise stress

Time
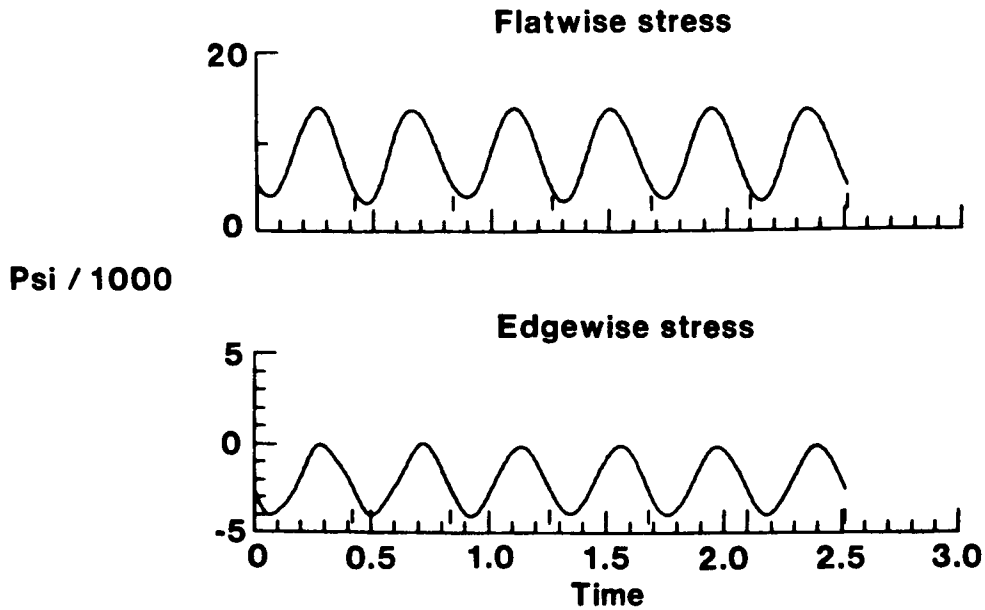
Figure 4. - Stress characteristics for imposed
yaw rate.

V_{wind} = 20 mph ΩR = 282 fps

Yaw, deg

Release

Time, sec

1/2 peak-to-peak stress, 1,000 psi

Flatwise

Edgewise

Time, sec

Figure 5. - Model experimental results.

242

FIXED PITCH WIND TURBINES

David B. Fenn and Larry A. Viterna

National Aeronautics and Space Administration
Lewis Research Center
Cleveland, Ohio 44135

ABSTRACT

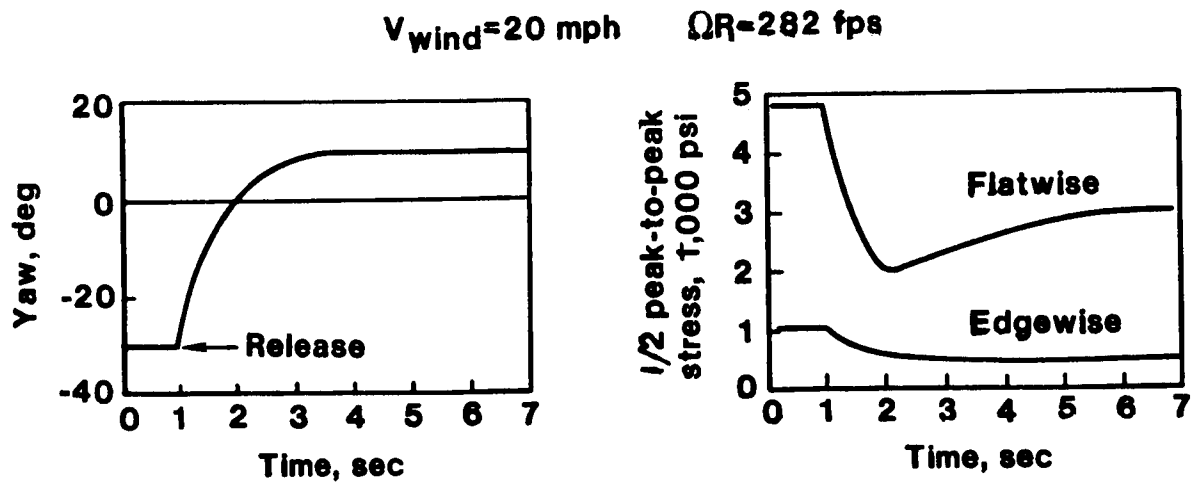Wind turbines designed for fixed pitch operation offer potential reductions in the cost of the machine by eliminating many costly components. Our studies have shown that a rotor can be designed which produces the same energy annually as Mod-0 but which regulates its power automatically by progressively stalling the blades as wind speed increases. Effects of blade twist, taper, root cut-out, and airfoil shape on performance are discussed.

Unfortunately, fixed pitch rotors are not self-starting when the pitch is set to maximize energy production per year. Various starting techniques are discussed.

INTRODUCTION

Fixed pitch wind turbines are being studied in an effort to produce machines which are less costly than the present variable pitch machines. These machines are intended for uses where load following is not required. The concept is not new. The Danes built a fixed pitch machine in the town of Gedser which operated successfully for many years. Our activity started with a study of the Gedser machine.

In principle the fixed pitch machine is relatively simple. The rotor is designed to stall progressively as the wind speed increases and thereby automatically limit the peak power. With the generator sized to accept the peak power that the rotor can produce, the machine can operate in any wind with no power control. Speed control is provided by synchronizing the generator to a large network--(just as it is in present wind turbines). Thus the fixed pitch machine appeared to have potential for lower cost; the larger generator required is inexpensive compared to the pitch change mechanisms, hydraulic systems and electronic controls required for the variable pitch machine.

It was recognized early that fixed pitch rotors would probably not be self-starting and that some special systems would be needed for synchronization. The objective of this paper is to describe our studies to date which have defined the type of blades needed for optimum performance and some alternative systems for starting and stopping the final pitch wind turbine.

OPTIMUM BLADE SHAPE

Our study of blade shapes was conducted using the computer code developed by Wilson. So far we have studied the effects of twist, airfoil section, taper,

and root cutout on performance. To achieve the same annual energy production with the smallest generator, the performance of the fixed pitch machine should approximate the characteristic of a fully pitchable wind turbine. Figure 1 is a comparison of the performance of a fixed pitch wind turbine and Mod-0 for the same annual energy production. In low winds the two are nearly alike. At 18 mph Mod-0 spills wind to hold constant power while the fixed pitch rotor increases its power output and starts to stall. At higher wind speeds more and more of the blades stall until at 35 mph no power is obtained at all.

Effect of Twist

Figure 2 is a plot of rotor power versus wind speed for three (3) rotors having different profiles. The untwisted blade appears superior because it produced a significantly lower peak power (lower installed capacity), more power in very high winds, and about the same power in low winds. In addition it is probably less costly to manufacture an untwisted blade.

Airfoil Section

Unlike a fully pitchable machine, the performance of a fixed pitch machine is dependent both upon the stall and the lift characteristic of the airfoil. The prediction of performance must be based on the best data available over the full range of angles of attack including post stall. Thick airfoils are preferable from a structural standpoint. The 23024 is the thickest 23000 series airfoil for which we have data. In figure 3 the performance of three candidate airfoils is presented. The GAW 1 and the 4424 are clearly inferior to the 23024 which produces more power in both the high and low wind regimes.

Effect of Taper

Figure 4 shows the performance of 3 blades with different taper profiles. The step tapered blade approximated the taper of the Mod-0 blade in 3 steps. It can be seen that the performance of the three blades is not very different. Thus it is possible to maintain the same airfoil section (23024 in this case) throughout the length of the blade. As the thickness varies for structural reasons the chord can be allowed to vary to maintain the same thickness to chord ratio (24%).

Effect of Root Cutout

Figure 5 shows the performance of 3 blades with different lengths of the blade root inoperative. The data show that almost no loss in power is incurred by root cutouts as high as 25%. With greater values power at the lower winds would be lost.

Performance of the Selected Blade

From the above data an untwisted, 23024, linearly tapered blade was selected for the fixed pitch machine. Its performance is compared to that of Mod-0 on figure 7. Both rotors produce the same energy annually and the peak power of the fixed pitch machine is only about 30 kW higher than Mod-0.

STARTING

Figure 7 shows the trade-off between annual power production and starting ability for a 3-bladed fixed pitch rotor. With a pitch angle of -2^0 the rotor produces 666,000 kWhr but requires 16 kW to motor start. With a pitch angle of -8^0 the rotor is self-starting but produces only 546,000 kWhr and requires a much larger generator. These data led to the conclusion that fixed pitch rotors are not self-starting.

Alternative starting systems are listed in figure 8. These systems are currently under investigation and it is too early to draw any conclusions.

Synchronous generators are best for power production but are difficult to motor and synchronize. The induction generator has a poorer power factor but good motoring torque and no synchronization problems.

It is theoretically possible to yaw the machine out of the wind to unstall the blades for starting. Once rotation starts we would yaw slowly back to the power position. The generator would be synchronized automatically when the speed reached synchronous.

A 2-position pitch system might be designed such that the outboard section of the blade is pitched for starting and then returned slowly to the power position without feedback control. Calculations show that at least 30% of the blade length would be required for the pitchable part.

Two methods of stopping the machine in the event that the load is lost are being considered: a deam-man brake and a small flap on the blade tip. Calculations show that a 3' flap is sufficient to stop a 125' diameter rotor.

CONCLUSIONS

We believe the fixed pitch rotor concept offers a potential reduction in wind turbine cost. Many costly and sometimes troublesome components can be eliminated.

There are starting problems which need to be solved and these are being investigated.

DISCUSSION

Q. Would you expect power from the grid to motor the rotor through and out of stall due to a high velocity gust?

A. That depends upon the design of the drive train: if torque can be transmitted from the generator to the rotor, the machine would motor through a period of high wind--otherwise the rotor would stop.

Q. How did not determine a start angle on the blade of only 8°?

A. We used Wilson's "prop" program to predict the speed vs. torque character-istics of a rotor with various pitch angles. Positive torque was found at all speeds with a pitch angle of 8°.

Q. What about 160 mph when stopped?

A. Actually, we design for a 120 mph wind striking the blade at 90° line. This is a onetime load which allows the stress to be 5 or 6 times greater than a fatigue stress would be. Consequently, the high wind requirement does not appear to adversly affect the design.

Q. What are the high wind (greater than cutout) and gusty air effects on blade limit loads and fatigue loads? Also what are the effects on drive system requirements to handle the cyclic drive torques?

A. So far we have only looked at operations in steady winds. The effect of gusts will be investigated later. We have not yet identified any changes in the drive train necessitated by changing from variable to fixed pitch rotors.

Q. With the loss of flatwise damping during the proposed stall operation, do you think upwind locating and guying, as with the Gedser machine, would be necessary?

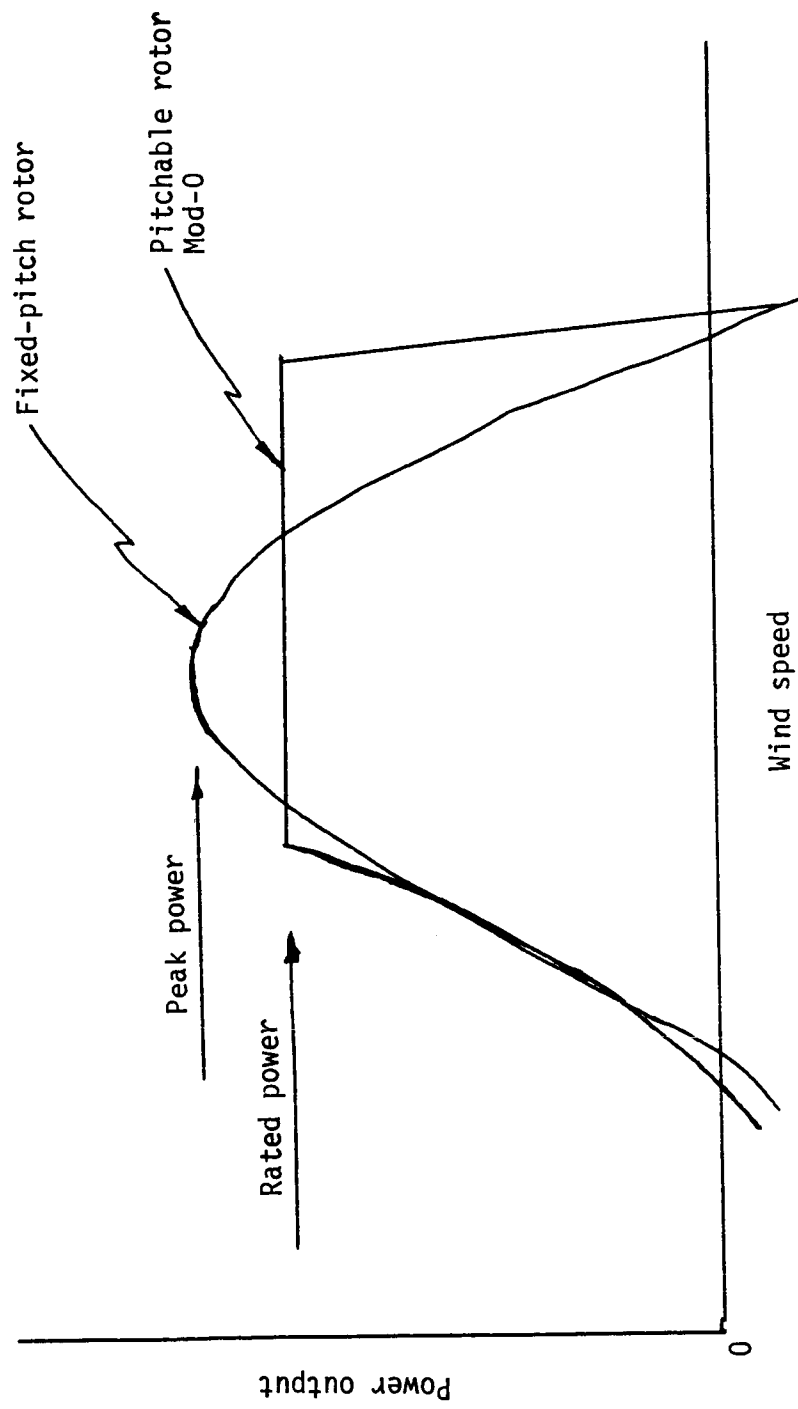A. No, but we need to and will examine stability.

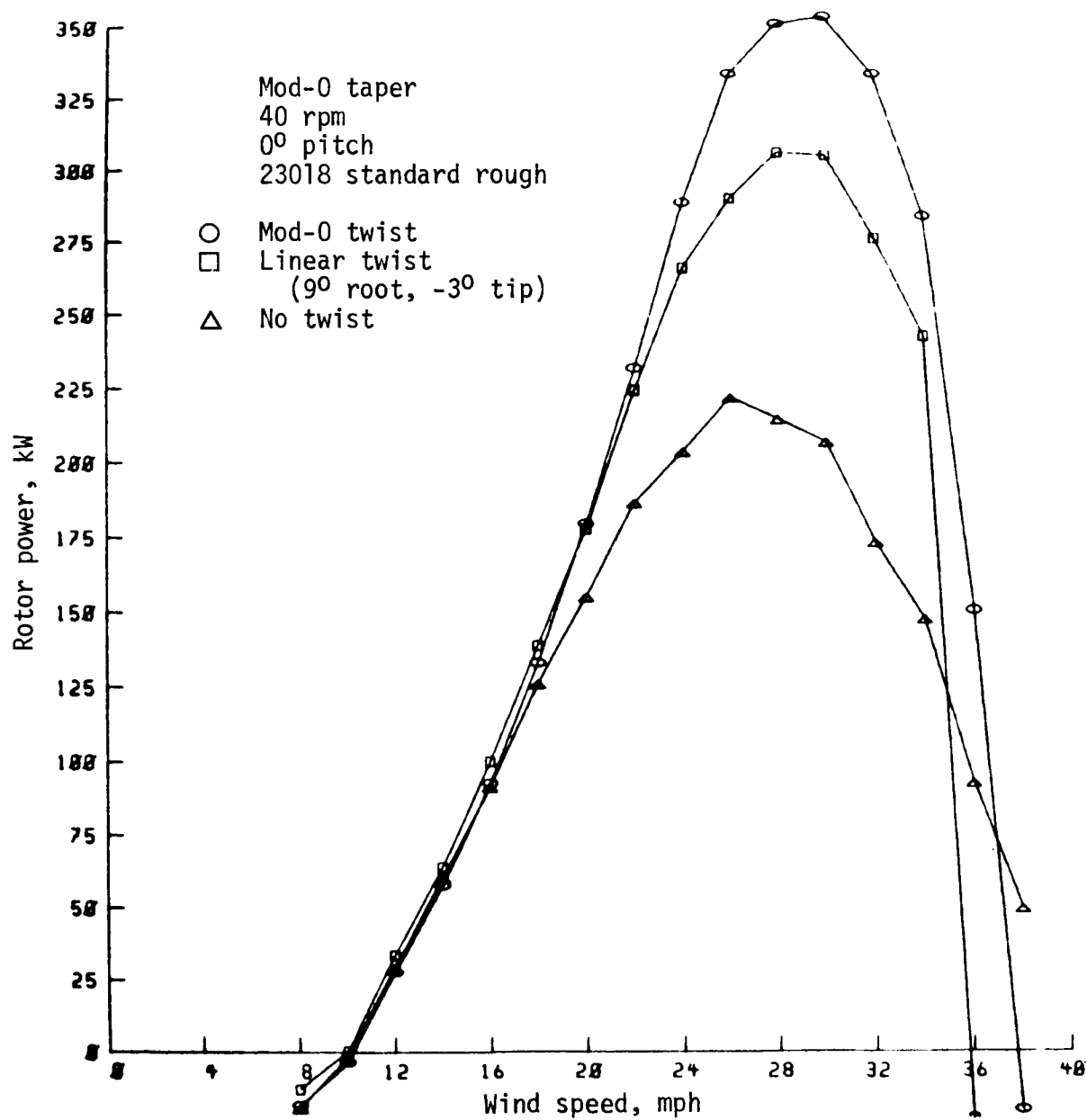Figure 1. - Fixed-pitch wind turbine performance.

Figure 2. - Effect of twist on fixed-pitch wind turbine power.
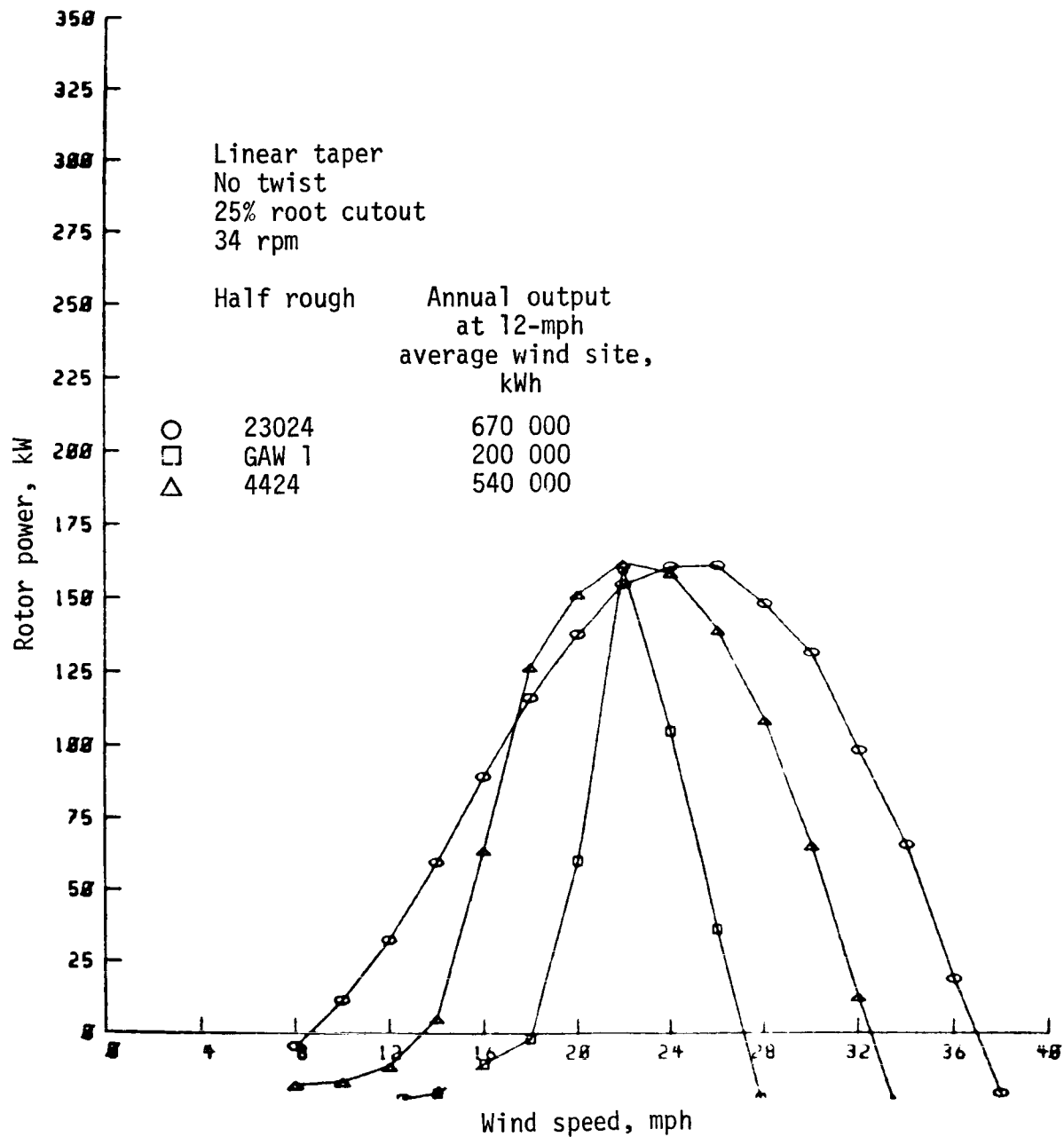
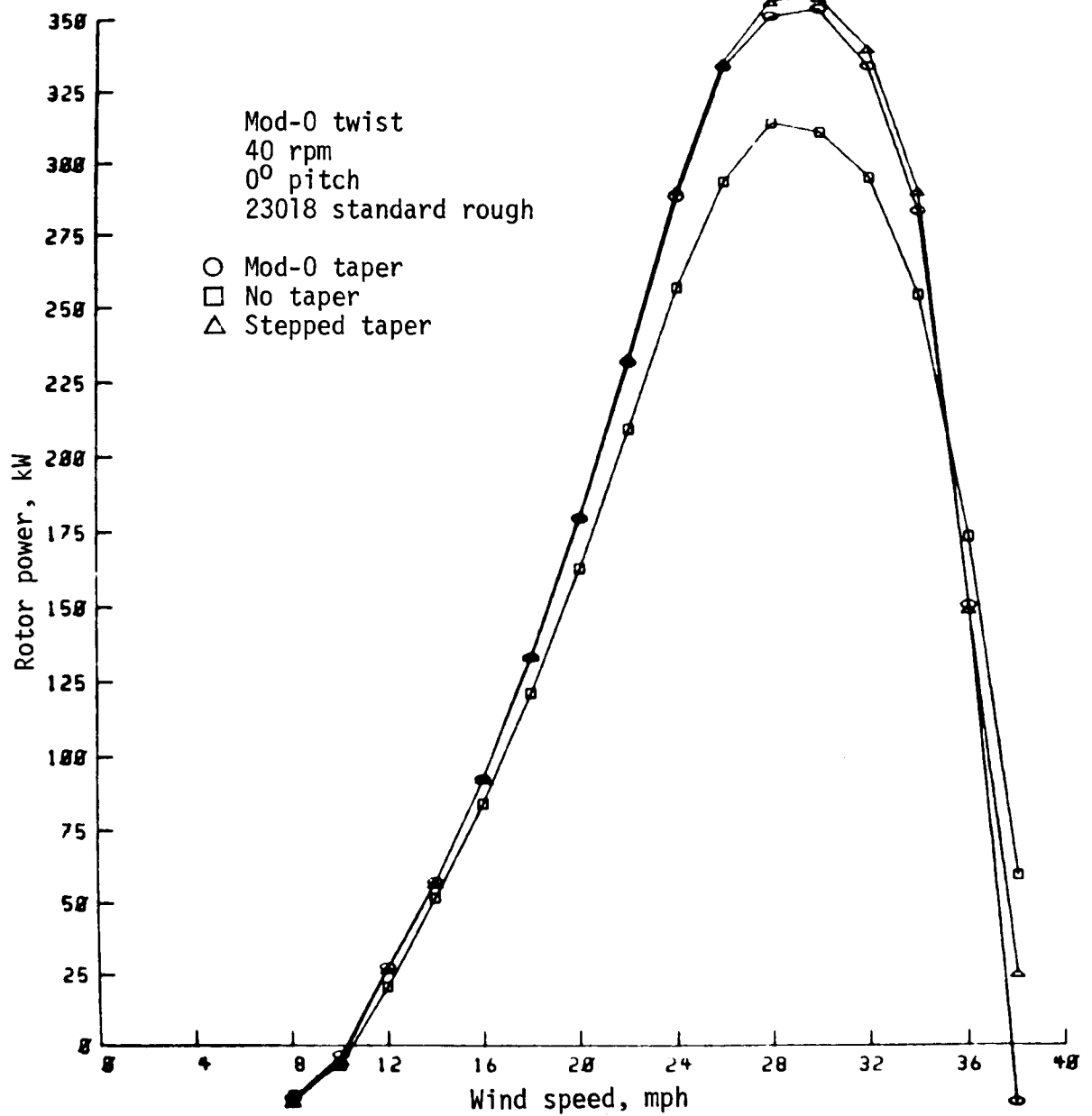Figure 3. - Various airfoils on a fixed-pitch rotor.

249

Figure 4. - Effect of taper on fixed-pitch wind turbine power.
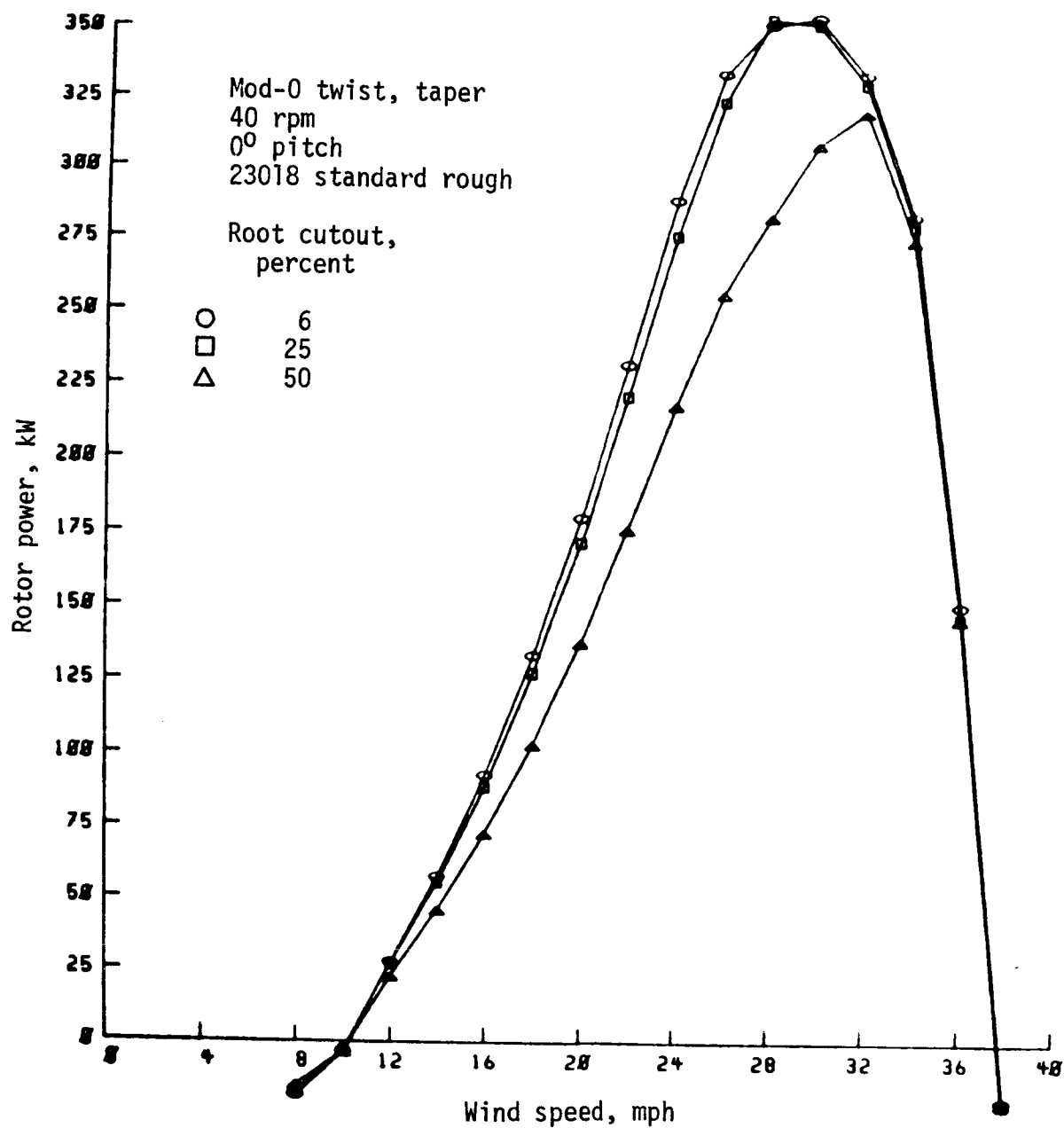
Figure 5. - Effect of root cutout on fixed-pitch wind turbine power.
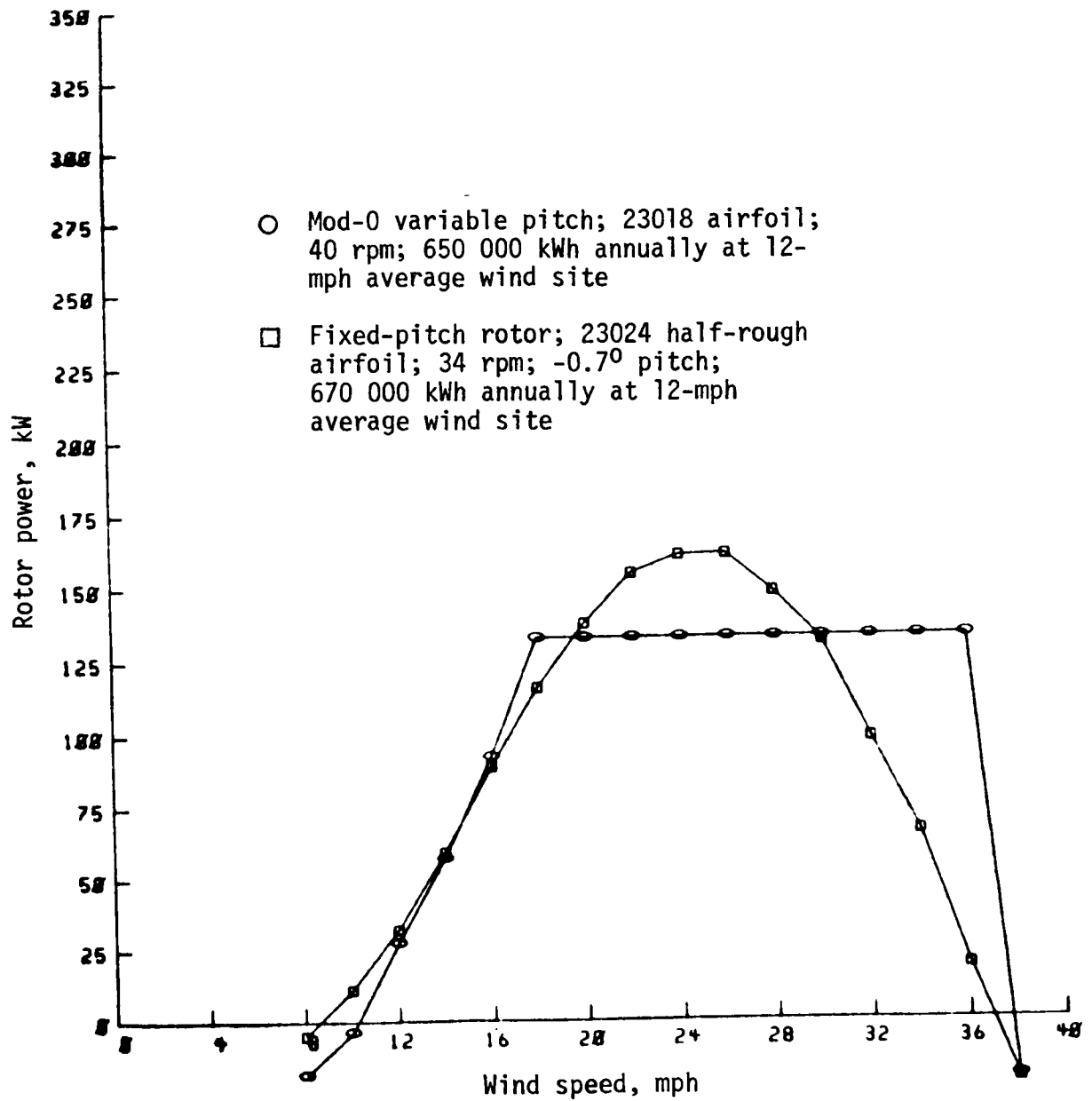
Figure 6. - Fixed-pitch rotor performance.

FIXED PITCH WIND TURBINE

Twist	Number of Blades	RPM	Angle	Peak Power	Annual Power	Power at Start
0	3	28	2^0	156 kW	666,000 kWhr	16 kW
0	3	28	8^0	249 kW	546,000 kWhr	0

Figure 7. - Starting ability versus annual power production.

FIXED PITCH WIND TURBINE

o Synchronous Generator - Motor Start

    o Clutch
    o Automatic Synchronizer

o Induction Generator - Motor Start

    o Poor Power Factor
    o Poor Efficiency at Low Power

o Yaw out of the Wind - Over Running Clutch

    o Automatic Synchronizer
    o Requires Experimental Verification

o Pitch Control on Blade Tip

    o Need 30% of Blade Length
    o More Complex Rotor

Figure 8. - Starting systems under investigation.

- Dead-man brake
    - Energized on loss of load
    - Scaleup effect

- Two-position tip flaps
    - Simple control
    - Approx. 4 ft^2 required

Figure 9. - Stopping systems for fixed-pitch wind turbines.

COMPOSITE BLADE FABRICATION

C. M. Minke

Hercules/Allegany Ballistics Laboratory
P. O. Box 210
Cumberland, MD   21502

ABSTRACT

A ten minute film presents the filament winding of the MOD 0 WTG Composite Blade. Various steps in the fabrication of tooling assembly, winding of spar and shell, and preparation for shipment are shown. Materials of fabrication are E glass roving and an epoxy resin.

DISCUSSION

Q. How does the winding angle (hence, longitudinal modulus) of the spar compare with the skin angle?

A. The winding angle ranged from about 30 to 40 degrees on both the spar and shell.

Q. How did you handle the problem of sag? Did you consider winding vertically rather than horizontally?

A. The unit was supported by a steady rest on all windings except the final windings to the tip. After winding and during cure, the blade was propped up.

Vertical winding would require a very expensive facility, which was not available.

RESEARCH OF LOW COST WIND GENERATOR ROTORS

Demeter G. Fertis
University of Akron
Akron, Ohio   44325

and

Robert S. Ross
Concept Development Institute, Inc.
1790 Stoney Hill Drive
Hudson, Ohio   44236

ABSTRACT

This feasibility program determined that it would be possible to signifi-
cantly reduce the cost of manufacturing wind generator rotors by making
them of cast urethane.   Goodyear developed several high modulus
urethanes which were structurally tested at the University of Akron.
A section of rotor was also cast and tested showing the excellent aero-
dynamic surface which results.   A design analysis indicated that a cost
reduction of almost ten to one can be achieved with a small weight in-
crease to achieve the some structural integrity as expected of current
rotor systems.

INTRODUCTION

Recently NASA has been given the task of trying to find some way that
wind energy could be harnessed at a large enough scale to become sig-
nificant as a world energy source.   In preliminary investigation NASA
has determined that large size windmills might be one solution to this
problem.   In their studies, however, they find that the cost of the initial
installation is considerable and if the overall system is to be economically
feasible, the initial cost of the equipment must be reduced.   These first
costs can be divided into three major components; 1) the rotor blades
themselves, 2) the tower that supports the equipment, and 3) the elec-
trical and electro-mechanical tie-ins.   In this particular program CDI
has proposed a solution for reducing the cost of the rotor blades.

In the first NASA installations and systems, rotor blades were based on
either propeller or airfoil design and fabrication techniques.   These
provided workable blades, but at a relatively high cost.   It appeared

that an entirely new approach would be required if a significant cost reduction was to be expected. CDI, therefore, looked to new materials and fabrication techniques as the solution to this problem. Since urethanes had a wide capability of structural properties, and they could be cast in low cost molds, where they generate their own internal heat, it appeared that these may be likely candidates for rotor components.

Through CDI, therefore, NASA funded a program to examine the physical properties of the urethanes both experimentally and analytically and to determine if full scale rotor blades could be made using this technique. The program involved not only physical testing of specimens, but also the fabrication of a model airfoil and a preliminary study of a full scale blade design to determine the practicability of the approach. The majority of the work was performed at the University of Akron and the Goodyear Tire & Rubber Company Research Laboratories.

MATERIAL EVALUATION

Urethanes are relatively new materials and, therefore, very little is known regarding their physical properties and structural behavior as a construction material. Two specific types of urethanes, microcellular foam and rigid foam, were selected for evaluation on this program. The properties examined were: density, tensile strength, compressive strength, shear strength, bearing strength, impact strength, creep resistance, fatigue strength, temperature effects and Poisson's ratio. Typical other behaviors examined were: hysteresis, modulus of elasticity, repeatability, experimental and analytical similarity, etc.

Using specimens 3/4" x 3/4" x 30" and three and four point loading systems, a large number of tests were conducted and data collected on load-deflection properties. The data proved to be very linear and creep was not significant for the most interesting formulations. Table 4 summarizes some of the properties obtained. Temperature effects were also briefly examined from 20°F to 150°F and appear to be within practical limits.

Fatigue tests were also conducted on tensile specimens at stress levels of 2200 psi at 5 and 10 cycles per second and went 2,000,000 cycles before being taken off the test machine. Strain gages tests were also conducted and they verified values of E of about 450,000 psi were achieved.

The test program indicated that the urethanes were a good structural material which behaved in a predictable engineering fashion and could be expected to perform as analytically shown similar to standard materials.

ROTOR DESIGN

This portion of the program consisted of two major areas: 1) The design of a test section to permit the casting of a urethane blade component which would demonstrate the structural capabilities of the material in a typical rotor blade configuration; and 2) the preliminary design of a full scale rotor blade that would permit the determination of a reasonable weight estimate.

For the purpose of this program a test section 7' long with a chord of 30" was planned. With a thickness of 15%, this represented a section of the 125' Mod O system at 80% of the radius. The model was made in two halves and cemented together. Two models were made and tested, one all urethane, and the other containing some typical reinforcing bars. This was to illustrate how readily metal could be used to vary the structural properties as needed.

The models were mounted in a cantilever fashion and tested to destruction in bending. Before this, however, they were tested in torque and were equipped with an accelerometer to check the natural frequency. As expected, the unit with reinforcing rods increased the stiffness of the test specimens. The surface was extremely smooth and did not require additional machinery.

The blade sections actually broke at stress concentration points at the root and indicated that the predicted structural properties were achieved. The blade was very stiff in torsion and was only tested up to 4° when 20,000 in-lbs was applied.

FULL SCALE ROTOR DESIGN ESTIMATES

Using design goal structural properties supplied by NASA on full scale preliminary designs of a 125' radius blade was made, assuming that it were to be cast urethane with metal stiffeners. It turned out that the

259

stiffeners criteria was the most critical and a blade using this technique would be slightly heavier than the present Mod O design to meet this structural goal. Since no attempt was made to optimize the designs, it is not known if the same weight could be achieved.

For casting purposes, the blade mold and fabrication costs were estimated and it was determined that costs in the vicinity of $2 to $3 per pound were not out of line, depending, of course, on the number of blades to be built. Size was not a limit in the technique considered.

It is now necessary to build and whirl test a set of blades as well as establish more precisely all the design parameters.

DISCUSSION

Q.   What would be the weight of a MOD O sized blade constructed from urethane?

A.   Preliminary estimates of blade weight vary from 2,750 to 3,300 pounds, which is slightly more than the present blade weight. Judicious design, however, could possibly bring it close to the same weight.

Q.   Do you have data and/or plans to obtain data on fatigue properties of your urethane foam samples?

A.   Samples of urethane were cycled at repeated tensile stress levels of 2,200 psi at speeds of 5 and 10 cycles per second and reached 2,000,000 cycles before being taken out of the machine. No visible signs of failure was present.

Q.   Are properties you showed for an isotropic material or did they include the high density of the skin which would form at the mold interface?

A.   The properties we showed did not include the ability to create a skin density at the mold surface greater than the rest of the specimen.

PLANS FOR

WIND ENERGY SYSTEM SIMULATION

Mark E. Dreier

Paragon Pacific, Inc.
1601 E. El Segundo Blvd.
El Segundo, California   90245

ABSTRACT

Two new analysis tools, one a digital computer code and the other a special purpose hybrid computer, are introduced. The digital computer program, the Root Perturbation Method or RPM, is a new implementation of the classic Floquet procedure which circumvents numerical problems associated with the extraction of Floquet roots. The hybrid computer, the Wind Energy System Time-domain simulator (WEST), yields real-time loads and deformation information essential to design and system stability investigations.

INTRODUCTION

In the realm of wind energy system simulation, the MOSTAB-HFW and WINDLASS digital computer programs have attained highly developed states for loads and deformation predictions. Except for empirical refinement of some data, and other minor adjustments, the ability to predict loads and deformations has been fully developed. The next task in the simulation problem is to determine the stability margins of the complex (coupled) aeroelastic-structural system present in the windmill designs, including the effects of periodic coefficients. Two methods for the solution of this problem are possible.

A rigorous stability analysis using digital techniques can be performed. This analysis would yield characteristic roots which reveal the system stability characteristics directly. The classic Floquet procedure is essential in this regard since it treats linear operators that are periodic functions of time.

An alternative method ties in real-time simulation of the system which would provide assessment of the system stability in the time domain, and an interactive ability to test different control algorithms. This paper introduces new concepts on these classic methods, both of which are planned for development in CY 1978.

PROPOSED DIGITAL STABILITY ANALYSIS PROGRAM

Overview of Floquet Method

In the past, digital verification of the stability of periodic systems has been treated using Floquet procedures. However, the Floquet procedures suffer from two very important drawbacks.

Firstly, in determining the stability of a system whose eigenvalues are, say, $\lambda_1, \lambda_2 \ldots \lambda_n$, the eigenvalues computed by the Floquet procedure are $\gamma_1, \gamma_2 \ldots \gamma_n$, where

$$\gamma_j = e^{T\lambda_j} \qquad j = 1, 2 \ldots n \qquad (1)$$

and T is the period of the physical system. Equation (1) says that the Floquet eigenvalues are exponentials of physical dynamic modes represented by $T\lambda_j$. While the values of λ_j will be spaced in magnitude to reflect the natural frequencies of the system, the γ_j's will be spread out due to the exponentiation. This results in considerable significant figure accuracy requirements in order to achieve even moderate accuracy in the calculations of λ. This effectively limits the number of dynamic modes that can be computed using practical computer implementation of the Floquet procedures.

The second difficulty with Floquet emerges when one notes that if

$$\lambda_j = a_j + i\,b_j \qquad (2)$$

is a solution to Equation (1), so is

$$\lambda_j = a_j + i\,(b_j + n2\pi) \qquad (3)$$

Hence, the imaginary part cannot be uniquely determined, but only within multiples of 2π.

262

The Root Perturbation Method

A new method for estimating the characteristic roots of linear systems with periodic coefficients has been proposed. The Root Perturbation Method (RPM) is an alternative implementation of the Floquet procedure, but circumvents the drawbacks of Floquet. The RPM begins by assuming a mean value of the constant coefficient matrix and determining the eigenvalues of that system. For example, if the system is modelled

$$\dot{x} - M(t)\, x \;=\; N(t)\, u \tag{4}$$

then the eigenvalues and eigenvectors μ and x are defined so that

$$M_o\, X \;=\; X\, U \tag{5}$$

where M_o is the mean value of $M(t)$ and U is the diagonal matrix made of the μ's. Defining the perturbation quantity

$$\overline{M}(t) \;\triangleq\; M(t) - M_o$$

and the vector

$$(6)$$

$$Z(\lambda) \;\triangleq\; e^{-u\lambda}\, X^{-1}\, \overline{M}(\lambda)\, X\, e^{u\lambda}$$

which is then used in the Neumann Series

$$H \;\triangleq\; \int_{\tau}^{\tau+t} Z(\lambda)\; d\lambda + \int_{\tau}^{\tau+t} Z(\lambda) \int_{\tau}^{\lambda} Z(\eta)\; d\eta\, d\lambda +$$

$$\int_{\tau}^{\tau+t} Z(\lambda) \int_{\tau}^{\lambda} Z(\eta) \int_{\tau}^{\eta} Z(\beta)\; d\beta\, d\eta\, d\lambda + \ldots \tag{7}$$

263

Some straightforward algebra will show that the sought characteristic roots, λ_j, are given by

$$\lambda_j = \mu_j + \frac{1}{T} \ln (h_{jj} + 1) \qquad j = 1, 2 \ldots n \qquad (8)$$

where h_{jj} are the diagonal elements of H defined in Equation (7).

The above equation is a perturbation result which should be much less susceptible to numerical difficulties. Also, since the log term is small, λ_j will be close to μ_j such that the 2π multiple associated with λ_j is easily discerned.

PROPOSED HYBRID SYSTEM FOR STABILITY AND CONTROL ANALYSIS

As mentioned earlier, another viable method to examine stability, loads and deformations of a wind turbine system is to construct a hybrid simulation model. Special purpose hybrid computers are especially attractive here since they can simulate real-time aeroelastic phenomena. At this time, construction of such a simulator is planned for CY 1978. Dubbed WEST (Wind Energy System Time-domain simulator), the same aeroelastic math models incorporated in MOSTAB-HFW (not stability derivative models!) will be solved simultaneously with the tower, pod and drive train models, to create real-time loads and deformation information for the entire system. WEST will be equipped with external potentiometers and a patch panel which allow the user to easily reconfigure the control system algorithms. The unit will be supported by a Digital Support System (DSS) that aids the programmer in modelling any number of physical system geometry changes. WEST will produce accurate time domain results (time histories) of the operation of a given wind turbine plant. A wind spectral synthesizer will also be incorporated in WEST, which will enable calculation of loads and motions in a statistical wind environment.

SUMMARY

Two useful new tools have been outlined and are currently planned for next year; these will provide methods of determining the stability, loads and motions of an entire wind energy system. The Root Perturbation Method, a post-processor for the WINDLASS system, implements the classic Floquet method in a new way which is less susceptible to numerical difficulties. The WEST special purpose hybrid computer uses the best features of both digital and analog technology to model a wind energy system in real time. Both of these new tools promise to be major contributors to the future study and evolution of wind turbine systems.

THE UMASS WIND FURNACE BLADE DESIGN

Duane E. Cromack

Mechanical Engineering Department
University of Massachusetts
Amherst, Massachusetts 01003

ABSTRACT

A brief description of the UMass Wind Furnace concept is presented along with some preliminary performance data. Particular emphasis is placed on the design, construction, and manufacturing procedure for the 32.5 foot diameter GRP blades.

INTRODUCTION

Conceptually the wind furnace is a simple heating system consisting of a wind turbine, solar flat plate collectors, a storage system, and a heat delivery system and is shown schematically in Fig. 1. This system and its operation are described in detail in ref. 1. Briefly, water in the thermal storage tank is heated by the solar collectors and by the electricity generated by the wind turbine. In turn, this water is used to heat the house by conventional base-board hot water convectors. At the present time, a gas fired hot air furnace serves as the auxiliary back-up heating system.

The wind turbine, the major component of the wind furnace system, consists of a 9.9 m (32.5 ft.) diameter, three-bladed downwind rotor atop an 18.3 m (60 ft.) steel stayed pole mast. Designed to operate at a tip-speed-ratio of 7.5, the machine should produce 25kW at 11.6 m/s (26 mph). The predicted and experimentally measured power output are shown in Fig. 2 as a function of wind speed. From cut-in speed of 2.7 m/s (6 mph) to rated speed of 11.6 m/s (26 mph) the rotor rpm continually increases and the 7.5 tip-speed-ratio is maintained. Above rated speed and up to 22.4 m/s (50 mph) the blades are automatically pitched towards feather thus maintaining a constant rated rpm of 167. At the cut-out speed of 22.4 m/s (50 mph), the blades are pitched to full feather and the machine stops.

BLADE CONSTRUCTION

Figure 3 is a sequence of photographs depicting the blade construction sequence. The skin is laid up over a male mold by applying epoxy resin to the cloth and smoothing it out with a squeege. After the skin is cured, the spar is laid-up and tape wound over a three-piece spindle. Before the spar cures, it is placed inside the skin which in turn is held in a female mold. After the spindle is removed and the shank mold put in place, pressure is applied inside with the pressure bag and the spar is cured while it bonds to the skin. The blade is completed by bonding the trailing edges of the skin together and attaching the steel sleeve over the shank portion. The pitch control sprocket attaches to the steel sleeve after the blade has been inserted into the rotor hub.

BLADE STRUCTURAL DESIGN

The UMass blades are patterned after the Brace Institute design and uses a NASA 4415 airfoil section (ref. 2) with a chord varying from 18 to 4 inches with approximately 47 degrees of twist along its 16.25 foot length. The blades are made of glass reinforced plastic (GRP), chosen because of its strength, ease of molding over a complex shaped mold, high durability, moderate cost and for its usefulness in making a small number of items of premium quality and of optimum thickness distribution on relatively inexpensive tools.

The blade was designed for two loading conditions: (1) stationary and un-feathered in a 150 mile-per-hour wind and (2) for maximum power in a 30 mile-per-hour wind representing a 50 percent overload based on rated power. The latter condition proved to be the most severe. A laminate schedule was obtained based on the calculated stresses and deflections that would place the elastic and aerodynamic axes nearly coincident with the 25 percent chord axis. A factor of safety of four was applied to account for aeroelastic effects and to provide as much rigidity as possible without significantly increasing the construction difficulty or material cost. The spar is a heavy laminate of pre-dominately unidirectional fabric tapering in thickness from the .5 radius to the tip. Several wraps of fiberglass tape reduce the likelihood of shear failure. The skin consists of several layers of balanced weave cloth tapering toward the tip. It is desirable to keep the skin no thicker than necessary for rigidity and impact damage to avoid shifting the elastic axis rearward. The cloth in the skin runs the length of the blade, thereby avoiding joints which could cause surface roughness.

The UMass Windfurnace has been up since November 1976 and operating automatically since September 1977. The blades have been left unpainted so that any deterioration can be detected - non has been observed to date.

REFERENCES

1. Cromack, D.E., "Design and Operational Aspects of the UMass Wind Furnace," Proceedings of the AWEA Conference, Boulder, Colorado, May 12-14, 1977.

2. Van Dusen, E.S., "Blade Structural Design; Wind Furnace Experiment," Energy Alternatives Program, University of Massachusetts, Amherst, Mass., 01003, TR/76/2, January 1976.

DISCUSSION

Q. What percent of the chord dimension does the spar fill?

A. The spar is 40 percent of the chord.

Q. Could you describe your gear drive system and performance characteristics?

A. The gear drive system consists of a truck differential and a silent chain and sprocket providing about an 11:1 speed up. The performance characteristics are shown in Figure 2 of this paper.
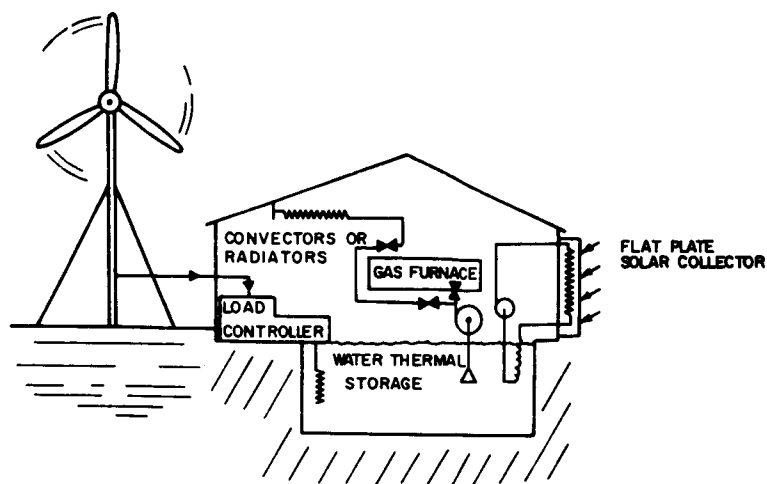
266

Figure 1. - Schematic of UMASS wind furnace.
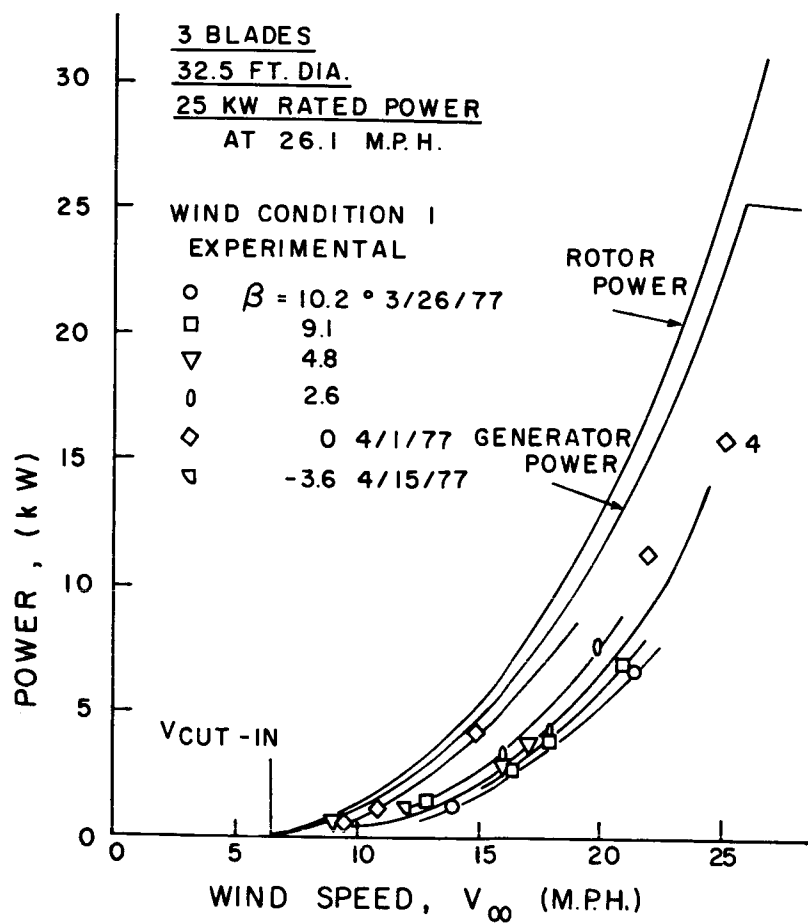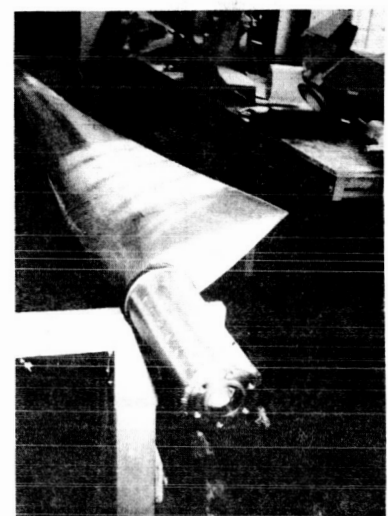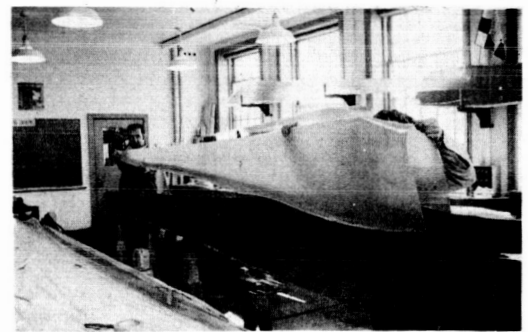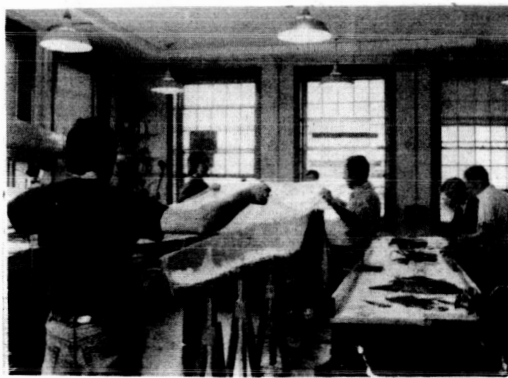

Figure 2. - Power as a function of wind speed.

(a)   (b)

Figure 3. - UMASS wind furnace blade construction sequence.

PANEL DISCUSSION SUMMARIES

DISCUSSION LEADER . . . . . DR. HOLT ASHLEY
                                 PROFESSOR AERONAUTICS AND ASTRONAUTICS
                                 STANFORD UNIVERSITY
                                 STANFORD, CALIFORNIA

SESSION CHAIRMAN . . . . . RONALD L. THOMAS
                                 DEPUTY PROJECT MANAGER
                                 WIND ENERGY PROJECT OFFICE
                                 NASA-LEWIS RESEARCH CENTER
                                 CLEVELAND, OHIO

INTRODUCTION

One purpose of the Workshop on Wind Turbine Structural Dynamics was to discuss future plans for large windturbines. This was accomplished by means of three panel discussions on the following subjects: (1) ANALYSIS METHODS, (2) STRUCTURAL CONFIGURATIONS, and (3) POWER TRAIN CONFIGURATIONS. Following each panel discussion, the audience was given an opportunity to ask questions and make comments. The main points put forward by both the panel and audience were then summarized by Dr. Holt Ashley (discussion leader), and Ronald L. Thomas (session chairman). Their summaries of each panel discussion follow:

PANEL I

SUBJECT: "ANALYSIS METHODS"

PANEL MEMBERS:

         DR. DAVID SPERA (NASA-LeRC)
         DR. JOHN DUGUNDJI (M.I.T.)
         MR. JACK ANDREWS (BOEING ENGINEERING & CONSTRUCTION)
         MR. CLYDE STAHLE (GENERAL ELECTRIC)
         MR. MARK DREIER (PARAGON PACIFIC)

SUMMARY:

DR. HOLT ASHLEY:

I'm sure you all realize that it doesn't matter what I say in this wrap-up summary, I'm going to make somebody mad. So put yourself in my position and be a little tolerant. I'll try to tell you what I think I heard.

With regard to the tools of analysis, we now have available a rich assortment of computer codes for predicting the dynamic response and stability of things that look like wind turbines. They are in remarkably good shape, perhaps, compared to the design tools that are used in many other areas of structural design. Also, the devices on which they are being used are pretty complicated,

and we are anticipating in the future quite a variety of configurations that differ from the ones which we are now in the process of verifying. So, although the tools are good, this is no time to shut the door on continued development of codes that are useful for analysis purposes. We're all pretty sure that F = MA. I think we also believe that the relations between stress, strain, internal loads, and so forth, can be described pretty well.

The aerodynamics is a relative, although not an absolute, weak spot. I would suggest that, in regard to the aerodynamic loads useful for forcing and stability, perhaps we're a little bit better off than the worse sorts of conditions that helicopters get into. This is because the vortex interactions are perhaps not as bad in these machines as they are in helicopters; although, on the other hand, helicopters tend to live in an environment that is not as dominated by the variability of the wind as these machines do. There is one clear need, and that is to continue to improve the characterization of that wind environment, as a statistical phenomenon in space and time, and to put that characterization into the codes. But we could be in considerably worse shape than, in fact, we are.

I also heard it agreed that design criteria are needed and have to be improved in an evolutionary way, as machines come along. It would be a mistake to freeze the criteria too simplistically in such a way that they constrain innovation and imagination in the future design of these machines, because it is not necessarily true that the low cost that you all seek so earnestly is going to be found in the type of "stiff" designs, as they were called, that are represented by Mod-0 and Mod-1.

One other thing about computer codes--there's a concept that I like, called an "acceptability index," that was mentioned by Mark Dreier. Let's see if we can all define that term as well as he seems to know how to define it, and let's use it to avoid the thing I talked about in my opening remarks: the misuse of computer codes. This involves the application of analytical tools in places where they don't belong. It's so easy to do, and it becomes easier as the codes become bigger, more complicated and more widely distributed from their source.

Wind tunnel testing-- there were clear differences of opinion there. I heard no one argue with Jack Andrews when he said that the Boeing Company felt that it was going to need some wind tunnel testing in connection with the development of the Mod-2 machine, which we hope is going to represent a bigger jump than, say, the Mod-1 is relative to the Mod-0. But we also recognize that, as a design verification tool, the wind tunnel has its limitations. It's not impossible, but it is difficult, to reproduce this wind environment.

Perhaps an equally important role of wind tunnel testing is as a way of verifying analytical methods, a task which is not as easy in the real world, full-scale environment. When you are doing that, you can then make simpler models and make those models and the codes that analyze them conform to one another. Thus you verify codes, which can then be used on more complicated, full-scale configurations, at least with a certain amount of luck and good judgment. We also heard a consensus plea for simple methods of analysis at the preliminary

design stage that would assist our understanding. They would also permit trade-off studies to be done in a simple way, without the enormous exercise of the computer.

With respect to the Mod-0 machine, it's seen by almost everyone as another useful way of verifying design tools. We heard several strong pleas that it be used as a test machine in various ways, following up, for example, on the current plan to reverse the direction of the rotor and thus essentially get two or three configurations for the price of one.

MR. RONALD THOMAS:

I'm not going to second guess on that, Holt. My final comment is, that if we are to get the cost down on these machines, we're going to have to get to the less stiff or soft systems. Right now the codes we're using in the wind turbine business are only verified for the stiff systems, and we've got to verify these codes for the soft systems. This may be done by using the small models, using the Mod-0, or whatever, but we've got to verify these codes as we get into these areas before we can commit to large designs. Thank you.

PANEL II

SUBJECT: "STRUCTURAL CONFIGURATIONS"

PANEL MEMBERS:

       DR. DAVID SPERA (NASA-LeRC)
       DR. KURT HOHENEMSER (WASHINGTON UNIVERSITY)
       MR. JACK ANDREWS (BOEING ENGINEERING & CONSTRUCTION)
       MR. CLYDE STAHLE (GENERAL ELECTRIC)
       MR. M. C. CHENEY, JR. (UNITED TECHNOLOGIES RESEARCH CENTER)
       MR. GLIDDEN DOMAN (HAMILTON STANDARD)

SUMMARY:

MR. RONALD THOMAS:

I'm going to try to summarize very briefly. First, the question of two versus three blades. I think the panel pretty much agrees that two is the preferred route if we can handle the cyclic loads: don't go to three blades unless you really have to. If, however, the cost of the blades is very low, then there may be an overall advantage to three blades. It is not merely a blade question but a whole wind turbine design question. If you do go to three, can you take enough material out of the whole machine to really make it worthwhile.

There seems to be some controversy as to the upwind versus downwind rotor. The upwind appears to offer some reduction in loads; however, as Clyde Stahle mentioned, maybe not all the factors were taken into consideration. There probably would be a reduction in loads, but not maybe quite as much as has been predicted. This needs further analysis and verification with Mod-0 tests.

On the question of stiffness versus softness, I think the panel very much believes that to really get the loads down, we probably are going to have to progress in the direction of softening up some of the areas. The analysis tools are here but this is an area where we're going to have to proceed in a slow and orderly fashion. We discussed the free yaw system quite a bit and I think that several of the panel members feel very strongly that this is something that should be tested on the Mod-0. There may be instabilities there, and I think there may be differences of opinion, or perhaps some of us maybe don't know quite well enough the magnitude of these instabilities, but it's certainly something that would be good to test on Mod-0. Once we have the analysis well enough in hand, we will test free-yaw on the Mod-0.

As far as the fixed pitch systems, I believe that the panel believes that there may be some advantages to going into the fixed pitch systems with the possibility of reducing costs. We possibly might want to use some control, and we discussed the cyclic versus the collective, and maybe not throw both of them out at the same time, but that may have some merit. It was pointed out that the fixed pitch system offers some possibility of softening up the rotor by going to a teetering hub. That concludes my summary.

DR. HOLT ASHLEY:

May I follow up? I'm just tempted to say that you did a very good job of summarizing; in regards to the kind of machines that you love, I don't think there is anything useful that I would have to add. On the other hand, I'm glad that Mr. Reuter brought up the vertical axis machines, because I accepted the invitation to come here under the impression that this was going to be a workshop on wind turbine structural dynamics. Actually, it turned out to be a very interesting workshop, but it was a workshop on horizontal-axis turbines of the kind that NASA is interested in. I think, with regard to the vertical-axis machines, we really have to say that they have good promise for certain kinds of applications that have not been recognized nearly as fully as the horizontal-axis machines by a great number of people. In turns out that the first windmills in the history of the world were vertical axis machines, if you want to look at your history books. As for their structural dynamic problems, I think I'm right in saying, from my study of the literature, that there may be a good deal more to learn as they are scaled up to the really large sizes which have potential for making contributions to the world's power problems. They're going to get into the same kind of "fun" that you people are already getting into, and they do present some extremely interesting opportunities for the kind of basic studies that John Dugundji talked about. They also will demand the development of better analysis and test tools. So what I come out on is that, if we feel the exercise here the last few days has been successful, we might want to recommend to an organization like Sandia or NRC, Canada, that a dynamics workshop on vertical-axis wind turbines might prove useful for them some day. It would certainly be a very interesting thing to participate in.

PANEL III

SUBJECT: "POWER TRAIN CONFIGURATIONS"

PANEL MEMBERS:

DR. MANUEL MARTINEZ-SANCHEZ (M.I.T.)
MR. ROBERT BARTON (GENERAL ELECTRIC)
MR. HAROLD GOLD (NASA-LeRC)
MR. ROBERT JONES (KAMAN AEROSPACE

SUMMARY:

MR. RONALD THOMAS:

Concerning the power quality of the wind turbine, it obviously depends on the size of the wind turbine and the size of the system it's going on. We've looked at Mod-O with its power oscillations. If you put Mod-O on the Clayton power system, there appears to be no major power quality concerns, but obviously if the wind turbine is a major part of the load, the people may not be happy with the power quality that the wind turbine is giving them. The better job we can do, the less problems we'll have. It all gets back down to doing the best we can with the least costs. So far as the technology goes in the drive train, I think the panel members believe that there are ways to reduce the cost and the weight of the drive train by possibly going to planetary systems and by making the drive train more flexible. Some believe the softer drive systems would result in improved power quality. There are many ways to design the drive train, but there aren't any that are clear cut winners over the conventional systems that we have. They have to be studied in detail and the overall costs and quality of the power output need to be better understood. I believe that as far as the stiffness versus flexibility issue goes, most of the people who prefer flexibility agree that flexibility is good as long as you have adequate controls, you are going to need more sophisticated controls than you do with the stiff systems. That wraps up my summary comments. Holt, do you have anything?

DR. HOLT ASHLEY:

Just a quickie, and I'm not sure if it's a technical comment. I think it's dangerous, if true, to let yourself be too unilaterally fascinated by the issue of fitting these machines into an existing large power grid. You'll notice that even Mr. English in his talk last night equivocated when I tried to get him to open up on that subject. I recognize that when it comes to selling budgets for this kind of RD&D in Congress and to our masters in Washington, we have to talk about the contribution that this type of machines might make within the framework of the Continental United States. But, I don't think we should lose sight of all kinds of interesting things that wind energy conversion systems might accomplish in remote places, for the needs of underdeveloped countries, and so forth. The fact is that all of your work is going to have an incidental contribution to make there, too. When you remove this grid synchronization requirement and look at some of those many other applications, the problems are really quite different. So don't lose sight of those possibilities too.

CONCLUSION:

<u>MR. RONALD THOMAS</u>:

Before we finish I would like to thank Dave Spera, who organized and chaired this whole three-day session, and also Joe Savino, who was the co-chairman, and Karen Wester who saw to the many, many details of the logistics. I think it's been a very interesting three days and it's been very helpful.

THE BRUSH WIND TURBINE GENERATOR AS DESCRIBED IN

SCIENTIFIC AMERICAN OF DECEMBER 20, 1890

David A. Spera

National Aeronautics and Space Administration
Lewis Research Center
Cleveland, Ohio 44135

ABSTRACT

An historic wind turbine generator is described which operated in Cleveland, Ohio, from 1888 to 1908. The machine had a 144-blade rotor 56 feet in diameter, a pivoted tower 60 feet high, and a maximum output of 12 kW DC. The description is based on an 1890 article in Scientific American journal.

INTRODUCTION

In 1888 Charles F. Brush, a prominent Cleveland, Ohio, industrialist erected a large windmill on his estate for the purpose of generating electricity to light his home. Brush had recently made his fortune through the invention and manufacture of practical arc lights and DC generators ("dynamos"). A Brush arc lighting system illuminated Cleveland's Public Square in 1879, an event which is often described as the world's first electric street lighting. Although the Brush wind turbine generator operated successfully for 20 years, it seems to have been overlooked in contemporary accounts of the historical development of windmills (see ref. 1, for example). The purpose of this brief paper is to acquaint the wind energy community with a machine which may prove to be the world's first practical wind turbine generator. It seems appropriate to do this by means of the text and illustrations of an 1890 article in Scientific American (ref. 2 and fig. 1), which is the most complete description available of the Brush windmill. This article, with minor editing to coordinate text and illustrations, is as follows:

MR. BRUSH'S WINDMILL DYNAMO

It is difficult to estimate the effect of an invention on existing practices and industries. Occasionally a new invention will appear which will greatly affect a whole range of allied inventions and industries in such a way as to entirely change time-honored customs, inaugurate new practices and establish new arts. The commercial development of electricity is a notable example of this.

After Mr. Charles F. Brush of Cleveland, Ohio, successfully accomplished practical electric illumination by means of arc lights, incandescent lighting was quickly brought forward and rapidly perfected. Gas lighting was also improved in various ways. Simultaneously with these, the electric distribution of power was carried forward, and important improvements were made in prime movers for driving dynamos. In this direction much has been done both in steam and water motors. Wind power has been repeatedly suggested for driving dynamos,

but the adaptation of the windmill to this use seems to have been a problem fraught with difficulties. Few have dared to grapple with it, for the question not only involved the motive power itself and the dynamo, but also the means of transmitting the power of the wheel to the dynamo, and apparatus for regulating, storing and utilizing the current. With the exception of the gigantic windmill and electric plant described herein, we do not know of a successful system of electric lighting operated by means of wind power.

Brush Residence (Figure 2)

Passing along Euclid Avenue in the beautiful city of Cleveland, one will notice the magnificent residence of Mr. Brush, behind which and some distance down the park may be seen, mounted high on a tower, the immense wheel which drives an electric lighting plant.

The house is furnished with 350 incandescent lights, varying from 10 to 50 candle power each. The lamps most commonly used are from 16 to 20 candle power, about 100 incandescent lights are in every day use. In addition to these lights there are two arc lights and three electric motors.

Brush Windmill (Figure 3)

The mill here shown, as well as all of the electrical apparatus used in connection with it, and the very complete system by which the results are secured, have been designed and carried out according to the plans of Mr. Brush and under his own personal supervision. As an example of thoroughgoing engineering work it cannot be excelled.

Every contingency is provided for, and the apparatus, from the huge wheel down to the current regulator, is entirely automatic. The wheel, which is 56 feet in diameter, is secured to the shaft and is provided with 144 blades, which are like those of screw propellers. The sail surface of the wheel is about 1,800 square feet, the length of the tail which turns the wheel toward the wind is 60 feet, and its width is 20 feet. The mill is made automatic by an auxiliary vane extending from one side, and serving to turn the wheel edgewise to the wind during a heavy gale. The tail may be folded against the tower parallel with the wheel, so as to present the edge of the wheel to the wind when the machinery is not in use.

Section View of Windmill Tower (Figure 4)

The tower is rectangular in form and about 60 feet high. It is mounted on a wrought iron gudgeon 14 inches in diameter and which extends 8 feet into the solid masonry below the ground level. The gudgeon projects 12 feet above the ground and enters boxes in the iron frame of the tower, the weight of the tower, which is 80,000 pounds, being borne by a step resting on the top of the gudgeon. The step is secured to a heavy spider fastened to the lower part of the frame of the tower.

To guard against extraordinary wind pressure, the tower is provided at each of its corners with an arm projecting downwardly and outwardly, and carrying a caster wheel very near but not in contact with the circular rail concentric

with the gudgeon. Ordinarily, these caster wheels do not touch the rail, but when the wind is very high, they come into contact with the rail and relieve the gudgeon from further strain.

In the upper part of the tower is journaled the main wheel shaft. This shaft is 20 feet long and 6½ inches in diameter. It is provided with self-oiling boxes 26 inches long, and carries the main pulley, which has a diameter of 8 feet and a face of 32 inches. The countershaft arranged below the wheel shaft is 3½ inches in diameter, it carries a pulley 16 inches in diameter, with a face of 32 inches, which receives the main belt from the 8 foot pulley on the wheel shaft. This is a double belt 32 inches wide. The countershaft is provided with two driving pulleys each 6 feet in diameter, with a face of 6½ inches, and the dynamo is furnished on opposite ends of the armature shaft with pulleys which receive belts from the drive wheels on the countershaft.

The dynamo is mounted on a vertically sliding support and partially counterbalanced by a weighted lever. It will be seen that the countershaft is suspended from the main shaft by the main belt, and the dynamo is partly suspended from the countershaft by the driving belts. In this way the proper tension of the belts is always secured, the total load on the dynamo belts being 1,200 pounds, and on the main belt 4,200 pounds. The ends of the countershaft are journaled in sliding boxes connected by equalizing levers which cause both ends of the shaft to move alike.

The current passes from the dynamo to contact shoes of polished and hardened steel carried by a cross bar on the tower, which shoes slide on annular plates surrounding the gudgeon. Conductors extend underground from these plates to the dwelling house.

Dynamo Room in Tower (Figure 5)

The pulleys are so proportioned that the dynamo, which is one of Mr. Brush's own design, makes fifty revolutions to one of the wheel. The speed of the dynamo at full load is 500 revolutions per minute, and its normal capacity at full load is 12,000 watts. The automatic switching devices are arranged so that the dynamo goes into effective action at 330 revolutions a minute, and an automatic regulator is provided which does not permit the electromotive force to run about 90 volts at any speed. The working circuit is arranged to automatically close at 75 volts and open at 70 volts. The brushes on the dynamo are rocked automatically as the load changes. The field of the dynamo is slightly compounded.

Storage Batteries (Figure 6)

In the basement of Mr. Brush's house there are 408 secondary battery cells arranged in twelve batteries of 34 cells each; these 12 batteries are charged and discharged in parallel; each cell has a capacity of 100 ampere hours. The jars which contain the elements of the battery are of glass, and each cell has its liquid covered with a layer of "mineral seal" oil, a quarter of an inch thick, which entirely prevents evaporation and spraying, and suppresses all odor.

Regulating System (Figure 7)

The automatic regulating devices are shown in one of the views of our engraving. At 1 are shown the voltmeters and ammeters employed in measuring the charging and discharging currents; at 2 is shown a series of indicators, one for each battery; 3 represents an electrically operated switch by means of which the current may be turned on or off the house mains by pressing push buttons in different portions of the house; 4 represents a ground detector, which is connected with the center of the battery and with the ground, so that should the conductor upon either end of the battery be grounded, the fact will be indicated by the movement of the index in one direction or the other from the zero point of the scale, thus showing not only that the battery is grounded, but indicating the grounded pole; 5 is a leakage detector connected up with the lamp circuits, and arranged to show any leakage from one conductor to the other; at 6 is shown a compound relay for operating the automatic resistance shown at 7. This resistance is placed between the batteries and the house mains, and is arranged to keep the voltage on the lamps constant at all times. In this device the resistance is secured by means of powdered carbon placed under varying pressure, the necessary movement being made by means of hydraulic pressure under the control of the relays.

Summary

It is found after continued use of this electric plant that the amount of attention required to keep it in working condition is practically nothing. It has been in constant operation more than two years, and has proved in every respect a complete success.

The reader must not suppose that electric lighting by means of power supplied in this way is cheap because the wind costs nothing. On the contrary, the cost of the plant is so great as to more than offset the cheapness of the motive power. However, there is a great satisfaction in making use of one of nature's most unruly motive agents.

CONCLUDING REMARKS

Operation of the Brush wind turbine generator was discontinued in 1908, at which time the rotor was removed. Between 1900 and 1908 the batteries were used only to power apparatus in Brush's basement laboratory, and city power replaced the battery system for house lighting. After 1908 the condition of the machine gradually deteriorated until it was dismantled in about 1931, shortly after Brush died. Efforts to locate remnants of the windmill have so far been unsuccessful. However, research continues on the design, manufacture, and operation of this historic wind machine.

REFERENCES

1. Golding, E. W.: The Generation of Electricity by Wind Power. John Wiley & Sons (New York), 1955.

2. Mr. Brush's Windmill Dynamo. Scientific American, vol. LXIII, no. 25, Dec. 20, 1890, cover and p. 389.
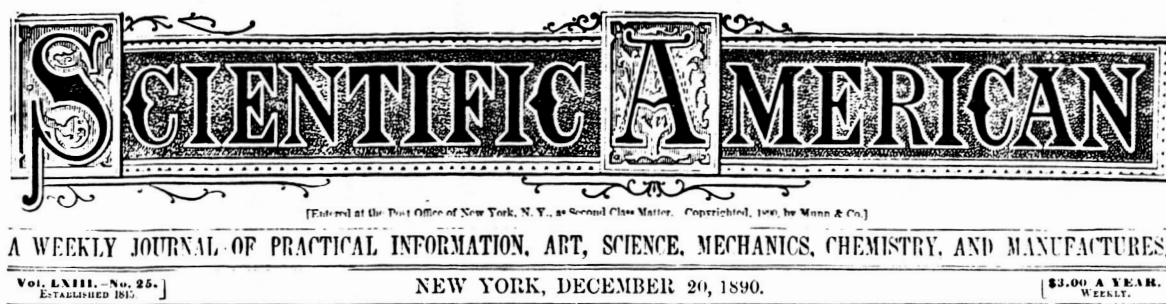
Figure 1. - Logo from cover of Scientific American.

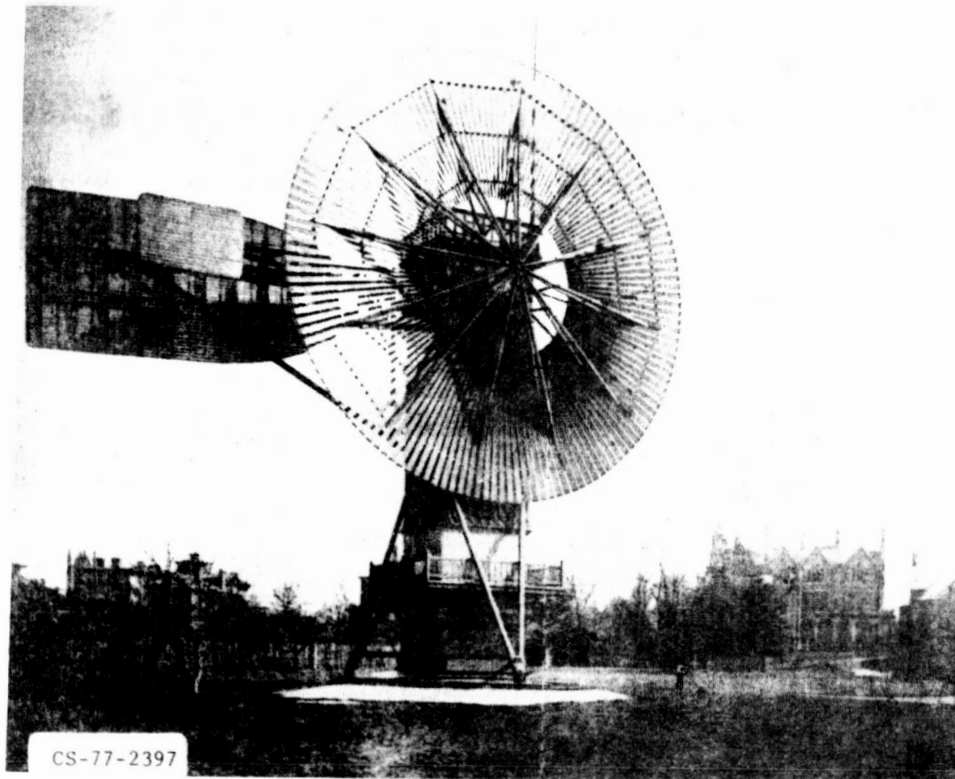Figure 2. - The Brush residence in Cleveland, Ohio,
as it appeared in 1890.

Figure 3. - The Brush wind turbine generator, which operated from 1888 to 1908. Rotor diameter, 56 ft; tower height, 60 ft; rated power, 12 kW, DC; rotor area, 1800 ft^2; tail area, 1200 ft^2.
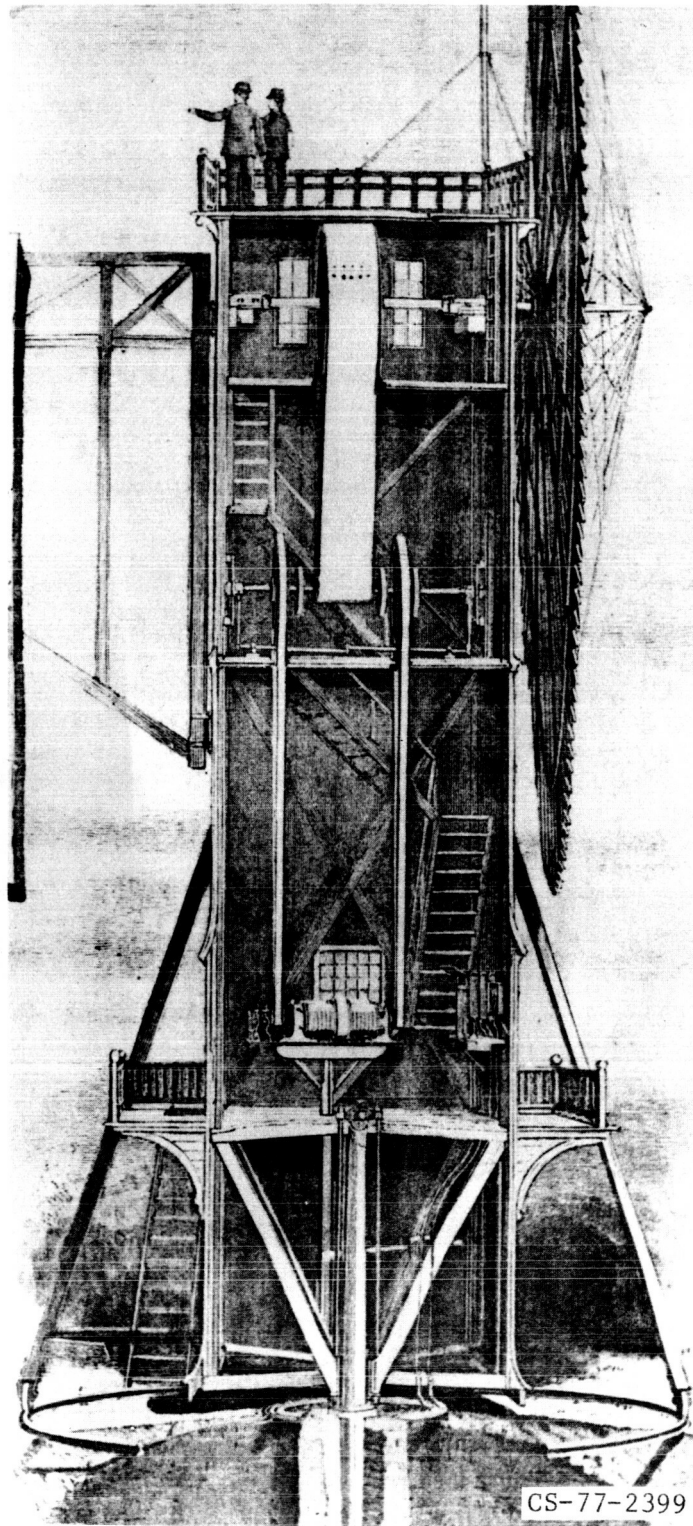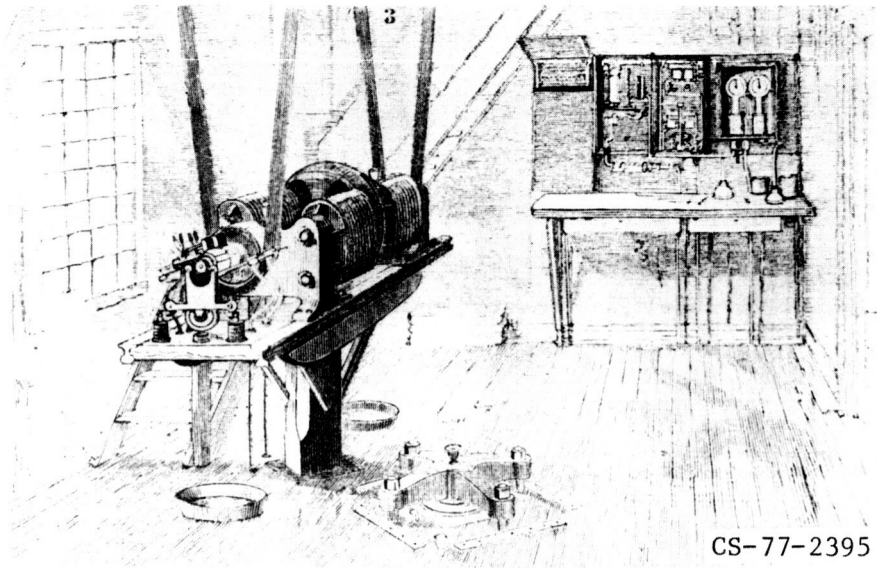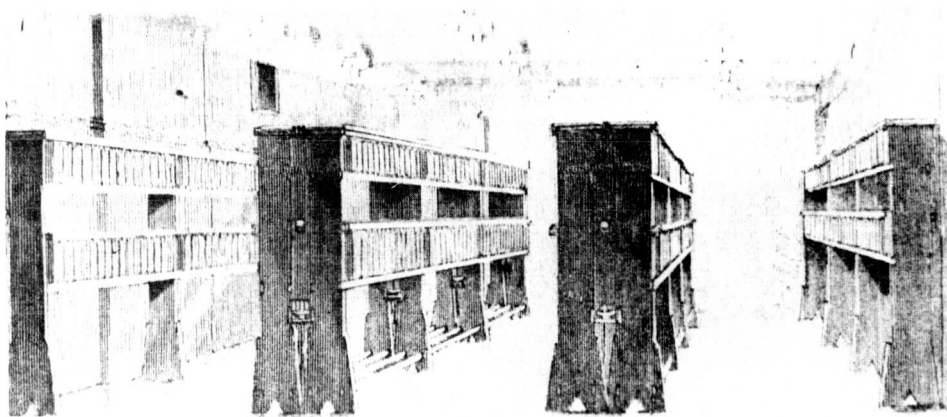
Figure 4. - Sectional view of tower. Pulley
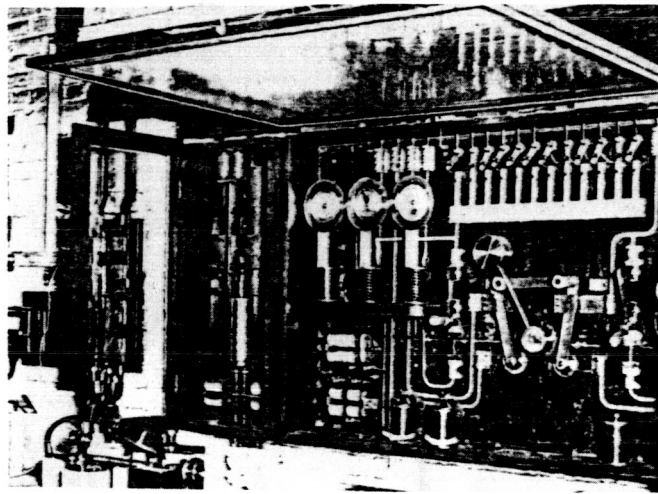ratio, 50 to 1; weight on pivot, 80 000 lb.

CS-77-2395

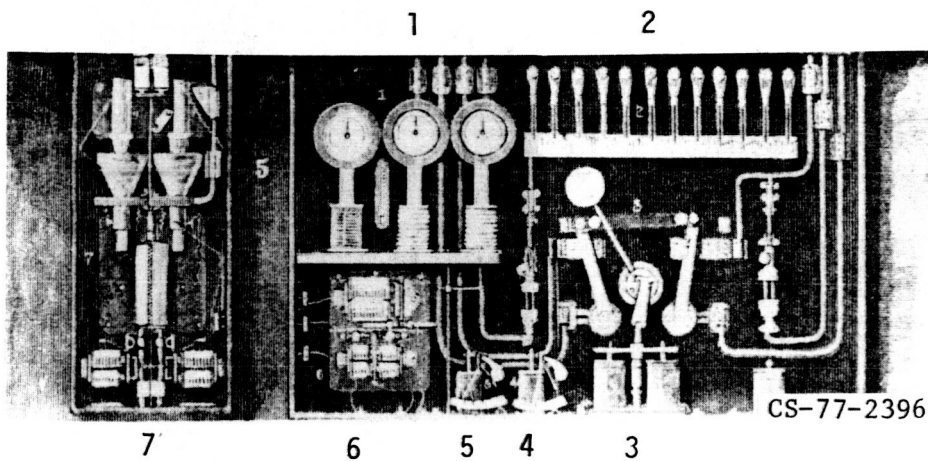Figure 5. - Dynamo room in tower. Generator rating, 12 kW
at 500 rpm.

CS-77-2394

Figure 6. - Battery room in basement of Brush residence.
Twelve batteries of 34 cells each; total capacity,
40 800 Ah).

(a) Photograph.

(b) Etching.

Figure 7. - Main control panel in residence.

1   Voltmeter and ammeters
2   Indicator switches for each battery
3   Main on-off switch
4   Battery ground detector
5   Lamp circuit leak detector
6   Voltage regulator relays
7   Voltage regulator variable resistance

ATTENDEES

Dan Ancona
DOE/Wind Systems Branch
600 E Street, NW
Washington, DC 20545

Jack Andrews (MS 8K-66)
Boeing Engineering and Construction
Box 3707
Seattle, WA 98124

Holt Ashley
Durand 369
Stanford University
Stanford, CA 94305

G. Mervin Ault (MS 3-5)
NASA-Lewis Research Center
21000 Brookpark Road
Cleveland, OH 44135

Robert Barton
General Electric Company
Box 8661 (7310)
Philadelphia, PA 19101

Joseph M. Baskin (8K-66)
Boeing Engineering and Construction
Box 3707
Seattle, WA 98124

Charles Butterfield
Rockwell International
Rocky Flats Plant
Box 464
Golden, CO 80401

Thomas P. Cahill (MS 49-6)
NASA-Lewis Research Center
21000 Brookpark Road
Cleveland, OH 44135

M. C. Cheney, Jr.
United Technologies Research
Silver Lane
East Hartford, CT 06108

William C. Cliff
Dept. of Atm. Science
Batelle,
Batelle Blvd.
Richland, WA 99352

John Combs (MS 21-4)
NASA-Lewis Research Center
21000 Brookpark Road
Cleveland, OH 44135

Duane Cromack
Mechanical Engineering Department
University of Massachusetts
Amherst, MA 01003

Glidden Doman
Hamilton Standard
Bradley Field
Windsor Locks, CT 06096

Mark Dreier
Paragon Pacific, Incorporated
1601 El Segundo Blvd.
El Segundo, CA 09245

John Dugundji
Aeronautics and Astronautics
MIT
Room 33-313
Cambridge, MA 02139

Robert E. English (MS 3-15)
NASA-Lewis Research Center
21000 Brookpark Road
Cleveland, OH 44135

Karl A. Faymon (MS 500-125)
NASA-Lewis Research Center
21000 Brookpark Road
Cleveland, OH 44135

David B. Fenn (MS 49-6)
NASA-Lewis Research Center
21000 Brookpark Road
Cleveland, OH 44135

Demeter G. Fertis
University of Akron
Akron, OH 44325

Patrick M. Finnegan (MS 49-6)
NASA-Lewis Research Center
21000 Brookpark Road
Cleveland, OH 44135

Vernon D. Gebben (MS 500-125)
NASA-Lewis Research Center
21000 Brookpark Road
Cleveland, OH 44135

Nicholas Giansante
Kaman Aerospace Corporation
Old Windsor Road
Bloomfield, CT 06002

John C. Glasgow (MS 49-6)
NASA-Lewis Research Center
21000 Brookpark Road
Cleveland, OH 44135

Harold Gold (MS 100-1)
NASA-Lewis Research Center
21000 Brookpark Road
Cleveland, OH 44135

John Gyekenyesi (MS 21-4)
NASA-Lewis Research Center
21000 Brookpark Road
Cleveland, OH 44135

Norman D. Ham
MIT
Room 33-410
Cambridge, MA 02139

Kermit Harner
Hamilton Standard
Bradley Field
Windsor Locks, CT 06096

William Hawersaat (MS 49-6)
NASA-Lewis Research Center
21000 Brookpark Road
Cleveland, OH 44135

Kirby Hiller (MS 100-1)
NASA-Lewis Research Center
21000 Brookpark Road
Cleveland, OH 44135

Kurt H. Hohenemser
Washington University
Box 1185
St. Louis, MO 63130

Robert H. Johns (MS 49-3)
NASA-Lewis Research Center
21000 Brookpark Road
Cleveland, OH 44135

Robert Jones
Kaman Aerospace Corporation
Old Windsor Road
Bloomfield, CT 06002

K. R. V. Kaza (MS 49-6)
NASA-Lewis Research Center
21000 Brookpark Road
Cleveland, OH 44135

H. S. Kirschbaum
Westinghouse Electric Corporation
Beulah Road
Pittsburgh, PA 15235

J. Koz
Hamilton Standard
Bradley Field
Windsor Locks, CT 06096

Ray Kvaternik
NASA-Langley Research Center
Hampton, VA 23665

Paul Manos (MS 86-2)
NASA-Lewis Research Center
21000 Brookpark Road
Cleveland, OH 44135

Tom Martin (MS 8K-66)
Boeing Engineering and Construction
Box 3707
Seattle, WA 98124

Dean R. Miller (MS 49-6)
NASA-Lewis Research Center
21000 Brookpark Road
Cleveland, OH 44135

C. M. Minke
Hercules/ABL
Box 210
Cumberland, MD 21502

Harold E. Neustadter (MS 49-6)
NASA-Lewis Research Center
21000 Brookpark Road
Cleveland, OH 44135

Robert C. Reuter, Jr.
Sandia Laboratories
Box 5800
Albuquerque, NM 87115

Timothy R. Richards (MS 49-6)
NASA-Lewis Research Center
21000 Brookpark Road
Cleveland, OH 44135

Robert S. Ross
Concept Development Institute
1790 Stoney Hill
Hudson, OH   44236

E. Rothman
Hamilton Standard
Bradley Field
Windsor Locks, CT   06096

Michael J. Salkind
NASA Headquarters
Washington, DC   20546

Manuel Martinez-Sanchez
MIT
Room 37-371
Cambridge, MA   02139

George S. Sarvay (MS 21-4)
NASA-Lewis Research Center
21000 Brookpark Road
Cleveland, OH   44135

Joseph M. Savino (MS 49-6)
NASA-Lewis Research Center
21000 Brookpark Road
Cleveland, OH   44135

Robert C. Seidel (MS 100-1)
NASA-Lewis Research Center
21000 Brookpark Road
Cleveland, OH   44135

William R. Shapton
University of Cincinnati
Mail Location 72
Cincinnati, OH   45221

Paul Sirocky (MS 21-4)
NASA-Lewis Research Center
21000 Brookpark Road
Cleveland, OH   44135

David A. Spera (MS 49-6)
NASA-Lewis Research Center
21000 Brookpark Road
Cleveland, OH   44135

Clyde Stahle (M 4018)
General Electric Company
Box 8661
Philadelphia, PA   19101

Forrest Stoddard
University of Massachusetts
Amherst, MA   01002

Timothy L. Sullivan (MS 49-6)
NASA-Lewis Research Center
21000 Brookpark Road
Cleveland, OH   44135

Donald Teague
DOE/Wind Systems Branch
Washington, DC   20545

Ronald L. Thomas (MS 49-6)
NASA-Lewis Research Center
21000 Brookpark Road
Cleveland, OH   44135

Robert Thresher
ERDA/Wind Systems Branch
35 E & NW, Apt 609
Washington, DC   20001

Marc K. Torrey (MS 49-6)
NASA-Lewis Research Center
21000 Brookpark Road
Cleveland, OH   44135

Andrew Trenka
Rockwell International
Rocky Flats Plant
Box 464
Golden, CO   80401

Larry A. Viterna (MS 49-6)
NASA-Lewis Research Center
21000 Brookpark Road
Cleveland, OH   44135

Karen J. Wester (MS 49-6)
NASA-Lewis Research Center
21000 Brookpark Road
Cleveland, OH   44135

Suey T. Yee (MS 21-6)
NASA-Lewis Research Center
21000 Brookpark Road
Cleveland, OH   44135

1. Report No. NASA CP-2034	2. Government Accession No.	3. Recipient's Catalog No.
4. Title and Subtitle WIND TURBINE STRUCTURAL DYNAMICS		5. Report Date March 1978
		6. Performing Organization Code
7. Author(s) Dean R. Miller, Lewis Research Center, editor		8. Performing Organization Report No. E-9518
		10. Work Unit No.
9. Performing Organization Name and Address National Aeronautics and Space Administration Lewis Research Center Cleveland, Ohio 44135		11. Contract or Grant No.
		13. Type of Report and Period Covered Conference Publication
12. Sponsoring Agency Name and Address Department of Energy Solar Energy Division Washington, D.C. 20545		14. Sponsoring Agency Code CONF-771148

15. Supplementary Notes

16. Abstract

A workshop on wind turbine structural dynamics was held at the NASA Lewis Research Center in Cleveland, Ohio, on November 15-17, 1977. Information was exchanged on the following topics:

- Methods for calculating dynamic loads
- Aeroelastic stability
- Wind loads, both steady and transient
- Critical design conditions
- Drive train dynamics
- Systems dynamics
- Behavior of operating wind turbines

17. Key Words (Suggested by Author(s)) Windpower; Windmill; Wind turbine; Vibratory loads; Rotor blade; Wind energy conversion; Aeroelasticity; Flutter; Modal analysis; Dynamic structural analysis	18. Distribution Statement Unclassified - unlimited STAR Category 44 DOE Category UC-60

19. Security Classif. (of this report) Unclassified	20. Security Classif. (of this page) Unclassified	21. No. of Pages 290	22. Price* A13